

Electronic Thesis and Dissertation Repository

9-15-2010 12:00 AM

Spatial and Temporal Risk Assessment for Water Resources Decision Making

Shohan S. Ahmad
University of Western Ontario

Supervisor
Slobodan P. Simonovic
The University of Western Ontario

Graduate Program in Civil and Environmental Engineering
A thesis submitted in partial fulfillment of the requirements for the degree in Doctor of
Philosophy
© Shohan S. Ahmad 2010

Follow this and additional works at: <https://ir.lib.uwo.ca/etd>

Recommended Citation

Ahmad, Shohan S., "Spatial and Temporal Risk Assessment for Water Resources Decision Making"
(2010). *Electronic Thesis and Dissertation Repository*. 20.
<https://ir.lib.uwo.ca/etd/20>

This Dissertation/Thesis is brought to you for free and open access by Scholarship@Western. It has been accepted for inclusion in Electronic Thesis and Dissertation Repository by an authorized administrator of Scholarship@Western. For more information, please contact wlsadmin@uwo.ca.

SPATIAL AND TEMPORAL RISK ASSESSMENT FOR WATER RESOURCES DECISION MAKING

(Spine title: Spatial & Temporal Water Resources Risk Assessment)

(Thesis format: Monograph)

By

Shohan S. Ahmad

Graduate Program in Engineering Sciences
Department of Civil and Environmental Engineering

A thesis submitted in partial fulfillment
of the requirements for the degree of
Doctor of Philosophy

The School of Graduate and Postdoctoral Studies
The University of Western Ontario
London, Ontario, Canada

© Shohan S Ahmad 2011

THE UNIVERSITY OF WESTERN ONTARIO
FACULTY OF GRADUATE STUDIES

CERTIFICATE OF EXAMINATION

Supervisor

Examining Board

Dr. Slobodan P. Simonovic

Dr. Raouf E. Baddour

Dr. Craig Miller

Dr. Micha Pazner

Dr. Niru Nirupama

The Thesis by

Shohan S. Ahmad

entitled:

**SPATIAL AND TEMPORAL RISK ASSESSMENT
FOR WATER RESOURCES DECISION MAKING**

is accepted in partial fulfillment of the
Requirements for the degree of
Doctor of Philosophy

Date : 15th September 2010

Lisa Hodgetts
Chair of Thesis Examination Board

ABSTRACT

Water resources systems are vulnerable to natural disasters such as floods, wind storms, earthquakes, and various meteorological events. Flooding is the most frequent *natural* hazard that can cause damage to human life and property. A new methodology presented in this thesis is capable of flood risk management by: (a) addressing various uncertainties caused by variability and ambiguity; (b) integrating objective and subjective flood risk; and (c) assisting the flood risk management based on better understanding of spatial and temporal variability of risk. The new methodology is based on the use of fuzzy reliability theory. A new definition of risk is used and described using three performance indices (i) a combined fuzzy reliability-vulnerability, (ii) fuzzy robustness and (iii) fuzzy resiliency. The traditional flood risk management relies on either temporal or spatial variability, but not both. However, there is a need to understand the dynamic characteristics of flood risk and its spatial variability. The two-dimensional (2-D) fuzzy set that relates the universe of discourse and its membership degree, is not sufficient to address both, spatial and temporal, variations of flood risk. The theoretical contribution of this study is based on the development of a three dimensional (3-D) fuzzy set.

The spatial and temporal variability of fuzzy performance indices – (i) combined reliability-vulnerability, (ii) robustness, and (iii) resiliency – have been implemented to (i) river flood risk analysis and (ii) urban flood risk analysis. The river flood risk analysis is illustrated using the Red River flood of 1997 (Manitoba, Canada) as a case study. The urban flood risk analysis is illustrated using the residential community of Cedar Hollow (London, Ontario, Canada) as a case study.

The final results of the fuzzy flood reliability analysis are presented using maps that show the spatial and temporal variation of reliability-vulnerability, robustness and resiliency indices. Maps of fuzzy reliability indices provide additional decision support for (a) land use planning, (b) selection of appropriate flood mitigation strategies, (c) planning emergency management measures, (d) selecting an appropriate construction technology for flood prone areas, and (e) flood insurance.

Key Words: Water resources, flood risk analysis, flood management, uncertainty analysis, fuzzy sets, spatial and temporal fuzzy performance indices, floodplain mapping, storm sewer modeling, disaster mitigation, Geographic Information System (GIS).

DEDICATION

I dedicate this thesis to my wonderful wife, Twiggy and my baby girl, Ereen who make my life meaningful and enjoyable.

ACKNOWLEDGEMENTS

I wish to express my deepest appreciation to Professor Slobodan P. Simonovic, the person that made all this research possible. He has provided an exceptional level of guidance and supervision throughout the years, and for that I am most grateful. His invaluable guidance and inspiration helped me grow confidence and develop both academically and personally. Thank you very much Professor.

I would like to thank the Department of Civil and Environmental Engineering at the University of Western Ontario, including faculty, staff, friends in the FIDS office, and fellow graduate students. Away from school my wife, Twiggy reminded me that there is life outside school, and kept me healthy and happy. Without her encouragement and support, this achievement could not have been possible. I would like to thank my parents, Dr. Sohrabuddin Ahmad and Mrs. Chaman Ara Ahmad; and Twiggy's parents, Dr. Md. Nurul Islam and Mrs. Saki Nazrin, who have always been a great encouragement for this great achievement. Special thanks to Taufiq and Tansu.

Finally, I am grateful to the Natural Sciences and Engineering Research Council (NSERC) of Canada for their very generous scholarships, which funded me throughout my time in Civil and Environmental Engineering at the University of Western Ontario.

TABLE OF CONTENTS

CERTIFICATE OF EXAMINATION.....	I
ABSTRACT	II
DEDICATION	IV
ACKNOWLEDGEMENTS.....	V
TABLE OF CONTENTS.....	VI
LIST OF FIGURES.....	X
LIST OF TABLES.....	XII
1 INTRODUCTION.....	1
1.1 WATER RESOURCES MANAGEMENT UNDER UNCERTAINTY	1
1.2 OBJECTIVE AND SUBJECTIVE UNCERTAINTY	6
1.3 SPATIAL AND TEMPORAL CHARACTERISTICS OF FLOOD RISK.....	7
1.4 OBJECTIVES OF THE RESEARCH.....	8
1.5 RESEARCH CONTRIBUTIONS	9
1.6 ORGANIZATION OF THE THESIS	9
2 LITERATURE REVIEW	12
2.1 WATER RESOURCES MANAGEMENT UNDER UNCERTAINTY	13
2.2 TYPES OF UNCERTAINTY.....	14
2.3 MODELING DYNAMIC PROCESS OF RIVER AND URBAN FLOODING.....	16
2.3.1 <i>HYDRODYNAMIC MODELING</i>	17
2.3.2 <i>SYSTEM DYNAMICS (SD) MODELING</i>	21
2.4 DEFINITION OF RISK.....	25
2.5 RISK IDENTIFICATION	26
2.6 PERFORMANCE INDICES.....	27
2.7 RELIABILITY ANALYSIS IN ENGINEERING SYSTEMS.....	27
2.7.1 <i>PROBABILISTIC APPROACH IN WATER RESOURCES MANAGEMENT</i>	28
2.7.2 <i>FUZZY SET APPROACH IN WATER RESOURCES FLOOD MANAGEMENT</i>	32

2.8	RELIABILITY ANALYSIS OF WATER RESOURCES SYSTEMS USING FUZZY PERFORMANCE INDICES	36
2.8.1	DEFINITION OF FAILURE.....	37
2.8.2	DEFINITION OF FUZZY SYSTEM STATE.....	41
2.8.3	DEFINITION OF COMPATIBILITY.....	43
2.8.4	COMBINED RELIABILITY-VULNERABILITY INDEX	44
2.8.5	ROBUSTNESS INDEX.....	46
2.8.6	RESILIENCY INDEX.....	46
3	METHODOLOGY FOR RIVER AND URBAN FLOOD RISK ANALYSIS	49
3.1	RIVER FLOOD RISK ANALYSIS	50
3.1.1	MODELING DYNAMIC PROCESSES OF RIVER FLOODING.....	51
	Hydrodynamic Modeling Approach	51
	System Dynamics Modeling Approach	55
3.1.2	RIVER FLOOD DAMAGE ANALYSIS.....	59
	Agricultural Damage.....	59
	Residential Damage.....	61
3.1.3	SPATIAL AND TEMPORAL VARIABILITY OF RIVER FLOOD RISK.....	63
3.1.4	A NEW METHODOLOGY FOR FUZZY RIVER FLOOD RISK ANALYSIS.....	65
	Definition of Partial Failure.....	66
	Spatial and Temporal Variability of Fuzzy Flood Damage	70
	Total Flood Damage.....	79
	Fuzzy Flood Compatibility.....	80
	Fuzzy Combined Reliability-Vulnerability Index	85
	Fuzzy Flood Recovery Time	92
	Fuzzy Resiliency Index.....	93
3.2	URBAN FLOOD RISK ANALYSIS.....	96
3.2.1	MODELING DYNAMIC PROCESSES OF URBAN FLOODING – HYDRODYNAMIC MODELING APPROACH	96
3.2.2	URBAN FLOOD DAMAGE ANALYSIS.....	100
3.2.3	SPATIAL AND TEMPORAL VARIABILITY OF URBAN FLOOD RISK.....	105
3.2.4	A NEW METHODOLOGY FOR FUZZY URBAN FLOOD RISK ANALYSIS	106
	Definition of Partial Failure.....	106
	Spatial and Temporal Variability of Fuzzy Flood Damage	109

<i>Total Urban Flood Damage</i>	116
<i>Fuzzy Flood Compatibility</i>	117
<i>Fuzzy Combined Reliability-Vulnerability Index</i>	118
<i>Fuzzy Robustness Index</i>	119
<i>Fuzzy Resiliency Index</i>	121
4 CASE STUDY	124
4.1 RIVER FLOOD RISK ANALYSIS: THE RED RIVER BASIN CASE STUDY	124
4.1.1 2D HYDRODYNAMIC MODELING OF THE RED RIVER CASE STUDY.....	130
4.1.2 SPATIAL AND TEMPORAL RISK ANALYSIS OF THE RED RIVER FLOOD OF 1997	134
4.1.3 RESULTS AND DISCUSSIONS.....	136
<i>Spatial and Temporal Variation of Water Surface Elevation</i>	136
<i>Verification of Result Obtained from MIKE 21 Model Simulation</i>	138
<i>Spatial and Temporal Variability of Flood Damage</i>	141
<i>Combined Fuzzy Flood Reliability-Vulnerability Index</i>	144
<i>Sensitivity Analysis of Combined Fuzzy Reliability-Vulnerability Index</i>	146
<i>Fuzzy Robustness Index</i>	150
<i>Fuzzy Resiliency Index</i>	152
4.1.4 SYSTEM DYNAMICS MODELING OF THE RED RIVER CASE STUDY	156
4.1.5 SPATIAL AND TEMPORAL FUZZY RISK ANALYSIS OF THE RED RIVER FLOOD OF 1997.....	163
4.1.6 RESULTS AND DISCUSSIONS.....	164
<i>Spatial and Temporal Variation of Flood Damage</i>	164
<i>Combined Fuzzy Flood Reliability-Vulnerability Index</i>	166
<i>Fuzzy Robustness Index</i>	168
<i>Fuzzy Resiliency Index</i>	170
4.2 URBAN FLOOD RISK ANALYSIS: CEDAR HOLLOW CASE STUDY.....	172
4.2.1 COUPLED 1D HYDRAULIC AND 2D HYDRODYNAMIC MODELING.....	173
4.2.2 URBAN FLOOD DAMAGE ANALYSIS.....	175
4.2.3 SPATIAL AND TEMPORAL URBAN FLOOD RISK ANALYSIS	178
4.2.4 RESULTS AND DISCUSSION:	179
<i>Spatial and Temporal Variability of Water Surface Elevations</i>	179
<i>Spatial and Temporal Variability of Flood Damage</i>	182

<i>Combined Fuzzy Flood Reliability-Vulnerability Index</i>	185
<i>Fuzzy Robustness Index</i>	187
<i>Fuzzy Resiliency Index</i>	189
5 SUMMARY AND CONCLUSIONS.....	190
5.1 FLOOD RELIABILITY ANALYSIS	191
5.1.1 RIVER FLOOD RISK ANALYSIS	194
2D Hydrodynamic Modeling.....	194
System Dynamics Modeling	197
5.1.2 URBAN FLOOD RISK ANALYSIS.....	200
5.2 THE USE OF SPATIAL AND TEMPORAL FUZZY RELIABILITY ANALYSIS IN PRACTICE.....	202
5.3 RECOMMENDATIONS FOR FUTURE WORK	205
5.3.1 INTELLIGENT DECISION SUPPORT SYSTEM	205
5.3.2 APPROPRIATE SHAPE OF FUZZY MEMBERSHIP FUNCTION.....	205
5.3.3 MULTI-OBJECTIVE DECISION SUPPORT SYSTEM	206
REFERENCES	207
APPENDIX: A (COMPUTATIONAL TOOLS FOR THE IMPLEMENTATION OF RIVER FLOOD RISK ASSESSMENT METHODOLOGY)	220
APPENDIX: B (COMPUTATIONAL TOOLS FOR THE IMPLEMENTATION OF URBAN FLOOD RISK ASSESSMENT METHODOLOGY)	239
CURRICULUM VITAE.....	252

LIST OF FIGURES

FIGURE 1.1: GREAT NATURAL DISASTERS 1950-2009, NUMBER OF EVENTS (AFTER MUNICH RE, NATCATSERVICE, 2010)	2
FIGURE 1.2: GREAT NATURAL DISASTERS 1950-2009, OVERALL AND INSURED LOSSES (AFTER MUNICH RE, NATCATSERVICE, 2010)	2
FIGURE 1.3: GREAT NATURAL DISASTERS 1950-2009, PERCENTAGE DISTRIBUTION (AFTER MUNICH RE, NATCATSERVICE, 2010)	3
FIGURE 1.4: SCHEMATIC OF CHAPTER 3.....	10
FIGURE 2.1: MAJOR SOUCES OF UNCERTAINTY (AFTER SIMONOVIC, 1997)	15
FIGURE 2.2: DEFINITION OF PROBABILISTIC RISK (AFTER GANOULIS 1994)	29
FIGURE 2.3: DIFFERENT PERCEPTION OF FAILURE (AFTER EL-BAROUDY AND SIMONOVIC, 2004)	38
FIGURE 2.4: FUZZY REPRESENTATION OF ACCEPTABLE FAILURE REGION (AFTER EL-BAROUDY AND SIMONOVIC, 2004)	39
FIGURE 2.5: TRIANGULAR SYSTEM-STATE MEMBERSHIP FUNCTION	42
FIGURE 2.6: TWO COMPLIANCE CASES (EL-BAROUDY AND SIMONOVIC, 2004)	43
FIGURE 2.7: COMPATIBILITY WITH DIFFERENT LEVELS OF PERFORMANCE MEMBERSHIP FUNCTIONS (EL-BAROUDY AND SIMONOVIC, 2004).....	45
FIGURE 2.8: FUZZY REPRESENTATION OF MAXIMUM RECOVERY TIME	47
FIGURE 3.1: SCHEMATIC OF (I) RIVER, AND (II) URBAN FLOOD RISK ANALYSIS.....	50
FIGURE 3.2: SINGLE CELL WITH INFLOW AND OUTFLOW.	58
FIGURE 3.3: GRAPHICAL RELATIONSHIP OF PERCENTAGE OF AVERAGE YIELD AND SEEDING DATE.....	60
FIGURE 3.4: DEPTH-DAMAGE RELATIONSHIP FOR A RING DIKED COMMUNITIES.....	63
FIGURE 3.5: 2-D FUZZY REPRESENTATION OF SPATIAL VARIABILITY IN ACCEPTANCE LEVEL OF PARTIAL FLOOD DAMAGE (AHMAD AND SIMONOVIC, 2007)	68
FIGURE 3.6: 3-D FUZZY REPRESENTATION OF SPATIAL AND TEMPORAL VARIABILITY IN ACCEPTANCE LEVEL OF PARTIAL FLOOD DAMAGE	68
FIGURE 3.7: 2-D FUZZY SET FOR TEMPORAL VARIABILITY OF FLOOD DAMAGE.....	72
FIGURE 3.8: 2-D FUZZY SET FOR SPATIAL VARIABILITY OF FLOOD DAMAGE.....	74
FIGURE 3.9: 3-D JOINT FUZZY SET OF FLOOD DAMAGE	75
FIGURE 3.10: CENTER OF GRAVITY OF THE 2-D FUZZY SET FOR TEMPORAL VARIABILITY ...	77
FIGURE 3.11: 2-D FUZZY SET FOR SPATIAL VARIABILITY OF FLOOD DAMAGE AT D_{i_g}	78
FIGURE 3.12: NEW 2-D FUZZY SET FOR SPATIAL AND TEMPORAL VARIABILITY OF FLOOD DAMAGE	78

FIGURE 3.13: OVERLAP AREA BETWEEN FLOOD DAMAGE MEMBERSHIP FUNCTION AND ACCEPTANCE LEVEL OF PARTIAL FLOOD DAMAGE MEMBERSHIP FUNCTION.....	81
FIGURE 3.14: WEIGHTED AREA CALCULATION FOR THE FLOOD DAMAGE MEMBERSHIP FUNCTION.....	83
FIGURE 3.15: FLOW CHART OF FUZZY COMBINED RELIABILITY-VULNERABILITY INDEX	88
FIGURE 3.16: FLOW CHART OF FUZZY ROBUSTNESS INDEX.....	90
FIGURE 3.17: FUZZY MEMBERSHIP FUNCTION OF RECOVERY TIME.....	94
FIGURE 3.18: LAYOUT OF PIPE AND STREET SYSTEM (AFTER MARK <i>ET AL</i> , 2004).....	98
FIGURE 3.19: FLOW FROM THE STREET SYSTEM INTO A PARTLY FULL PIPE (AFTER MARK <i>ET AL</i> , 2004).....	98
FIGURE 3.20: FLOW TO THE STREETS FROM A PIPE SYSTEM WITH INSUFFICIENT CAPACITY (AFTER MARK <i>ET AL</i> , 2004).....	99
FIGURE 4.1: CANADIAN PORTION OF THE RED RIVER BASIN (AFTER WINNIPEG FREE PRESS).....	125
FIGURE 4.2: SCHEMATIC DIAGRAM OF THE FLOOD CONTROL STRUCTURES.....	129
FIGURE 4.3: SCHEMATIC DIAGRAM OF THE INFRASTRUCTURE IN THE STUDY AREA.....	130
FIGURE 4.4: TOPOGRAPHIC DATA OF THE RED RIVER CASE STUDY.....	132
FIGURE 4.5: SCHEMATIC DIAGRAM OF 2-D MODELING APPROACH.....	133
FIGURE 4.6: GUI WITH PREDEFINED PARTIAL LEVEL OF FLOOD DAMAGE FOR RED RIVER FLOOD 1997.....	135
FIGURE 4.7: WATER SURFACE ELEVATION (M) IN RED RIVER FLOOD IN 1997.....	137
FIGURE 4.8: SATELLITE IMAGE (LEFT) AND SIMULATED FLOODED AREA (RIGHT) ON MAY 1, 1997.....	138
FIGURE 4.9: COMPARISON OF OBSERVED AND SIMULATED WATER ELEVATIONS (IN METER) AT RED RIVER NEAR ST ADOLPHE.....	139
FIGURE 4.10: COMPARISON OF OBSERVED AND SIMULATED WATER LEVELS AT FLOODWAY INLET.....	139
FIGURE 4.11: SPATIAL AND TEMPORAL VARIATION OF FLOOD DAMAGE (\$ PER 625 SQ. METER).....	142
FIGURE 4.12: FUZZY COMBINED RELIABILITY-VULNERABILITY INDEX.....	145
FIGURE 4.13: SENSITIVITY ANALYSIS ON COMBINED RELIABILITY-VULNERABILITY INDEX TO THE SHAPE.....	149
FIGURE 4.14: FUZZY ROBUSTNESS INDEX.....	151
FIGURE 4.15: FUZZY RESILIENCY INDEX.....	155
FIGURE 4.16: TOPOGRAPHIC DATA OF THE RED RIVER CASE STUDY.....	156
FIGURE 4.17: STUDY AREA DIVIDED INTO CELLS.....	159
FIGURE 4.18: FLOW ROUTING SECTOR.....	161

FIGURE 4.19: CONTROL SCREEN OF THE RED RIVER SECTION SIMULATION MODEL.	163
FIGURE 4.20: GUI WITH PREDEFINED PARTIAL LEVEL OF FLOOD DAMAGE	164
FIGURE 4.21: SPATIAL AND TEMPORAL VARIATION OF FLOOD DAMAGE (\$ PER 4 SQ. KM)	165
FIGURE 4.22: FUZZY COMBINED RELIABILITY-VULNERABILITY INDEX	167
FIGURE 4.23: FUZZY ROBUSTNESS INDEX	169
FIGURE 4.24: FUZZY RESILIENCY INDEX.....	171
FIGURE 4.25: LOCATION OF CEDAR HOLLOW, LONDON, ON.....	172
FIGURE 4.26: 500 YEAR 6-HOUR DESIGN RAINFALL	175
FIGURE 4.27: FIA BASED STRUCTURE DEPTH-DAMAGE CURVE, TWO OR MORE STORIES WITH BASEMENT (SCAWTHORN, 2006).....	176
FIGURE 4.28: ROAD BLOCKAGE VS. PERCENT DAMAGE RELATIONSHIP	177
FIGURE 4.29: GUI WITH PREDEFINED PARTIAL LEVEL OF FLOOD DAMAGE FOR CEDAR HOLLOW.....	178
FIGURE 4.30: SPATIAL AND TEMPORAL VARIATION OF WATER SURFACE ELEVATION (METER).....	180
FIGURE 4.31: SPATIAL AND TEMPORAL VARIATION OF DIRECT DAMAGE	182
FIGURE 4.32: SPATIAL AND TEMPORAL VARIATION OF INDIRECT DAMAGE	183
FIGURE 4.33: SPATIAL AND TEMPORAL VARIATION OF TOTAL FLOOD DAMAGE	184
FIGURE 4.34: FUZZY COMBINED RELIABILITY-VULNERABILITY INDEX	186
FIGURE 4.35: FUZZY ROBUSTNESS INDEX	188

LIST OF TABLES

TABLE 4.1: COMPARISON OF RECORDED AND MODELED PEAK WATER LEVELS (FT) FOR 1997.....	140
TABLE 4.2: AREA IN SQUARE KM CORRESPONDING TO VALUES OF COMBINED RELIABILITY-VULNERABILITY INDEX	148

1 INTRODUCTION

1.1 WATER RESOURCES MANAGEMENT UNDER UNCERTAINTY

Uncertainty can have important implications on water resources management. All water management decisions should take uncertainty into account. The diversity of sources of uncertainty in water resources management pose a great challenge to ensure a satisfactory and reliable system performance. Sometimes the implications of uncertainty are the risks associated with the potential and significant effects of poor water resources system performance. Adopting high safety factors by considering all unknown sources of risk (standard-based engineering practice) is one of the ways to avoid uncertainty. However, a high safety factor without quantifying different sources of uncertainty would make the solution infeasible. Therefore it is necessary to quantify known sources of uncertainty. Managers need to understand the nature of the underlying threats in order to identify, assess and manage the risks associated with uncertainty. The inability to do so is likely to result in adverse impacts on systems performance, and in extreme cases such as natural hazards, i.e. floods, cyclones, tsunamis etc, this can result in catastrophic performance failures. Quantification of uncertainty in natural hazard risk management can reduce the loss of lives and damage to properties. According to Simonovic (2011) the longer time period records (traced back to 1900 while more reliable after 1950) show an increasing trend in the number of disasters (Figure 1.1), their overall and insured losses (Figure 1.2), and economic impact (Figure 1.3).

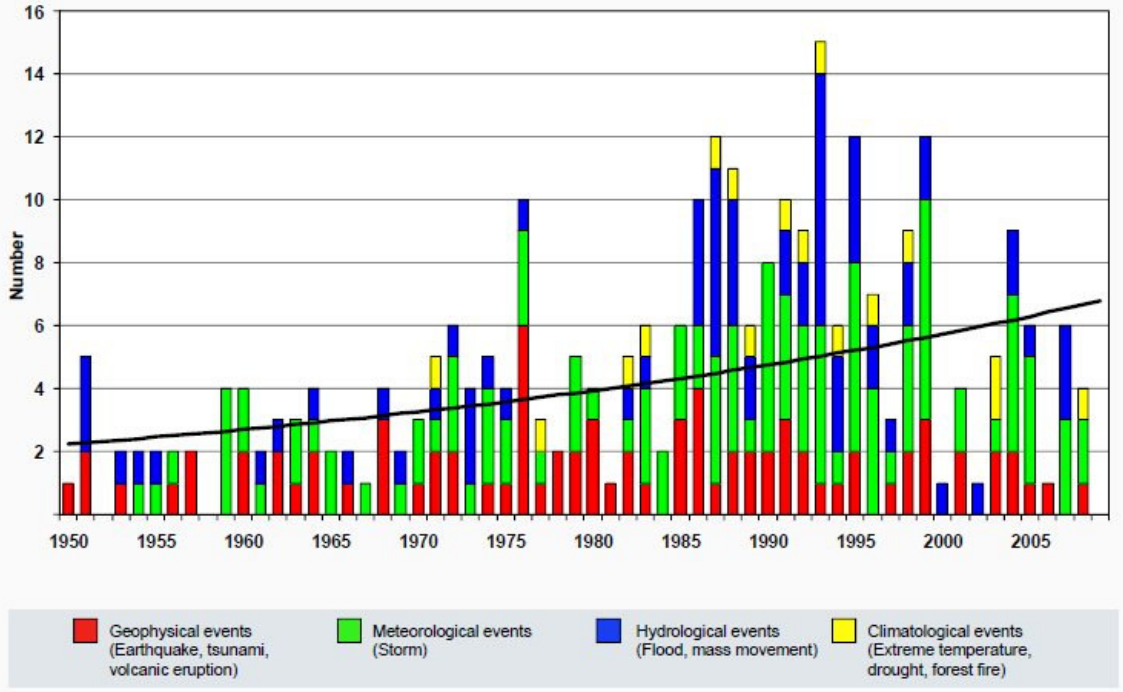


Figure 1.1: Great natural disasters 1950-2009, number of events (after Munich Re, NatCatService, 2010)

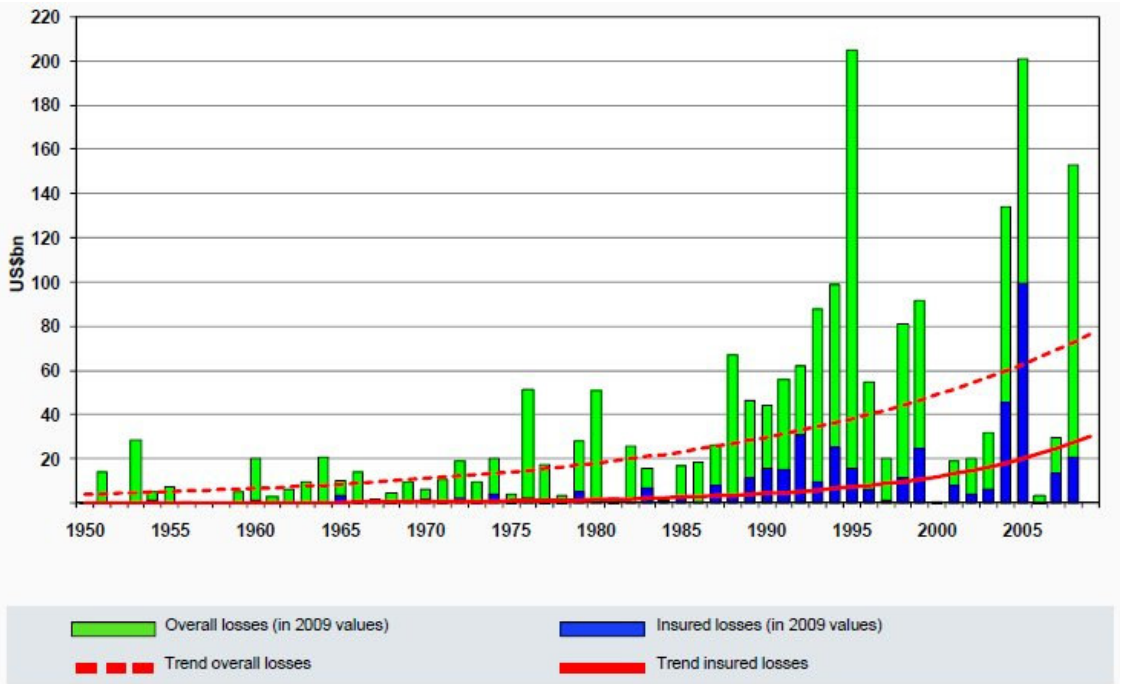


Figure 1.2: Great natural disasters 1950-2009, Overall and insured losses (after Munich Re, NatCatService, 2010)

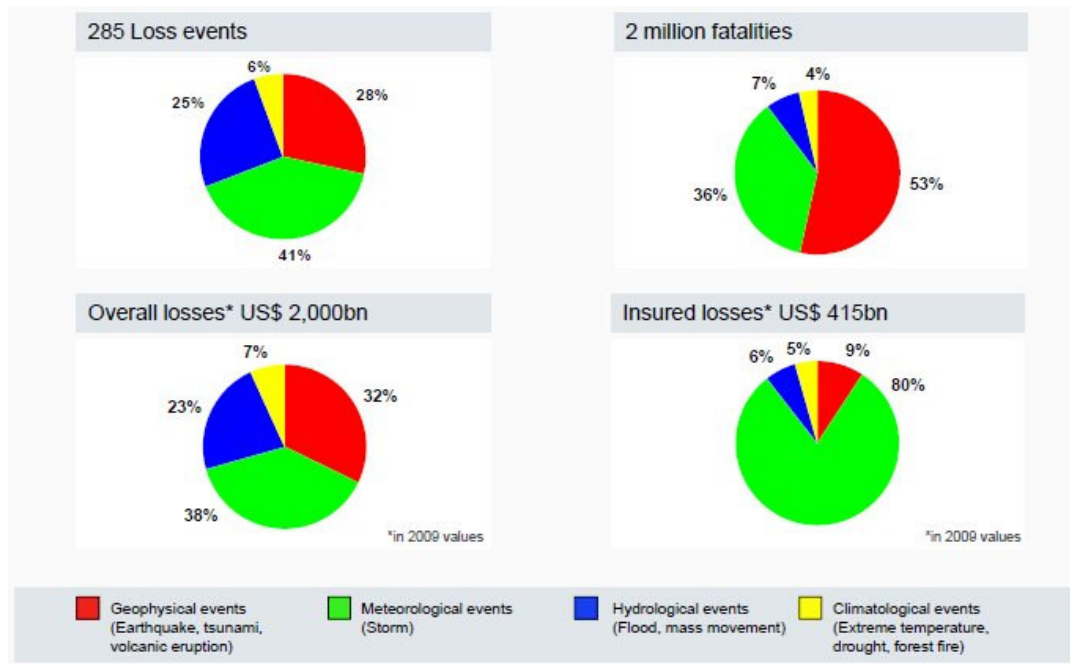


Figure 1.3: Great natural disasters 1950-2009, percentage distribution (after Munich Re, NatCatService, 2010)

In 2000, Mozambique was affected by a devastating flood that made half a million people homeless and caused 700 deaths (Wheater, 2005). The devastating flood of Central Europe in 2002 required the widespread evacuation of many towns and cities, with property damage estimated at 21.5 billion euros (Kron, 2005; Wheeler, 2010). On July 26, 2005, the flooding that took place in Mumbai (Bombay) affected approximately 5 million people and led to 1000 deaths. 940 millimeters of rainfall was recorded in this single event. Flooding in Central Europe in August 2005 caused fatalities in Germany, Switzerland, Austria, Romania and Bulgaria (Wheater, 2010). Among recent incidents, a flood of southern China in June 2010 affected more than 29 million people and inundated 1.6 million hectares of agricultural land. More than two million people were evacuated and 195,000 houses collapsed, with direct economic losses amounting to approximately 5.03 billion euros (IFRC, 2010). During May to June, 2010 the devastating floods in

Central Europe affected Austria, the Czech Republic, Germany, Hungary, Poland, Slovakia, Serbia and Ukraine. Poland was the worst affected and the city of Kraków declared a state of emergency. As a result of the devastating flood 37 people were killed and approximately 23,000 people were evacuated. Poland estimated an economic loss of 2.5 billion euros (Euronews, 2010).

Urban flooding also poses a major threat to many cities around the world. Higher frequency of urban flooding, which occurs mostly in developing countries, has made it necessary for the development of a more efficient urban flood management plan. Heavy rainfall, combined with an insufficient capacity of sewer systems, can cause urban flooding. In February 2002, 50 people were killed and 200,000 people made homeless in Indonesia as a result of heavy rainfall that led to urban flooding (Mark *et al.*, 2004). In 2000, Mumbai experienced a major flooding event in which 15 lives were lost and that caused immeasurable inconveniences for many people living in that region. In Dhaka City (Bangladesh), due to an insufficient capacity of storm sewer systems, a small rainfall event can cause serious problems. In September 1996, Dhaka City was paralyzed as a result of urban flooding. In 1983, Bangkok (Thailand) remained flooded for almost 6 months and reported infrastructure damage was approximately \$146 million (Mark *et al.*, 2004). On August 19, 2005, a two to three hour period of extremely heavy rainfall hit the Greater Toronto Area and quickly caused an accumulation of storm water in the storm sewer systems, which resulted in flooding across the city. This single rain event cost the city an estimated \$34 million. In addition, the Insurance Bureau of Canada estimated that over \$400 million was paid out to private citizens to cover the flood damage to basements

caused by this single storm event (River Sides, 2005). Toronto was not alone in experiencing first hand the destructive potential of flooding. In February 2010, heavy rain lashed the Portuguese resort island of Madeira, turning some streets in the capital, Funchal, into raging rivers of mud, water and debris. The mudslides and flooding killed at least 42 people and more than 120 other people were reported as injured (CBC news, 2010). In April, 2010, landslides and floods set off by the heavy rains killed at least 95 people in the city of Rio de Janeiro. In addition to obstructing roads and other infrastructure, the devastation caused by this flood resulted in hundreds of people becoming homeless, virtually paralyzing the economic activity of Brazil's second largest city (Reuters, 2010).

Ganoulis (1994) argues that engineering risk assessment and reliability analyses provide a general methodology for the quantification of uncertainty and, as a result, should be used to determine the safety of an engineering system. Risk assessment is an essential component of sustainable flood management, and is becoming more important with the increase in population density and the intensifying effects of climate change. There is a scientific consensus that climate change is resulting in higher average temperatures, rising sea levels, change in precipitation patterns and change in frequency and severity of extreme hydrological conditions – floods and droughts. A larger population affects the sustainability of land use, safe economic development in flood prone areas, and in general leads to greater flood vulnerability.

There are two principal types of measures being considered for the management of river

floods: (a) structural measures; and (b) non-structural measures (Simonovic, 1999 among others). The most common structural interventions used today are: (i) levees or flood walls; (ii) diversion structures; (iii) channel modifications; and (iv) flood control reservoirs. For management of urban floods, the structural measures now deal with efficient storm sewer system and infiltration basin. Furthermore, the structural measures are becoming more frequently combined with non-structural measures, such as flood zoning, flood warning, waterproofing, and flood insurance. Levy and Hall (2005) introduced the important concept of “living with flood”, which requires a high public awareness of actual flood risks. The quantification of all uncertainties and the spatial and temporal representation of flood risk contributes to a higher level of awareness and may reduce the effects of flood damage to both people and material.

1.2 OBJECTIVE AND SUBJECTIVE UNCERTAINTY

There are many types of uncertainty in the flood management process, ranging from hydrologic, hydraulic, geotechnical, and structural uncertainty, to economic, environmental, ecological, social and political uncertainty. According to Slovic (2000) and Simonovic (2002) a major part of the confusion implicit in flood risk analysis relates to an inadequate distinction between three fundamental concepts of probability and risk: (i) Objective risk (real, physical), R_o , and objective probability, p_o , which is the property of real physical systems; (ii) Subjective risk, R_s , and subjective probability, p_s ; and (iii) Perceived risk, R_p , which is related to an individual’s feeling of fear in the face of an undesirable and possible event. Probability is here defined as the degree of belief in a statement. R_s and p_s are not properties of the physical systems under consideration (but

may be some function of R_o and p_o). Similarly, R_p is not a property of the physical systems but is related to fear of the unknown. Moreover, R_p may be a function of R_o , p_o , R_s , and p_s . Because of the confusion between the concepts of objective and subjective flood risk, many characteristics of subjective risk are also believed to be valid for objective risk. Indeed, it is almost universally assumed that the imprecision of human judgment is equally prominent and destructive for all water resources risk evaluations and all risk assessments. The popular methods used by society to manage flood risk appear to be dominated by considerations of perceived and subjective risks, while it is the objective risks that kill people, damage the environment and create property loss (Simonovic and Ahmad, 2007).

1.3 SPATIAL AND TEMPORAL CHARACTERISTICS OF FLOOD RISK

Flood risk assessments have three main characteristics: (i) spatial structure and relationships among risk characteristics; (ii) interactions among the spatial risk characteristics; and (iii) changes or alterations in temporal risk characteristics. Any effort to understand and describe the dynamics of flood risk assessment requires the ability to deal with these interrelated aspects. Traditional modeling approaches focus on either temporal or spatial variation, but not both. There is an important feedback between time and location in space, i.e., temporal variability of risk is affected by the change of spatial characteristics of risk. To understand risk dynamics, patterns in time and location in space need to be examined together. Therefore, to better understand dynamic characteristics of flood risk, a new modeling framework is required that not only captures the dynamic processes in time and location in space but also integrates different modeling

tools required for solving complex flood risk management problems. Modeling environments that can link social, economic, and environmental consequences of flood risks are fundamental to an understanding of the impacts of proposed management decisions. An integrated modeling framework can enhance our ability to understand complex flood management processes, and can also assist in generating adequate information/scenarios in order to help decision-making.

1.4 OBJECTIVES OF THE RESEARCH

The main objectives of the research presented here are (a) to provide the methodology for flood risk assessment while taking into consideration the spatial and temporal variability of various objective and subjective uncertainties in flood management, and (b) to provide a methodology possessing the capability to spatially and temporally represent integrated flood risk. The presented research develops three fuzzy performance indices: (1) combined reliability-vulnerability index, (2) robustness index, and (3) resiliency index, for spatial and temporal reliability analysis of riverine and urban floods. This new methodology is not limited by the shape of the membership function in any way. The shape of the membership function that best represents the flood damage should be selected on the basis of the available damage information and the stakeholder's domain knowledge. The existing literature offers various methods for the development of appropriate membership functions that combine data, expert opinion and stakeholder's preferences. Despic and Simonovic (2000) provide a methodology for developing an appropriate membership function for flooding. Since the main focus of this thesis is on the development of a methodology for spatial and temporal reliability analysis of floods,

a triangular fuzzy membership function is used for the purposes of illustration. Sensitivity analyses are also performed using a trapezoidal membership function to emphasize the importance on choosing the right membership function.

1.5 RESEARCH CONTRIBUTIONS

The traditional two-dimensional (2-D) fuzzy set representation is not sufficient to handle both spatial and temporal information. The theoretical foundation of this study is based on the development of a three dimensional (3-D) fuzzy set representation of the flood risk that includes spatial and temporal variability. In order to describe the spatial and temporal variability in the risk preferences of decision makers, the proposed methodology extends the partial flood damage concept (El-Baroudy and Simonovic, 2004) to a 3-D representation. The practical contribution of this research is the development of a flood risk management approach capable of:

- addressing uncertainty caused by spatial and temporal variability and ambiguity;
- integrating objective and subjective risks; and
- assisting flood management decision making by providing a better understanding of spatial and temporal variability of risk.

1.6 ORGANIZATION OF THE THESIS

This thesis contains five chapters. The first chapter is a general introduction to flood risk assessment. The second chapter contains a literature review on water resources management (mainly focusing on floodplain management) under uncertainty, modeling dynamic processes, and risk analysis. This chapter describes the theory of fuzzy

performance indices developed by El-Baroudy and Simonovic (2004) that forms the basis of the research presented in this thesis. The third chapter provides the methodology adopted for the spatial and temporal extension of the fuzzy reliability analysis of flood risk. The third chapter presents the mathematical formulation in two parts:

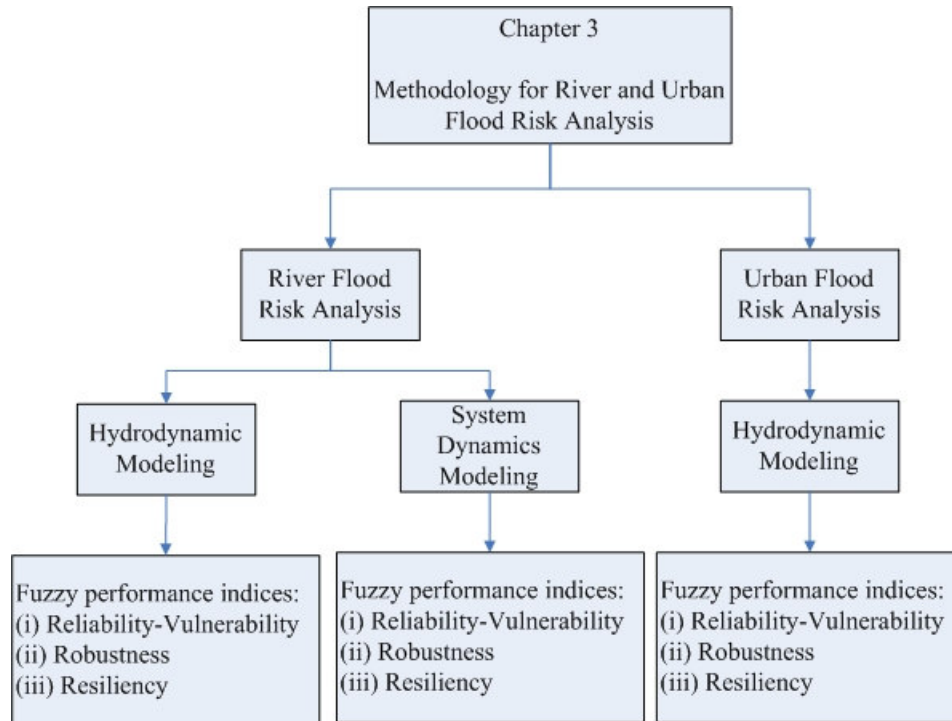


Figure 1.4: Schematic of Chapter 3

- (a) the first part describes the methodology of spatial and temporal reliability analysis for *river flooding*. The dynamic process of overland flooding is addressed using two modeling tools: (i) hydrodynamic modeling, and (ii) system dynamics (SD) modeling. The results of these two models are water surface elevations for different time steps and locations in space. The presented methodology then uses the water surface elevations to determine spatial and temporal variation of flood

damage, and develops the fuzzy performance indices to spatially and temporally represent reliability-vulnerability, robustness and resiliency for river flood risk.

(b) the second part describes the methodology used for the spatial and temporal reliability analysis for *urban flooding*. The dynamic interaction between the storm sewer network and overland flow is addressed using a hydrodynamic modeling tool. Due to the inadequate capability of the SD approach to dynamically link a storm sewer model with an overland flow model, SD modeling is inappropriate to address overland flooding for an urban flood context. As such, the hydrodynamic modeling is used to simulate the dynamic process of overland urban flooding. The hydrodynamic model generates water surface elevations for different time steps and locations, which are used to determine the spatial and temporal variation of flood damage. The methodology then develops the fuzzy performance indices to spatially and temporally represent reliability-vulnerability, robustness and resiliency of urban flood risk.

Chapter four demonstrates the applicability of the proposed approach for two case studies: (i) Red River flood risk analysis, Manitoba, Canada, and (ii) Urban flood risk analysis for London, Ontario, Canada. Finally, summaries and conclusions of the research are presented in chapter five.

2 LITERATURE REVIEW

Engineering risk and reliability analysis is a general methodology for the quantification of uncertainty and the evaluation of its consequences for the safety of engineering systems (Ganoulis, 1994). Risk identification is the first step in any risk analysis, where all sources of uncertainty are clearly detailed. Quantification of risk is the second step, where uncertainties are measured using different system performance indices and figures of merit such as reliability, vulnerability, robustness and resiliency. The existence of different types of uncertainty creates many challenges in water resources planning, design and management. Therefore reliability analysis in water resources management relies greatly on the proper quantification of different sources of uncertainty.

This chapter first introduces different types of uncertainty, i.e. inherent spatial and temporal variability associated with water resources management. The chapter then focuses on different modeling approaches to address the dynamic process of water resources system (such as flood risk), and their spatial variability. The dynamic characteristics of flood risk and its spatial variability are difficult to understand due to the inherent complexity of human and natural systems. Traditional modeling approaches focus on either temporal or spatial variation, but not both. There is a need to understand the dynamic processes and their interaction in time and location in space. In case of water resources systems, particularly for flood processes, different modeling tools are required that capture dynamic processes in time and location in space. The dynamic process of overland flooding is presented in this research using two modeling tools: (i) hydrodynamic modeling, and (ii) system dynamics (SD) modeling. The chapter then

reviews different approaches used in the framework of reliability analyses of engineering systems. The chapter focuses on the fundamentals of the probabilistic reliability analysis. This part focuses on the use of performance indices for evaluating risk and reliability in water resources management. Since the probabilistic approach faces great challenges in addressing uncertainty related to human subjectivity and ambiguity, this chapter sheds light on the importance of subjective uncertainty in water resources management and shows the capability of different methods to overcome the shortcomings and limitations of probabilistic reliability analysis. Next, this chapter introduces the fuzzy set theory as a complementary approach for assessing uncertainty related to water resources systems and focuses on the use of fuzzy performance indices for reliability analysis.

2.1 WATER RESOURCES MANAGEMENT UNDER UNCERTAINTY

Tung and Yen (2005) define uncertainty as “the occurrence of uncontrollable events”. Decisions in engineering-based systems design, planning, and management are made with uncertainty, the sources of which are many and diverse. Ang and Tang (1984) point out that there is uncertainty in all engineering-based systems because these systems rely on the modeling of physical phenomena that are either inherently random or difficult to model with a high degree of accuracy. All water management decisions should take uncertainty into account. Implications of uncertainty may be risks in the sense of significant potential unwelcome effects of water resources system performance. Accordingly, if analysis of the performance of a water resources system does not adequately consider different types and sources of uncertainty, the extent of damage posed by flooding will be significantly higher than it otherwise would have been. With

these in mind, managers need to understand the nature of the underlying threats in order to identify, assess and manage risk. Failure to do so is likely to result in adverse impacts on performance, and in extreme cases, major performance failures.

2.2 TYPES OF UNCERTAINTY

Different classifications of types and sources of uncertainty exist in the literature depending on the considered aspect of uncertainty. For example, uncertainty in water resources systems can be attributed to hydrologic, structural, environmental, social, economical, and operational aspects. Tung and Yen (2005) list some of those classifications. According to Simonovic (1997) and NRC (2000) the taxonomy of uncertainty includes: (1) natural variability and (2) knowledge uncertainty (Figure 2.1). Natural variability deals with variability inherent to the physical world, viz. events that can be described as “random”. Simonovic (1997) further categorized natural variability, i.e. randomness, into i) temporal variability, ii) spatial variability, and iii) individual heterogeneity. Temporal variability describes the time dependent fluctuations, while spatial variability describes the space dependent fluctuations. In this thesis spatial variability refers to location dependent fluctuations. Individual heterogeneity includes all other sources of variability. The second type of uncertainty, knowledge uncertainty, deals with a lack of understanding of events or processes. According to Simonovic (1997), knowledge uncertainty reflects our limited ability to represent real world phenomena with a mathematical model for effective analysis, which can have an effect on i) model formulation, ii) parameter estimation, and iii) decision-making. Knowledge uncertainty emerges, for the most part, as a result of insufficient data or information of the events or

processes (NRC, 2000).

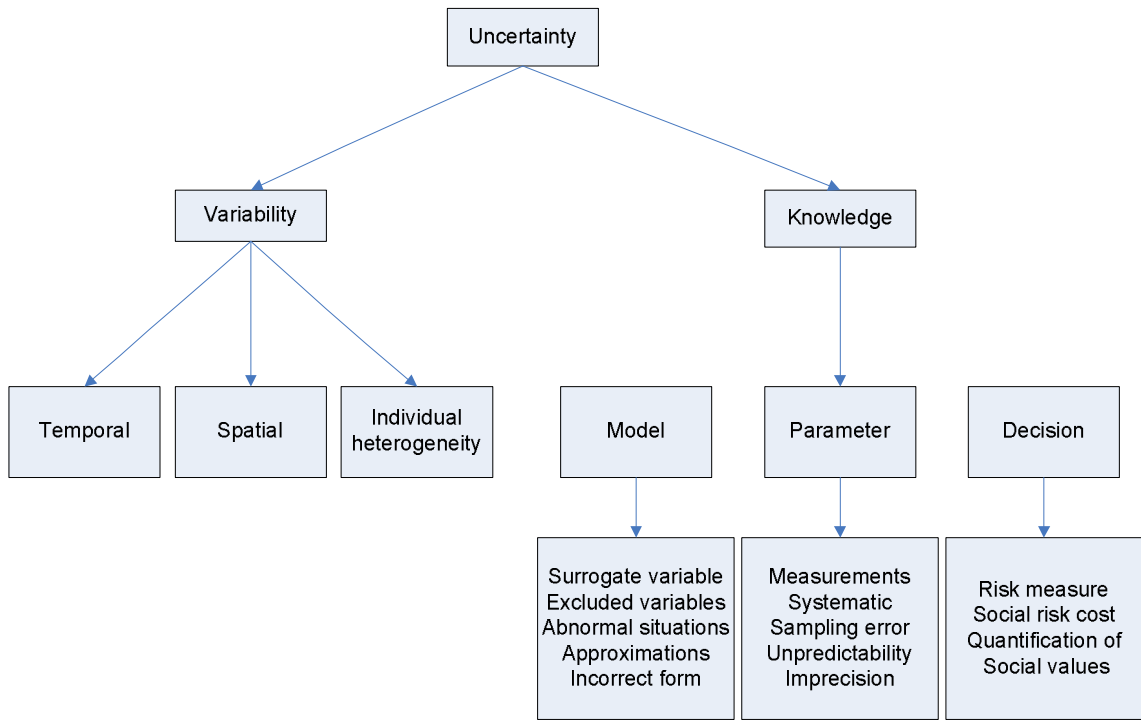


Figure 2.1: Major sources of uncertainty (after Simonovic, 1997)

In flood risk management variability is mainly associated with the spatial and temporal variation of the main hydrologic variables (precipitation, river flow, etc). The temporal variability of flow results in variations of flood water level. The shape of the hydrograph can have a significant impact on the extent of flood damage. Depending on the rainfall intensity, rainfall duration, and the direction of storm movement, there can be a wide range of hydrograph shapes. Spatial and temporal variability of these factors may augment or reduce peak flow, cause either a gradual or rapid rise to peak value, and also result in gradual or rapid recession of the hydrograph. Gradual recession of the hydrograph increases the duration of submergence, which may cause significant damage

to agricultural crops, infrastructure and property. In flood risk management spatial variability is also associated with floodplain characteristics such as land-use, terrain elevation, channel network, vegetation, roughness, soil characteristics, porosity, etc. For example, areas closer to the river and with a lower elevation are highly prone to significant flood damage compared to areas further away from the river with higher elevations. As floods recede, areas with higher elevation are more quickly dried and are ready to seed before areas closer to the river and with lower elevations. Uncertainty in spatial and temporal variability arises due to our inability to accurately measure, calculate or estimate the value of such factors.

In flood risk management, the uncertainty pertaining to the physical characteristics of the water resources system is partly about variability. Uncertainty is, in part, also about lack of knowledge or ambiguity. Both variability and ambiguity are associated with a lack of clarity, which arises because of the typical lack of system performance history and records, human error, subjectivity, faulty assumptions, bias and ignorance.

2.3 MODELING DYNAMIC PROCESS OF RIVER AND URBAN FLOODING

Risk in water resources management requires the understanding of three main characteristics: (i) spatial structure and the relationships among risk characteristics; (ii) interactions among the spatial risk characteristics; and (iii) changes or alterations in risk characteristics over time (Simonovic, 2007). In order to deal with the dynamic characteristics of flood, it is essential to understand and describe all of its interrelated characteristics. However, the important interactions of spatial and temporal

characteristics of flood risk have not been fully considered in traditional modeling approaches. Normally such approaches focus on either temporal or spatial variation, but not both. There is a need to understand the important interactions between time and location in space, i.e., how the temporal variability of risk is affected by a change in the spatial characteristics of risk. Therefore in order to properly address risk dynamics, the spatial and temporal characteristics of risk need to be examined together. The work presented in this thesis focuses on the development of a new modeling framework that not only captures dynamic processes in time and location in space but also integrates different modeling tools required for solving complex river and urban flood management problems. Ahmad and Simonovic (2004) introduced three modeling paradigms: (i) cellular automata (CA), (ii) geographic information system (GIS), and (iii) system dynamics (SD), which exhibit the potential for describing dynamic processes in time and location in space. In this research, system dynamics (SD) is presented as a strong modeling tool for modeling the spatial and temporal characteristics of overland flooding. This research also introduces hydrodynamic modeling as another strong tool capable of modeling the dynamic interactions on the propagation of river and urban flooding, and also for addressing the spatial and temporal variability of overland flow. The following sections provide a brief description of the strengths, weaknesses and applicability of these two modeling approaches - (i) hydrodynamic modeling, and (ii) system dynamics modeling – for addressing overland flooding in flood risk management.

2.3.1 HYDRODYNAMIC MODELING

Hydrodynamic modeling is able to address the spatial and temporal variability in flood

water depth, velocity, and the extent of inundation of a flooding event, all of which are very important in flood risk analysis. Flows for which flood water depth and velocity vary, not only with location in space but also with time, are considered as transient or unsteady flow. In rivers and floodplains, flows can be considered as steady for the purposes of an approximate representation of overland flooding in time and location in space. However, for more accurate modeling, the analysis of overland flooding requires considering the flow as unsteady or transient. In 1871, Barrède Saint-Venant formulated the basic theory that considered the analysis of unsteady flow through the coupling of the continuity and momentum equations. Modeling of fluid flow is possible either as one-dimensional, where the direction of flow is predetermined and thereby making approximation or as two-dimensional, where the direction of flow is not predetermined, and is therefore not restricted.

The hydrodynamic modeling used in this research is presented as a powerful tool for addressing river and urban flooding and also for modeling spatial and temporal variability in flood water level, discharge, velocity, etc. Flow in rivers and through pipes can be accurately modeled considering one-dimensional representation. However, consideration of one-dimensional representation will not accurately model overland flooding. Therefore the flow should be considered as unsteady or transient while modeling overland flooding in two-dimensions. Since an analytical solution of the Saint-Venant equations is not possible, the complete Saint-Venant equations must be solved numerically for overland flooding. The most common numerical solutions to the Saint-Venant equations are the finite element and finite difference methods.

There are a number of studies that compare one-dimensional (1-D) and two-dimensional (2-D) approaches in river flood modeling (Horritt and Bates, 2002; Lin et. al., 2006). In confined channels, such as pipe networks, the 1D sewer model can provide acceptable results as long as the water is contained within the street network (Mark *et. al.*, 2004). If the water overflows the curbs and flows overland, the flow may change direction. Under these circumstances the 1D model should not be used, and the 2D model becomes the preferred choice. Leandro, *et al.* (2009) also concluded that 1D models can provide an adequate approximation of flow in confined channels (such as rivers, pipes and streets), however 2D models give better results for the flow over terrain. Early urban hydrologic models did not have the capability to model the excess flow from the manholes as overland flooding. The surcharged flow remained atop of the manholes until the capacity of the sewer networks was at a maximum. When sewer network capacity became available, the excess water was allowed to drain back into the storm sewer network (Rossman, 2005; Zhong, 1998). This shortcoming in the earlier storm sewer models was overcome by introducing links between surface networks and pipe networks (Leandro *et al.*, 2009).

The use of hydrodynamic modeling in river and urban flooding is becoming very common as the result of: (i) the time needed for the numerical modeling of full Saint Venant equations has become more acceptable, (ii) an increased availability of high resolution topographic data, such as LIDAR, which is required as input into the 2D hydrodynamic model, and (iii) the accumulation of more detailed and accurate results of water level, velocity, discharge etc that are essential for effective river and urban flood

investigation (Smith, *et. al.*, 2006).

Some examples of the commercial tools used for 1D river modeling are HEC-RAS (Hydraulic Engineering Center, 2010), MIKE 11 (DHI, 2008,(a)) and SOBEK (WLI|Delft Hydraulics, 2005). For 1D pipe flow modeling, examples include MOUSE (DHI, 2004), MIKE URBAN (DHI, 2009), XP-SWMM (XP Software, 2010), EPA SWMM (EPA, 1995) and PC-SWMM (CHI, 2006). For 2D overland flow modeling examples include MIKE 21 (DHI, 2008,(b)), TUFLOW (Phillips *et. al.*, 2005), SOBEK, GSSHA (Charles *et. al.*, 2006), RMA2 (Barbara *et. al.*, 2006). The commercial hydraulic/hydrodynamic models, such as MIKE URBAN (DHI, 2009) or Infoworks CS (Wallingford Software, 2006) have the capability to model the dynamic interactions between surface networks and pipe/sewer networks by using a weir or an orifice equation (Kawaike and Nakagawa, 2007; Mark *et al.*, 2004; Nasello and Tucciarelli, 2005, Leandro *et. al.*, 2007). Recently there has been a growing trend towards integrating two or more hydrodynamic models to overcome the weakness in linkage between two models. Examples of such models are (1D/2D) MOUSE-MIKE21, which couples the 1D MOUSE pipe/sewer model with the 2D MIKE21 overland model (Carr and Smith, 2006); the (1D/2D) SOBEK Urban, which couples the 1D SOBEK flow with 2D Delft FLS (Bolle *et al.*, 2006); or TUFLOW. The current trend in river flood modeling is to couple a 1D river model with a 2D overland/surface flow model, and in the case of urban flood modeling, a 1D pipe flow model is coupled with a 2D overland flow model. In certain cases all of the three models – (i) 1D river model, (ii) pipe flow model, and (iii) overland flow model – may be coupled together. Researchers have attempted to compare the 1D/1D and 1D/2D couple

models (Kaushik, 2006; Chen *et al.*, 2007). More recently, Leandro, *et al.* (2009) provided a comparison between a 1D sewer model coupled with a 1D surface network model (1D/1D) and a 1D sewer model coupled with a 2D overland/surface flow model (1D/2D).

There are certain limitations in 2D hydrodynamic modeling, such as computation time, requirement of more data, etc. The computation time in 2D modeling is significantly higher compared to 1D modeling (Paquier *et al.*, 2003; Lhomme *et al.*, 2006). However, it should be noted that the 1D hydrodynamic model does not provide satisfactory results for solving overland flow, in which case 2D hydrodynamic modeling is required.

2.3.2 SYSTEM DYNAMICS (SD) MODELING

System Dynamics (SD) is a rigorous method of system description, which facilitates feedback analysis via a simulation model of the effects of alternative system structures and the control policies of system behaviour (Simonovic, 2009). The advantages of system dynamics simulation include: (a) facilitating the simplicity of use of system dynamics applications; (b) a greater applicability of the general principles of system dynamics to social, natural, and physical systems; (c) the ability to address how structural changes in one part of a system might affect the behaviour of the system as a whole; (d) a combined predictive (determining the behaviour of a system under particular input conditions) and learning (the discovery of unexpected system behaviour under particular input conditions) functionality; and (e) an active involvement of stakeholders in the modeling process. The strength of the system dynamics approach is

largely in representing temporal processes. SD models, however, do not adequately represent spatial processes. For example, SD models can be used for the analysis of different flood management policies and the estimation of flood damages (as a function of time). However, SD modeling provides no easy way to represent damage topographically. A simple SD model is therefore inadequate for developing an overland flood model that can capture both spatial and temporal variability in the propagation of flood flows. Given that SD is adept at representing temporal processes (with a limited capacity for spatial modeling), and GIS is useful for spatial modeling (with a limited capacity for temporal representation), the logical step in the development of a more comprehensive methodology is the integration of SD with GIS to model the spatio-temporal dynamics of engineering systems.

System dynamics has a long history as a modeling paradigm with its origin in the work of Forrester (1961), who developed the subject to provide an understanding of strategic problems in complex dynamic systems. System dynamics is grounded in control theory and the modern theory of nonlinear dynamics. More details on SD modeling can be found elsewhere (Sterman, 2000; Ford, 1999; and Coyle, 1996). System Dynamics is a promising approach for modeling complex dynamic systems. SD has been successfully applied to policy analysis in the area of business (Sterman, 2000), health care (Royston et al., 1999), and environmental management (Ford, 1999; and Sudhir et al., 1997). The concepts and applications of system dynamics approaches to a variety of problems have been discussed by several authors (Sterman, 2000; Forrester, 1961; and Coyle, 1996). System dynamics is becoming increasingly popular for modeling water resource systems.

Palmer (1998) has done extensive work in river basin planning using SD. Keyes and Palmer (1993b) used SD simulation modeling for drought studies. Matthias and Frederick (1994) have used SD techniques to model sea-level rise in coastal areas. Fletcher (1998) has used system dynamics as a decision support tool for the management of scarce water resources. Simonovic, *et. al.*, (1997) and Simonovic and Fahmy (1999) have used a SD approach for long-term water resources planning and in policy analysis for the Nile River Basin in Egypt. The SD approach has been used to model reservoir operation for flood control (Ahmad and Simonovic, 2000a), operation of multiple reservoirs for hydropower generation (Teegavarapu and Simonovic, 2000), calculation of flood damages (Ahmad and Simonovic, 2000b), and analysis of the economic aspects of flood management policies (Ahmad and Simonovic, 2000c). Simonovic (2002) has used SD to develop a world water model. Li and Simonovic (2001) have developed a SD model for predicting floods from snowmelt in North American prairie watersheds. Ahmad and Simonovic (2001c) used SD as a decision support tool for the evaluation of impacts of flood management policies. The spatial system dynamics approach (SSD) developed by Ahmad and Simonovic (2004) can model dynamic processes in time and location in space with certain limitations.

The strength of the system dynamics approach is in its ability to represent temporal processes. SD models are excellent tools for planning and policy analysis. SD models, however, do not adequately represent spatial processes. For example, system dynamics models can be used for the analysis of different flood management policies and the estimation of flood damages (as a function of time). Given the strength of SD in

representing temporal processes with restricted spatial modeling capabilities, and the competency of GIS for spatial modeling with limited representation of temporal aspects, a logical alternative is the integration of system dynamics with GIS to model spatial dynamic systems. Attempts have been made to add spatial dimensions to system dynamics models. These attempts can be divided into two categories: (a) introducing spatial dimensions into the system dynamics model (implicit approach) or (b) translating system dynamics model equations to run in GIS. The first approach does not represent spatial dimensions in an explicit manner. The Mono Lake model is an example of this approach (Ford, 1999). In this model spatially important features of the system are represented with one or two aggregate relationships. The complex shape of the Mono basin affects the water flow, which is modeled by two non-linear functions: (a) surface area – volume curve; and (b) elevation - volume curve. The second approach of adding a spatial dimension to the system dynamics models involves translating SD model equations into a programming language and interfacing with GIS. For instance, Costanza et al. (1990) combined a GIS with a system dynamics model for ecological modeling. They used *Stella* (HPS Inc., 2001) to develop ecological models and then translated the model into *Fortran* through a separate program to interface with the GIS. To study the effects of fire on landscape patterns Baker (1992) interfaced four models with a GIS to control the simulation, data handling, and display. A decision support software package, *Extend* and *EML* (Environmental Modeling Language), were used by Theobald and Gross (1994) to explore landscape dynamics (a fire spread and population model). They combined SD, GIS and CA to provide spatial-temporal modeling capabilities for landscape dynamics. Work on modeling mobile individuals in dynamic landscapes is

reported by Westervelt and Hopkins (1999) using software packages IMPORT/ DOME, GRASS, and SME (Spatial Modeling Environment). In these studies, the work is focused on spatial modeling (emphasis on GIS) and SD is used to bring the dynamic modeling (temporal aspect) capability into the GIS environment. Since system dynamics model equations are translated to run within a GIS, a drawback of the approach used in these studies is the loss of the interactive power of SD (changes cannot be made during simulation). The main limitation in all the attempts that have been made so far for a combined spatio-temporal dynamic modeling, is that the relationship between time and location in space is not explicit.

2.4 DEFINITION OF RISK

A standardized and overarching definition of risk is perhaps unachievable. Numerous definitions can be found in the relevant literature as authors continue to define risk in their own way. Simonovic (1997) defined risk as a measure of the probability and severity of adverse effects. Simonovic and Ahmad (2007) further defined risk as the “significant potential unwelcome effect of water resources system performance or the predicted or expected likelihood that a set of circumstances over some time frame will produce some harm that matters”. Haines (1998) defines the risk analysis process as “a set of logical, systematic and well-defined activities that provide the decision maker with a sound identification, measurement, quantification, and evaluation of the risk associated with certain natural phenomena or man made activities.” Normally, risk is equated with the probability of failure or the probability of load exceeding resistance. Other symbolic expressions equate risk with the sum of uncertainty and damage or the quotient of

hazards divided by safeguards (Lowrance, 1976). According to Simonovic and Ahmad (2007) there are three cautionary measures surrounding risk that must be taken into consideration: (i) risk cannot be represented objectively by a single number alone, (ii) risk cannot be quantified on strictly objective grounds, and (iii) risk should not be labeled as *real*. Regarding the caution of viewing risk as a single number, the multidimensional character of risk can only be aggregated into a single number by assigning implicit or explicit weighting factors to various numerical measures of risk. Since these weighting factors must rely on necessarily biased value judgments, the resulting single metric for risk cannot therefore be deemed objective. Since risk cannot be expressed objectively by a single number, it is not possible to rank risks on strictly objective grounds. Finally, since risk estimates are evidence-based, risks cannot be strictly labeled as *real*. Rather, they should be labeled as inferred, at best.

2.5 RISK IDENTIFICATION

Risk identification is the first step in any risk analysis, where all sources of uncertainty are clearly detailed. Risk and reliability analysis can be used to assess the safety of any engineering system (Ganoulis, 1994). Classical reliability analysis uses the load-resistance approach (which is widely used in structural reliability analysis). Load, l , is a variable that reflects the behaviour of the system under certain external conditions of stress loading, while resistance, r , is a characteristic variable which describes the capacity of the system to resist an external load. Failure occurs when the load exceeds the resistance, while the system is considered safe if resistance exceeds or is equal to the load Ganoulis (1994):

FAILURE or INCIDENT : $l > r$

SAFETY or RELIABILITY : $l \leq r$

The quantification of risk is the second step in any risk analysis, whereby uncertainties are measured using different system performance indices such as reliability, vulnerability, robustness and resiliency. Importantly, the quantification of uncertainties involved in floodplain management can be used to mitigate the risks of flood damage.

2.6 PERFORMANCE INDICES

Performance Indices (PI) are measures of how well a system performs under various loading conditions. Safety of the system under uncertainty can be represented by the performance indices. Hashimoto *et al.* (1982a and 1982b) suggest reliability, resiliency, vulnerability and robustness as performance indices to evaluate the performance of water resources systems. Duckstein *et al.* (1987) mention incident-related performance indices such as grade of service, quality of service, speed of response, incident period, availability, economic index vector, in addition to the PIs suggested by Hashimoto *et al.* (1982a and 1982b).

2.7 RELIABILITY ANALYSIS IN ENGINEERING SYSTEMS

Probability theory and fuzzy set theory are the main approaches used in the risk and reliability analysis of engineering systems. The probabilistic approach and the fuzzy approach are described in the following sections as tools for reliability analysis.

2.7.1 PROBABILISTIC APPROACH IN WATER RESOURCES MANAGEMENT

Analysis in the probabilistic approach involves describing load and resistance as belonging to respective possible probability distributions. Uncertainty in both load and resistance is introduced through the use of random variables. Therefore, the system reliability is realistically measured in terms of probability. The principal objective of the probabilistic reliability analysis is to ensure, in terms of probability, that load does not exceed resistance throughout a specified time horizon in terms of probability.

Ganoulis (1994) states that by considering the system variables as random, uncertainties can be quantified on a probabilistic framework. Load, l , and resistance, r , are taken as random variables L and R , with the following probability distribution and probability density distribution functions:

$F_L(l), f_L(l)$: load

$F_R(r), f_R(r)$: resistance

In the probabilistic framework, the simple definition of failure is when the load exceeds the resistance. Thus probability of failure or risk is defined by the following relation:

$$P_F = P(R < L) \tag{2.1}$$

The quantity P_F is obtained by the joint probability density function $f_{LR}(l,r)$ of the random variables R and L . Figure 2.2 shows the risk P_F above the bisectrice line $L=R$ that can be calculated by integrating the following equation.

$$P_F = P(L > R) = \int_0^\alpha \left(\int_0^l f_{LR}(l, r) dr \right) dl \quad (2.2)$$

Equation (2.2) is a general expression to quantify the risk in a probabilistic framework.

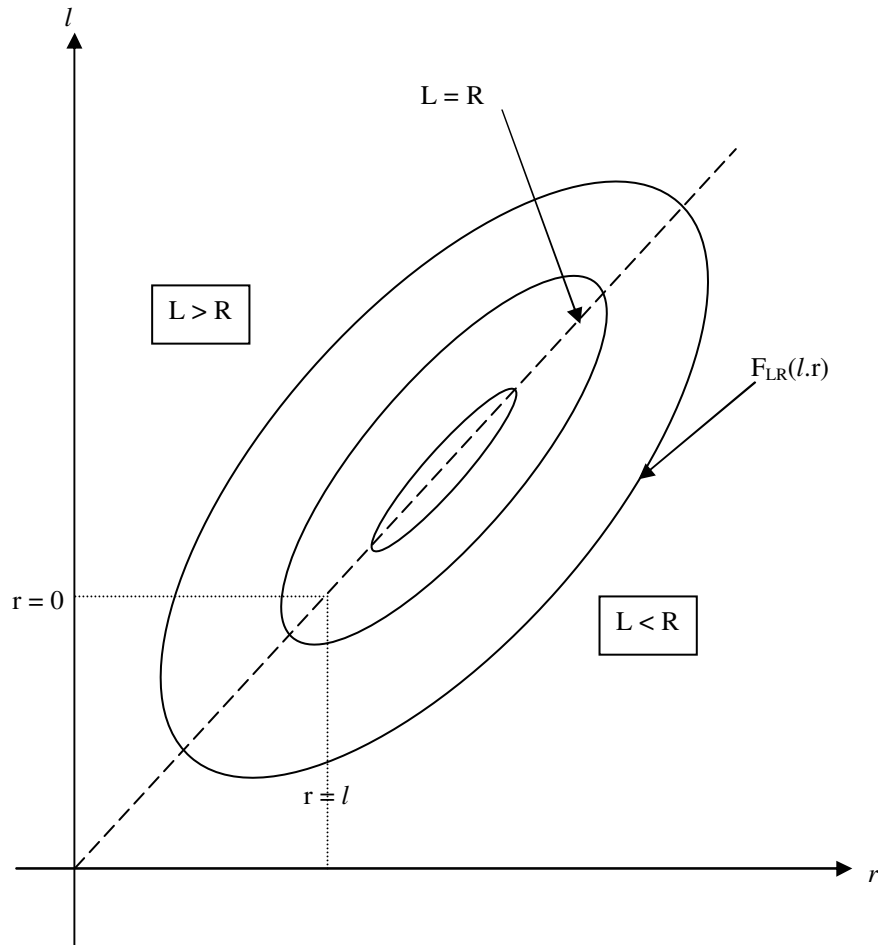


Figure 2.2: Definition of probabilistic risk (after Ganoulis 1994)

The intensive calculations involved in this approach require prior knowledge of the probability density functions of both load and resistance and/or their joint probability distribution functions. The amount of data required to perform such calculations is usually insufficient and even if data are available to estimate these distributions, approximations are almost always necessary to calculate system reliability, (Ang and

Tang, 1984).

In flood risk analysis the probabilistic (stochastic) risk analysis approach has been extensively used. Normally, expected annual flood loss computation (HEC, 1989) is used to address the hydrologic (flood-frequency analysis), hydraulic (rating curve development) and economic uncertainties (stage damage analysis) in flood risk analysis. Quite often this analysis is subject to data insufficiency and inaccuracy; knowledge uncertainty in selecting an appropriate modeling tool and model parameters; and complete ignorance of subjective and perceived aspects of flood risk.

There are several approximate methods available to overcome the problem of data insufficiency and consideration of objective and subjective uncertainties at the same time. For example, researchers (Tung and Yen, 2005) have suggested that in some cases it is possible to use the normal representation of non-normal distributions as a practical alternative that is based on the central limit theory. In this case, data requirements for estimating the first two moments of the assumed normal distribution are very high. Another approach to avoid the problem of data insufficiency is the use of subjective judgment of the decision-maker to estimate the probability distribution of a random event, i.e. subjective probability (Vick, 2002). The third approach is the integration of judgment with the observed information using Baye's theory (Ang and Tang, 1984). The problem with Bayesian reliability analysis is that the selection of prior distribution does not often reflect the true uncertainty inherent to the system. The choice of subjective probability distribution, in these two approaches, presents difficulties in the translation of

prior knowledge into meaningful probability distribution, especially for multi-parameter problems (Press, 2003). Therefore, accuracy of the derived distributions is strongly dependent on the realistic estimation of the decision-maker's judgment (El-Baroudy and Simonovic, 2004).

The probabilistic approach usually fails to address subjective and perceived risks. People utilize the concept of risk to increase their understanding of various uncertainties and to develop their capacity to cope with the negative impacts of disasters. The concepts of failure and risk imply different meanings for different people. Slovic (2000) stresses the difference in risk perception, i.e. acceptance of failure, or judgmental and heuristics beliefs. Studies of the probabilistic information processing show that people do not use the proper probabilistic principles in judging the likelihood of a certain event. However, subjective probability is used to quantify engineering judgment about the likelihood of the occurrence of an uncertain event, the existence of an unknown condition, or the confidence in the truth of a proposition, (Vick, 2002).

An innovative framework is proposed in this work for: (a) integrating different perspectives of flood risk; (b) performing flood risk assessments; and (c) developing flood risk management strategies for an entire river basin. It is typically the case that the public awareness of flood disasters is generally quite low, owing largely to the fact that people tend to underestimate or ignore entirely the extent to which they are financially and personally vulnerable to the effects of flooding. This phenomenon can be explained by pointing to the common tendency to assess flood risk on the basis of past experiences

of damage. If, for instance, a previous flood did not cause significant damage to a community and its population, we can reasonably assume that the flood prevention measures in place will not have adequately taken into account the likelihood and risk of a more severe flood event in the future. Progress in flood risk prevention and flood disaster mitigation is thus contingent on the likely harm experienced by the people affected. This directly affects investments in flood risk prevention and mitigation measures as well as the development of legislation, standardization and governmental regulations and control. The framework developed in this research provides support for the broad range of decision-making processes related to flood management.

2.7.2 FUZZY SET APPROACH IN WATER RESOURCES FLOOD MANAGEMENT

Fuzzy set theory was developed to address people's judgmental beliefs, or subjective uncertainty, and their basis in a lack of knowledge. In comparison to the probability theory, fuzzy set theory has a certain degree of freedom with respect to aggregation operators, types of fuzzy sets (membership functions), etc., which allows for its adaptability to different contexts (Zimmerman, 1996). In the last twenty years, fuzzy set theory and fuzzy logic have contributed successfully to technological development in different areas of application, for instance mathematics, algorithms, standard models, and real-world problems of different kinds (Zimmermann, 1996). Zimmerman (1996) classifies the variety of applications of the fuzzy set approach as follows:

- Mathematical applications that extend the classical applications of set theory into

topology, algebra and logic, etc.;

- Algorithmic applications in the field of mathematical programming and control algorithms;
- Standard models applications such as transportation models and inventory models; and
- Real-world problems such as operations research and empirical research.

The application of the fuzzy set approach in the field of water resources management has grown over the last two decades (Simonovic, 2009, Chapter 6). Uncertainty, or the lack of knowledge and complexity of water resources systems, is expected to be of growing importance in the near future, which supports the need to provide trust in the application of the fuzzy set theory (El-Baroudy and Simonovic, 2004). It should be noted that both probability theory and fuzzy set theory are capable of handling different facets of uncertainty. Both approaches are complementary and the use of one of them does not exclude the need for the other.

The fuzzy set approach is widely used in water resources multi-objective decision making under uncertainty (Kacprzyk and Nurmi, 1998; Bender and Simonovic, 2000; Despic and Simonovic, 2000; Borsuk et al., 2001; Prodanovic and Simonovic, 2002; Simonovic and Nirupama, 2005 among others). El-Baroudy and Simonovic (2004) used fuzzy set theory in the field of water resource reliability analysis and proposed three fuzzy reliability indices: (1) a combined reliability-vulnerability index, (2) a robustness index, and (3) a resiliency index. These indices were successfully tested using a case study of the London

regional water supply system. Among the more recent applications of fuzzy set theory to flood management is the work of Akter and Simonovic (2005). Their work is applied to flood management in the Red River Basin, Manitoba, Canada, and allowed for a discrete ranking of alternatives using multiple objectives and input from a large number of stakeholders. The floodplain management process in the Red River basin involves numerous stakeholders. They include different levels of government, different agencies, private organizations, interest groups and the general public. They all have different and specific needs and responsibilities during all stages of floodplain management—planning, emergency management and flood recovery. Currently, the Government of Manitoba, Canada is responsible for decision-making about floodplain management measures. The decision-making process involves consulting different organizations for their technical input. Concerns of the general public about the alternatives are gathered through public hearings and workshops. Economic analysis plays an important role in formulating plans for reducing flood damages and making operational decisions during an emergency.

However, little attention has been given to the environmental and social impacts of floods. Different studies of the Red River flooding and numerous interviews with its stakeholders indicate that a consideration of the social impacts of the flood event is of prime importance for a successful implementation of any floodplain management policy. Akter and Simonovic (2005) have used fuzzy set and fuzzy logic techniques to successfully represent the imprecise and vague information in many fields, and so their work signals a significant contribution to the development of an effective way to represent uncertainties. To obtain a value from the diversified opinions of a large number

of stakeholders, where subjective uncertainty plays a major role, Akter and Simonovic (2005) have used fuzzy set theory and fuzzy logic to address two issues: (1) collection of views of a large number of stakeholders, with a consideration of the numerous uncertainties present in their opinions; and (2) ranking of different flood management alternatives under uncertainty. Their work is the driving force behind our decision to choose fuzzy set theory for an accurate representation of subjective data/lack of knowledge in the river and urban flood management process.

Pioneering applications of fuzzy set theory to spatial analyses can be found in Guesgen (2005); Shi *et al.* (2005); and Verstraete *et al.* (2005); among others. However, the application of fuzzy sets that consider both spatial and temporal variability is very rare in the case of floodplain management. To capture the spatial uncertainty in water resources decision making, Simonovic and Nirupama (2005) have developed Spatial Fuzzy Compromise Programming (SFCP) by introducing spatial variability in Fuzzy Compromise Programming. In SFCP, the fuzzified distance metric value is analyzed for the best alternative for every raster cell. There is a number of fuzzified distance metrics from various alternatives in every raster cell. The largest fuzzified distance metric from each cell is then chosen as the best solution for that particular location (Simonovic and Nirupama, 2005). Ahmad and Simonovic (2007) used the fuzzy performance indices developed by El-Baroudy and Simonovic (2004) to address the spatial variability of flood risk using fuzzy set theory. Ahmad and Simonovic (2007) integrated GIS technology with fuzzy flood risk estimation to develop a spatial representation of flood risk. However they did not consider the temporal variability of uncertainties in flood risk

analysis.

The work presented in this thesis deals with spatial and temporal uncertainties associated with flood risk management. It is difficult to represent ambiguity and imprecision using probabilistic methods or Bayesian analysis. Since fuzzy set theory is more appropriate for representing uncertainty, it is utilized in water resources decision making. The existing fuzzy approaches are used extensively in multi-objective decision making or to capture inherent fuzziness of spatial objects. However, the existing methods are not capable of addressing spatial and temporal variability of risk. Since flood risk analysis is spatial and temporal in nature and inherently loaded with uncertainties, an approach is required that will provide (a) the methodology to represent spatial and temporal variability in flood data, and (b) the methodology to spatially and temporally represent flood risk. The proposed methodology of spatial and temporal representation of flood risk is based on the fuzzy performance indices developed by El-Baroudy and Simonovic (2004). The following section includes a detailed review of the fuzzy performance indices developed by El-Baroudy and Simonovic (2004), which were used to represent the risk of water resources systems.

2.8 RELIABILITY ANALYSIS OF WATER RESOURCES SYSTEMS USING FUZZY PERFORMANCE INDICES

Water resources systems are subject to a wide range of possible future conditions. Uncertainty associated with the quantification of these conditions possesses a great challenge to water resources systems management, particularly as the satisfactory and

reliable performance of a system cannot easily be guaranteed (El-Baroudy and Simonovic, 2004). Normally, water resources systems include collections of different types of sub-systems that are connected in complicated networks that extend over and serve broad geographical regions. As a result, water resources systems are at risk due to natural hazards or anthropogenic causes, whether unintentionally or intentionally (i.e. terrorist acts) facilitated (El-Baroudy and Simonovic, 2004). Probabilistic reliability analysis is widely used to deal with the problem of uncertainty in water resources systems. Invariably though, the application of probabilistic reliability analysis is affected by the well-known engineering problem of data insufficiency. Fuzzy set theory, on the other hand, is developed to try to capture people's judgmental beliefs or, as mentioned before, the uncertainty that is caused by lack of knowledge. Fuzzy set theory and fuzzy logic have contributed successfully to technological development in different applications to real-world problems (Zimmermann, 1996). This study explores the utility of the fuzzy performance indices that is suggested by El-Baroudy and Simonovic (2004), for spatial and temporal reliability analysis of floods.

2.8.1 DEFINITION OF FAILURE

The failure state, as defined by set theory, occurs when resistance (ground level or embankments) falls below the load (water level). A margin of safety, $M < 0.0$ (i.e., the difference between load and resistance), or safety factor, $\Theta < 0.0$ (i.e., the ratio between load and resistance), can be used as performance functions and are shown in Figure 2.3. Water levels may vary significantly and ground surfaces may be subject to change as well. As a result, it is difficult to predict their real values with certainty.

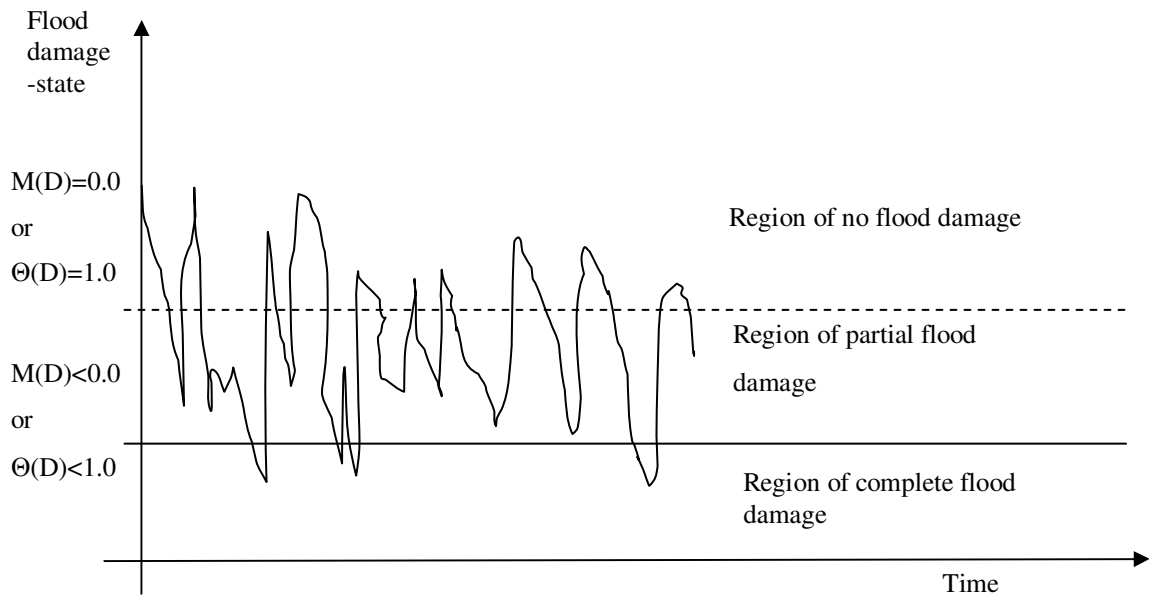


Figure 2.3: Different perception of failure (after El-Baroudy and Simonovic, 2004)

As an example, consider the case where the water level in a river rises above a certain limit and flood waters begin to overflow the embankment. This could result in devastating consequences such as erosion of the embankment or complete failure of the embankment. The level at which the embankment can withstand the rising water may be uncertain or the change in water level may not be accurately known. Thus, the extent of damage that defines failure may vary significantly depending upon the preference of the decision-maker.

It is practical to use the concept of partial failure when dealing with ambiguous quantities. These ambiguous quantities can be better described by fuzzy theory rather than classical set theory. El-Baroudy and Simonovic (2004) state that if the value of the margin of safety or factor of safety is below m_1 (or θ_1) then it falls in the complete

failure region and the fuzzy membership function is zero (Figure 2.4). Similarly, if the value of the margin of safety or factor of safety is more than m_2 (or θ_2) then it will be in the complete safety region and the value of fuzzy membership function will be 1. Any value of the margin of safety or the factor of safety between m_1 (or θ_1) and m_2 (or θ_2) implies that the system is in the acceptable failure region.

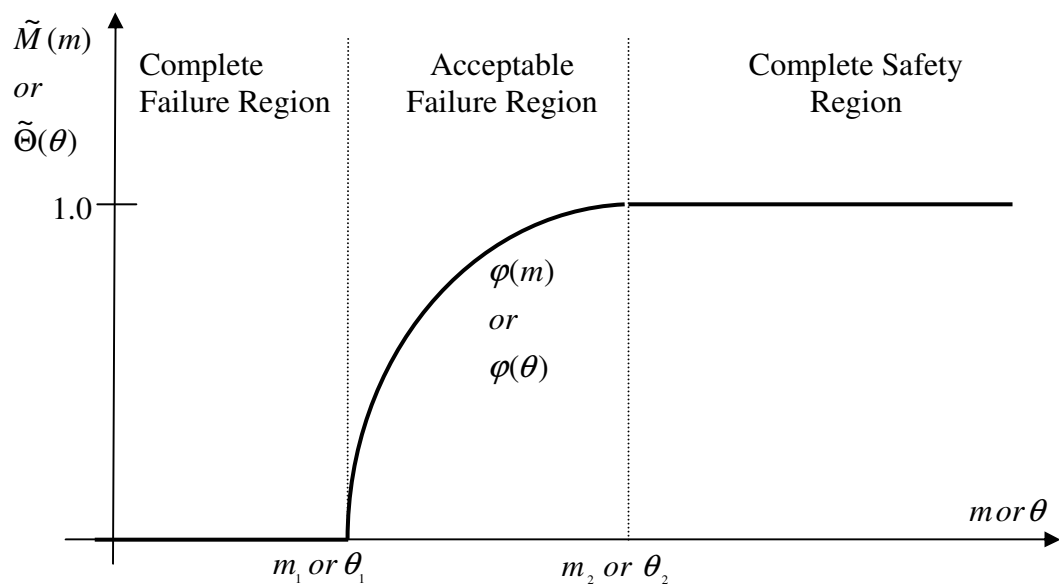


Figure 2.4: Fuzzy Representation of Acceptable Failure Region (after El-Baroudy and Simonovic, 2004)

The acceptable level of performance defined by fuzzy membership function is:

$$\tilde{M}(m) = \begin{cases} 0, & \text{if } m \leq m_1 \\ \varphi(m), & \text{if } m \in [m_1, m_2] \\ 1, & \text{if } m \geq m_2 \end{cases}$$

or (2.3)

$$\tilde{\Theta}(\theta) = \begin{cases} 0, & \text{if } \theta \leq \theta_1 \\ \varphi(\theta), & \text{if } \theta \in [\theta_1, \theta_2] \\ 1, & \text{if } \theta \geq \theta_2 \end{cases}$$

where:

\tilde{M} is the fuzzy membership function of margin of safety;

$\varphi(m)$ and $\varphi(\theta)$ are functional relationships that represent the subjective view of the acceptable risk;

m_1 and m_2 are the lower and upper bounds of the acceptable failure region, respectively;

$\tilde{\Theta}$ is the fuzzy membership function of factor of safety; and

θ_1 and θ_2 are the lower and upper bounds of the acceptable failure region, respectively.

High system reliability is reflected through the use of high values of margin of safety (or factor of safety), i.e., high values for both m_1 and m_2 (or θ_1 and θ_2). The difference between m_1 and m_2 (or θ_1 and θ_2) inversely affects the system reliability, i.e., the higher the difference the lower the reliability (El-Baroudy and Simonovic, 2004). Therefore, El-Baroudy and Simonovic (2004) define the reliability measure (LR) of an acceptable level of performance as:

$$LR = \frac{m_1 \times m_2}{m_2 - m_1}$$

or (2.4)

$$LR = \frac{\theta_1 \times \theta_2}{\theta_2 - \theta_1}$$

Since failure is defined by a lower bound, upper bound, and the function $\varphi(m)$ or $(\varphi(\theta))$, which are subjectively defined, this approach is an effective tool in capturing the subjectivity of decision-makers in risk perception.

2.8.2 DEFINITION OF FUZZY SYSTEM STATE

Fuzzy membership function has been used to calculate the resulting margin of safety (or factor of safety) as a representation of the system state at any given time (El-Baroudy and Simonovic, 2004). Thus,

$$\tilde{M} = \tilde{X}(-)\tilde{Y}$$

and (2.5)

$$\tilde{\Theta} = \tilde{X}(/)\tilde{Y}$$

where;

\tilde{M} is the fuzzy margin of safety;

\tilde{X} is the fuzzy resistance capacity;

\tilde{Y} is the fuzzy load requirement;

$(-)$ is the fuzzy subtraction operator;

(/) is the fuzzy division operator; and

$\tilde{\Theta}$ is the fuzzy factor of safety.

As data insufficiency and lack of knowledge in water resources systems are common problems, both load (water level) and resistance (ground level) can be represented as fuzzy sets. The margin of safety (or factor of safety) membership function can be represented using the system state.

Figure 2.5 shows a system state defined by a triangular membership function, where u_1 is the lower bound value, u_2 is the modal value, and u_3 is the upper bound value of the membership.

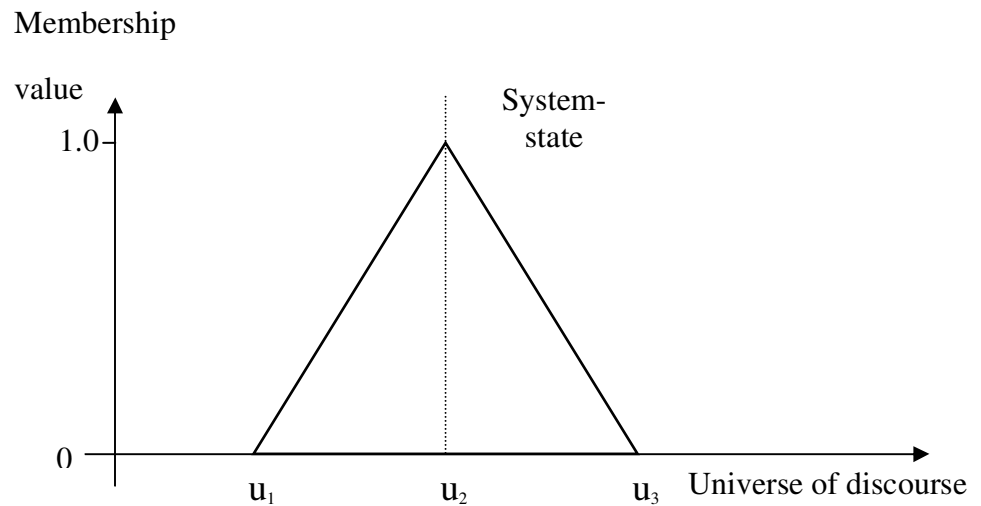


Figure 2.5: Triangular system-state membership function

2.8.3 DEFINITION OF COMPATIBILITY

The extent to which two fuzzy sets match is measured by comparing two fuzzy membership functions. El-Baroudy and Simonovic (2004) define compatibility as the extent to which a fuzzy system state membership function matches a predefined acceptable level of performance membership function. El-Baroudy and Simonovic (2004) define compliance as:

$$\text{Compliance} = \frac{\text{Overlap area between system state and acceptable level of performance}}{\text{Total area of system state membership function}}$$

Figure 2.6 shows two different cases of compatibility. The system state membership function in the first case partially falls within the acceptable level of performance and in the second case the system state membership function falls completely within the acceptable level of performance.

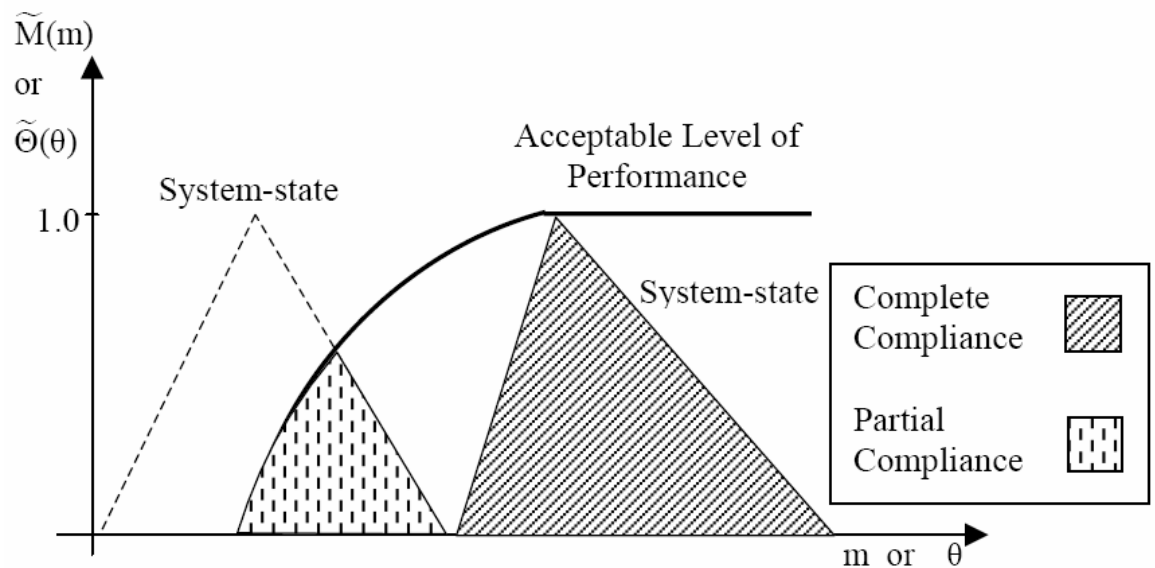


Figure 2.6: Two compliance cases (El-Baroudy and Simonovic, 2004)

It is preferable to have a larger overlap area than a smaller overlap area. A larger overlap area represents more compliance with the acceptable level of performance. As the area with high membership values is more significant than an area with low membership values, El-Baroudy and Simonovic (2004) consider the weighted area approach when studying the compliance of the system state membership function with an acceptable level of performance membership function.

$$Compatibility\ Measure\ (CM) = \frac{Weighted\ Overlap\ area}{Weighted\ area\ of\ system\ state\ function} \quad (2.6)$$

2.8.4 COMBINED RELIABILITY-VULNERABILITY INDEX

“Reliability and vulnerability are used to provide a complete description of system performance in case of failure and to determine the magnitude of the failure event” (El-Baroudy and Simonovic, 2004). A predefined acceptable level of performance is established by assigning values to the lower and upper bounds m_1 and m_2 (or θ_1 and θ_2) shown in Equation 2.7. Then the compliance of the system state with the acceptable level of performance is measured. Higher compatibility with a predefined acceptable level of performance reflects better system performance. Therefore, several acceptable levels of performance must be defined to reflect the differences in perception of risk (El-Baroudy and Simonovic, 2004). Figure 2.7 illustrates three acceptable levels of performance that reflect a decision-maker’s perception of risk: highly satisfactory, satisfactory and risky performance.

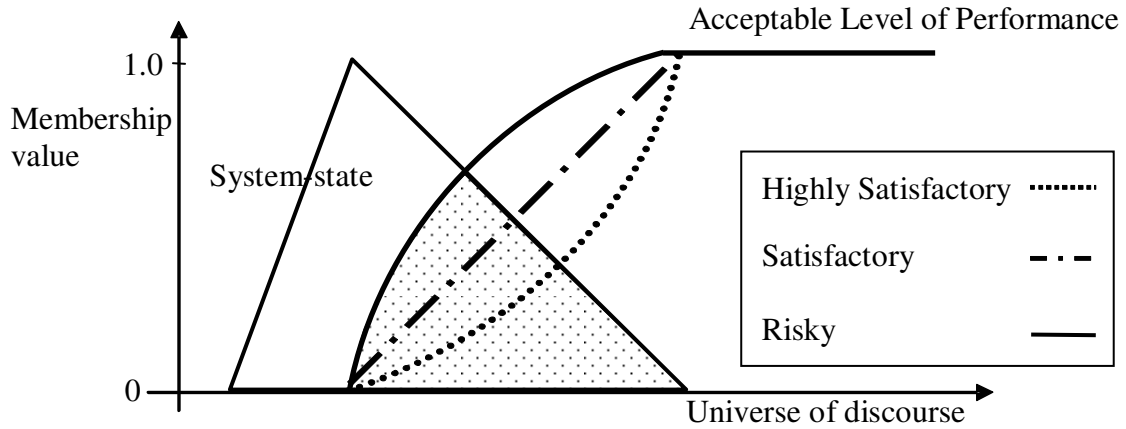


Figure 2.7: Compatibility with different levels of performance membership functions
(El-Baroudy and Simonovic, 2004)

According to El-Baroudy and Simonovic (2004) a reliability index is expressed as

$$RE_f = \frac{\max_{i \in K} \{CM_1, CM_2, \dots, CM_i\} \times LR_{\max}}{\max_{i \in K} \{LR_1, LR_2, \dots, LR_i\}} \quad (2.7)$$

where:

RE_f is the combined fuzzy reliability-vulnerability index;

LR_{\max} is the reliability measure of acceptable level of performance corresponding to the system-state with maximum compatibility value;

LR_i is the reliability measure of the i -th acceptable level of performance;

CM_i is the compatibility measure for system-state with the i -th acceptable level of performance; and

K is the total number of the defined acceptable levels of performance.

2.8.5 ROBUSTNESS INDEX

Hashimoto et al. (1982b) introduce robustness as a measure of a system's ability to adapt to a wide range of possible future load conditions at little additional cost. El-Baroudy and Simonovic (2004) redefine this concept in fuzzy environment as the change in compatibility measure that reflects the change in future conditions. The robustness index in terms of compatibility measure is:

$$RO_f = \frac{I}{CM_1 - CM_2} \quad (2.8)$$

where:

RO_f is the fuzzy robustness index;

CM_1 is the compatibility measure before the change in conditions; and

CM_2 is the compatibility after the change in conditions.

Therefore, the higher the change in compatibility measure, the lower the value of fuzzy robustness index. A decrease in robustness index indicates lower system adaptability to new conditions. If the change in compatibility measure is low, then the fuzzy robustness index will be high and the system's ability to adapt to new conditions will also be higher.

2.8.6 RESILIENCY INDEX

Hashimoto et al. (1982a) describe resiliency as the time required for a system to recover from a failure state. El-Baroudy and Simonovic (2004) represent this recovery time in terms of fuzzy sets. Different fuzzy system state membership functions arise from

different types of failure according to the system's recovery times. Kaufmann and Gupta (1985) consider the maximum recovery time of various types of failure as the system's recovery time. El-Baroudy and Simonovic (2004) also consider this maximum recovery time in generating the fuzzy resiliency index.

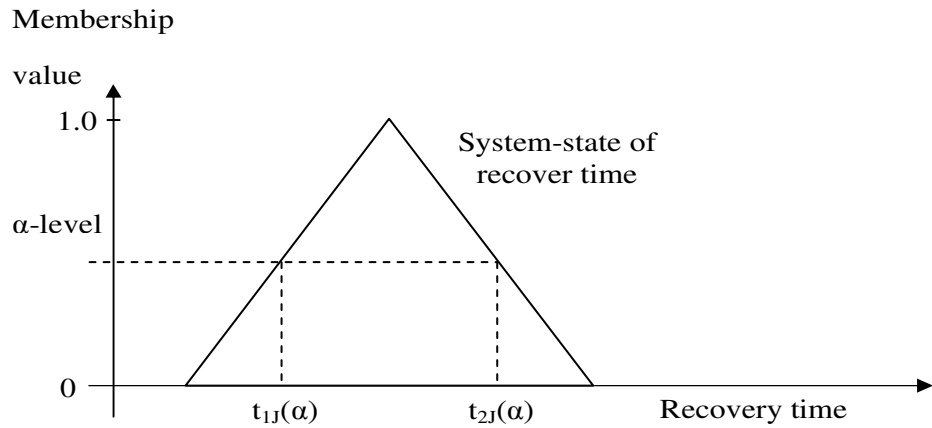


Figure 2.8: Fuzzy representation of maximum recovery time

If $t_{1j}(\alpha)$ is the lower bound of the j -th recovery time and $t_{2j}(\alpha)$ is the upper bound of the j -th recovery time at α -level (Figure 2.8) from the J number of failure events then the system fuzzy maximum recovery time at α -level is,

$$\tilde{T}(\alpha) = \left(\max_{j \in J} [t_{1_1}(\alpha), t_{1_2}(\alpha), \dots, t_{1_j}(\alpha)], \max_{j \in J} [t_{2_1}(\alpha), t_{2_2}(\alpha), \dots, t_{2_j}(\alpha)] \right) \quad (2.9)$$

El-Baroudy and Simonovic (2004) express resiliency as the inverse value of the centre of gravity of the maximum fuzzy recovery time. Their resiliency index is:

$$RS_f = \left[\frac{\int_{t_1}^{t_2} t \tilde{T}(t) dt}{\int_{t_1}^{t_2} \tilde{T}(t) dt} \right]^{-1} \quad (2.10)$$

where;

RS_f is the fuzzy resiliency index;

$\tilde{T}(t)$ is the system fuzzy maximum recovery time;

t_1 is the lower bound of the support of the system recovery time ; and

t_2 is the upper bound of the support of the system recovery time.

The inverse relation given in Equation (2.10) implies that the longer the recovery time, the lower is a system's ability to recover from the failure state and the lower is its resilience. Similarly, a shorter recovery time means that a system possesses a heightened ability to recover from failure and therefore exhibits greater resilience.

The suggested fuzzy performance indices are used to handle different fuzzy representations. In addition, these indices comply with the conceptual approach of the fuzzy set theory.

3 METHODOLOGY FOR RIVER AND URBAN FLOOD RISK ANALYSIS

This chapter presents a methodology for assessing inherent spatial and temporal uncertainty associated with river and urban flooding. Traditional modeling approaches focus on either temporal or spatial variability, but not both. There is a need to understand the dynamic characteristics of flood risk and their relationships with spatial variability. The main objective of the chapter is to present an original methodology for the river and urban flood risk management that is capable of (a) addressing uncertainty caused by spatial and temporal variability and ambiguity; (b) integrating objective and subjective risks; and (c) assisting flood management decision making so that it is based on a better understanding of spatial and temporal variability of risk. This chapter has two sections: (i) *river flood risk analysis*, and (ii) *urban flood risk analysis*. For *river flood risk analysis* the concept of overland flooding is based on two approaches: (a) hydrodynamic modeling, and (b) system dynamics modeling. For *urban flood risk analysis* the concept of overland flooding is based on hydrodynamic modeling only. The schematic representation in Figure 3.1 briefly shows the steps taken in this research for (i) river flood risk analysis, and (ii) urban flood risk analysis.

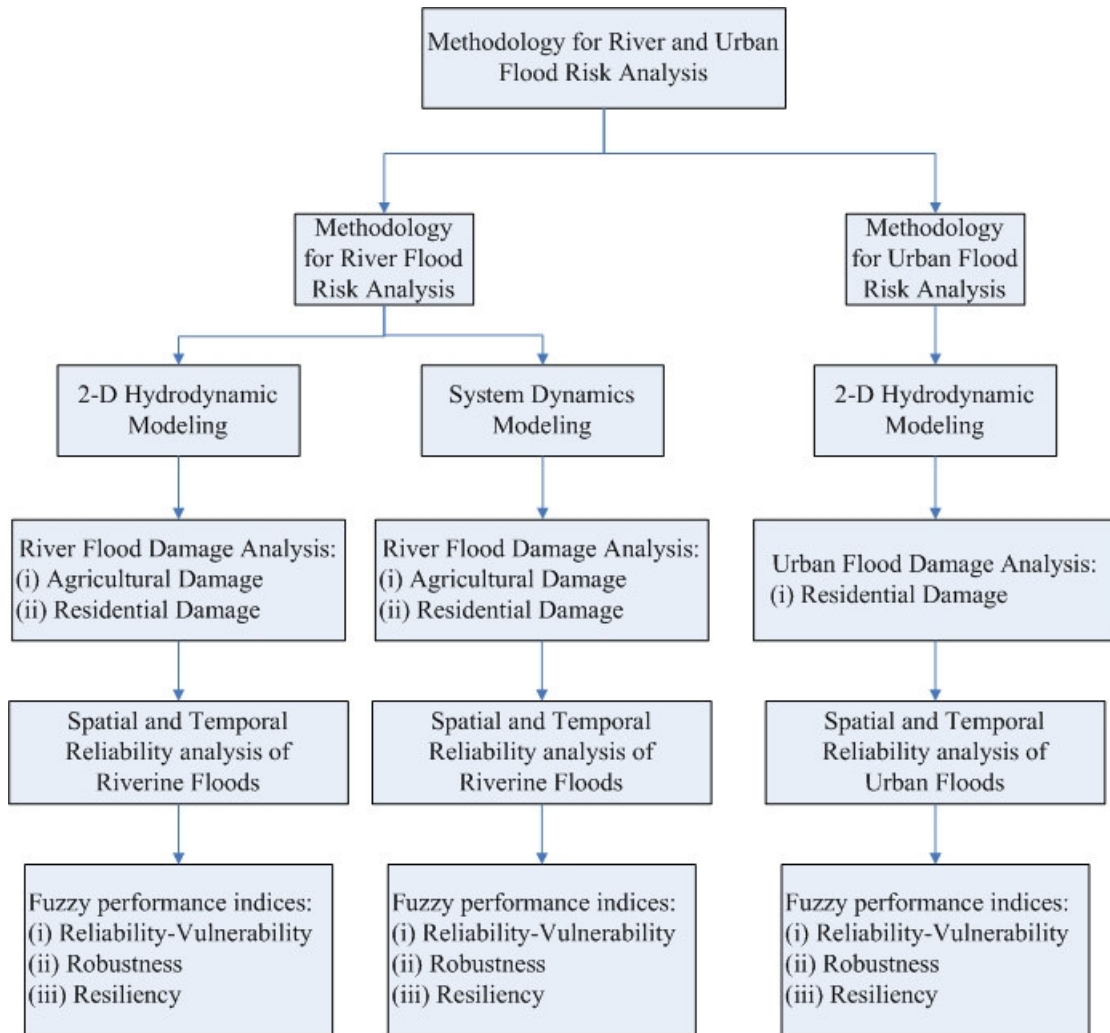


Figure 3.1: Schematic of (i) river, and (ii) urban flood risk analysis

3.1 RIVER FLOOD RISK ANALYSIS

Flood inundation maps representing spatial and temporal variability of flood water elevations are generated for the river flood risk analysis process. The following section briefly describes the conceptual models/tools for overland flooding used in this research for river flood risk analysis.

3.1.1 MODELING DYNAMIC PROCESSES OF RIVER FLOODING

Hydrodynamic Modeling Approach

1-D or fully 2-D hydrodynamic modeling approaches may be used for river flooding depending on the objectives of the study, available data, computational resources, accuracy requirement and real-time operational efficiency.

The theory of 1-D hydrodynamic modeling is based on the assumptions that water is incompressible and homogeneous, i.e., without significant variation in density and the bottom slope is small. The water-lengths are large as compared to water-depths. This ensures that the flow everywhere can be regarded as having a direction parallel to the bottom, i.e., vertical accelerations can be neglected and a hydrostatic pressure variation along the vertical can be assumed. The basic equations for 1-D hydrodynamic modeling are derived considering conservation of mass and momentum. Considering the hydraulic resistance and the lateral inflow, the equations can be written as (DHI, 2008 (a)):

$$\frac{\partial Q}{\partial x} + \frac{\partial A}{\partial t} = q \quad (3.1)$$

$$\frac{\partial Q}{\partial x} + \frac{\partial}{\partial x} \left(\frac{\alpha Q^2}{A} \right) + gA \frac{\partial h}{\partial x} + \frac{gQ|Q|}{C^2 AR^*} = 0 \quad (3.2)$$

where

A = Flow area (m²)

R* = Resistance radius (m)

C = Chezy's Resistance coefficient (m^{1/2}/s)

g	=	Acceleration due to gravity (m/s^2)
h	=	Stage above horizontal reference level (m)
Q	=	discharge (m^3/s)
α	=	momentum distribution coefficient
q	=	Lateral inflow (m^2/s)

In two-dimensional hydrodynamic models the following basic equations for the conservation of mass and momentum are used to describe the flow and water level variations (DHI, 2008 (b)):

(a) Continuity

$$\frac{\partial \zeta}{\partial t} + \frac{\partial p}{\partial x} + \frac{\partial q}{\partial y} = 0 \quad (3.3)$$

(b) X-Momentum

$$\begin{aligned} \frac{\partial p}{\partial t} + \frac{\partial}{\partial x} \left(\frac{p^2}{h} \right) + \frac{\partial}{\partial y} \left(\frac{pq}{h} \right) + gh \frac{\partial \zeta}{\partial x} + \frac{gp\sqrt{p^2 + q^2}}{c^2 \cdot h^2} - \frac{1}{\rho_w} \left[\frac{\partial}{\partial x} (h\tau_{xx}) + \frac{\partial}{\partial y} (h\tau_{xy}) \right] \\ - \Omega q - fv v_x + \frac{h}{\rho_w} \frac{\partial}{\partial x} (p_a) = 0 \end{aligned} \quad (3.4)$$

(c) Y-Momentum

$$\begin{aligned} \frac{\partial p}{\partial t} + \frac{\partial}{\partial y} \left(\frac{q^2}{h} \right) + \frac{\partial}{\partial x} \left(\frac{pq}{h} \right) + gh \frac{\partial \zeta}{\partial y} + \frac{gq\sqrt{p^2 + q^2}}{c^2 \cdot h^2} - \frac{1}{\rho_w} \left[\frac{\partial}{\partial y} (h\tau_{yy}) + \frac{\partial}{\partial x} (h\tau_{xy}) \right] \\ + \Omega q - fv v_y + \frac{h}{\rho_w} \frac{\partial}{\partial y} (p_a) = 0 \end{aligned} \quad (3.5)$$

Where:

$h(x,y,t)$ = water depth (m);

$\zeta(x,y,t)$ = surface elevation (m);

$p,q(x,y,t)$ = flux densities in x and y-directions ($m^3/s/m$) = (uh,vh); (u,v) = depth averaged velocities in x- and y- directions;

$c(x,y)$ = Chezy resistance ($m^{1/2}/s$);

g = acceleration due to gravity (m/s^2);

$f(v)$ = wind friction factor;

$\Omega(x,y)$ = Coriolis parameter, latitude dependent (S^{-1});

$P_a(x,y,t)$ = atmospheric pressure (kg/m^2);

ρ_w = density of water (kg/m^3);

x,y = space coordinates (m);

t = time (s);

$\tau_{xx}, \tau_{xy}, \tau_{yy}$ = components of effective shear stress;

$V, V_x, V_y(x,y,t)$ = wind speed and components in x- and y- direction (m/s);

In very flat floodplains with complex topographic features, which are often due to the presence of infrastructure, flood wave propagation is not a one-dimensional phenomenon. To accurately capture the lateral flows, a two-dimensional modeling approach is required. In 2-D modeling, equations of continuity and momentum are written in two dimensions and results are calculated at each grid point in the solution domain. Thus only a fine spatial resolution (dx) can be used. Accordingly, 2-D modeling requires a lot of computer memory and makes computing time slow.

Contrary to a 1-D modeling approach, where results (water levels and discharges) can only be obtained at points where cross-section information is available, 2-D modeling results are available at every grid point in the solution domain. Moreover, discharges and velocities are available in two dimensions, i.e. along the flow and in the lateral direction.

The main advantage of using the 2-D approach is that it provides information on variable discharges and velocities in both x and y direction at each grid point and at each computational interval. The computation of velocity profiles in two dimensions allows the accurate representation of flood wave propagation and offers a better prediction of the effects of river training, scouring and sediment transport processes. The assessment of impacts of any proposed change in the river, such as dikes, training walls and dredging, begins by determining the local changes in velocities. Velocity predictions can also be used for navigation purposes. The information on the distribution of average velocity at any section can also assist fisheries research and management. Thus a 2-D model can be used to assess the impact of proposed changes, such as dredging and changes in channel configuration, and any addition or removal of flood control structures.

Water level accuracy may be improved by using a two-dimensional model that can better resolve bathymetry and flow features. Water levels are required primarily for flood forecast, floodway operation and river management. Water level information can be used to verify existing floodplain contingency preparations. Since the 2-D model provides an accurate flow field, it can serve as the basis of a contaminant model to assess the effects of predicted or present loading.

In terms of data the most important requirement for 2-D modeling of a river system is an accurate description of the topography and bathymetry of river and floodplains. Prediction of water levels depends heavily on an accurate representation of floodplain. Other necessary data can be divided into three groups: basic model parameters, calibration parameters, and boundary conditions. Basic model parameters include model grid size and extent, time step and length of simulation, and the type of output required and its frequency. Bed resistance and wind friction factors are required parameters for calibration. Hydrographic boundary conditions can be specified as a constant or variable (in time and location in space) water level or flux at each open model boundary, as a constant or variable source or sink anywhere within the model, and/or as an initial free surface level may be applied over the entire model. The basic output of the model is water surface elevation and flux densities in x- and y-directions. The derived output includes water particle velocity and flow direction. Output results are computed at each grid point for each time step.

Due to significant requirements of topographic data and computational time for two-dimensional modeling, a one-dimensional approach is the preferred choice for modeling floods, especially in very large basins. However, with advances in the ability of topographic data to capture and process techniques, and advancement in parallel computing, two-dimensional modeling applications are becoming increasingly feasible in river flooding.

System Dynamics Modeling Approach

System dynamics approach is used in this research for modeling river flooding. The

presence of feedback and the interaction between time and location in space, with support from GIS, make the proposed modeling approach suitable for implementation in river flooding. The following section describes the theoretical concept of river flooding in two sections: (i) flow description in floodplains, and (ii) river flow.

The representation of natural processes of flow in both floodplains and river is possible. However, the resulting model would be very complex (Bedient and Huber, 1988). Models of hydrologic systems are generally based on simplifying assumptions that are put into place to reduce the complex description to a set of simpler descriptive processes. Chow *et al.* (1988) proposed the control volume approach that provides a conceptual model applicable to hydrologic systems in general. Hydrologic models are developed by relating the input (into the control volume) with the output, using a system response or transformation. Therefore the first task in modeling is the definition of the control volume. There are several approaches to defining a control volume for routing applications. The most common of these can be grouped into three classes: (i) a watershed based approach (river reaches and associated land draining directly into river), (ii) a source to sink routing approach (involves subdividing the land surface into smaller segments and routing the flow from each segment directly to a discharge location), and (iii) a cell-to-cell routing approach.

A cell-to-cell routing approach is used in this research to describe overland flow in the floodplains. In the cell-to-cell routing approach the land surface is divided into segments, routing flow from one segment to the next until it arrives at a final point. The cell-to-cell

routing approach assumes the land surface within each of these segments to be homogenous. For convenience and computational efficiency, the land segments used are often equal sized cells. However, irregularly shaped land segments are also applicable in this approach. The land segment defines the control volume in a cell-to-cell routing approach. Using a unique response function, inputs to each segment are transferred to the next downstream segment. The response function is expected to capture the essence of the various flow processes occurring within the control volume. There are several cell-to-cell routing models for overland flow found in the relevant literature: Vörösmarty et al. (1989), Miller et al. (1994), Sausen et al. (1994), Kite et al. (1994), Naden (1992), and Asante (2000). The routing method used in this research is based on the work of Coe (1997), who proposed a methodology that marked an improvement to Miller's cell-to-cell approach by using natural depressions in the land surface to determine the cell storage. In this model, the application of a grid divides the land surface into routing cells. Discharge occurs only when the cell storage is exceeded. Consequently, the discharge rate turns out to be a function of the difference between the amount of water in the cell and its storage capacity. The storage capacity of each cell is determined by filling the sinks in a finer resolution grid. The regions without internal drainage are assigned a storage of zero. The main reason for the selection of a cell-to-cell routing approach for overland flooding in this research is that, compared to source to sink routing, which requires a transfer function, cell storage has a physical basis and can be calculated using GIS.

The Von Neumann neighborhood scheme is used for cell-to-cell routing. The scheme allows water from each cell to move to one or more of its four neighboring cells. The

excess water (more than storage capacity) is distributed to four neighboring cells in descending order of slope difference. A single cell with inflow and outflow is shown in Figure 3.2.

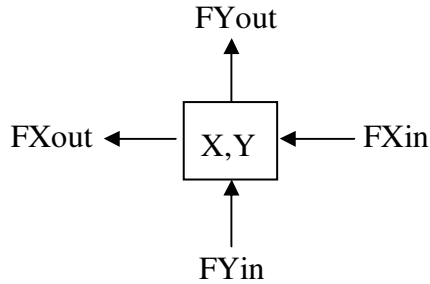


Figure 3.2: Single cell with inflow and outflow.

The water stored in each cell can be mathematically described as (Ahmad and Simonovic, 2004):

$$V[X,Y](t) = V[X,Y](t - dt) + (FXin[X,Y] + FYin[X,Y] + Qrain[X,Y] - FXout[X,Y] - FYout[X,Y] - Evap[X,Y]) * dt \quad (3.6)$$

The Equation (3.6) states that the volume (V) of water in cell X, Y at time t is a function of volume in the same cell at previous time step plus inflow (from neighboring cells in X and Y direction and rain) minus outflow (to neighboring cells in an x and y direction and evaporation).

The Muskingum method (Chow et al. 1988) has been used for routing flow in the river. A detailed description of the Muskingum method is given in Appendix A. Overland flow and river flow is modeled in system dynamics simulation environment whereby basic

building blocks, i.e. stocks, flows, connectors, and converters, are used to describe the model structure. Water volume in each cell is represented by a stock. Flows are used for inflows and outflows to model changes in water over time. Converters are used to provide information to the model and operate the system using logical/mathematical functions. The flow routing sector describes the movement of water from cell to cell. Terrain information, such as surface elevation, ground slope and storage capacity in the cell, affects the flow from one cell to another.

3.1.2 RIVER FLOOD DAMAGE ANALYSIS

In this research agricultural and residential damage is assessed as a result of river flooding. An innovative approach is introduced here to describe spatial and temporal variability of flood damage.

Agricultural Damage

Agricultural damage is assessed in this study based on the delay to seed and, as a result, on the delay of the crop yield (KGS, 2000). Agricultural damage assessment is carried out by the following four steps:

Step One: Determine Date of Flood Recession From Flood Stage Hydrograph:

From 2D hydrodynamic and system dynamics models the spatial and temporal variability of flood water elevations are determined. Flood stage hydrographs are generated for every location of the agricultural land in the case study area, which provides the model

with a flood recession date. From the stage hydrograph, the first date of seeding and the expected yield for the crop are determined for i -th time step at j -th location. As floods recede, areas with higher elevation are exposed first and are ready to seed before locations closer to the river and with lower elevation.

Step Two: Add Additional Time to Flood Recession Date for Field Drying:

Additional time, i.e. a drying period, is added to the date of flood recession to allow the agricultural land to completely dry before seeding. In this study, a 14 day time frame was used as the drying period to account for one rainfall event during this period.

Step Three: Determine Percent of Average Yield:

The relative yield is then determined from the graphical relationship between the relative yield and seeding date (Figure 3.3).

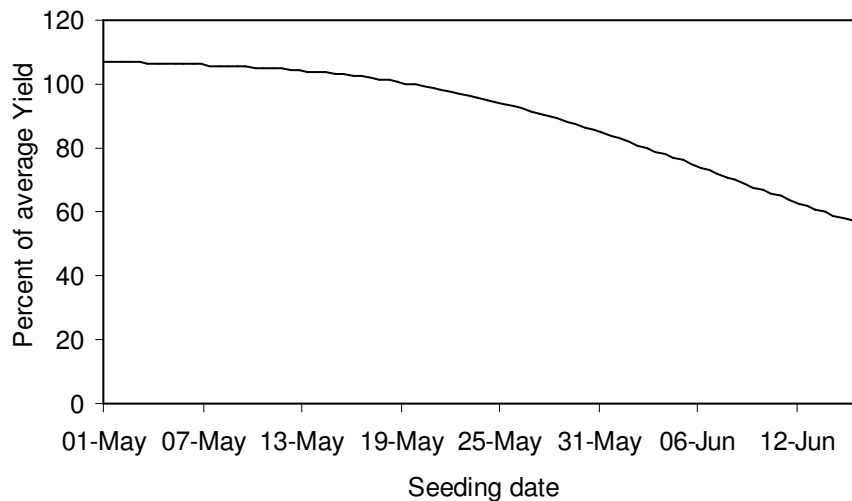


Figure 3.3: Graphical relationship of percentage of average yield and seeding date

Step Four: Assess Agricultural Damage:

Agricultural damage is assessed using the corresponding value of the relative yield from Figure 3.3 (KGS, 2000).

Agricultural damage is calculated as

$$D_{ij} = (100 - Y_j)\% \times A_j \times P_j \quad (3.7)$$

Where

D_{ij} is the agricultural damage for i -th time step at j -th location;

Y_j is the expected yield (as a function of seeding date) at j -th location (bushels/acre);

A_j is the area of the grid cell at j -th location; and

P_j is three year average price of crop (\$/bushel)

Residential Damage

For residential and ring-dike communities (i.e. a roughly circular dike to prevent overflow of lowlands and to retain floodwater), a depth damage function (KGS, 2000) is used to estimate the incremental damage to a town's infrastructure. For the ring-diked communities, the initial damage level is assumed to be 5% of the total damage, which then rises linearly to 100% when flood water level reaches the top of the dike (Figure 3.4). Once the flood water level exceeds the top level of the dike, infrastructural damage is shown by a vertical line at the right of the chart that represents the total potential damage to infrastructure as a percentage ($X\%$) of the total reported damage. Since time is required to recover from flood damage, the maximum flood damage of ring-diked

communities is assumed to remain the same, even after the flood waters have receded. Information such as the top level of the dike, level of incipient flooding, the initial flood damage level, the area within the ring-dike, total reported flood damage and total potential infrastructure damage for each ring-dike community are required for the damage assessment model. The output of the damage analyses are shown by maps representing the spatial and temporal variability of flood damage.

Total reported damage for location j in a ring dike community

$$G_j = \frac{\text{Total Reported Damage for a community} \times \text{Area of grid cell, } A_j}{\text{Area of Ring Dyke}} \quad (3.8)$$

Following logical statements of IF-THEN-ELSE structure are used to determine damage D_{ij} for i -th time step at j -th location;

IF Water Elevation < Base level of incipient flooding THEN $D_{ij} = 0$

ELSEIF Base level of incipient flooding \leq Water Elevation \leq Top level of dike

$$\text{THEN } D_{ij} = \frac{(\text{Water level} - \text{Base level of incipient flooding}) \times \frac{(100 - 5)}{100} \times G_j}{\text{Top level of dyke} - \text{Base level of incipient flooding}} + \frac{5}{100} \times G_j$$

ELSEIF Water Elevation > Top level of dike

$$\text{THEN } D_{ij} = \frac{\text{Total Potential Infrastructure Damage}}{\text{Total Reported Damage}} \times G_j \quad (3.9)$$

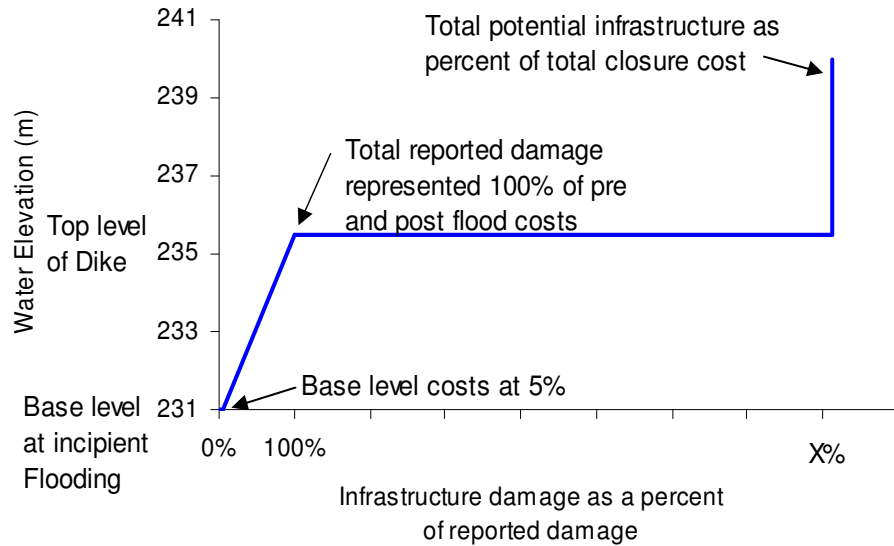


Figure 3.4: Depth-damage relationship for a ring diked communities

3.1.3 SPATIAL AND TEMPORAL VARIABILITY OF RIVER FLOOD RISK

There are many sources of uncertainty associated with river flood risk analysis. The floodplain maps and flood damage assessments are subject to uncertainty due to lack of data and other ambiguities. Fuzzy membership functions are used to account for the uncertainty of a variable (or variables) used in flood risk analysis. Different shapes of membership functions, such as triangular, trapezoidal, Gaussian, exponential, etc., are used to express uncertainty. In flood risk management uncertainty is associated mainly with the spatial and temporal variability of hydrologic variables (precipitation, river flow, etc). Temporal variability of flow results in variations of flood water level. Depending on the spatial and temporal variability of rainfall intensity, rainfall duration and the direction of storm movement, there can be a wide range of shapes of hydrographs. The spatial and temporal variability of these factors may augment or reduce peak flow, cause gradual or

rapid rise to peak value, and also result in gradual or rapid recession of the hydrograph. A gradual recession of the hydrograph increases the duration of submergence, which may cause significant damage to agricultural crops, infrastructures and properties. In flood risk management, spatial variability is also associated with floodplain characteristics such as land-use, terrain elevation, channel network, vegetation, roughness, soil characteristics, porosity, etc. For example, areas closer to the river and with a lower elevation are highly prone to significant flood damage compared to areas further away from the river with a higher elevation. As floods recede, areas with a higher elevation are first to be exposed and are ready to seed before areas closer to the river and with lower elevation. Fuzzy set theory is used to represent spatial and temporal uncertainty for flood risk analysis

For example, the uncertainty in the inflow value (or a water level) can be expressed using a triangular or trapezoidal membership function, which is meant to convey the notion that the inflow value (or a water level value) is concentrated around one or a range of modal values. In general, uncertainty in the inflow value, water level, hydraulic properties and terrain elevation can result in uncertainty in the floodplain map. There can also be uncertainty in flood damage analysis. The shape of the membership function needs to be carefully taken into consideration as it significantly affects the representation of an uncertain value. Accordingly, there is uncertainty even in the selection of the type of membership function. In this study, the spatial and temporal uncertainty of these variables are considered in order to develop the methodology for a spatial and temporal reliability analysis of riverine and urban floods.

3.1.4 A NEW METHODOLOGY FOR FUZZY RIVER FLOOD RISK ANALYSIS

The new methodology presented here uses three fuzzy performance indices: (i) a combined reliability-vulnerability index, (ii) a robustness index, and (iii) a resiliency index (El-Baroudy and Simonovic, 2004) for spatial and temporal reliability analysis of floods. The calculation of reliability indices depends on the exact definition of the unsatisfactory state of a system. The methodology developed in this work is based on an innovative concept of partial failure first introduced by El-Baroudy and Simonovic (2004). Partial failure (Figure 2.4) is defined by the introduction of subjective levels of acceptance partial flood damage. The boundary of the acceptance partial failure region is ambiguous. The acceptance partial failure region varies with time and locations and also changes from one stakeholder to the other, depending on the personal perception of risk. Methodology developed in this thesis requires generating the system state membership function and the predefined acceptance level of partial failure membership function. For example, in flood management, the system state membership function can represent the uncertainty with flood water level, while the acceptance level of partial failure membership function can define the region of partial failure as the region between the complete failure state (i.e. when flood water level results in the complete failure of the flood protection embankment and also a complete inundation of the protected area) and the acceptable failure level (i.e. the flood water level has overtopped the flood protection embankment without causing complete failure, and therefore results in a partial inundation of the protected area). Since the fuzzy sets are capable of representing the notion of imprecision better than the ordinary sets, fuzzy set theory has been used in this

work to describe various aspects of risk.

Ahmad and Simonovic (2007) successfully extended fuzzy reliability analysis into a spatial fuzzy reliability analysis for taking explicitly into consideration spatial variability of flood risk management. However, Ahmad and Simonovic (2007) did not consider the temporal variability in flood risk analysis. Therefore both spatial and temporal variability associated with flood risk management has not yet been fully addressed. In order to understand the dynamic characteristics of flood risk and its spatial variability, an original methodology is presented in this thesis that extends the fuzzy performance indices of El-Baroudy and Simonovic (2004) to address spatial and temporal variability of riverine floods.

Definition of Partial Failure

The spatial and temporal variability of the acceptance level of partial flood damage is addressed in this work by introducing the temporal dimension to the 2-D fuzzy set of the acceptance level of partial flood damage (Figure 3.5) (Ahmad and Simonovic, 2007). This 3-D (Figure 3.6) representation of the acceptance level of partial flood damage captures the spatial and temporal variability of flood damage. The acceptance level of partial flood damage is represented as a fuzzy membership function, $\tilde{M}_{ij}(D_{ij})$, based on the flood damage value D_{ij} for i -th time step at j -th location (Figure 3.6).

$$\tilde{M}_{ij}(D_{ij}) = \left\{ \begin{array}{ll} 1 & \text{if } D_{ij} \leq D_{ij1} \\ \varphi_k(D_{ij}) & \text{if } D_{ij} \in [D_{ij1}, D_{ij2}] \\ 0 & \text{if } D_{ij} \geq D_{ij2} \end{array} \right\} \quad (3.10)$$

where,

D_{ij} is the flood damage for i -th time step at j -th location;

$\tilde{M}_{ij}(D_{ij})$ is the fuzzy membership function of margin of safety for i -th time step at j -th location;

D_{ij1} and D_{ij2} are lower and upper bounds of the acceptance level of partial flood damage for i -th time step at j -th location;

$\varphi_k(D_{ij})$ are functional relationships representing the subjective levels of acceptance of the partial risk for i -th time step at j -th location;

k ($= 1, 2, 3$) is the type of the acceptance level of partial flood damage membership function.

$k = 1$ denotes the conservative acceptance level of partial flood damage membership function for i -th time step where $i \in [0, i_1]$ is for rising limb of the stage/discharge hydrograph;

$k = 2$ denotes neutral acceptance level of partial flood damage membership function for i -th time step where

$i \in [i_1, i_2]$ is for peak part of the stage/discharge hydrograph;

$k = 3$ denotes risky acceptance level of partial flood damage membership function for i -th time step where $i \in [i_2, i_3]$ is for recession limb of the stage/discharge hydrograph;

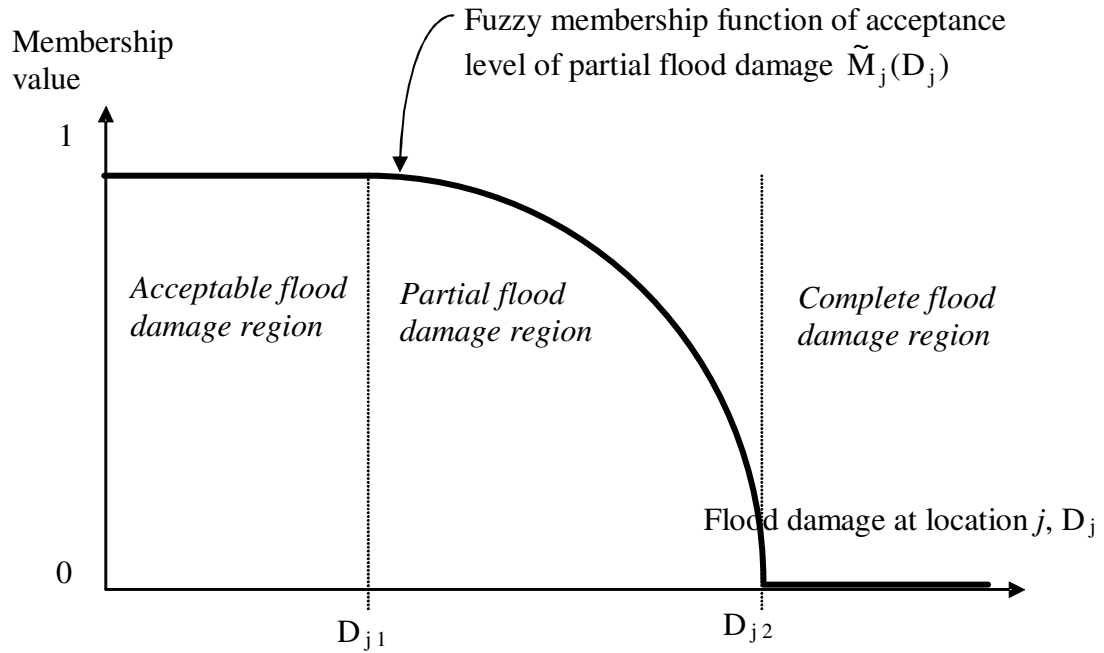


Figure 3.5: 2-D Fuzzy representation of spatial variability in acceptance level of partial flood damage (Ahmad and Simonovic, 2007)

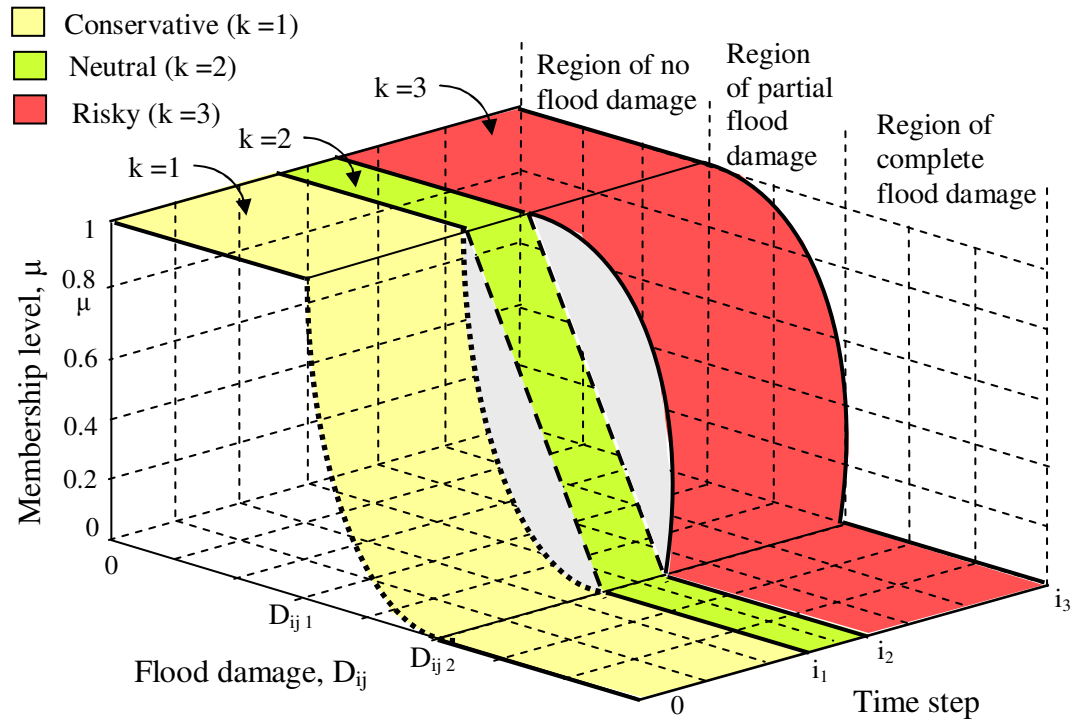


Figure 3.6: 3-D Fuzzy representation of spatial and temporal variability in acceptance level of partial flood damage

The perception of flood risk and damage level varies with the time step of the stage and/or discharge hydrograph, precisely because this variation is predicated on the decision maker's preference towards the shape of the membership function $\tilde{M}_{ij}(D_{ij})$. To reflect the subjectivity of the decision maker different time steps of the hydrograph are assigned to different shapes: rising limb with a conservative acceptance level; crest with a neutral acceptance level; and recession limb with a risky acceptance level of partial flood damage membership functions. The perception of flood risk and damage level also varies with space for various land use patterns, i.e. residential and agricultural. In comparison to areas further away from the river, areas near the river that are highly prone to significant flood damage may be assigned different shapes of membership function $\tilde{M}_{ij}(D_{ij})$ based on the decision maker's perception of flood risk and damage level. The shape of the membership function $\tilde{M}_{ij}(D_{ij})$ can be changed with time and location by assigning the value to the lower bound, D_{ij1} and/or the upper bound, D_{ij2} of the acceptance level of partial flood damage.

If the value of flood damage exceeds D_{ij2} , then the region suffers complete damage (Figure 3.6). In this case the membership function $\tilde{M}_{ij}(D_{ij})$ value is equal to zero. If the value of flood damage is below D_{ij2} but exceeds D_{ij1} , then the region suffers partial flood damage. The membership function, $\tilde{M}_{ij}(D_{ij})$ of the acceptance level of partial flood damage, attains its maximum value of one if the value of flood damage is below D_{ij1} .

The Reliability Measure (LR_{ij}) of the partial level of flood damage is calculated for i -th

time step at location j as follows:

$$LR_{ij} = \frac{D_{ij1} \times D_{ij2}}{D_{ij2} - D_{ij1}} \quad \text{where } D_{ij2} > D_{ij1} \quad (3.11)$$

Using almost crisp definition of the partial failure region by selecting close values for D_{ij1} and D_{ij2} will result in a very high LR_{ij} value. This, however, will not affect the values of the proposed fuzzy performance indices. The subjectivity of decision makers, in selecting D_{ij1} and D_{ij2} , will always result in a degree of ambiguity of risk perception. This alternate definition of failure can accommodate different risk perceptions through the individual selection of the lower and upper bounds of the region of partial damage, and also the shape of the membership function $\tilde{M}_{ij}(D_{ij})$.

Spatial and Temporal Variability of Fuzzy Flood Damage

A fuzzy approach to river flood risk assessment generally involves a 2-D fuzzy set (Li et. al., 2007) with one dimension representing the universe of discourse of variability and the other dimension representing its membership degree. The 2-D fuzzy set is appropriate for representing either spatial or temporal variability of river flood damage, but not both of them. A new approach is proposed here that will address both spatial and temporal variability in river flood damage. The representation of spatial and temporal variability of river flood damage is considered in the following four steps:

(a) 2-D Fuzzy Set for Temporal Variability of River Flood Damage

Determining the temporal variation of river flood damage is performed by considering the uncertainty related to changing flow. Uncertainty related to properties of spatial variability is not considered in determining temporal variability of river flood damage. Agricultural damage is determined as a function of the flood recession date. Flood damage in residential areas is determined using a depth-damage relationship. Uncertainty in flood water level is the result of our inability to accurately measure, calculate or estimate the flow value. Since a probabilistic approach usually fails to address factors of uncertainty related to human error, subjectivity, and the lack of historical records and data, a fuzzy set approach is used. Temporal uncertainty of river flood damage is described in this study using a two dimensional (2-D) fuzzy set with one dimension representing the value of river flood damage for i -th time step, D_i and the other its membership degree. The definition of this 2-D fuzzy set of river flood damage is given by

$$\begin{aligned} \bar{A} &= \{(D_i, \tilde{S}_i(D_i)) \mid \forall D_i \in D\} \\ 0 &\leq \tilde{S}_i(D_i) \leq 1 \end{aligned} \tag{3.12}$$

where

\bar{A} denotes 2-D fuzzy set for temporal variability of flood damage;

D_i is the flood damage for i -th time step in the universe of discourse D ; and

$\tilde{S}_i(D_i)$ denotes membership degree of the 2-D fuzzy set.

In the case of a triangular membership function (Figure 3.7), the fuzzy river flood

damage function $\tilde{S}_i(D_i)$ can be defined for i -th time step as:

$$\tilde{S}_i(D_i) = \left\{ \begin{array}{ll} 0 & \text{if } D_i \leq D_{i \text{ Min}} \\ \frac{D_i - D_{i \text{ Min}}}{D_{i \text{ Mean}} - D_{i \text{ Min}}} & \text{if } D_i \in [D_{i \text{ Min}}, D_{i \text{ Mean}}] \\ \frac{D_{i \text{ Max}} - D_i}{D_{i \text{ Max}} - D_{i \text{ Mean}}} & \text{if } D_i \in [D_{i \text{ Mean}}, D_{i \text{ Max}}] \\ 0 & \text{if } D_i \geq D_{i \text{ Max}} \end{array} \right\} \quad (3.13)$$

where,

$\tilde{S}_i(D_i)$ is the flood damage membership function for i -th time step;

$D_{i \text{ Mean}}$ is the modal value of flood damage for i -th time step; and

$D_{i \text{ Min}}, D_{i \text{ Max}}$ are the lower and the upper bounds of flood damage for i -th time step.

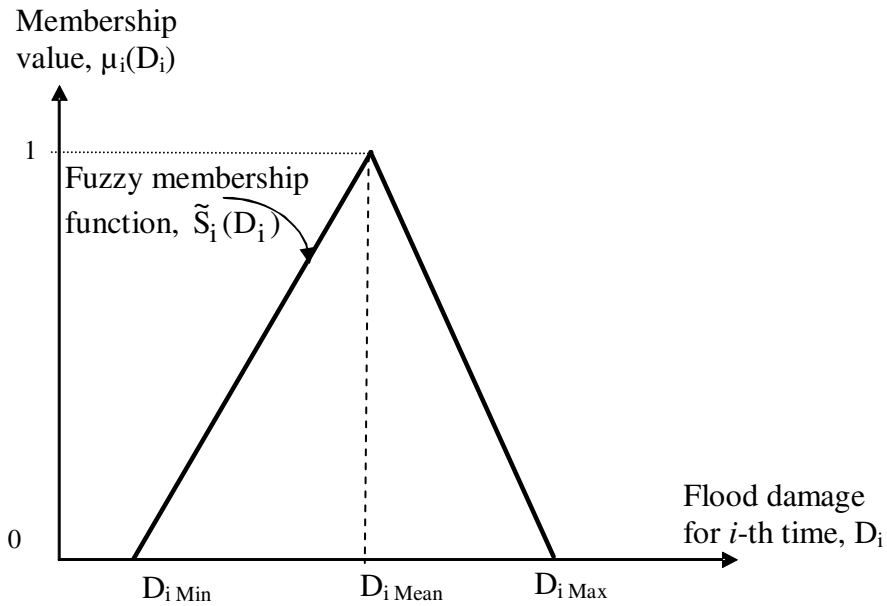


Figure 3.7: 2-D fuzzy set for temporal variability of flood damage

(b) 2-D Fuzzy Set for Spatial Variability of River Flood Damage

Determining the spatial variation of river flood damage is performed by considering the uncertainty related to properties that change with the location in the floodplain. Temporal variability resulting from the change in properties with time is not considered in determining spatial variability of river flood damage. Agricultural damage depends, for example, on the spatial distribution of different types of crops. The methodology developed in this work considers average crop damage as a property of location. In the case of residential areas, infrastructure/property damage and depth-damage relationships are also considered to be location dependent. These location dependent properties are subject to uncertainty due to lack of data, human error, etc. Therefore the fuzzy set approach is used to capture spatial variability of flood damage. The spatial variability of flood damage is described in this study using a two dimensional (2-D) fuzzy set with one dimension representing the value of flood damage at j -th location, D_j and the other its membership degree. The definition of this 2-D fuzzy set of river flood damage at j -th location is given by

$$\begin{aligned} \bar{B} &= \{(D_j, \tilde{S}_j(D_j)) \mid \forall D_j \in D\} \\ 0 &\leq \tilde{S}_j(D_j) \leq 1 \end{aligned} \tag{3.14}$$

where

\bar{B} denotes 2-D fuzzy set for spatial variability of flood damage;

D_j is the flood damage at j -th location in the universe of discourse D ; and

$\tilde{S}_j(D_j)$ denotes membership degree of the 2-D fuzzy set.

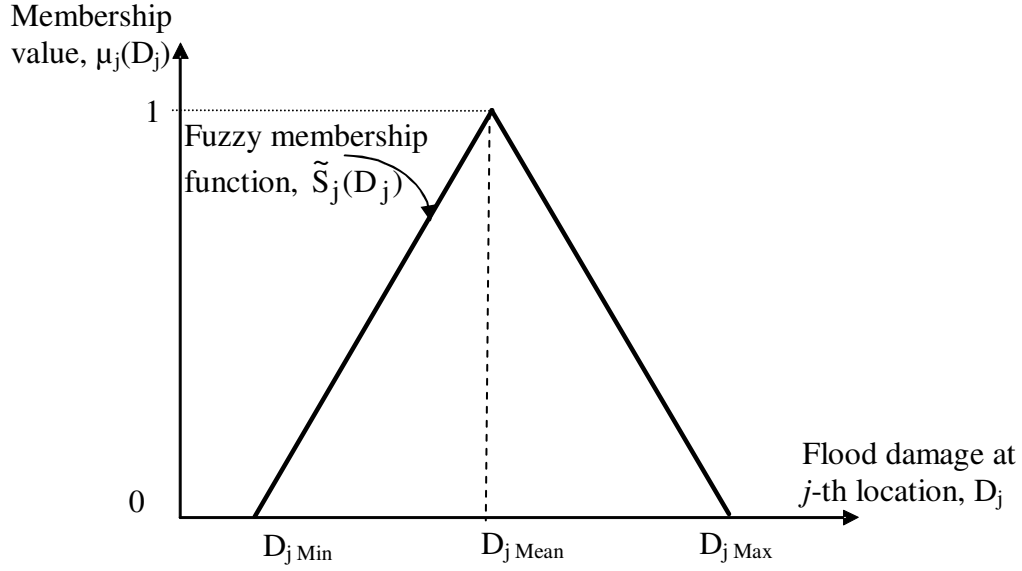


Figure 3.8: 2-D fuzzy set for spatial variability of flood damage

In the case of a triangular membership function shape (Figure 3.8), the fuzzy river flood damage function $\tilde{S}_j(D_j)$ can be defined at j -th location as:

$$\tilde{S}_j(D_j) = \left\{ \begin{array}{ll} 0 & \text{if } D_j \leq D_{j \text{ Min}} \\ \frac{D_j - D_{j \text{ Min}}}{D_{j \text{ Mean}} - D_{j \text{ Min}}} & \text{if } D_j \in [D_{j \text{ Min}}, D_{j \text{ Mean}}] \\ \frac{D_{j \text{ Max}} - D_j}{D_{j \text{ Max}} - D_{j \text{ Mean}}} & \text{if } D_j \in [D_{j \text{ Mean}}, D_{j \text{ Max}}] \\ 0 & \text{if } D_j \geq D_{j \text{ Max}} \end{array} \right\} \quad (3.15)$$

where,

$\tilde{S}_j(D_j)$ is the flood damage membership function at j -th location;

$D_{j \text{ Mean}}$ is the modal value of flood damage at j -th location; and

$D_{j \text{ Min}}, D_{j \text{ Max}}$ are the lower and the upper bounds of flood damage at j -th location.

(c) 3-D Fuzzy Set for Spatial and Temporal Variability of Flood Damage

The 2-D fuzzy sets developed in this study for – i) temporal variability of flood damage, and ii) spatial variability of flood damage – are used to capture various sources of temporal and spatial uncertainty, respectively. However, neither i) nor ii) is capable of representing the combined uncertainty of the river flood risk that is both spatial and temporal in nature. Therefore, a new three dimensional fuzzy set (3-D fuzzy set) is developed in this thesis to fully address the spatial and temporal uncertainty and subjectivity associated with river flood damage. A 3-D fuzzy set (Li et. al., 2007) is developed (Figure 3.9) with the first dimension used for the temporal variability of flood damage D_i , the second dimension for the spatial variability of flood damage D_j , and the third dimension for the membership degree.

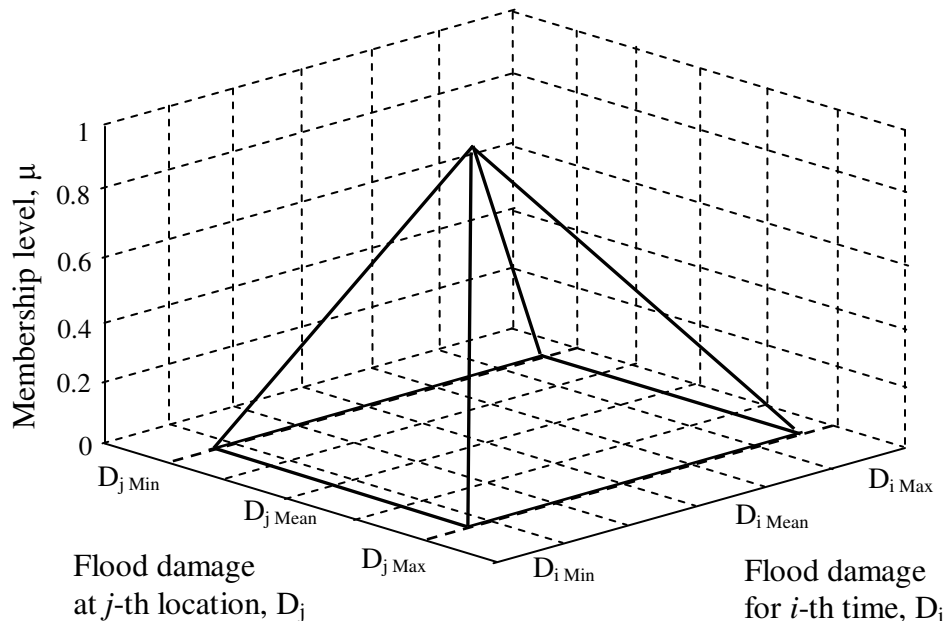


Figure 3.9: 3-D joint fuzzy set of flood damage

The joint membership function of the river flood damage provides a visualization of the spatial and temporal variability in river flood damage at any membership level. This 3-D fuzzy set represents spatial and temporal variability in river flood damage at every spatial location and at every time step. The definition of the 3-D fuzzy set is given as follows:

$$\begin{aligned} \bar{V} &= \{(D_i, D_j), \mu_{\bar{V}}(D_i, D_j) \mid \forall D_i \in D, D_j \in D\} \\ 0 &\leq \mu_{\bar{V}}(D_i, D_j) \leq 1 \end{aligned} \quad (3.16)$$

where

\bar{V} denotes 3-D fuzzy set for spatial and temporal variability of flood damage;

D_i is the flood damage in time for i -th time step in the universe of discourse D ;

D_j is the flood damage at j -th location in the universe of discourse D ; and

$\mu_{\bar{V}}(D_i, D_j)$ denotes membership degree of the 3-D fuzzy set.

(d) Dimension Reduction

The 3-D fuzzy set is used to quantify uncertainty in river flood damage that changes with time and location. However, the complexity of the 3-D spatial and temporal components of the fuzzy set may cause difficulty in the risk analysis process. In this study the reliability assessment (later described in this Chapter) is based on the comparative analysis of two membership functions: (a) river flood damage membership function; and (b) the predefined acceptance level of partial river flood damage membership function. For i -th time step, the acceptance level of partial river flood damage results in a 2-D fuzzy set. In order to compare with a 2-D fuzzy set of acceptance level of partial river flood damage, the *3-D fuzzy set for spatial and temporal variability of river flood damage*

needs to be represented by a 2-D fuzzy set. In practice, the *3-D fuzzy set for spatial and temporal variability of river flood damage* can be approximated by performing a dimension reduction operation, which consists of constructing a 2-D fuzzy set for river flood damage at a particular location at a particular point in time. The dimension reduction operation uses the centroid operation in Equation (3.17) to determine the centre of gravity (Figure 3.10) of the *2-D fuzzy set for temporal variability of river flood damage* in *i*-th time step.

$$D_{i_G} = \left[\frac{\int_{D_{i_{\min}}}^{D_{i_{\max}}} D_i \tilde{S}_i(D_i) dD}{\int_{D_{i_{\min}}}^{D_{i_{\max}}} \tilde{S}_i(D_i) dD} \right] \quad (3.17)$$

where,

D_{i_G} denotes centre of gravity of the 2-D fuzzy set temporal variability of flood damage.

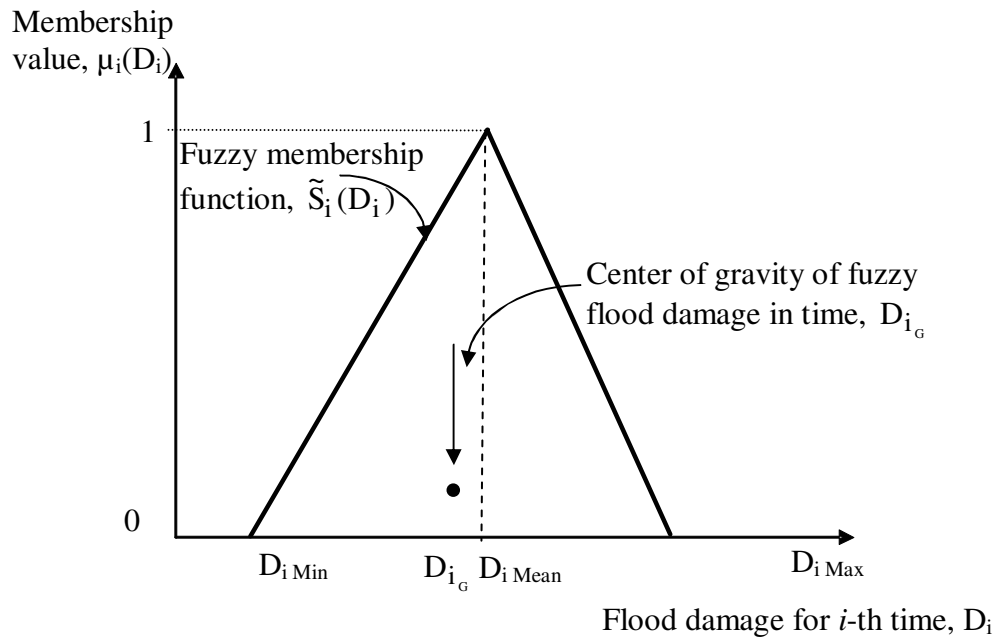


Figure 3.10: Center of gravity of the *2-D fuzzy set for temporal variability of flood damage*

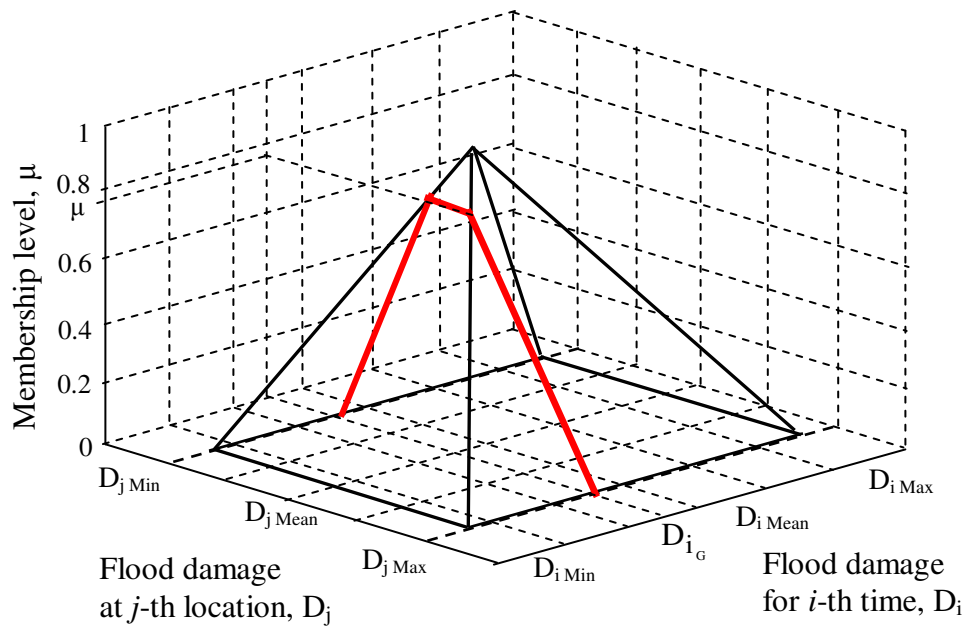


Figure 3.11: 2-D fuzzy set for spatial variability of flood damage at D_{i_g}

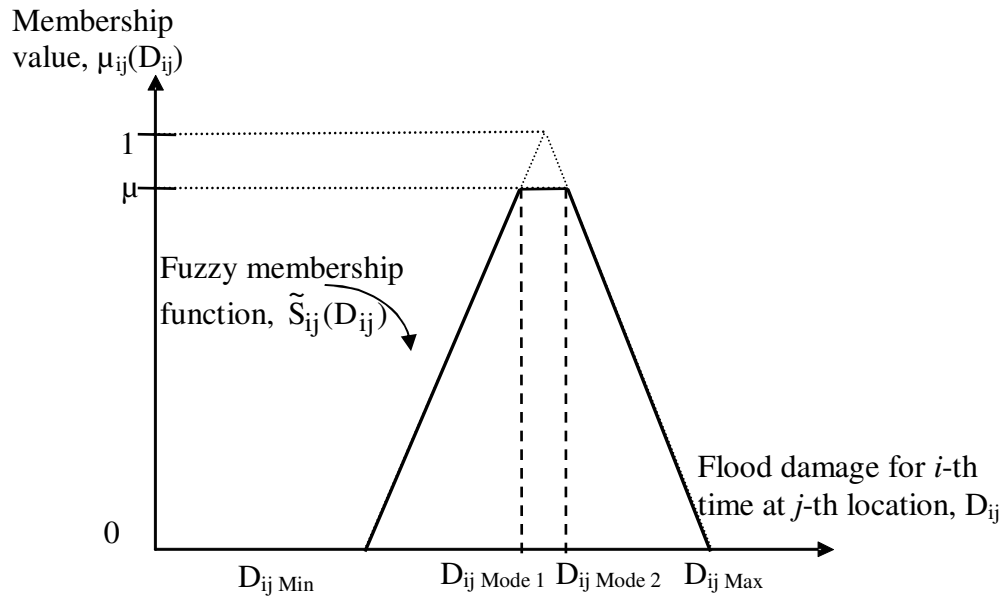


Figure 3.12: New 2-D fuzzy set for spatial and temporal variability of flood damage

From the 3-D fuzzy set a new 2-D fuzzy set is generated by calculating a 2-D fuzzy set for spatial variability of flood damage at the center of gravity D_{i_g} (Figure 3.11) of the 2-D fuzzy set for temporal variability of flood damage. The new 2-D fuzzy set is an approximate representation of the 3-D fuzzy set for spatial and temporal variability of flood damage. This new 2-D fuzzy set generates a trapezoidal flood damage membership function (Figure 3.12) defined in Equation (3.18), which represents spatial and temporal variability in river flood damage.

$$\tilde{S}_{ij}(D_{ij}) = \left\{ \begin{array}{ll} 0 & \text{if } D_{ij} \leq D_{ij \text{ Min}} \\ \frac{D_{ij} - D_{ij \text{ Min}}}{D_{ij \text{ Mode 1}} - D_{ij \text{ Min}}} & \text{if } D_{ij} \in [D_{ij \text{ Min}}, D_{ij \text{ Mode 1}}] \\ \frac{D_{ij \text{ Max}} - D_{ij}}{D_{ij \text{ Max}} - D_{ij \text{ Mode 2}}} & \text{if } D_{ij} \in [D_{ij \text{ Mode 2}}, D_{ij \text{ Max}}] \\ 0 & \text{if } D_{ij} \geq D_{ij \text{ Max}} \end{array} \right\} \quad (3.18)$$

where,

$\tilde{S}_{ij}(D_{ij})$ is the flood damage membership function for i -th time step at j -th location;

$D_{ij \text{ Mode 1}}$ and $D_{ij \text{ Mode 2}}$ are the modal values for i -th time step at j -th location; and

$D_{ij \text{ Min}}$ and $D_{ij \text{ Max}}$ are the lower and the upper bounds of flood damage for i -th time step at j -th location.

Total Flood Damage

The methodology presented here proposes the following equation (Equation 3.19) to capture the dynamic characteristics of river flood risk and its spatial variability:

$$D_T = \int_{i=0}^T \left[\int_{x=\alpha}^{\beta} \int_{y=v}^{\omega} F(D(x, y, i)) dx dy \right] di \quad (3.19)$$

where,

D_T denotes total flood damage;

x denotes x co-ordinate of the center of a grid cell at location j , $x \in [\alpha, \beta]$;

y denotes y co-ordinate of the center of a grid cell at location j , $y \in [v, \omega]$;

i denotes time step, $i \in [0, T]$; and

$F(D(x, y, i))$ denotes a function of flood damage with respect to space (x -coordinate, y co-ordinate) and time (i).

The integration in Equation (3.19) over the entire region and time horizon results in the total flood damage. This representation of flood risk has the potential for increasing our understanding of its dynamic character in time and location.

Fuzzy Flood Compatibility

The basis for reliability assessment in this study is the comparative analysis of two membership functions: (a) river flood damage membership function shown in Equation (3.18); and (b) the predefined acceptance level of partial river flood damage membership function shown in Equation (3.10). The purpose of the comparative analysis is to capture the extent to which the two fuzzy sets match (Figure 3.13). According to Zimmermann (1996) and Simonovic (2009), the extent of overlap between the two membership functions, represented as a fraction of the total area of the flood damage membership function, illustrates clearly the fuzzy compliance between the river flood damage

membership function and the acceptance level of partial river flood damage membership function.

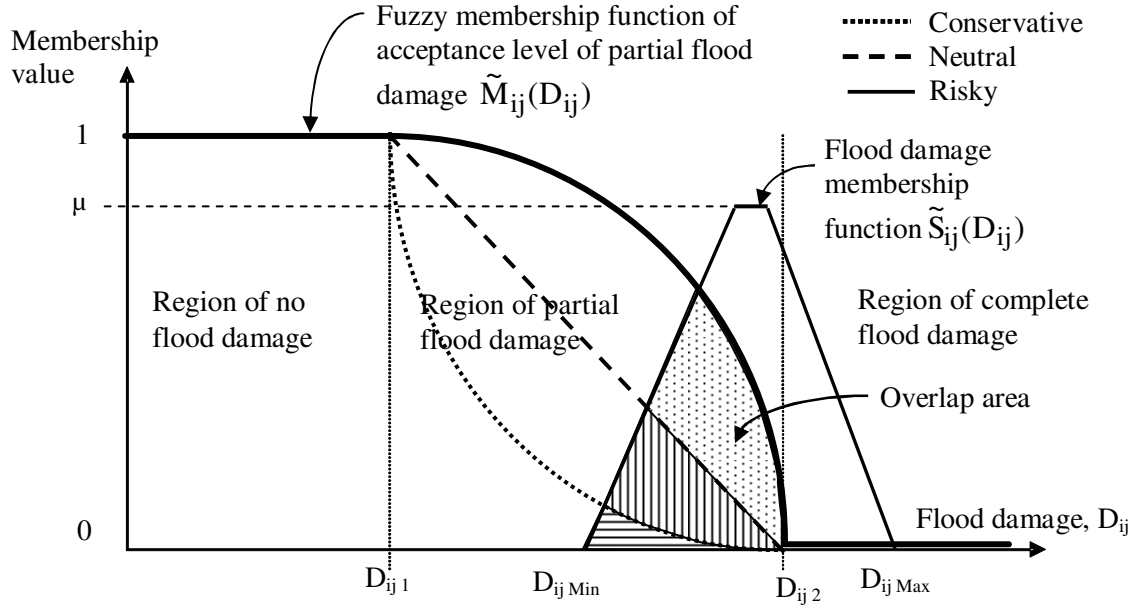


Figure 3.13: Overlap area between flood damage membership function and acceptance level of partial flood damage membership function

The compliance of two fuzzy membership functions can be mathematically presented using the fuzzy compatibility measure:

$$\text{Compatibility Measure, } CM_{ij} = \frac{OA_{ij}}{A_{ij}} \quad (3.20)$$

where,

CM_{ij} is the fuzzy compatibility for i -th time step at j -th location;

OA_{ij} is the overlap area for i -th time step at j -th location; and

A_{ij} is the total area under the flood damage membership function for i -th time step at j -th

location.

Verma and Knezevic (1996) state that an overlap in the area of high significance (area with high membership values) is preferable to an overlap in a low significance area. Thus, the fuzzy compliance takes into account the weighted area approach which modifies Equation (3.20) into:

$$CM_{ij} = \frac{WOA_{ij}}{WA_{ij}} \quad (3.21)$$

where,

CM_{ij} is the compatibility measure for i -th time step at j -th location;

W is the weight of the incremental area in terms of value of the membership function

WOA_{ij} is the weighted overlap area between the flood damage membership function and the partial level of flood damage membership function for i -th time step at j -th location; and

WA_{ij} is the weighted area of the flood damage membership for i -th time step at j -th location.

The calculation of the fuzzy compatibility measure is presented for the river flood damage membership function $\tilde{S}_{ij}(D_{ij})$, as shown in Figure 3.14. At any particular α -cut of width $d\alpha$, the corresponding left and right values of the universe of discourse are:

$$\begin{aligned}
D_{ij\ 11} &= D_{ij\ \text{Min}} + (D_{ij\ \text{Max}} - D_{ij\ \text{Min}}) \tilde{S}_{ij\ \alpha}(D_{ij\ 11}) \\
D_{ij\ 12} &= D_{ij\ \text{Min}} + (D_{ij\ \text{Max}} - D_{ij\ \text{Min}}) \tilde{S}_{ij\ \alpha}(D_{ij\ 12}) \\
D_{ij\ r1} &= D_{ij\ \text{Min}} + (D_{ij\ \text{Max}} - D_{ij\ \text{Min}}) \tilde{S}_{ij\ \alpha}(D_{ij\ r1}) \\
D_{ij\ r2} &= D_{ij\ \text{Min}} + (D_{ij\ \text{Max}} - D_{ij\ \text{Min}}) \tilde{S}_{ij\ \alpha}(D_{ij\ r2})
\end{aligned}
\tag{3.22}$$

where,

$\tilde{S}_{ij\ \alpha}(D_{ij})$ is the α -cut of fuzzy flood damage membership function for i -th time step at j -th location;

$D_{ij\ 11}$ is the first left (lower) flood damage value for i -th time step at j -th location;

$D_{ij\ 12}$ is the second left (upper) flood damage value for i -th time step at j -th location;

$D_{ij\ r1}$ is the first right (lower) flood damage value for i -th time step at j -th location; and

$D_{ij\ r2}$ is the second right (upper) flood damage value for i -th time step at j -th location.

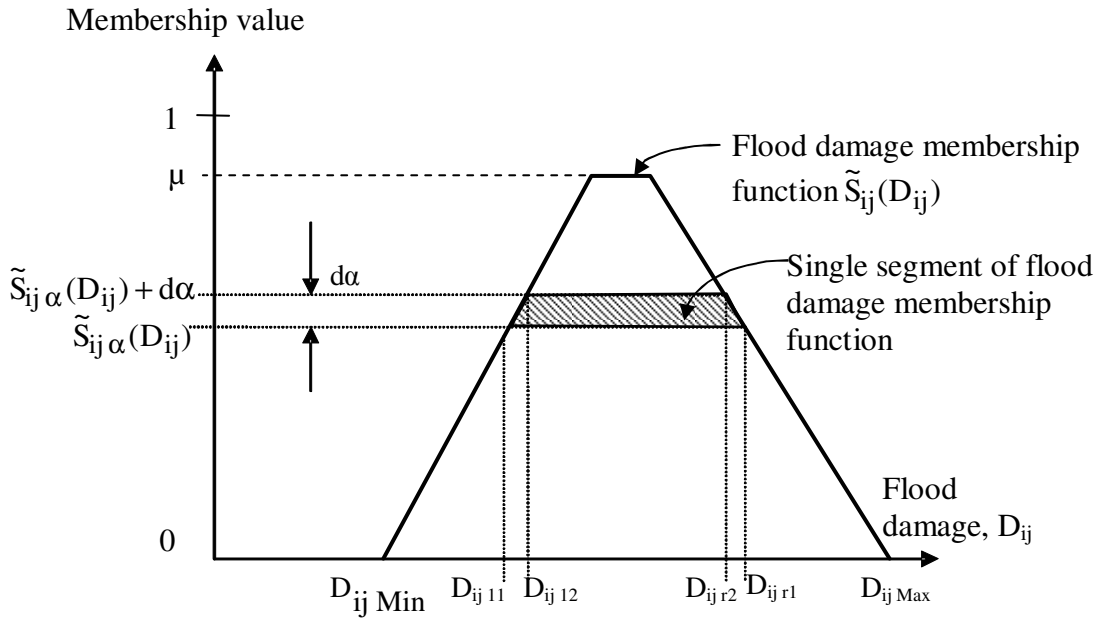


Figure 3.14: Weighted area calculation for the flood damage membership function

The area of the incremental α -cut for i -th time step at j -th location is calculated as follows:

$$dA_{ij} = \frac{(D_{ijr1} - D_{ijl1}) + (D_{ijr2} - D_{ijl2})}{2} d\alpha \quad (3.23)$$

The weight of this incremental area is the average value of the membership function:

$$W = \frac{\tilde{S}_{ij\alpha}(D_{ijl1}) + \tilde{S}_{ij\alpha}(D_{ijl2})}{2}$$

or

$$W = \frac{\tilde{S}_{ij\alpha}(D_{ijr1}) + \tilde{S}_{ij\alpha}(D_{ijr2})}{2} \quad (3.24)$$

As a result, the weighted area for i -th time step at j -th location equals:

$$dA_{w\ ij} = \left[\frac{(D_{ijr1} - D_{ijl1}) + (D_{ijr2} - D_{ijl2})}{2} d\alpha \right] \cdot \left[\frac{\tilde{S}_{ij\alpha}(D_{ijl1}) + \tilde{S}_{ij\alpha}(D_{ijl2})}{2} \right] \quad (3.25)$$

Integration of Equation 3.25 over the entire domain of α -cut values, i.e. from 0 to μ , results in the weighted area of the flood damage membership function, WA_{ij} for i -th time step at j -th location:

$$\begin{aligned}
WA_{ij} &= \int dA_{w\ ij} \\
&= \int_{\alpha=0}^{\mu} \left[\frac{(D_{ij\ r1} - D_{ij\ l1}) + (D_{ij\ r2} - D_{ij\ l2})}{2} d\alpha \right] \cdot \left[\frac{\tilde{S}_{ij\ \alpha}(D_{ij\ l1}) + \tilde{S}_{ij\ \alpha}(D_{ij\ l2})}{2} \right] d\alpha \quad (3.26)
\end{aligned}$$

Similar calculations apply to the overlap area (Figure 3.13) between the flood damage membership function and the predefined partial flood damage level membership function. The weighted area of the overlap for i -th time step at j -th location, WOA_{ij} , is calculated for determining the fuzzy compliance measure.

Fuzzy Combined Reliability-Vulnerability Index

Fuzzy reliability and fuzzy compatibility of two input membership functions are used in mathematical derivation of the fuzzy combined reliability-vulnerability index. “Reliability and vulnerability are used to provide a complete description of system performance in case of failure and to determine the magnitude of the failure event” (El-Baroudy and Simonovic, 2004). Fuzzy combined reliability-vulnerability index for flood risk assessment is calculated using:

$$RE_{ij} = \frac{\max_{f \in K} \{CM_{ij1}, CM_{ij2}, \dots, CM_{ijf}\} \times LR_{ij\ max}}{\max_{f \in K} \{LR_{ij1}, LR_{ij2}, \dots, LR_{ijf}\}} \quad (3.27)$$

where:

RE_{ij} is the fuzzy combined reliability-vulnerability index for i -th time step at j -th location;

$LR_{ij\ max}$ is the fuzzy reliability of the acceptance level of partial flood damage

corresponding to the maximum compatibility value for i -th time step at j -th location;

LR_{ijf} is the fuzzy reliability of the f -th acceptance level of partial flood damage for i -th time step at j -th location;

CM_{ijf} is the fuzzy compatibility for flood damage with the f -th acceptance level of partial flood damage for i -th time step at j -th location; and

$K (= f)$ is the total number of the defined acceptance levels of partial flood damage.

A flow chart in Figure 3.15 shows the process adopted for the calculation of the fuzzy combined reliability-vulnerability index. Computation of the fuzzy combined reliability-vulnerability index starts with the first i -th time step at j -th location. Flood damage is determined for i -th time step at j -th location. The next step deals with the generation of a *2-D fuzzy set for temporal variability of flood damage* and a *2-D fuzzy set for spatial variability of flood damage*. To describe the overall spatial and temporal uncertainty, a *3-D joint fuzzy membership function of flood damage* is generated for i -th time step at j -th location. Then the dimension reduction operation using Equation (3.17) calculates the center of gravity D_{i_g} of the *2-D fuzzy set for temporal variability of flood damage* to compress the *3-D joint fuzzy set* into a *2-D fuzzy set for spatial variability of flood damage* at D_{i_g} . This new 2-D trapezoidal fuzzy set is termed in this study as *2-D fuzzy set for spatial and temporal variability of flood damage* that represents both spatial and temporal variability. The program then proceeds to the next j -th location and follows the process described above to generate a *2-D fuzzy set for spatial and temporal variability of flood damage* for i -th time at next j -th location (grid cell). Once all the locations (grid cells) have been taken into consideration, the program generates fuzzy flood damage

maps for every j -th location in i -th time step. When all the locations (grid cells) have been taken into consideration, the program then generates the lower bound, the modal value, and the upper bound of the fuzzy flood damage maps for every grid cells for i -th time step.

The next step deals with the generation of the acceptance levels of partial flood damage and the computation of the weighted overlap area to determine the compliance level (Figure 3.15). In order to illustrate the range of stakeholder's preferences, three partial levels of flood damage are chosen in this study. They capture: (i) conservative acceptance level (for rising limb of the hydrograph); (ii) neutral acceptance level (for crest of the hydrograph); and (iii) risky acceptance level (for recession limb of the hydrograph). The acceptance levels of partial flood damage also differ for residential land and agricultural land. Thus the acceptance levels of partial flood damage are assigned according to location and time. The range of stakeholder's preferences is considered with different acceptance levels of partial flood damage. The computation of the weighted overlap area for f acceptance levels of partial flood damage determines the compliance level. Then fuzzy compatibility is calculated using Equation (3.21). The acceptance levels of partial flood damage result in raster maps with corresponding fuzzy compatibility values. Then Equation (3.27) is used to develop a single map containing the fuzzy combined reliability-vulnerability index for every j -th location in i -th time step.

Once the calculation is finished for the i -th time step, the program proceeds to the next i -th time step. The program follows the same approach described above to

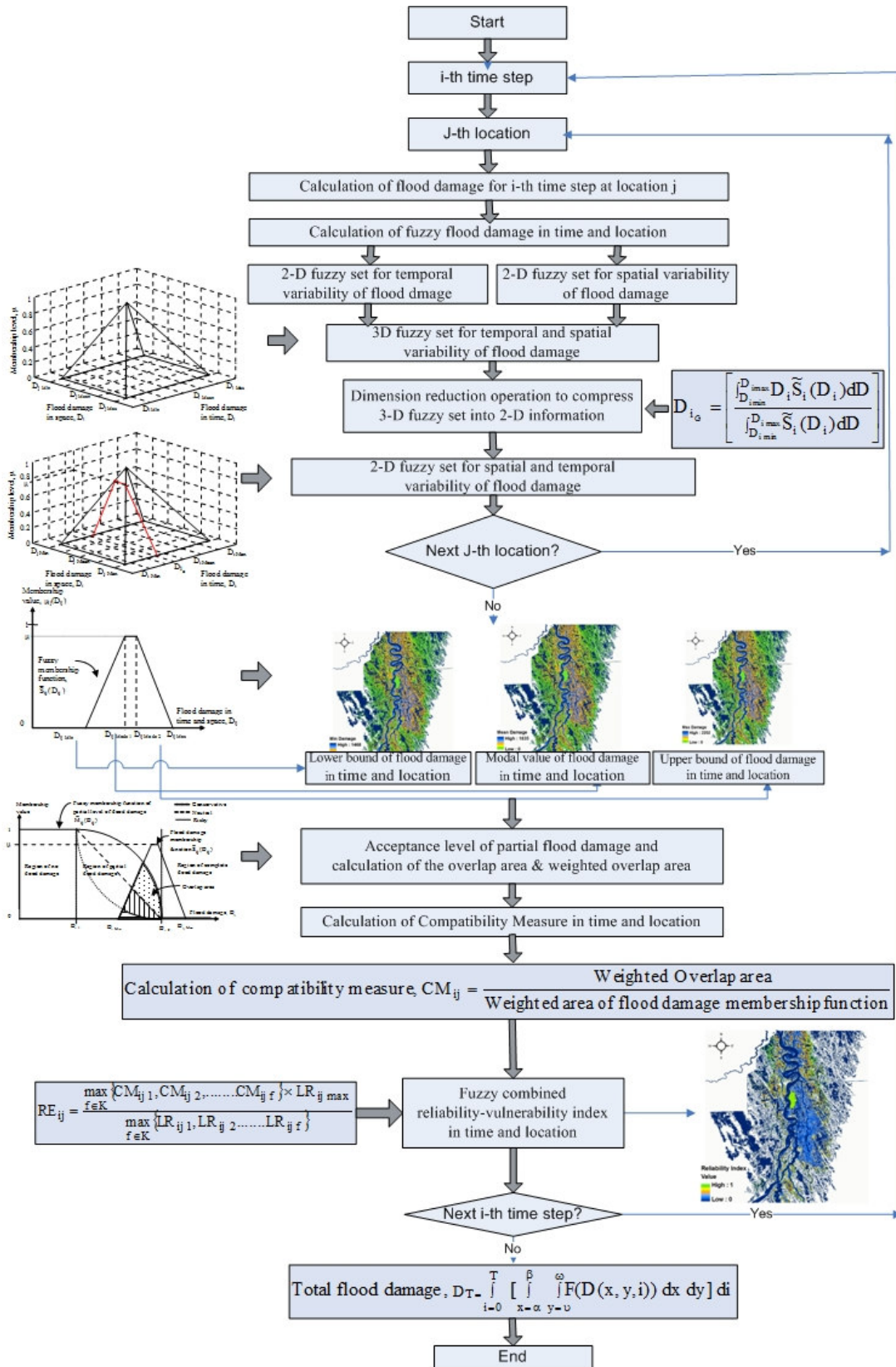


Figure 3.15: Flow chart of fuzzy combined reliability-vulnerability index

generate fuzzy combined reliability-vulnerability index for all locations (grid cells) at each time step. Once the program finishes calculation for all the time steps, total flood damage is calculated using Equation (3.19).

Fuzzy Robustness Index

The adaptability of the system to the change in the acceptance level of partial flood damage is spatially and temporally variable. Two maps containing compatibility measure values are used as inputs in the following Equation:

$$RO_{ij} = \frac{1}{CM_{ij1} - CM_{ij2}} \quad (3.28)$$

where:

RO_{ij} is the fuzzy robustness index for i -th time step at j -th location;

CM_{ij1} is the compatibility measure before the change in the partial level of flood damage for i -th time step at j -th location; and

CM_{ij2} is the compatibility measure after the change in the partial level of flood damage for i -th time step at j -th location.

The fuzzy robustness index is calculated as the inverse of the difference in compatibility values between the two acceptance levels of partial flood damage for each location and time. This inverse relation implies that the higher the change in compatibility the lower the fuzzy robustness value.

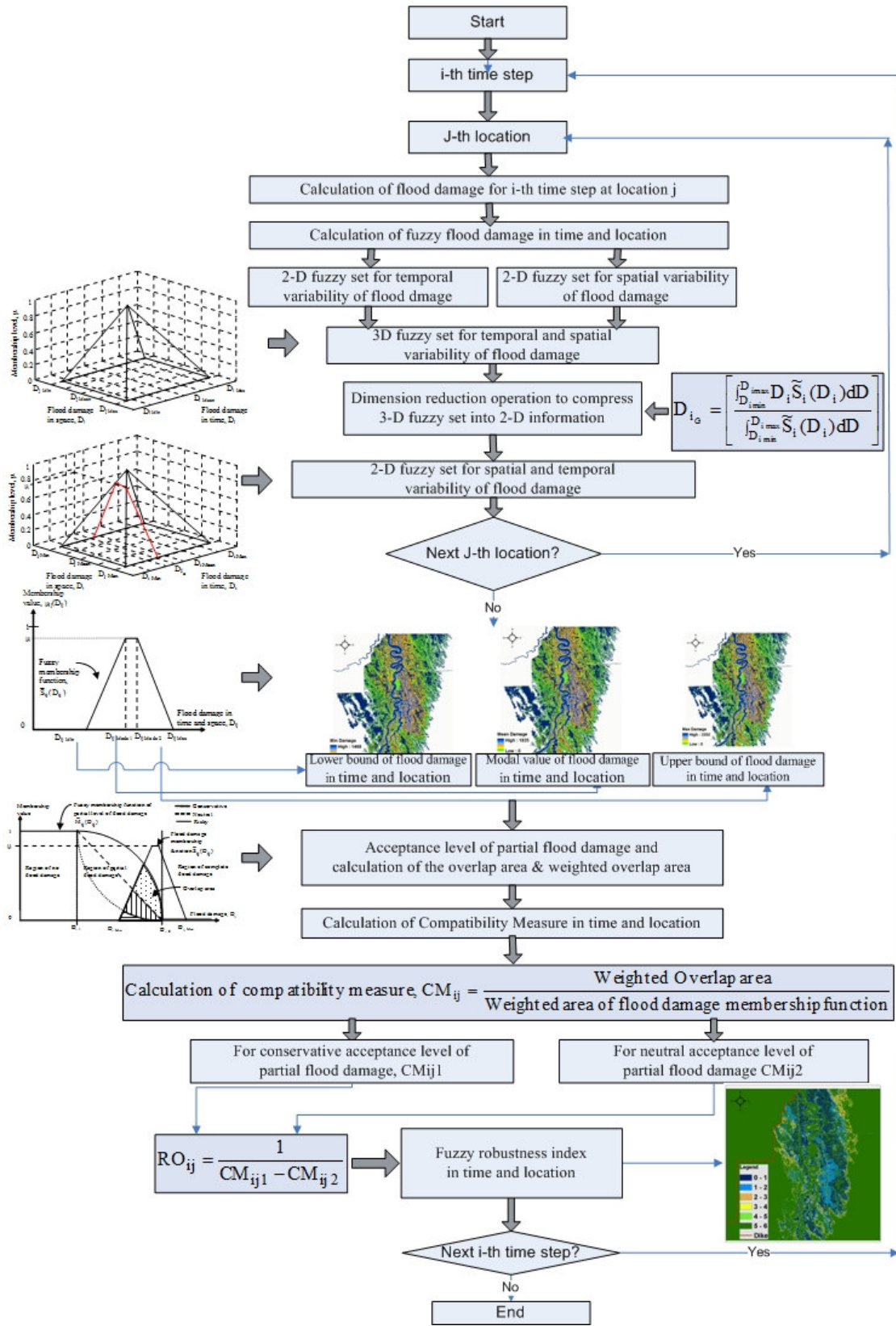


Figure 3.16: Flow chart of fuzzy robustness index

The calculation process of fuzzy robustness index is illustrated with a flow chart in Figure 3.16. The process of the fuzzy robustness index is identical up to the step where it considers the compatibility measure. The calculation of fuzzy robustness index also starts with the first i -th time step at j -th location. The next steps considers the generation of a 2-D fuzzy set for temporal variability of flood damage, a 2-D fuzzy set for spatial variability of flood damage, and a 3-D joint fuzzy set for both spatial and temporal variability of flood damage for i -th time step at j -th location. The dimension reduction operation using Equation (3.17) compresses the 3-D joint fuzzy set into a 2-D trapezoidal fuzzy set for spatial and temporal variability of flood damage, which is used to represent both spatial and temporal uncertainty. The program then proceeds to the next j -th location (grid cell) and follows the process described above to generate a 2-D fuzzy set for spatial and temporal variability of flood damage for i -th time at next j -th location (grid cell). When all the locations (grid cells) have been taken into consideration, the program then generates the lower bound, the modal value, and the upper bound of the fuzzy flood damage maps for every grid cells for i -th time step.

In the next step, the acceptance levels of partial flood damage are set. Then the computation of the weighted overlap area is used to determine the compliance level (Figure 3.16). For the illustration of methodology, two acceptance levels of partial flood damage are used to determine the robustness index in time and location: (i) conservative, and (ii) neutral. As a result, two maps of fuzzy compatibility are obtained from two acceptance levels of partial flood damage. In the next step Equation (3.28) is used to determine the fuzzy robustness index.

Once the calculation is finished for the i -th time step, the program proceeds to the next i -th time step. The program follows the same approach described above to generate a fuzzy robustness index for all j -th locations (grid cells) at each i -th time step. The program stops when it finishes the calculation of the fuzzy robustness index for all the i -th time steps.

Fuzzy Flood Recovery Time

Failures of engineering systems (in our case flood protection systems) may vary according to a number of factors, and for each type of failure the system might have a different recovery time. The time required to recover from the failure state can be represented as a fuzzy set to account for the uncertainty (imprecision) in its determination. Based on local factors (such as land-use type, available resources to help flood victims, etc.), an appropriate shape membership function is derived for every grid cell in space and at every time step. This derivation offers a more accurate representation of the recovery time. From a series of fuzzy membership functions developed for various types of failure and for different locations, the maximum recovery time is chosen to represent the system recovery time (Kaufmann and Gupta, 1985):

$$\tilde{T}_{ij}(\alpha) = \left(\max_{k=K} [t_{ij1_1}(\alpha), t_{ij1_2}(\alpha), \dots, t_{ij1_k}(\alpha)], \max_{k=K} [t_{ij2_1}(\alpha), t_{ij2_2}(\alpha), \dots, t_{ij2_k}(\alpha)] \right) \quad (3.29)$$

Where,

$\tilde{T}_{ij}(\alpha)$ is the system fuzzy maximum recovery time at α -cut for i -th time step at j -th location;

$t_{ij1_k}(\alpha)$ is the lower bound of the k -th recovery time at α -cut for i -th time step at j -th location;

$t_{ij2_k}(\alpha)$ is the upper bound of the k -th recovery time at α -cut for i -th time step at j -th location; and

K is total number of failure events.

Fuzzy Resiliency Index

The resiliency index measures the ability of a system to recover from the failure state. A resilient community is able to recover quickly from a flood disaster. After a disaster, post-flood recovery involves restoring all systems to normal or near normal condition. As a measure of the ability to recover, the time necessary to recover from flood is determined on the basis of water drainage, damage assessment, provisions for flood assistance to flood victims, time for rebuilding or repairing, and return to normal life (Morris-Oswald and Simonovic, 1997; Simonovic, 1999).

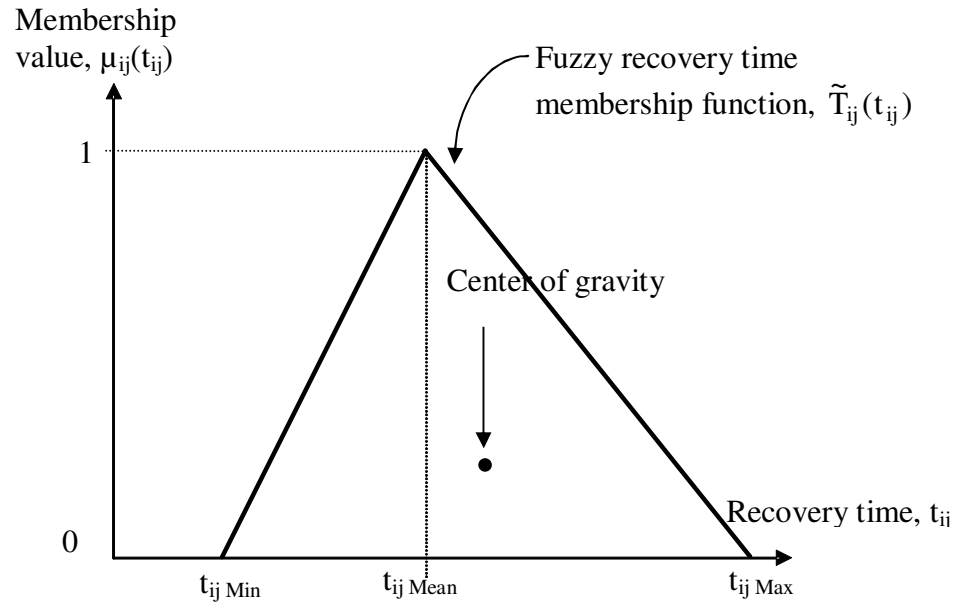


Figure 3.17: Fuzzy membership function of recovery time

The extent of flood damage to structures in residential areas and agricultural lands is a key factor in assessing the time required to recover from the flood damage. In most cases, high recovery cost corresponds to longer recovery time and vice-versa. Based upon this assumption, a recovery time vs. flood damage relationship is generated in this research for assessing the recovery time for residential and ring-diked communities in the post-flood stage. For agricultural areas the flood recovery time is assessed based on the flood recession date. For illustration purposes, a triangular fuzzy membership function is assigned to represent uncertainty in flood recovery time. The triangular shape of the membership function conveys the notion that the minimum and maximum recovery time values ($t_{ij \text{ Min}}$ and $t_{ij \text{ Max}}$) are concentrated around the modal value of the recovery time $t_{ij \text{ Mean}}$ and expressed mathematically as follows (Figure 3.17):

$$\tilde{T}_{ij}(t_{ij}) = \left\{ \begin{array}{ll} 0 & \text{if } t_{ij} \leq t_{ij \text{ Min}} \\ \frac{t_{ij} - t_{ij \text{ Min}}}{t_{ij \text{ Mean}} - t_{ij \text{ Min}}} & \text{if } t_{ij} \in [t_{ij \text{ Min}}, t_{ij \text{ Mean}}] \\ \frac{t_{ij \text{ Max}} - t_{ij}}{t_{ij \text{ Max}} - t_{ij \text{ Mean}}} & \text{if } t_{ij} \in [t_{ij \text{ Mean}}, t_{ij \text{ Max}}] \\ 0 & \text{if } t_{ij} \geq t_{ij \text{ Max}} \end{array} \right\} \quad (3.30)$$

where,

$\tilde{T}_{ij}(t_{ij})$ is the membership function of the flood recovery time for i -th time step at j -th location;

$t_{ij \text{ Mean}}$ is the modal value of the flood recovery time for i -th time step at j -th location; and $t_{ij \text{ Min}}, t_{ij \text{ Max}}$ are the lower and upper bounds of the flood recovery time for i -th time step at j -th location.

The inverse of the center of gravity of the recovery time is used to represent the resiliency. The fuzzy resiliency index is calculated as:

$$RI_{ij} = [CG_{ij}]^{-1} = \left[\frac{\int_{t_{ij \text{ Min}}}^{t_{ij \text{ Max}}} t_{ij} \tilde{T}_{ij}(t_{ij}) dt}{\int_{t_{ij \text{ Min}}}^{t_{ij \text{ Max}}} \tilde{T}_{ij}(t_{ij}) dt} \right]^{-1} \quad (3.31)$$

where,

RI_{ij} is the spatial fuzzy resiliency index for i -th time step at j -th location;

CG_{ij} is the center of gravity of the recovery time membership for i -th time step at j -th location; and

$\tilde{T}_{ij}(t_{ij})$ is the fuzzy recovery time membership function for i -th time step at j -th location.

3.2 URBAN FLOOD RISK ANALYSIS

Urban floods, in particular, may result in a high flood risk in areas with a high population density, major economic activities, a high concentration of infrastructure, and high property values (Pelling, 2003). Due to ongoing trends of population growth and an increase in the frequency and magnitude of river floods, both of which can be attributed to climate change, urban areas are at an increasingly greater risk for severe flood damage. Work presented in this research focuses on urban floods that result from heavy precipitation. Flood inundation maps representing flood water elevation are first generated for urban flood risk analysis. A one dimensional (1D) storm sewer model is coupled with a two dimensional (2D) overland flow model to produce flood inundation maps. After generation of the flood inundation maps, a damage analysis is performed and then fuzzy performance indices are developed to represent urban flood reliability-vulnerability, robustness and resilience (Figure 3.1).

The following section briefly describes the concept of a 1D/2D coupled hydrodynamic model and its use in this research to model the dynamic process of urban flooding.

3.2.1 MODELING DYNAMIC PROCESSES OF URBAN FLOODING – HYDRODYNAMIC MODELING APPROACH

Modeling the dynamic processes of urban flooding has become one of the main objectives in recent years in the field of hydraulics and urban hydrology. Urban flooding involves complex interactions between overland flows on the streets and flooding flows from sewer networks and rivers. The hydraulic models used to understand the physical

processes involved in urban flooding normally vary from one dimensional (1-D) to two dimensional (2-D) hydrodynamic models. Recent developments have led to an innovative concept that allows for a coupled (sewer/surface) hydraulic model, i.e. a one-dimensional (1-D) sewer model is coupled with a two-dimensional (2-D) surface flow model. The modeling approach used in this research also involves the integration of a 1-D sewer model and a 2-D surface flow model to describe the dynamic interaction between overland flows on the streets and storm sewer networks.

There are several causes that might be responsible for urban flooding, such as heavy precipitation, overland flows from river, etc. Usually the runoff starts as overland flow on the streets. This overland flow then enters the sewer network, i.e. the pipe network through manholes. Figure 3.18 shows how the manholes connect the street network with the sewer network.

The amount of water entering the sewer network depends on the intake capacity of the drainage system. If the intake capacity of the drainage system is sufficient then most of the runoff volume may be transported through the underground pipe system (Figure 3.19).

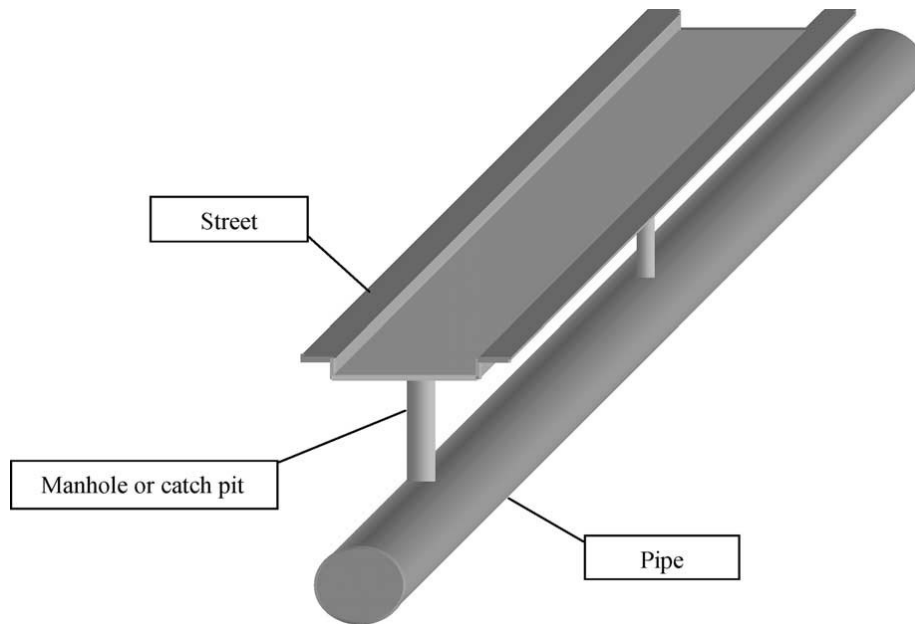


Figure 3.18: Layout of pipe and street system (after Mark *et al.*, 2004)

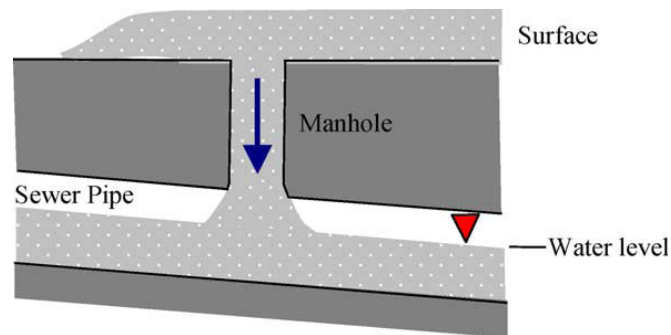


Figure 3.19: Flow from the street system into a partly full pipe (after Mark *et al.*, 2004)

However if the intake capacity is limited then only a small fraction of the runoff volume will enter the sewer networks, while the rest of the runoff volume will be transported on the surface. In such cases, the water may return back from the pipe networks to the street system, thereby causing surface flooding (Figure 3.19).

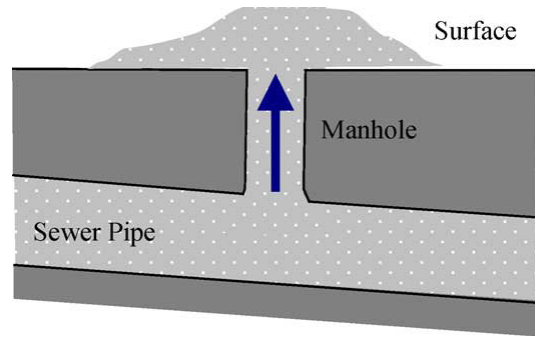


Figure 3.20: Flow to the streets from a pipe system with insufficient capacity (after Mark *et al.*, 2004)

In this research, the drainage system consists of a 1-D pipe flow model and a 2-D surface flow model. Computation of the unsteady flow in the 1-D pipe flow model is based on solving the 1-D Saint Venant equations, i.e. equations for the conservation of continuity (Equation 3.1) and momentum (Equation 3.2). The 2-D surface flow model solves the full 2D Saint Venant equation numerically, i.e. equations for the conservation of continuity (Equation 3.3), momentum in x direction (Equation 3.4), and momentum in y direction (Equation 3.5). The 1-D pipe flow model and the 2-D surface flow model constitute dynamically interconnected networks that route the rainfall runoff simultaneously. Manholes function as key features for exchanging flow between the sewer networks and street networks. This exchange of water is computed using the orifice equation, weir equation, or an exponential function. In this research the orifice equation is used as a function to drain ponded areas. The quantity of water flow and direction is determined based on the orifice equation (DHI, 2009).

$$Q_{UM2I} = \text{sign}(H_U - H_{M2I}) C \text{Min}(A_M, A_I) \sqrt{2g |H_U - H_{M2I}|} \quad (3.32)$$

Where

Q_{UM21} is the flow rate between 1D sewer model and 2D surface flow model,

H_U is the water level in the 1D sewer model,

H_{M21} is the water level in the surface flow model,

C is the orifice coefficient,

$\text{Min}(A_M, A_I)$ is the cross sectional area of the manhole in 1D sewer model or the inlet depending on which is smaller, and

g is the acceleration due to gravity.

3.2.2 URBAN FLOOD DAMAGE ANALYSIS

Flood damage analysis is an essential part of the urban flood risk management. Economic, social and ecological aspects should be considered while assessing urban flood risk (Kubal et al., 2009). Economic risk assessment is mostly based on the damage to residential buildings, industrial facilities, commercial buildings, transport facilities, etc. Social risk assessment focuses on the size of a population affected by urban flooding. Due to stress and psychological trauma, some flood victims may face severe psychological and emotional effects (Gruenwald, 2001; Kubal et al., 2009). Children and elderly people are the most vulnerable demographics in the case of an extreme flood event. Urban floods may further cause changes in the environment leading to ecosystem imbalances (Apel et. al., 2004). Normally, urban flood risk analysis is based on the assessment of economic damages. Due to a general lack of knowledge and the unavailability of required data, the social and ecological impacts of flood events are

generally not considered in the risk assessment process. Due to the limited scope of this research, urban flood risk analysis is being based mainly on the economic assessment of flood damage such as direct damage to buildings, and indirect damage to flood victims residing in affected residential areas. In this thesis total economic damage for a residential area is carried out by the following three steps

(i) Step One: Assessment of Direct Damage:

Direct damage usually considers the damage to buildings and infrastructure that is caused by urban flooding. Normally a depth-damage and depth-percent damage approach is used to assess direct damage. The depth-damage approach defines stage-damage relationships based on the available data (i.e. the data that is available from past instances of flood damage). Developing an individual depth-damage relationship for each type of structure is time consuming and expensive (Stuart, 1985). Furthermore the depth-damage relationship can only be used for a short period of time. On the other hand, the depth-percent damage function, a plot of floodwater depth versus percent damage, is widely used in practice due to ease application. A depth-damage relationship can be easily constructed by multiplying the percentage damage with a replacement value. Thus multiple stage-damage relationships can be constructed from one depth-percent damage relationship by changing only the replacement value. Accordingly, a depth-percent damage relationship is selected in this research to determine the extent and severity of damage to buildings (N.B. though the potential damage related to other forms of infrastructure is pertinent to flood risk management, this research focuses primarily on the damage related to buildings). Scawthorn *et al.*, (2006) used the depth-damage

functions for buildings developed by the Federal Insurance Administration (FIA), which are termed “credibility-weighted” depth-damage curves in their HAZUS Flood Model. Since in this research urban flood risk analysis is limited to residential areas, the FIA based depth-percent damage curve for two or more storied buildings (Scawthorn et. al, 2006) is used for determining direct damage. The percent of damage will be higher with increase in flood water level. If the percentage of damage has reached a certain threshold value then the building is considered to be a total loss. In this research the threshold value is considered at 50 percent damage of the replacement cost. Beyond this threshold value it is assumed that the building should be demolished and rebuilt.

(ii) Step Two: Assessment of Indirect Damage:

Besides physical damage on urban structures, in particular buildings, urban flooding can have a tremendous impact on business sectors in the sense that any kind of service interruption may result in a loss of money. For instance, regional suppliers depend heavily on conducting essential tasks in a certain/limited time frame, so if their level of efficiency is interrupted, this will have further consequences for those businesses that rely on the timely delivery of goods and services. Buyers/customers of these products will thus also face a great deal of inconvenience due to the interruptions as a result of urban floods. Any kind of service interruptions in industry, the transportation sector, and even the dislocation of communication services may cause tremendous economic damage, and this damage may further increase as a result of chain reactions, or the “ripple effect”, in business sectors (Scawthorn et. al, 2006). These kinds of losses are termed in this research as indirect economic damage. The length of time needed to restore business

operation can have significant impacts on the extent of indirect damage. The higher the restoration time required to return a system back to its normal running state, the more costly is the economic damage likely to be, and vice-versa. In such an event, the indirect damage may also be calculated in terms of loss of wages and even loss of employment as the result of the concomitant economic losses in business sectors.

In this research the urban flood risk analysis is mainly limited to residential areas. Therefore damage assessment is not directly linked to commercial and industrial areas. However, an innovative approach is used in this research that indirectly considers business loss for flood victims residing in affected residential areas. The methodology developed in this research is highly dependent on preparing a survey for the residents living in the flood affected areas. The detailed investigation carried out by this research focuses primarily on the likely consequences of service interruption and small business closure in the case of a flood event. For example, if a residential area is flooded then residents would likely face problems that may prevent them from going to work. If residents do not have any other alternative for making up for lost productivity, then it could result in a loss of wage. In the case of an important business meeting or a work project that needs to be completed within a certain period of time, the absence of the manager/client may lead to economic loss, the extent of which may be extremely high. In a residential area, the level and extent of these kinds of problem that a resident/labourer might face points to the diverse disruption in daily activities caused by flood events, thereby resulting in what this study has termed indirect damage. It is obvious that if residents face fewer road blockage as a result of urban flooding, then they will likely

experience little or no trouble in traveling to their workplace, however if the number of road blockage is quite high then the consequences may be significant in terms of indirect damage. The methodology used for determining indirect damage, in this research, is therefore based on number of road blockage vs. percentage damage relationship. This would be different in each case study and should not be used without detailed investigation.

(c) Step Three: Assessment of Total Urban Flood Damage

A weighted approach is used where direct damage and indirect damage are assigned with weights to assess total urban flood damage according to the following Equation:

$$\text{Total Damage} = \frac{\text{Direct Damage (\%)} \times w_1 + \text{Indirect Damage (\%)} \times w_2}{w_1 + w_2} \quad (3.33)$$

Where

w_1 is the weight of direct damage

w_2 is the weight of indirect damage

The weights assigned for direct damage and indirect damage should be carefully assessed. These weights are highly subjective and vary from one person to another based on their individual's perception of risk. Assessment of total urban flood damage would change based on the weights assigned to the direct damage and indirect damage.

3.2.3 SPATIAL AND TEMPORAL VARIABILITY OF URBAN FLOOD RISK

There are many sources of uncertainty associated with urban flood risk analysis. Urban flood damage assessment is subject to uncertainty due to a lack of data and ambiguity. In urban flood risk analysis uncertainty is mainly associated with spatial and temporal variability in urban stormwater hydrology, which includes variables such as precipitation; drainage area size, shape and orientation; ground cover and soil type; slope of terrain; vegetation; roughness; porosity; storage potential (wetlands, ponds, reservoir etc.); characteristics of drainage system, etc. Depending on the spatial and temporal variability of rainfall intensity, rainfall duration, and direction of storm movement there can be wide range of shapes of rainfall hyetographs. Spatial and temporal variability of these factors may augment or reduce the peak of the hyetograph.

The depth-damage relationship can also change with residential, commercial and industrial areas. This depth-damage relationship is spatially variable based on the type of structure, i.e. one, two or more stories, presence of basement, etc. Fuzzy membership functions are used to account for the uncertainty associated with variables used in urban flood risk analysis. Different shapes of membership functions, such as triangular, trapezoidal, Gaussian, exponential, etc., are used to express uncertainty. For example, the temporal uncertainty in the rainfall data can be expressed using a fuzzy triangular or trapezoidal membership function. In this study spatial and temporal uncertainty of these variables are considered in order to develop the methodology for spatial and temporal urban flood risk analysis using fuzzy performance indices.

3.2.4 A NEW METHODOLOGY FOR FUZZY URBAN FLOOD RISK

ANALYSIS

This section introduces the adaptation of the new methodology of three fuzzy performance indices: (i) a combined reliability-vulnerability index, (ii) a robustness index, and (iii) a resiliency index, for spatial and temporal variability of flood risk analysis in urban flood management. The approach to urban flood risk assessment uses a similar methodology (as described in section 3.1.4) as the one used for river flood risk analysis. It is based on the use of three fuzzy performance indices for addressing spatial and temporal variability in flood risk. Urban flood reliability analysis requires a definition of the unsatisfactory state of a system. Since there can be uncertainty associated in defining the failure state, the partial failure concept discussed in Section 3.1.4.1 is used to define the subjectivity in acceptance level of partial flood damage for urban flood risk analysis. Similarly, the methodology for urban flood risk analysis requires generating the system state membership function and the predefined acceptance level of partial flood damage membership function. Fuzzy set theory is used to address uncertainty related to urban flood management. The methodology presented here describes the development of fuzzy performance indices particularly for the spatial and temporal uncertainties inherent to urban flood management.

Definition of Partial Failure

The spatial and temporal variability of the acceptance level of partial flood damage for urban flood reliability analysis is addressed using the 3-D representation (Figure 3.6) of the partial level of flood damage (as described in section 3.1.4) as the one used for river

flood risk analysis. The shape of the acceptance level of partial flood damage membership function changes with time and location. This 3-D representation allows for the capturing of spatial and temporal variability in the acceptance level of partial flood damage that is based on decision makers' preferences for urban flood risk analysis. The acceptance level of partial urban flood damage is represented as a fuzzy membership function, $\tilde{M}_{ij}(D_{ij})$, based on the flood damage value D_{ij} in time and location in space (Figure 3.6). Acceptance level of partial urban flood damage membership function $\tilde{M}_{ij}(D_{ij})$ is defined using an equation similar to Equation 3.10, which is as follows:

$$\tilde{M}_{ij}(D_{ij}) = \left\{ \begin{array}{ll} 1 & \text{if } D_{ij} \leq D_{ij1} \\ \varphi_k(D_{ij}) & \text{if } D_{ij} \in [D_{ij1}, D_{ij2}] \\ 0 & \text{if } D_{ij} \geq D_{ij2} \end{array} \right\}$$

where,

D_{ij} is the flood damage for i -th time step at j -th location;

$\tilde{M}_{ij}(D_{ij})$ is the fuzzy membership function of margin of safety for i -th time step at j -th location;

D_{ij1} and D_{ij2} are lower and upper bounds of the acceptance level of partial flood damage for i -th time step at j -th location;

$\varphi_k(D_{ij})$ are functional relationships representing the subjective view of the partial risk for i -th time step at j -th location;

k ($= 1, 2, 3$) is the type of the acceptance level of partial flood damage membership function.

$k = 1$ denotes the conservative acceptance level of partial flood damage membership

function for i -th time step where $i \in [0, i_1]$ is for rising limb of the rainfall hyetograph;

$k = 2$ denotes neutral acceptance level of partial flood damage membership function for i -th time step where

$i \in [i_1, i_2]$ is for peak part of the rainfall hyetograph;

$k = 3$ denotes risky acceptance level of partial flood damage membership function for i -th time step where $i \in [i_2, i_3]$ is for recession limb of the rainfall hyetograph;

In the case of river flood risk analysis, the perception of flood risk and damage level varies with the time step of the stage and/or discharge hydrograph. However, in urban flood risk analysis the perception of flood risk and damage level varies with the time step of the rainfall hyetograph, which is based on the decision maker's preference towards the shape of the membership function $\tilde{M}_{ij}(D_{ij})$. Similarly, different time steps of the rainfall hyetograph are assigned to different shapes to reflect the subjectivity of the decision maker in urban flood risk analysis process: rising limb with conservative level of acceptance; a crest with neutral level of acceptance; and a recession limb with a risky acceptance level of partial flood damage. The perception of urban flood risk and damage level also varies spatially for different land use patterns, i.e. residential, industrial, commercial, etc. For example, in residential areas the distance of land parcels from the exit of a community may determine the shapes of the membership function $\tilde{M}_{ij}(D_{ij})$. In the case of an emergency evacuation, residents living further away from the exit are prone to higher flood risk, compared to the residents living closer to the exit. Therefore, based on the decision maker's perception of flood risk and damage level, different shapes of membership function $\tilde{M}_{ij}(D_{ij})$ may be assigned for different land parcels. The shape

of the membership function $\tilde{M}_{ij}(D_{ij})$ can be changed with time and location by assigning the value to the lower bound, D_{ij1} and/or the upper bound, D_{ij2} of partial level of urban flood damage.

If the value of urban flood damage exceeds D_{ij2} , then the region suffers complete damage (Figure 3.6). In this case the membership function $\tilde{M}_{ij}(D_{ij})$ value is equal to zero. If the value of urban flood damage is below D_{ij2} but exceeds D_{ij1} , then the region suffers partial urban flood damage. The membership function, $\tilde{M}_{ij}(D_{ij})$ of the acceptance level of partial urban flood damage attains its maximum value of one if the value of urban flood damage is below D_{ij1} .

The Reliability Measure (LR_{ij}) of the partial level of urban flood damage is calculated for i -th time step at j -th location $\tilde{M}_{ij}(D_{ij})$ using an equation similar to Equation 3.11, which is as follows:

$$LR_{ij} = \frac{D_{ij1} \times D_{ij2}}{D_{ij2} - D_{ij1}} \quad \text{where } D_{ij2} > D_{ij1}$$

Spatial and Temporal Variability of Fuzzy Flood Damage

The representation of spatial and temporal uncertainty in urban flood damage is assessed in this research based on the generation of a 3-D fuzzy set (Li et. al., 2007) that captures both spatial and temporal variability in urban flood damage. The methodology uses the

following four steps for representation of spatial and temporal variability of urban flood damage, a similar approach (as described in section 3.1.4) as the one used for river flood risk analysis:

(a) 2-D Fuzzy Set for Temporal Variability of Urban Flood Damage:

The temporal variation of urban flood damage is determined considering the uncertainty related to time variant properties by changing rainfall intensity only. Spatial uncertainty is not considered in determining temporal variability of urban flood damage. The methodology developed in this work considers the urban flood water level as the main source of temporal uncertainty in urban flood damage analysis. Urban flood damage, in residential areas, is determined using a depth-percent damage relationship. Thus, temporal variation of flood water level directly affects the variation of percent flood damage. Uncertainty in flood water levels is the result of our inability to accurately measure, calculate or estimate the flow value. A triangular fuzzy membership function is selected in this study to describe the temporal uncertainty of urban flood damage (Figure 3.7). The fuzzy membership function, representing the temporal variability of urban flood damage, is a two dimensional (2-D) fuzzy set with one dimension representing urban flood damage in i -th time, D_i and the other its membership degree. The definition of this *2-D fuzzy set for temporal variability of urban flood damage* is defined using an equation similar to Equation 3.12, which is as follows:

$$\bar{A} = \{(D_i, \tilde{S}_i(D_i)) \mid \forall D_i \in D\}$$

$$0 \leq \tilde{S}_i(D_i) \leq 1$$

where

\bar{A} denotes 2-D fuzzy set for temporal variability of flood damage;

D_i is the flood damage for i -th time step in the universe of discourse D ; and

$\tilde{S}_i(D_i)$ denotes membership degree of the 2-D fuzzy set.

In the case of a triangular membership function, the fuzzy urban flood damage function

$\tilde{S}_i(D_i)$ can be defined for i -th time step using an equation similar to Equation 3.13, which is as follows:

$$\tilde{S}_i(D_i) = \left\{ \begin{array}{ll} 0 & \text{if } D_i \leq D_{i \text{ Min}} \\ \frac{D_i - D_{i \text{ Min}}}{D_{i \text{ Mean}} - D_{i \text{ Min}}} & \text{if } D_i \in [D_{i \text{ Min}}, D_{i \text{ Mean}}] \\ \frac{D_{i \text{ Max}} - D_i}{D_{i \text{ Max}} - D_{i \text{ Mean}}} & \text{if } D_i \in [D_{i \text{ Mean}}, D_{i \text{ Max}}] \\ 0 & \text{if } D_i \geq D_{i \text{ Max}} \end{array} \right\}$$

where,

$\tilde{S}_i(D_i)$ is the flood damage membership function for i -th time step;

$D_{i \text{ Mean}}$ is the modal value of flood damage for i -th time step; and

$D_{i \text{ Min}}, D_{i \text{ Max}}$ are the lower and the upper bounds of flood damage for i -th time step.

(b) 2-D Fuzzy Set for Spatial Variability of Urban Flood Damage

Spatial variability of urban flood damage is determined by considering only the uncertainty related to location variant properties. Temporal variability is not considered in determining spatial variation of urban flood damage. In the case of residential areas, the type of structures, whether it is one storied, two storied or more, with or without

basement, location of land parcel, etc. will determine its property value and the type of depth-percent damage relationships that should be considered. Therefore the property value, as well as the depth-percent damage relationship, is location dependent. Thus, spatial variation of infrastructure/property value and depth-percent damage relationships directly affects the variation of urban flood damage. The fuzzy set approach is used to address spatial uncertainty with location variant properties. The spatial variability of uncertainty of urban flood damage is described in this study using a two dimensional (2-D) fuzzy set with one dimension representing the value of urban flood damage at j -th location, D_j and the other for its membership degree. The definition of this *2-D fuzzy set for spatial variability of flood damage* using an equation similar to Equation 3.14, which is as follows:

$$\bar{B} = \{(D_j, \tilde{S}_j(D_j)) \mid \forall D_j \in D\}$$

$$0 \leq \tilde{S}_j(D_j) \leq 1$$

where

\bar{B} denotes 2-D fuzzy set for spatial variability of flood damage;

D_j is the flood damage at j -th location in the universe of discourse D ; and

$\tilde{S}_j(D_j)$ denotes membership degree of the 2-D fuzzy set.

In the case of a triangular membership function shape (Figure3.8), the fuzzy urban flood damage membership function $\tilde{S}_j(D_j)$ can be defined for j -th location using an equation similar to Equation 3.15, which is as follows:

$$\tilde{S}_j(D_j) = \left\{ \begin{array}{ll} 0 & \text{if } D_j \leq D_{j \text{ Min}} \\ \frac{D_j - D_{j \text{ Min}}}{D_{j \text{ Mean}} - D_{j \text{ Min}}} & \text{if } D_j \in [D_{j \text{ Min}}, D_{j \text{ Mean}}] \\ \frac{D_{j \text{ Max}} - D_j}{D_{j \text{ Max}} - D_{j \text{ Mean}}} & \text{if } D_j \in [D_{j \text{ Mean}}, D_{j \text{ Max}}] \\ 0 & \text{if } D_j \geq D_{j \text{ Max}} \end{array} \right\}$$

where,

$\tilde{S}_j(D_j)$ is the flood damage membership function at j -th location;

$D_{j \text{ Mean}}$ is the modal value of flood damage at j -th location; and

$D_{j \text{ Min}}, D_{j \text{ Max}}$ are the lower and the upper bounds of flood damage at j -th location.

(c) 3-D Fuzzy Set for Spatial and Temporal Variability of Urban Flood Damage

2-D fuzzy sets for i) temporal variability of urban flood damage, and ii) spatial variability of flood damage, can address inherent temporal and spatial uncertainty, respectively. As described in Section 3.1.4, since neither i) nor ii) of the 2-D fuzzy sets are capable of representing the combined uncertainty of the urban flood risk that is both spatial and temporal in nature, a three dimensional fuzzy set (3-D fuzzy set) (Figure 3.9) is used to capture the inherent spatial and temporal uncertainty and subjectivity associated with the urban flood damage.

A 3-D fuzzy set (Li et. al., 2007) representing spatial and temporal variability of urban flood damage is developed (Figure 3.9) with the first dimension used for the urban flood damage for i -th time step, D_i ; the second dimension for the urban flood damage at j -th location, D_j ; and the third dimension its membership degree. This 3-D fuzzy flood set of urban damage represents both spatial and temporal uncertainty in urban flood damage at

every spatial location for every time step. The definition of *3-D fuzzy set for spatial and temporal variability of urban flood damage* using an equation similar to Equation 3.16, which is as follows:

$$\bar{V} = \{(D_i, D_j), \mu_{\bar{V}}(D_i, D_j) \mid \forall D_i \in D, D_j \in D\}$$

$$0 \leq \mu_{\bar{V}}(D_i, D_j) \leq 1$$

where

\bar{V} denotes 3-D fuzzy set for spatial and temporal variability of flood damage;

D_i is the flood damage in time for i -th time step in the universe of discourse D ;

D_j is the flood damage at j -th location in the universe of discourse D ; and

$\mu_{\bar{V}}(D_i, D_j)$ denotes membership degree of the 3-D fuzzy set.

(d) Dimension Reduction

3-D fuzzy set for spatial and temporal variability of urban flood damage represents spatial and temporal uncertainty related to urban flood management. The application of the developed methodology in urban flood management is also based on a comparative analysis of two membership functions: (a) urban flood damage membership function, and (b) predefined acceptance level of partial urban flood damage membership function, a similar approach (as described in section 3.1.4) as the one used for river flood risk analysis. Similarly, for i -th time step, the predefined acceptance level of partial urban flood damage results in a 2-D fuzzy set. For purposes of comparison with the 2-D fuzzy set of predefined acceptance level of partial urban flood damage, the *3-D fuzzy set for spatial and temporal variability of urban flood damage* needs to be represented by a 2-D

fuzzy set. Therefore, the *3-D fuzzy set for spatial and temporal variability of urban flood damage* is approximated by performing a dimension reduction operation, resulting in a 2-D fuzzy set for urban flood damage at a particular location at a particular point in time. The dimension reduction operation, as described in Section 3.1.4, is used to determine the centre of gravity (Figure 3.10) of the *2-D fuzzy set for temporal variability of urban flood damage* in *i*-th time step. The dimension reduction operation in urban flood risk analysis uses a centroid operation using an equation similar to Equation 3.17, which is as follows:

$$D_{i_G} = \left[\frac{\int_{D_{i_{\min}}^D}^{D_{i_{\max}}^D} D_i \tilde{S}_i(D_i) dD}{\int_{D_{i_{\min}}^D}^{D_{i_{\max}}^D} \tilde{S}_i(D_i) dD} \right]$$

where,

D_{i_G} denotes centre of gravity of the 2-D fuzzy set temporal variability of flood damage.

From the 3-D fuzzy set a new 2-D fuzzy set is generated by calculating a *2-D fuzzy set for spatial variability of flood damage* at the center of gravity D_{i_G} (Figure 3.11) of the *2-D fuzzy set for temporal variability of flood damage*. The new 2-D fuzzy set is an approximate representation of the *3-D fuzzy set for spatial and temporal variability of flood damage*. This new 2-D fuzzy set generates a trapezoidal flood damage membership function (Figure 3.12), which represents spatial and temporal variability in urban flood damage. This new trapezoidal membership function is defined using an equation similar to Equation 3.18, which is as follows:

$$\tilde{S}_{ij}(D_{ij}) = \left\{ \begin{array}{ll} 0 & \text{if } D_{ij} \leq D_{ij \text{ Min}} \\ \frac{D_{ij} - D_{ij \text{ Min}}}{D_{ij \text{ Mode 1}} - D_{ij \text{ Min}}} & \text{if } D_{ij} \in [D_{ij \text{ Min}}, D_{ij \text{ Mode 1}}] \\ \frac{D_{ij \text{ Max}} - D_{ij}}{D_{ij \text{ Max}} - D_{ij \text{ Mode 2}}} & \text{if } D_{ij} \in [D_{ij \text{ Mode 2}}, D_{ij \text{ Max}}] \\ 0 & \text{if } D_{ij} \geq D_{ij \text{ Max}} \end{array} \right\}$$

where,

$\tilde{S}_{ij}(D_{ij})$ is the flood damage membership function for i -th time step at j -th location;

$D_{ij \text{ Mode 1}}$ and $D_{ij \text{ Mode 2}}$ are the modal values for i -th time step at j -th location; and

$D_{ij \text{ Min}}$ and $D_{ij \text{ Max}}$ are the lower and the upper bounds of flood damage for i -th time step at j -th location.

Total Urban Flood Damage

The methodology uses the equation (Equation 3.19) to capture the dynamic characteristics of urban flood risk and its spatial variability:

$$D_T = \int_{i=0}^T \left[\int_{x=\alpha}^{\beta} \int_{y=v}^{\omega} F(D(x, y, i)) dx dy \right] di$$

Where,

D_T denotes total flood damage;

x denotes x co-ordinate of the center of a grid cell at location j , $x \in [\alpha, \beta]$;

y denotes y co-ordinate of the center of a grid cell at location j , $y \in [v, \omega]$;

i denotes time step, $i \in [0, T]$; and

$F(D(x, y, i))$ denotes a function of flood damage with respect to space (x -coordinate, y co-ordinate) and time (i)

Using this equation it is possible to determine the total urban flood damage over the entire location and time.

Fuzzy Flood Compatibility

The urban flood reliability assessment conducted in this study is based on the comparative analysis of two membership functions: (a) urban flood damage membership function; and (b) the predefined acceptance level of partial urban flood damage membership function. As described in Section 3.1.4, the purpose of the comparative analysis is to capture the extent to which the two fuzzy sets match (Figure 3.13). The compliance of the two fuzzy membership functions in urban flood risk assessment can be quantified for the fuzzy compatibility measure using an equation similar to Equation 3.20, which is as follows:

$$\text{Compatibility Measure, } CM_{ij} = \frac{OA_{ij}}{A_{ij}}$$

where,

CM_{ij} is the fuzzy compatibility for i -th time step at j -th location;

OA_{ij} is the overlap area for i -th time step at j -th location; and

A_{ij} is the total area under the flood damage membership function for i -th time step at j -th location.

Verma and Knezevic (1996) state that an overlap in the area of high significance (area with high membership values) is preferable to an overlap in a low significance area.

Thus, the compliance takes into account the weighted area approach, such that the compatibility measure can be calculated using Equation 3.21 as following:

$$CM_{ij} = \frac{WOA_{ij}}{WA_{ij}}$$

where,

CM_{ij} is the compatibility measure for i -th time step at j -th location;

W is the weight of the incremental area in-terms of value of the membership function

WOA_{ij} is the weighted overlap area between the flood damage membership function and the partial level of flood damage membership function for i -th time step at j -th location;

and

WA_{ij} is the weighted area of the flood damage membership for i -th time step at j -th location.

For more information on the calculation process of compatibility measure for i -th time step at j -th location, CM_{ij} , please see Section 3.1.4.

Fuzzy Combined Reliability-Vulnerability Index

Fuzzy combined reliability-vulnerability index is used in this research to determine the performance of the sewer system for urban flood risk management. The fuzzy combined reliability-vulnerability index is calculated using an equation similar to Equation 3.27, which is as follows:

$$RE_{ij} = \frac{\max_{f \in K} \{CM_{ij1}, CM_{ij2}, \dots, CM_{ijf}\} \times LR_{ij \max}}{\max_{f \in K} \{LR_{ij1}, LR_{ij2}, \dots, LR_{ijf}\}}$$

where:

RE_{ij} is the fuzzy combined reliability-vulnerability index for i -th time step at j -th location;

$LR_{ij \max}$ is the fuzzy reliability of the acceptable level of partial flood damage corresponding to the maximum compatibility value for i -th time step at j -th location;

LR_{ijf} is the fuzzy reliability of the f -th acceptable level of partial flood damage for i -th time step at j -th location;

CM_{ijf} is the fuzzy compatibility for flood damage with the f -th acceptable level of partial flood damage for i -th time step at j -th location; and

$K (= f)$ is the total number of the predefined acceptable levels of partial flood damage.

A flow chart in Figure 3.15 shows the process adopted for the calculation of the fuzzy combined reliability-vulnerability index for river flood risk management. The computation of a fuzzy combined reliability-vulnerability index, used in the case of urban flood risk analysis, is determined based on a similar approach (as described in section 3.1.4) as the one used for river flood risk analysis.

Fuzzy Robustness Index

The fuzzy robustness index is used to measure the ability of the system to adapt to a wide range of possible future conditions. In urban flood management, the fuzzy robustness index measures the adaptability of the system to the change in the partial level of urban

flood damage. The fuzzy robustness index is determined using an equation similar to Equation 3.28, which is as follows:

$$RO_{ij} = \frac{1}{CM_{ij1} - CM_{ij2}}$$

where:

RO_{ij} is the fuzzy robustness index for i -th time step at j -th location;

CM_{ij1} is the compatibility measure before the change in the acceptable level of partial flood damage for i -th time step at j -th location; and

CM_{ij2} is the compatibility measure after the change in the acceptable level of partial flood damage for i -th time step at j -th location.

The fuzzy robustness index is calculated as the inverse of the difference in compatibility values between the two acceptable levels of partial urban flood damage for each location and time. This inverse relation implies that the higher the change in compatibility the lower the fuzzy robustness value.

A flow chart in Figure 3.16 shows the process adopted for the calculation of the fuzzy robustness index for river flood risk management. The computation of the fuzzy robustness index, used in the case of urban flood risk analysis, is determined based on a similar approach (as described in section 3.1.4) as the one used for river flood risk analysis.

Fuzzy Resiliency Index

In urban flood risk management the resiliency index measures the ability of the system to recover from the failure state. In case of an urban flood disaster, post-flood recovery involves restoring all systems to normal or near normal condition. The time required to recover from the failure state depends largely on economic losses related to building repair, replacement costs, building content losses, relocation expenses, income losses, wage losses, etc.. A community that is able to recover quickly from such losses would be considered to be highly resilient.

In this research the extent of urban flood damage (as described in Section 3.2.2) in terms of (i) direct damage, and (ii) indirect damage in residential areas is considered a key factor in assessing the recovery time. If the extent of either (i) or (ii), and in worse cases both (i) and (ii), are high then the recovery cost will be more and therefore will correspond to a longer recovery time, and vice-versa. Based upon this assumption, a recovery time vs. flood damage relationship is generated in this research for illustration of the methodology only. This hypothetical recovery time vs. flood damage relationship could assess the recovery time for residential communities in the post-flood stage. In the interest of illustration, a triangular fuzzy membership function (Figure 3.17) is used to represent uncertainty in urban flood recovery time. The triangular shape of the membership function conveys the notion that the minimum and maximum recovery time values ($t_{ij \text{ Min}}$ and $t_{ij \text{ Max}}$) are concentrated around the modal value of the recovery time $t_{ij \text{ Mean}}$ and is expressed using an equation similar to Equation 3.30, which is as follows:

$$\tilde{T}_{ij}(t_{ij}) = \left\{ \begin{array}{ll} 0 & \text{if } t_{ij} \leq t_{ij \text{ Min}} \\ \frac{t_{ij} - t_{ij \text{ Min}}}{t_{ij \text{ Mean}} - t_{ij \text{ Min}}} & \text{if } t_{ij} \in [t_{ij \text{ Min}}, t_{ij \text{ Mean}}] \\ \frac{t_{ij \text{ Max}} - t_{ij}}{t_{ij \text{ Max}} - t_{ij \text{ Mean}}} & \text{if } t_{ij} \in [t_{ij \text{ Mean}}, t_{ij \text{ Max}}] \\ 0 & \text{if } t_{ij} \geq t_{ij \text{ Max}} \end{array} \right\}$$

where,

$\tilde{T}_{ij}(t_{ij})$ is the membership function of the flood recovery time for i -th time step at j -th location;

$t_{ij \text{ Mean}}$ is the modal value of the flood recovery time for i -th time step at j -th location; and

$t_{ij \text{ Min}}$, $t_{ij \text{ Max}}$ are the lower and upper bounds of the flood recovery time for i -th time step at j -th location.

Similar to determining the resiliency index in the case of river flood risk analysis, the process adopted here also uses the inverse of the center of gravity of the urban flood recovery time to represent the resiliency in the urban flood scenario. Therefore the fuzzy resiliency index is calculated using an equation similar to Equation 3.31, which is as follows:

$$RI_{ij} = [CG_{ij}]^{-1} = \left[\frac{\int_{t_{ij \text{ Min}}}^{t_{ij \text{ Max}}} t_{ij} \tilde{T}_{ij}(t_{ij}) dt}{\int_{t_{ij \text{ Min}}}^{t_{ij \text{ Max}}} \tilde{T}_{ij}(t_{ij}) dt} \right]^{-1}$$

where,

RI_{ij} is the spatial fuzzy resiliency index for i -th time step at j -th location;

CG_{ij} is the center of gravity of the recovery time membership for i -th time step at j -th location; and

$\tilde{T}_{ij}(t_{ij})$ is the fuzzy recovery time membership function for i -th time step at j -th location.

4 CASE STUDY

The methodology used for the fuzzy reliability analysis and its application to river and urban flooding is described in Chapter 3. The necessary information for carrying out the computations for (i) river flood risk analysis, and (ii) urban flood risk analysis is described in Chapter 4. For the river flood risk analysis, the presented methodology is illustrated using the Red River flood of 1997 (Manitoba, Canada) as a case study. For urban flood risk analysis, the presented methodology is illustrated using the residential community of Cedar Hollow, London, Ontario as a case study. This Chapter presents the two case studies and the final results of the spatial and temporal variation of fuzzy performance indices: (i) combined reliability-vulnerability, (ii) robustness, and (iii) resiliency, presented using maps, for river flood risk analysis in the Red River basin, and urban flood risk analysis of Cedar Hollow community of London, Ontario.

4.1 RIVER FLOOD RISK ANALYSIS: THE RED RIVER BASIN CASE STUDY

The Red River originates in the north-central United States and flows north. It forms the boundary between North Dakota and Minnesota and enters Canada at Emerson, Manitoba. It continues northward to Lake Winnipeg. From its origin to its outlet in Lake Winnipeg, the river is 563 km long. The Red River basin covers 116,500 km² (exclusive of the Assiniboine River and its tributary, the Souris), of which nearly 103,500 km² is within the USA. The remaining 13,000 km² is in Canada. In the city of Winnipeg, the Red River is joined by its major tributary, the Assiniboine River, from the west. The Canadian portion of the Red River basin is shown in Figure 4.1. In this study the Red River basin, which is comprised of the community of St. Agathe to the south of the

Winnipeg floodway in Manitoba, Canada, is used to illustrate the applicability of the proposed fuzzy performance indices for flood risk analysis. The specific characteristics of the Red River basin include flat topography, frequent flooding, a river passing through Winnipeg, and the presence of flood control structures such as diversions, a floodway, dikes and a reservoir. The operational strategy of the major protection works, such as gates, a floodway and diversions, is in place to provide the necessary protection for Winnipeg.

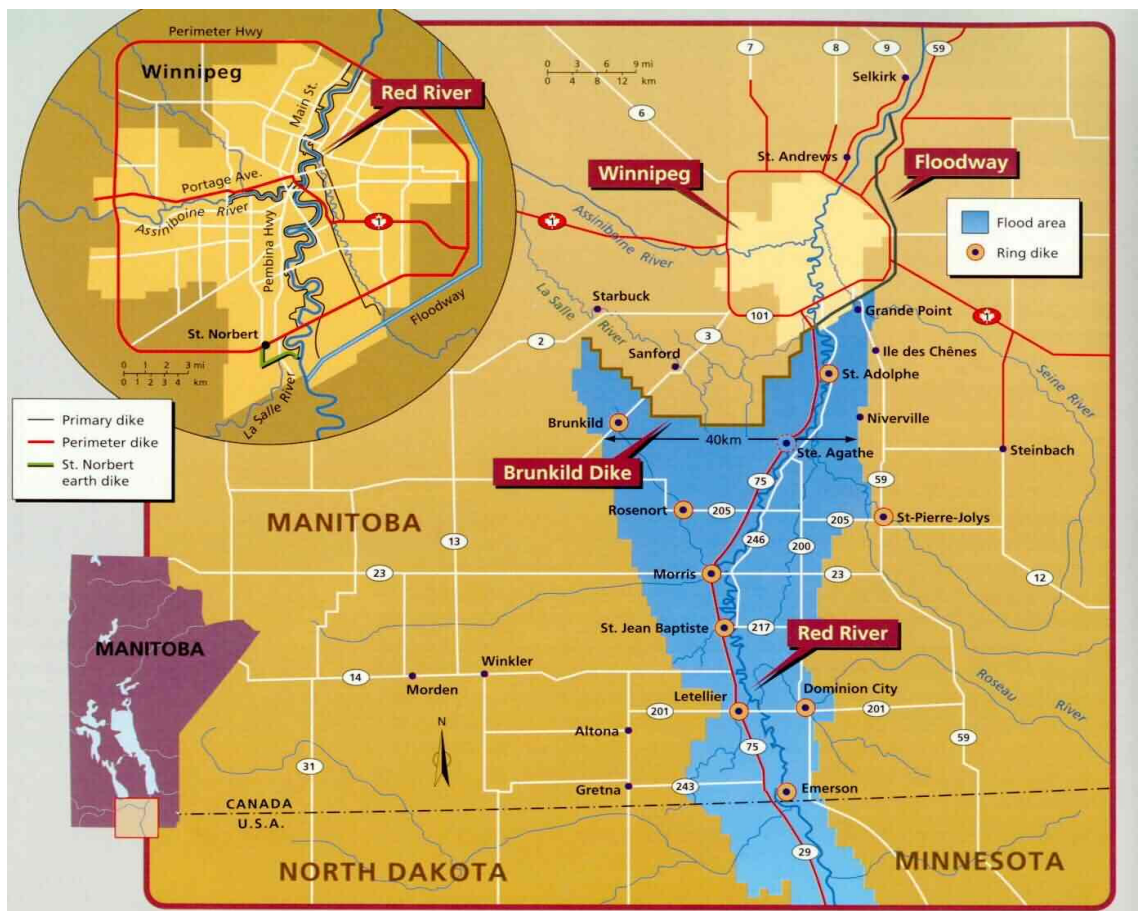


Figure 4.1: Canadian portion of the Red River basin (after Winnipeg Free Press).

The Red River valley is a highly productive agricultural area serving local, regional and international food needs. The Red River basin has a sub-humid to humid continental

climate with moderately warm summers, cold winters, and rapid changes in daily weather patterns. Extreme temperature variations are the norm. On average the Red River basin's mean monthly temperature ranges from -15 degrees to +20 degrees Celsius. About three-quarters of the basin's approximately 50 cm of annual precipitation occur from April through September, with almost two-thirds falling during May, June and July. November through February are the driest months (IJC, 1997). Flow records show that approximately 80% of the peak flows at the Redwood Bridge in Winnipeg come from the main stem of the Red River. Furthermore, a very large portion of these peak flows, some 80 percent or more, originate from within the United States.

The basin is remarkably flat. The slope of the river averages about 0.05 meters per km. The basin is about 100 km across at its widest. During major flooding events the entire valley becomes a floodplain. The drainage area of the Red River has two basic types of topography. The central portion of the area, extending east and west of the river is the bed of the former glacial lake Agassiz. This region is a broad, flat plain with very gentle slopes. As a result, once the river overflows its banks a very large area is subject to flooding. Surrounding the plain is a rough and higher upland region. Because of the gentle slopes that characterize this former lakebed, the Red River and the lower end of its tributaries normally do not develop a velocity that is sufficiently strong enough to cut channels adequate to carry higher flows. Therefore it fails to mitigate flood risk when Red River and its tributaries are posed by higher flows.

The soil covering the Red River plains consists of highly plastic clay, which is able to

hold large quantities of water and, with changes in moisture content, demonstrates high swelling and shrinking characteristics. These characteristics make this soil type a very poor material foundation, which is further compounded by the instability and vulnerability to mud slides of the riverbanks in many areas. These hydrologic, meteorological, and topographic factors are all very important in understanding the flooding in the basin. Further details on the study area can be found in IJC (1997). The characteristics of flooding in the area are also discussed in detail by the Royal Commission (1958).

The earliest flood recorded in the Red River basin was in 1826. However, anecdotal evidence refers to larger flood events that date back as early as the late 1700s. Between 1862 and 1948, there are records of few major floods of the Red River. The 1826 flood is the largest flood in the recorded history of the Red River basin. Other than the 1826 flood, the 1997 flood exceeds the rest of the flood events.

The Red River basin experienced heavy precipitation in the fall of 1996 (10 cm above average). The winter of 1996-1997 was very severe. Record or near record snowfall occurred throughout the basin. The Red River basin also experienced heavy early spring precipitation and the temperatures were unreasonably high, such that they resulted in a major meltdown of snow. Records show that the Red River started to flood on March 30. In Winnipeg floodwaters were at their crest level on May 4, 1997. About 2000 km² or 5% of Manitoba's farm lands were flooded. Approximately 28000 Manitobans (6000 from Winnipeg) were evacuated. The damage from the 1997 flood event is in the hundreds of

millions of dollars.

After the 1950 flood, the Canadian portion of the Red River basin was designed using major flood management planning strategies. A commission was set up (Royal Commission, 1958) that recommended the construction of several flood control structures in the basin. Construction of elevated dikes and pumping stations within the City of Winnipeg were initiated in 1950. The Red River Floodway (completed in 1966) represented a major flood control work in the Red River basin. It was constructed to reduce flooding in the city of Winnipeg by diverting water from the Red River. In the early 1970s, construction of a series of ring dikes around communities in the Red River basin was initiated as a flood protection measure. A schematic diagram of flood control structures in the Canadian portion of the Red River basin is shown in Figure 4.2. The Portage Diversion was constructed to divert the water in the Assiniboine River to Lake Manitoba through a diversion channel with a water holding capacity 710 m³/s.

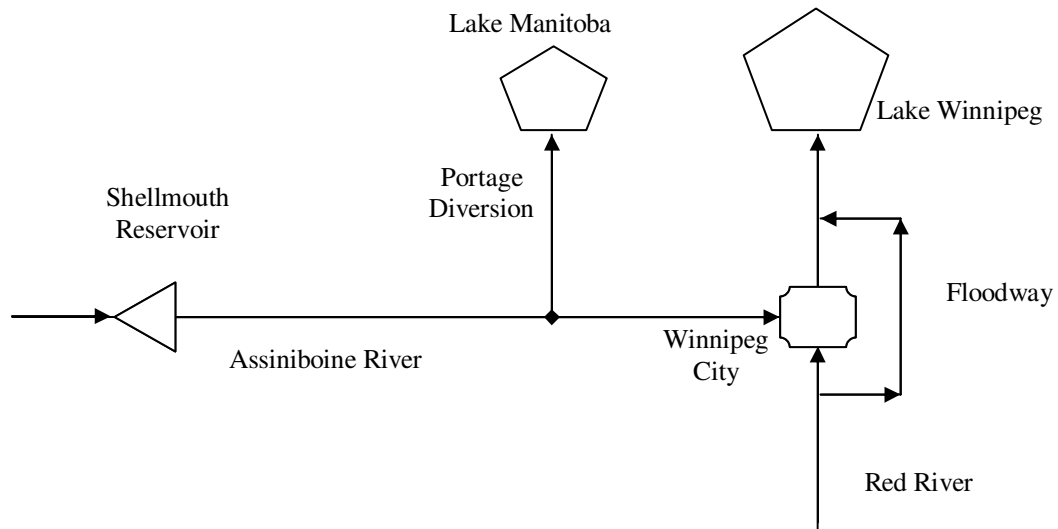


Figure 4.2: Schematic diagram of the flood control structures.

The so-called “Flood of the Century” data from 1997 are used in this case study. Two modeling tools are used to simulate the overland flooding in the Red River basin: (i) MIKE 21 (DHI, 2008), a two-dimensional hydrodynamic modeling tool, and (ii) Stella, a system dynamics modeling tool. The focus area for the study is taken from south of the Winnipeg floodway to the town of St. Agathe. The St. Agathe town was completely flooded during the 1997 flood event. The flow in this area went predominantly beyond the x-section of the river once the flood had arrived. The pockets formed by highways 330, 305, 75 and the CN railway line are shown in Figure 4.3. This made the task of 2-D hydrodynamic modeling very challenging in this region.

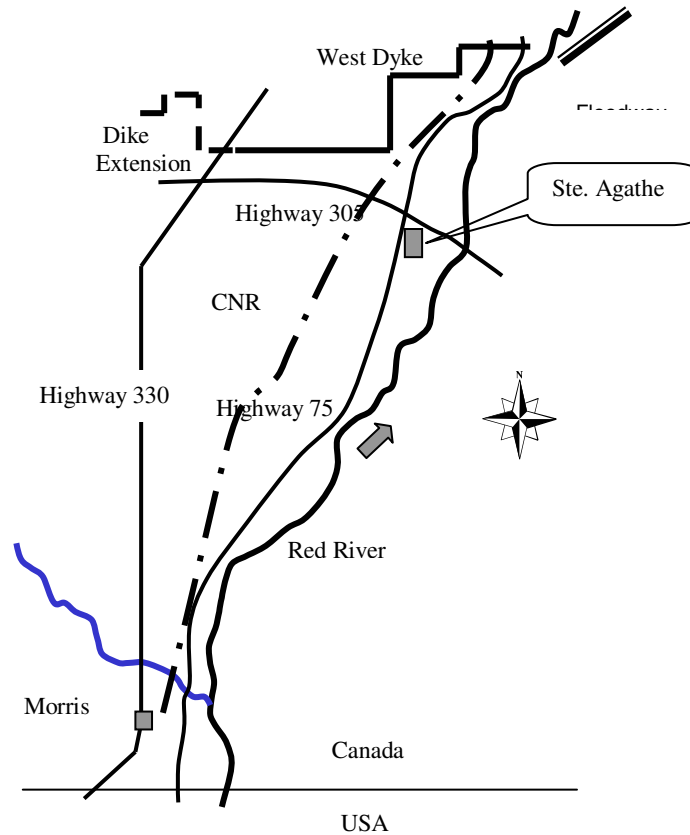


Figure 4.3: Schematic diagram of the infrastructure in the study area

4.1.1 2D HYDRODYNAMIC MODELING OF THE RED RIVER CASE STUDY

The data required for 2-D hydrodynamic modeling can be divided into two categories: (i) hydrologic data, and (ii) topographic data.

(i) Hydrologic Data

Hourly data of the Red River discharge near Ste. Agathe (St. No. 05OC012), and hourly stage data taken above the Red River Floodway control structure (St. No. 05OC021), both of which are used in this study, are collected from the Water Survey of Canada (WSC). Hourly wind data recorded at the Winnipeg airport is also used. Hourly

discharges at the Red River near Ste. Agathe and hourly water levels below the floodway are used as upstream and down stream boundary conditions, respectively. The data required for calibration include the Manning's roughness coefficient for river and floodplains, the eddy viscosity, and a wind friction coefficient. The main criteria for calibration consisted of matching the extent and depth of flooding produced by the MIKE 21 hydrodynamic model with the extent of flooding obtained from aerial photographs taken during the 1997 flood.

(ii) Topographic Data

The topographic data set used for this study is provided by the IJC. This data set appears in the form of ArcInfo GRID files (5m by 5m) and is derived from LIDAR airborne surveys (LaserMap Images Plus, 1999). The area covered by this data is 688 km², from south of the Winnipeg floodway to Ste. Agathe. This area is covered by 43 sheets, where each sheet covers 16 square kilometers (4 km × 4 km). The projection for this data set is UTM NAD83 Zone 14 (North) and for the Vertical Datum is CGVD1928. Figure 4.4 shows one sheet covering the case study area within the Red River basin.

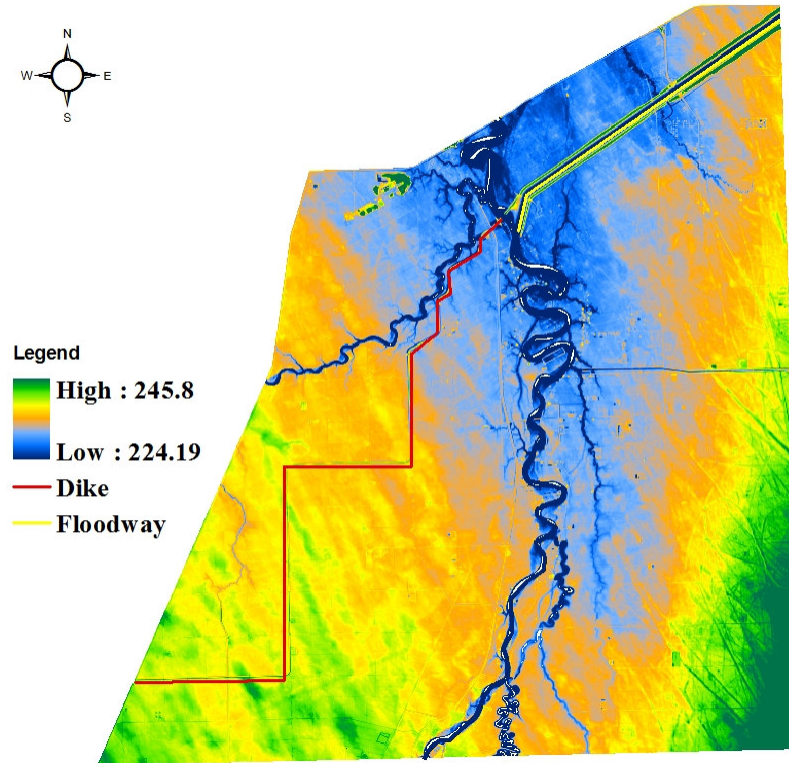


Figure 4.4: Topographic data of the Red River Case study

Hydrodynamic Modeling Approach

The schematic diagram of the MIKE 21 hydrodynamic modeling approach is presented in Figure 4.5. First, the hydrodynamic module is selected. Since LIDAR data does not include the cross-sectional information on the main branch of the Red River this information is taken from old data sets. A digital elevation model (DEM) is generated from this topographic data set by processing the data in GIS. The DEM was processed in GIS, thereby giving it a spatial resolution of 25m. This DEM is then converted to an ASCII format (x,y,z coordinates) using scripts written in AML (ArcView Macro Language). This conversion is required to import data in the MIKE 21 model as a bathymetry file. The simulation period is then chosen. In this case, the simulation period

spans from 22 April, 1997 to 31 May, 1997. A time step of 2 seconds is used. Boundary locations, source and sink locations, and flooding and drying depth, are used as basic parameter inputs in the hydrodynamic model. MIKE 21 uses a detailed description of topography and additional terms in mass and momentum equations. Therefore, MIKE 21 requires more time and computational resources to simulate a hydrologic event. In this case study, the computation time in MIKE 21, with a time step of 2 seconds and a spatial resolution of 25 m is around 12 days.

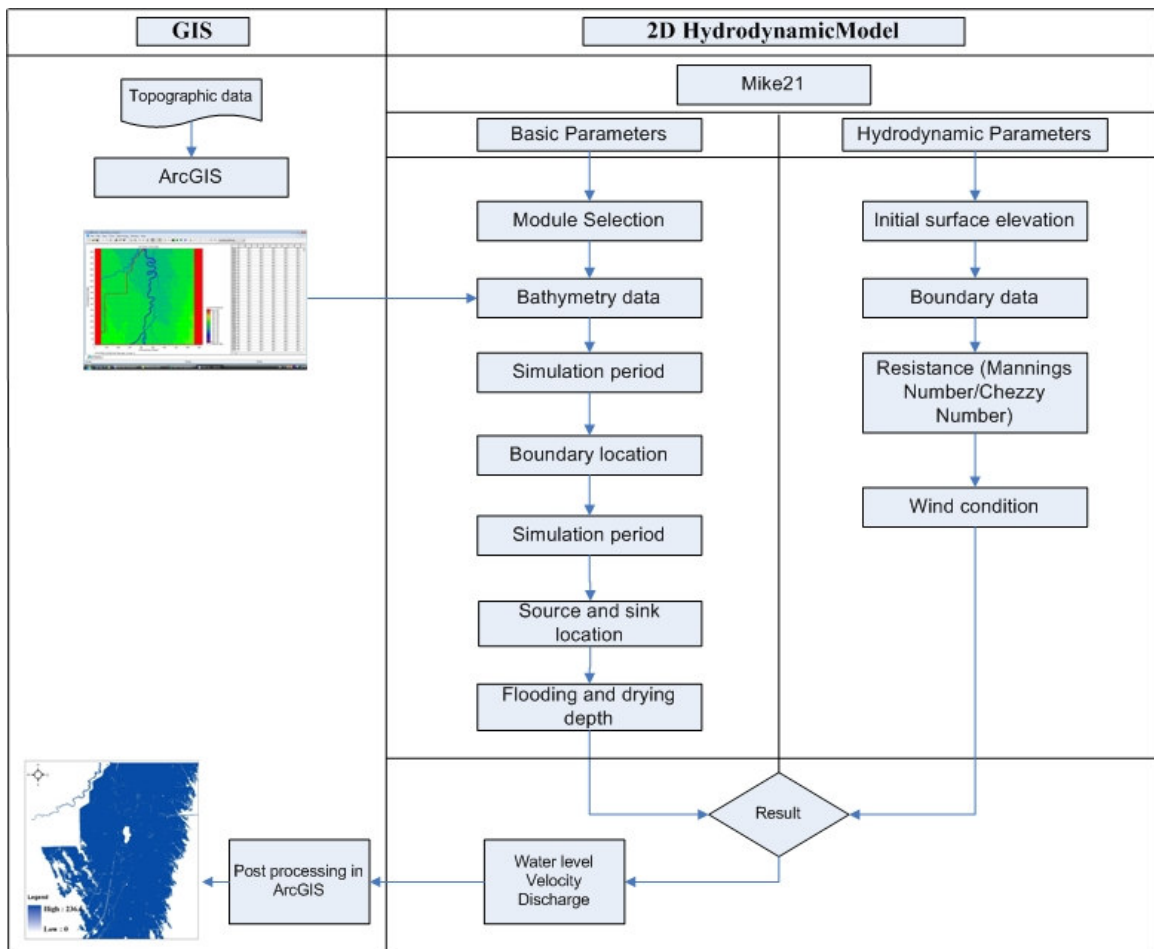


Figure 4.5: Schematic diagram of 2-D modeling approach.

Flooding and drying banks are important in the floodplains as well as along the main river channel. MIKE 21 incorporates drying and flooding banks in a robust manner without excessive smoothing of bathymetry. Whenever the water level at a particular grid falls below the user defined value, this grid is taken out of the calculation of the flooded area. When water level in that cell reaches a certain threshold value then that particular cell is added into calculation of the flooded area. Initial surface elevation, boundary conditions (upstream and downstream), and calibration parameters, are also provided for the MIKE 21 model. For boundary conditions in the MIKE 21 model, hourly stage data taken above the Red River Floodway control structure (St. No. 05OC021) and hourly discharge near Ste. Agathe (St. No. 05OC012), are taken as the upstream and downstream boundary conditions, respectively. The model requires calibration using trial and error procedures. However, to provide for a better comparison with MIKE 11, this study decided to use the Manning's roughness coefficient (n) value 0.067 for the floodplains reported by Klohn-Crippen (1999). After the calibration of the model, different flooding scenarios were explored. The results of MIKE 21 can either be viewed directly or they can be displayed over topographic data through GIS. The model output includes water surface elevation, and velocity and discharge in x- and y-directions.

4.1.2 SPATIAL AND TEMPORAL RISK ANALYSIS OF THE RED RIVER FLOOD OF 1997

The spatial and temporal fuzzy risk analysis of the Red River flood of 1997 is performed using Equations (3.27), (3.28) and (3.31). The fuzzy flood damage membership functions for agricultural land and residential land (including ring-diked communities) are

developed based on the flood damage data. The compliance of the flood damage membership function with different partial levels of flood damage membership functions (Figure 4.6) are assessed for i -th time step at j -th location.

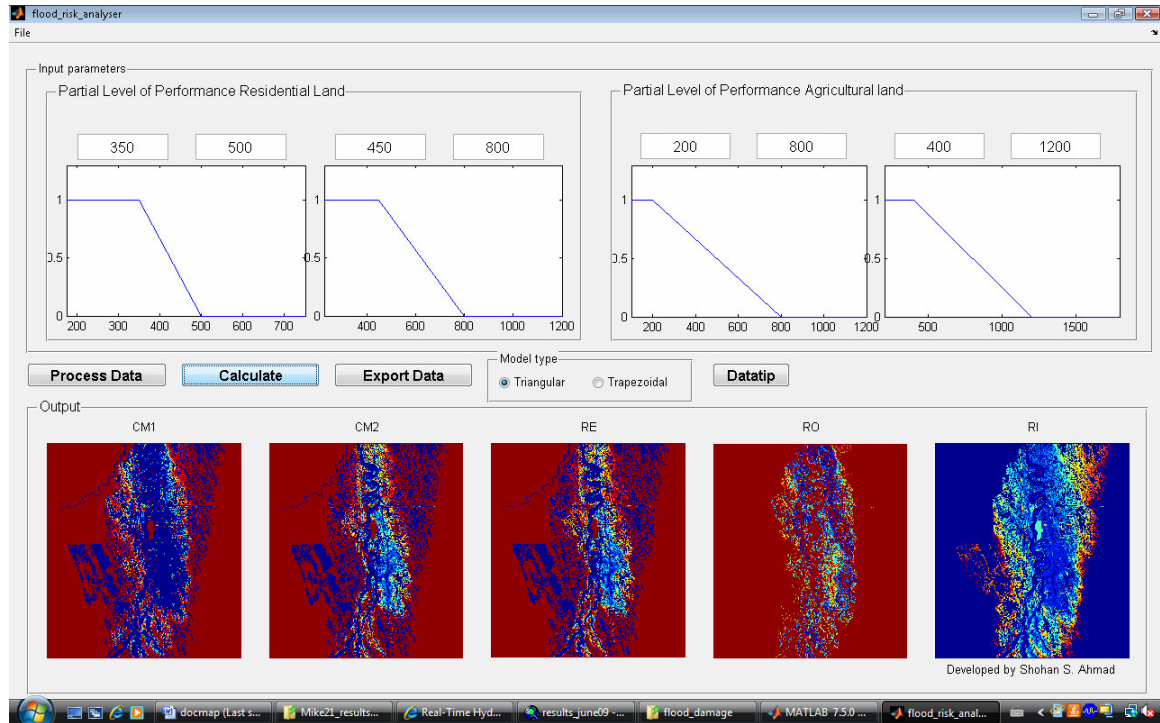


Figure 4.6: GUI with predefined partial level of flood damage for Red River Flood 1997

The maximum value of compatibility is combined for i -th time step at j -th location to determine the fuzzy combined reliability-vulnerability index. The inverse of the difference in compatibility values between two partial levels of flood damage represent the fuzzy robustness index. The fuzzy robustness index measures the adaptability to change in the partial level of flood damage. The time to recover from flood damage is determined using a flood recession time and recovery time-damage relationship. Uncertainty in the value of recovery time is accounted for by using a fuzzy membership function. Ability to recover from a failure state is represented by a fuzzy resiliency index.

4.1.3 RESULTS AND DISCUSSIONS

Spatial and Temporal Variation of Water Surface Elevation

Water surface elevation for the 1997 Red River flood event is simulated using the 2-D hydrodynamic model (MIKE 21). Figure 4.7 shows the water surface elevation at selected time steps. The movement of flood water in the floodplain is observed from the MIKE 21 simulation. It can be observed that on April 23, 1997, the floodplain in the case study region is completely dry. On April 26, 1997, areas closer to the river (mostly agricultural) are flooded. Due to the presence of Z-dike and control structures in the Red River basin, which are used to protect Winnipeg from flooding, some interesting patterns of flood wave propagation can be observed (Figure 4.7). On May 3, 1997, most of the Red River basin is completely flooded. On May 3, 1997, the community of Ste. Agathe remains flooded (Figure 4.7). The community of St. Adolphe is protected by ring dikes during the 1997 flood event. From the MIKE 21 simulation, it can be observed that the flow was obstructed by the operation of the control structures. The impact of the Z-dike is also visible as water was hitting the dike and the flow direction was changing and approaching south on the Red River basin. On May 17, 1997, areas further away from the river have recovered from flooding, while most areas closer to the river remain flooded. On May 21, 1997, most of the areas have become dry, while some pocketholes still containing stagnant water remain flooded.

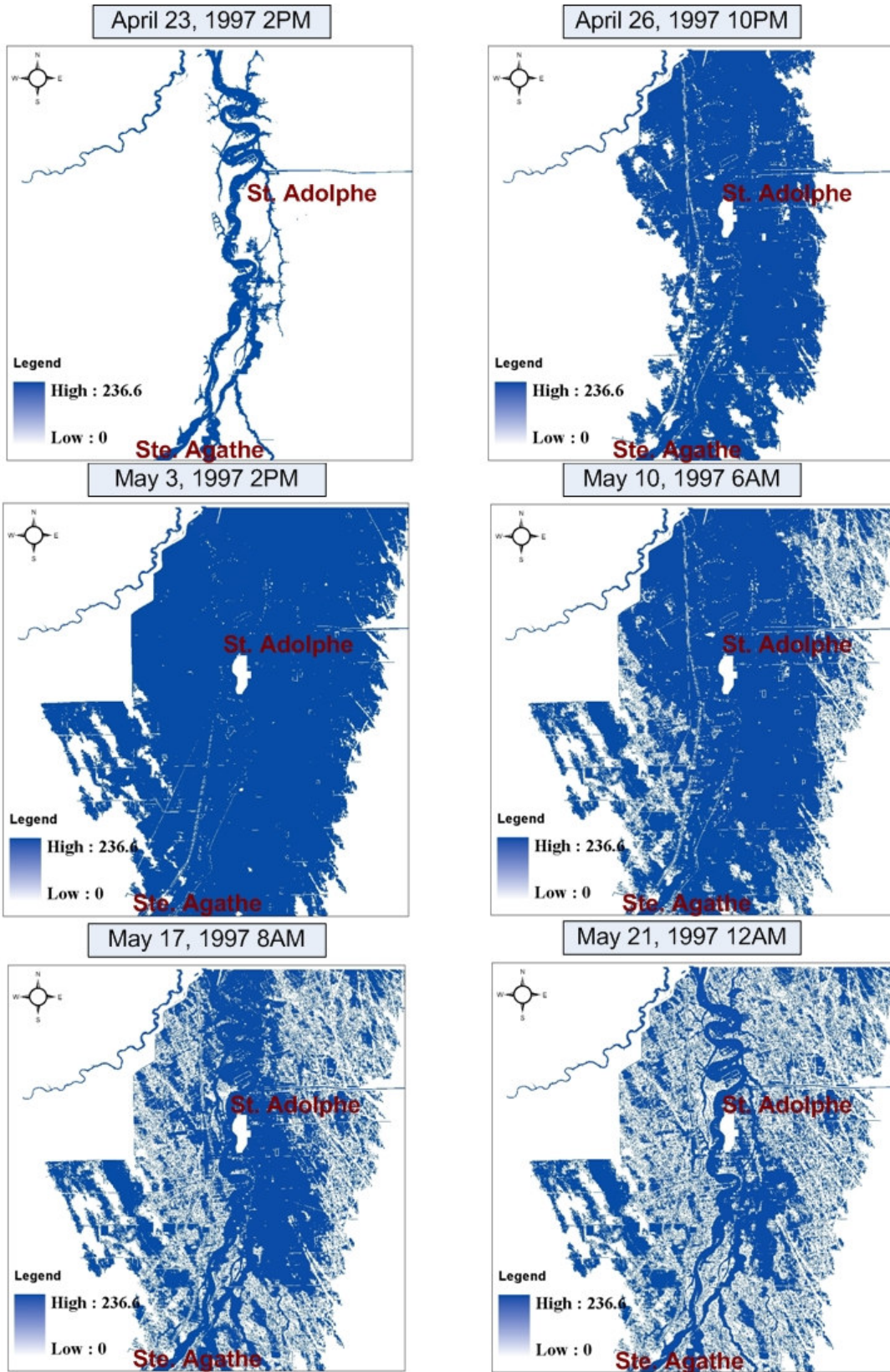
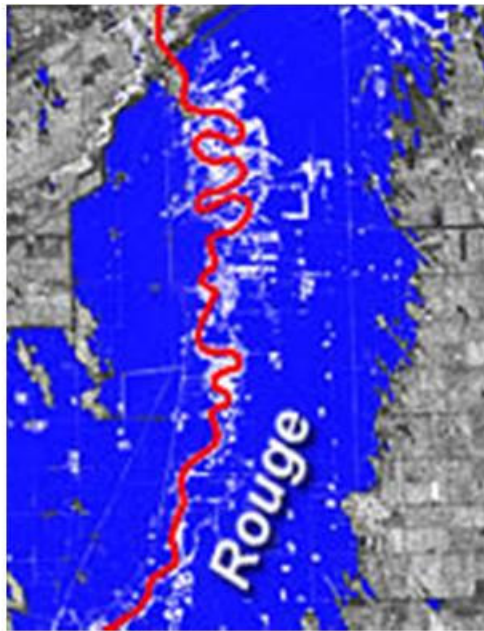


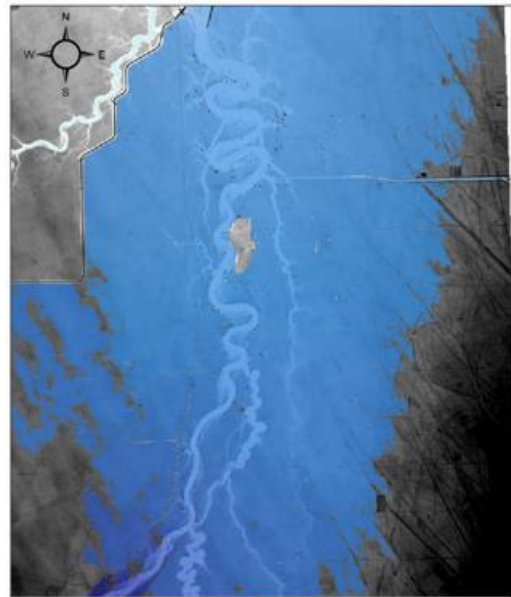
Figure 4.7: Water surface elevation (m) in Red River flood in 1997

Verification of Result Obtained from MIKE 21 Model Simulation

The results of the MIKE 21 simulation are verified by comparing the extent of flooding with satellite images taken on May 1, 1997 (Figure 4.8), and also with the observed water levels at Red River near St. Adolphe (Figure 4.9), Ste Agathe and the floodway inlet (Figure 4.10). Overall, the MIKE 21 model results were satisfactory for assessing the flooding of the Red River in 1997 in the region from Ste. Agathe to the Red River Floodway control structure (south border of the City of Winnipeg).



Satellite Image, RADARSAT. May 1, 1997 7:32AM
Source: Canadian Center for Remote Sensing



Simulated flooded area on May 1, 1997 8:00 AM

Figure 4.8: Satellite Image (Left) and simulated flooded area (Right) on May 1, 1997

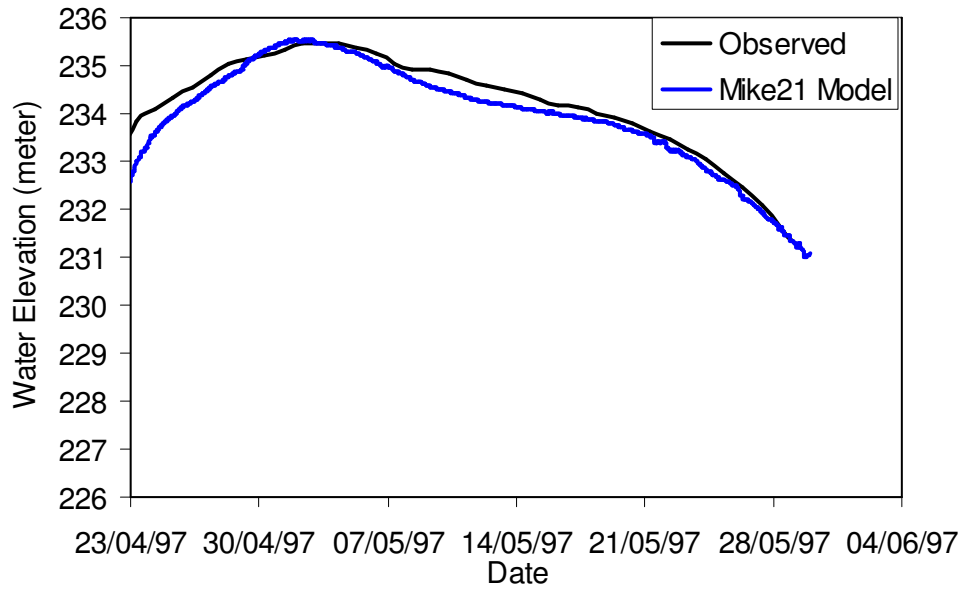


Figure 4.9: Comparison of observed and simulated water elevations (in meter) at Red River near St Adolphe

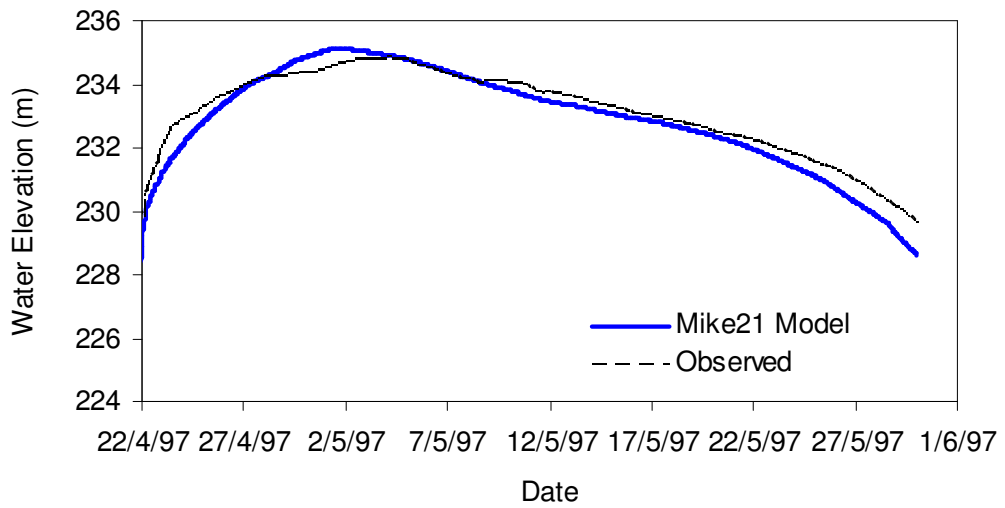


Figure 4.10: Comparison of observed and simulated water levels at floodway inlet.

A comparison of results obtained using MIKE 21 and results reported by Klohn-Crippen (1999) using MIKE 11 are shown in Table 4.1.

Table 4.1: Comparison of recorded and modeled peak water levels (ft) for 1997

Location	Observe Peak (m)	Model Peak (m) MIKE 11*	Model Peak (m) MIKE 21	Difference in peak (MIKE 21 and Observed)
Main River				
Ste. Agathe	236.67	236.58	236.60	-0.07
Ste. Adolphe	235.45	235.45	235.7	+0.25
Floodway Inlet	235.15	235.15	235.3	+0.15
Floodplain				
Ste. Agathe	237.6	237.6	237	-0.6

* MIKE 11 results are taken from Klohn-Crippen (1999)

There are some errors in peak water levels when the MIKE 21 results are compared with observed data. The model results may improve if un-gauged inflow from tributaries joining the Red River between Ste. Agathe and the Winnipeg floodway inlet are considered. Another factor that may attribute to the error is the interoperability between GIS and the 2D hydrodynamic model, MIKE 21. Since LIDAR is not capable of penetrating the water surface, LIDAR data does not provide any information on river cross-sections. River cross-section data are combined with the LIDAR data to prepare a complete topography. This process can attribute to error due to datum correction and georeferencing.

Another important factor that may attribute to error is that MIKE 21 does not have the capability to explicitly model the operation of the floodway and control structure. MIKE 21 has the option of using a sink function, which is used in this study as an indirect way to incorporate floodway operations to create diversion of flow. The problem with this approach is the sink function only affects the continuity equation. The momentum term is unaffected in the Saint-Venant equation. Therefore, it is not possible to capture the backwater effects due to the operation of the floodway.

Spatial and Temporal Variability of Flood Damage

Agricultural and residential damage for the Red River basin is shown using a red (light to dark) color ramp, with red representing a location with high damage and white representing a location with low damage (Figure 4.11). Each section of the flooded agricultural area has a unique seeding date. In this study agricultural damage is assessed based on the seeding date and this damage is observed over the time period bounded by the date of submergence and the seeding date (considering any additional time required for drying, if needed). Damage analyses show that on April 23, 1997, there was no damage in the floodplain. On April 26, 1997, however, agricultural areas closer to the river were flooded and show considerable flood damage. On May 3, 1997, more agricultural land is submerged and flood damage is significantly higher. Agricultural damage was experienced during the period from April 26, 1997 to May 21, 1997.

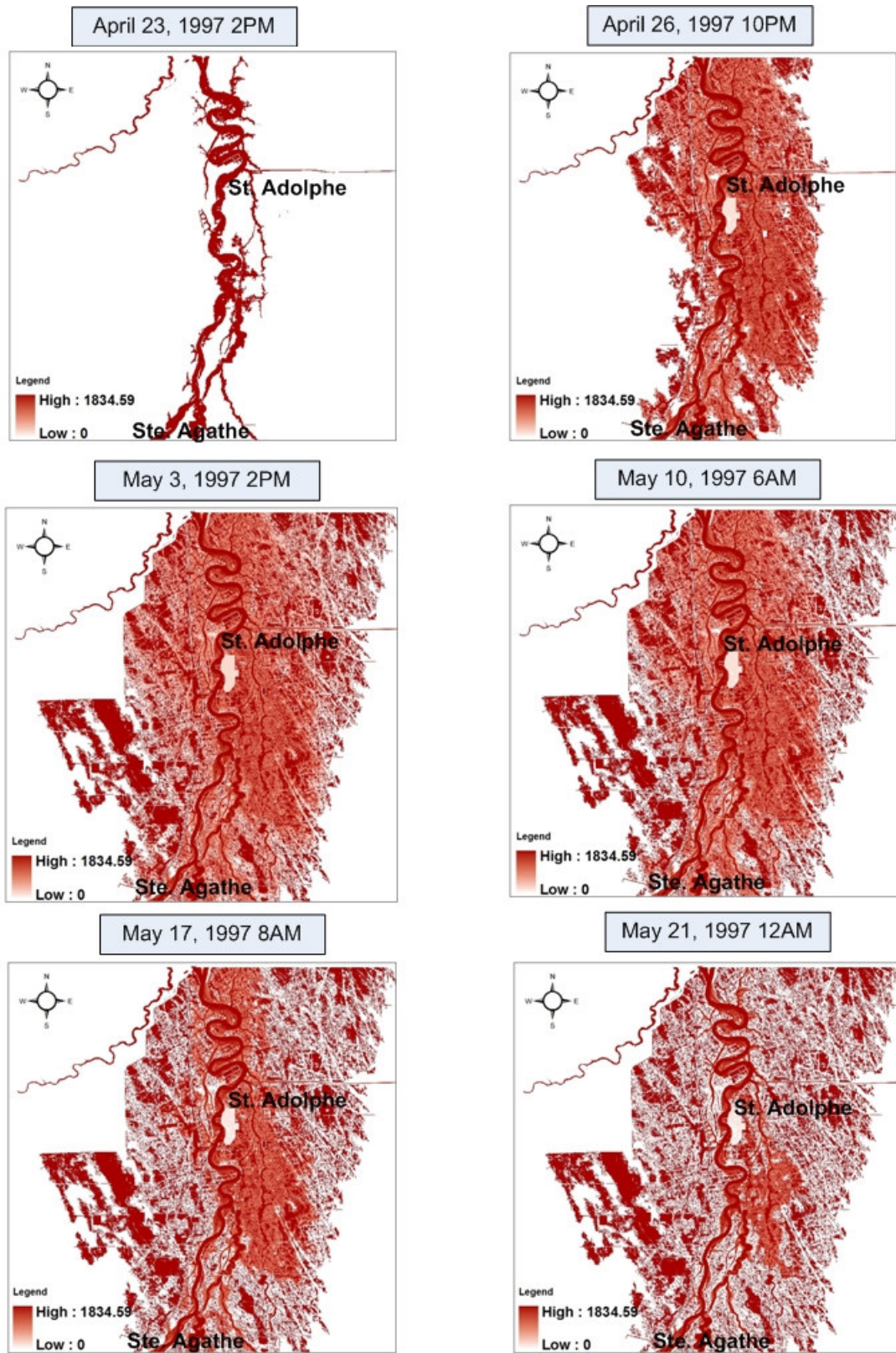


Figure 4.11: Spatial and temporal variation of flood damage (\$ per 625 sq. meter)

As the seeding date of May 21, 1997 approaches, much of the agricultural land shows zero damage. There is some agricultural land in the floodplain where flood water remained stagnant over a long period. The major delay in initiating the seeding date caused the damage in those locations to be significantly higher than it otherwise would have been (Figure 4.11).

A temporal analysis of damage to ring-diked communities shows that when the flood water level was at the base level of incipient flooding, then the damage to infrastructure was 5% of the total reported damage. On April 26, 1997, when flood waters were rising, the community of Ste. Agathe and St. Adolphe experienced a minor increase in infrastructural damage costs related to pre-emptive flood fighting measures (Figure 4.11). The ring-diked community of St. Adolphe was protected from flooding, and on May 3, 1997 infrastructural damage cost reached its highest level for pre-emptive flood fighting (diking and cleanup) and infrastructure repair (roads, bridges, culverts, ditches, sewer and water) (Figure 4.11). However, due to a breach of the dike, the community of Ste. Agathe was completely flooded. Figure 4.11 shows that on May 3, 1997, the community of Ste. Agathe experienced severe infrastructure damage, which is represented in this study as the total potential infrastructure damage based on pre-emptive flood fighting costs, post-flood clean-up costs and loss of infrastructure. Since infrastructure damage repair requires a significant amount of time to be completed, by May 21, 1997, damage value remained the same.

Combined Fuzzy Flood Reliability-Vulnerability Index

The combined reliability and vulnerability index for the Red River basin is expressed using a color ramp, with blue representing the location with lowest reliability and white the location with highest reliability (Figure 4.12). Reliability and vulnerability values for a region or a location of particular interest can be easily identified using the color ramp. The combined fuzzy flood reliability-vulnerability index value ranges from 0 (dark blue) to 0.33 (light blue). Orange marks the areas of higher reliability and lower vulnerability in comparison with the regions closer to the river. The value of the combined fuzzy flood reliability-vulnerability index in this region is between 0.34 (dark orange) and 0.58 (light orange). The transition to regions with high reliability is indicated by the value of the combined index in the range of 0.59 (dark yellow) to 0.75 (light yellow). Green marks the regions that are safer and less vulnerable to floods, where the index value is between 0.76 and 0.90. Regions with the highest reliability are shown in white color with an index value between 0.91 and 1.0.

The combined fuzzy reliability and vulnerability index map shows that on April 23, 1997, agricultural land and ring-diked communities were not affected by flooding, but that on April 26, 1997, areas closer to the river started showing a lower level of reliability and a higher level of vulnerability (Figure 4.12). On May 3, 1997, the larger area was flooded and showed a lower reliability and a higher vulnerability. May 10, 1997, shows a decrease in agricultural areas with low reliability and high vulnerability. On May 21, 1997, the agricultural area with no flooding shows high reliability and low vulnerability. On April 26, 1997, the ring-diked community of St. Adolphe and Ste. Agathe has a

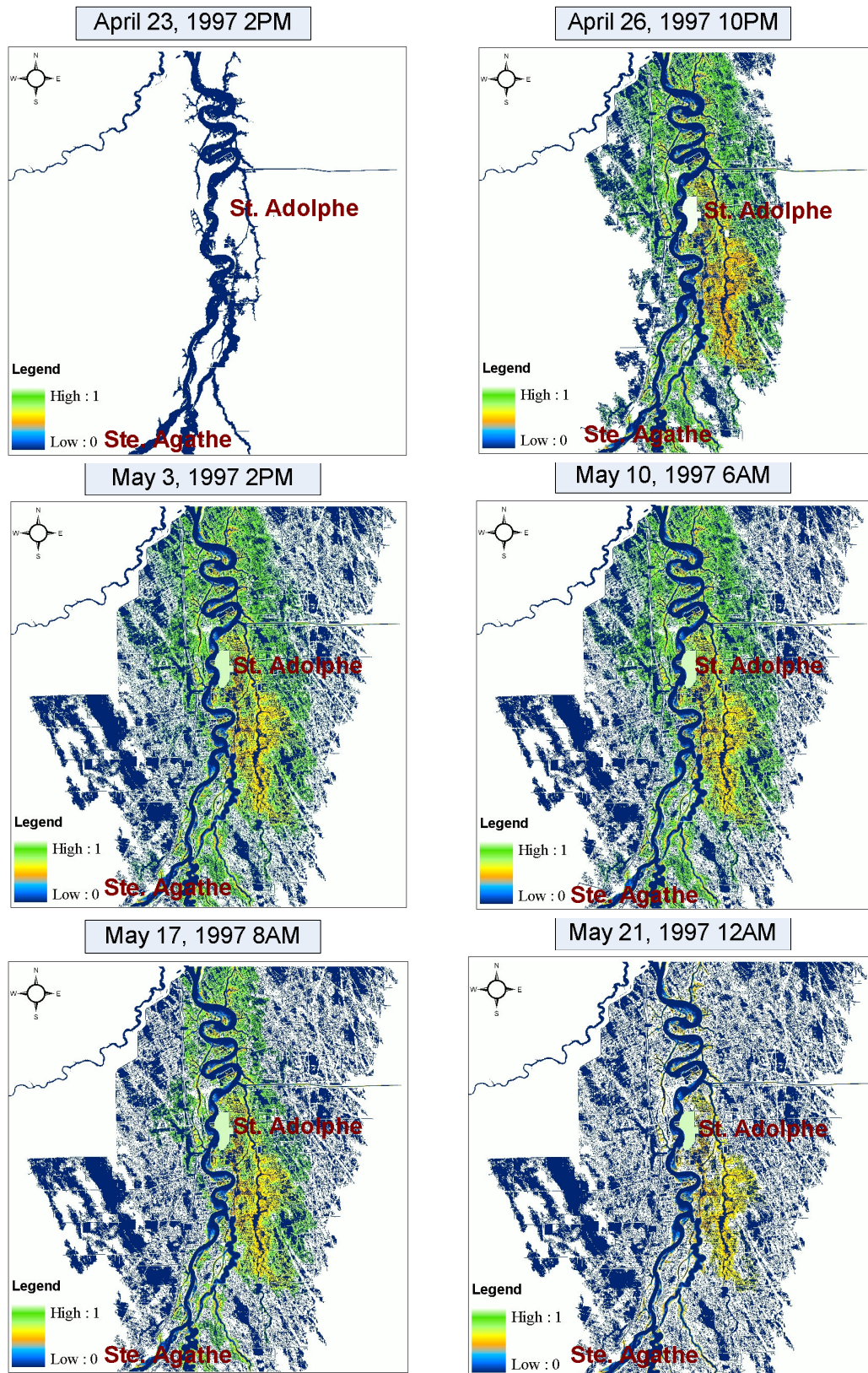


Figure 4.12: Fuzzy combined reliability-vulnerability index

reliability index of 1, indicating the highest reliability, whereas on May 3, 1997, due to an increase in infrastructure damage, the reliability index for the community of Ste. Adolphe decreased from 1 to 0.95 still indicating high reliability. However, for the community of St. Agathe, the reliability index decreased to 0 indicating very low reliability (Figure 4.12).

Sensitivity Analysis of Combined Fuzzy Reliability-Vulnerability Index

The analysis presented in this thesis was conducted by using membership function shapes selected by the researchers without real input from the stakeholders. Therefore, the analyses were performed for two shapes, triangular and trapezoidal membership functions, in order to test the sensitivity of the combined fuzzy reliability-vulnerability index to the shape of the membership function. A flow chart in Figure 3.15 shows the process adopted for the calculation of the fuzzy combined reliability-vulnerability index where a triangular fuzzy membership function shape is used to develop 2-D fuzzy sets for (i) temporal variability of flood damage, and (ii) spatial variability of flood damage. Sensitivity analyses were performed using trapezoidal membership functions for the 2-D fuzzy sets, while a similar procedure (as shown in flow chart in Figure 3.15) is followed to determine the combined reliability-vulnerability index. The effect of the different shape of membership function is assessed by comparative analyses of the reliability-vulnerability maps, as shown in Figure 4.13. Maps of the combined reliability and vulnerability index of May 3, 1997 for the triangular and trapezoidal membership functions for the Red River basin (Figure 4.13) were developed using the same color ramp as in Figure 4.12. A different color ramp is used to represent the map (Figure 4.13)

showing a difference in the combined reliability-vulnerability index. The increase in the combined reliability-vulnerability index value ranges from 0 (dark blue) to 0.024 (dark green). Blue represents locations with a lower increase in the combined reliability-vulnerability index value, which ranges from 0 (dark blue) to 0.007 (light blue). Orange marks the areas with higher increases in reliability. The value of the increase in combined reliability-vulnerability index in this region is between 0.008 (dark orange) and 0.013 (light orange). The transition to regions with a higher increase in reliability is indicated in the range between 0.014 (dark yellow) and 0.016 (light yellow). For St. Adolphe, the reliability index increased by 0.015 when the shape of the fuzzy membership function changed from trapezoidal to triangular. Green marks the regions that show the highest increase in reliability value, between 0.017 and 0.024. It is evident that when compared to a trapezoidal fuzzy membership function, a triangular fuzzy membership function results in a higher combined reliability-vulnerability index.

The quantitative analysis of the maps of combined reliability-vulnerability index (Figure 4.13) for May 3, 1997 is provided in Table 4.2. About 114 km² of the region under consideration has zero compatibility and therefore no impact on the shape of the membership function. About 307 km² of the region has a combined reliability-vulnerability index of 1 for the trapezoidal membership function. As the membership function is changed to a triangular shape, it results in a 2.95% increase in area within the study region that has a combined reliability-vulnerability index of 1.

Table 4.2: Area in square Km corresponding to values of combined Reliability-Vulnerability Index

Combined Reliability-Vulnerability Index on May 3, 1997	Area in square Km corresponding to values of combined Reliability-Vulnerability Index using		Change in area in square Km corresponding to values of combined reliability-vulnerability index for changing fuzzy membership function from trapezoidal to triangular
	Triangular fuzzy membership function	Trapezoidal fuzzy membership function	
0.05	114.76	114.76	0.00
0.1	0.40	0.40	0.00
0.15	0.403	0.94	-0.54
0.2	0.53	0.86	-0.33
0.25	1.43	0.56	0.87
0.3	0.45	0.45	0.00
0.35	0.41	0.41	0.00
0.4	0.90	0.90	0.00
0.45	1.031	1.94	-0.92
0.5	0.91	1.98	-1.07
0.55	4.730	2.74	1.98
0.6	3.05	5.24	-2.19
0.65	5.51	5.63	-0.11
0.7	3.51	1.21	2.30
0.75	4.64	6.98	-2.34
0.8	5.15	5.63	-0.49
0.85	4.92	5.61	-0.69
0.9	5.21	5.27	-0.06
0.95	11.44	10.82	0.62
1	310.77	307.82	2.95

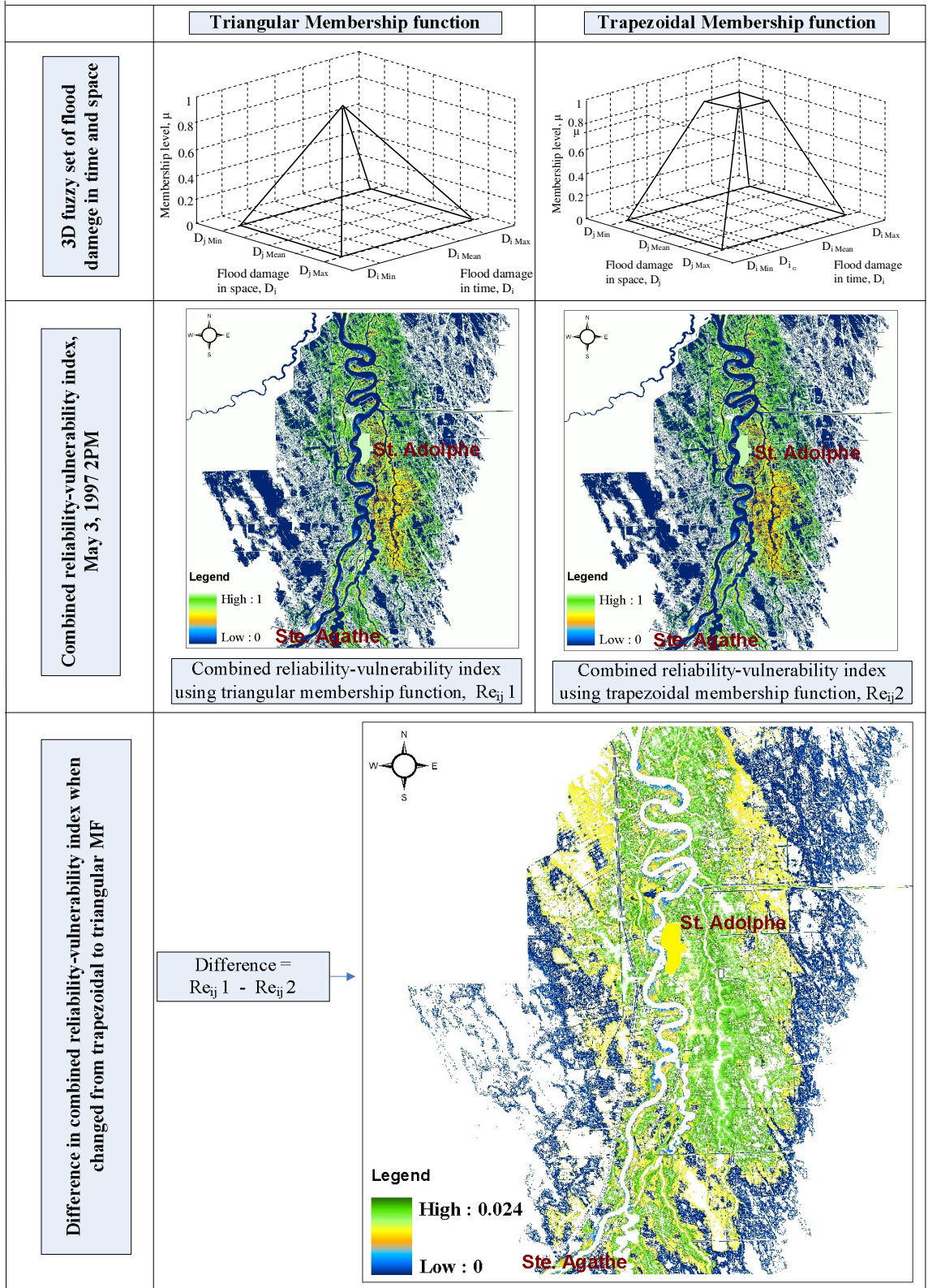


Figure 4.13: Sensitivity analysis on combined reliability-vulnerability index to the shape

Fuzzy Robustness Index

A fuzzy robustness index is calculated for the 1997 Red River basin flood in order to assess the ability of the area to adapt to the change in partial levels of flood damage. In the Red River case study a fuzzy robustness index is developed based on the two defined partial levels of flood damage. The fuzzy robustness index of a system depends upon the change in fuzzy compatibility. The higher the change in compatibility measure, the lower is the value of robustness index and vice-versa. The higher the value of the robustness index, the higher the system's ability to adapt to changing conditions.

The robustness index for the Red River case ranges from 0 (lowest) to 6 being (highest), which measure the level of robustness. The range of values of the fuzzy robustness index for the Red River basin is shown with a new reclassification that has (Figure 4.14) 6 zones. This is meant to produce a better representation of fuzzy robustness index maps. The range of 0 to 1, shown by dark blue, represents regions with the lowest robustness. These regions have a very low ability to adapt to the change in partial levels of flood damage. Light blue marks areas of low robustness where the robustness index ranges from 1 to 2. These areas have a slightly higher robustness compared to the regions shown in dark blue. Orange marks the areas that have a higher robustness compared to areas shown in light blue. The value of robustness index in this region is between 2 and 3. Areas in yellow have a robustness index in the range of 3 to 4. The transition to high robustness is shown in light green, which represents regions with values of robustness index ranges between 4 to 5. These regions have a high ability to adapt to change in partial levels of flood damage. Regions with the highest robustness index are shown in

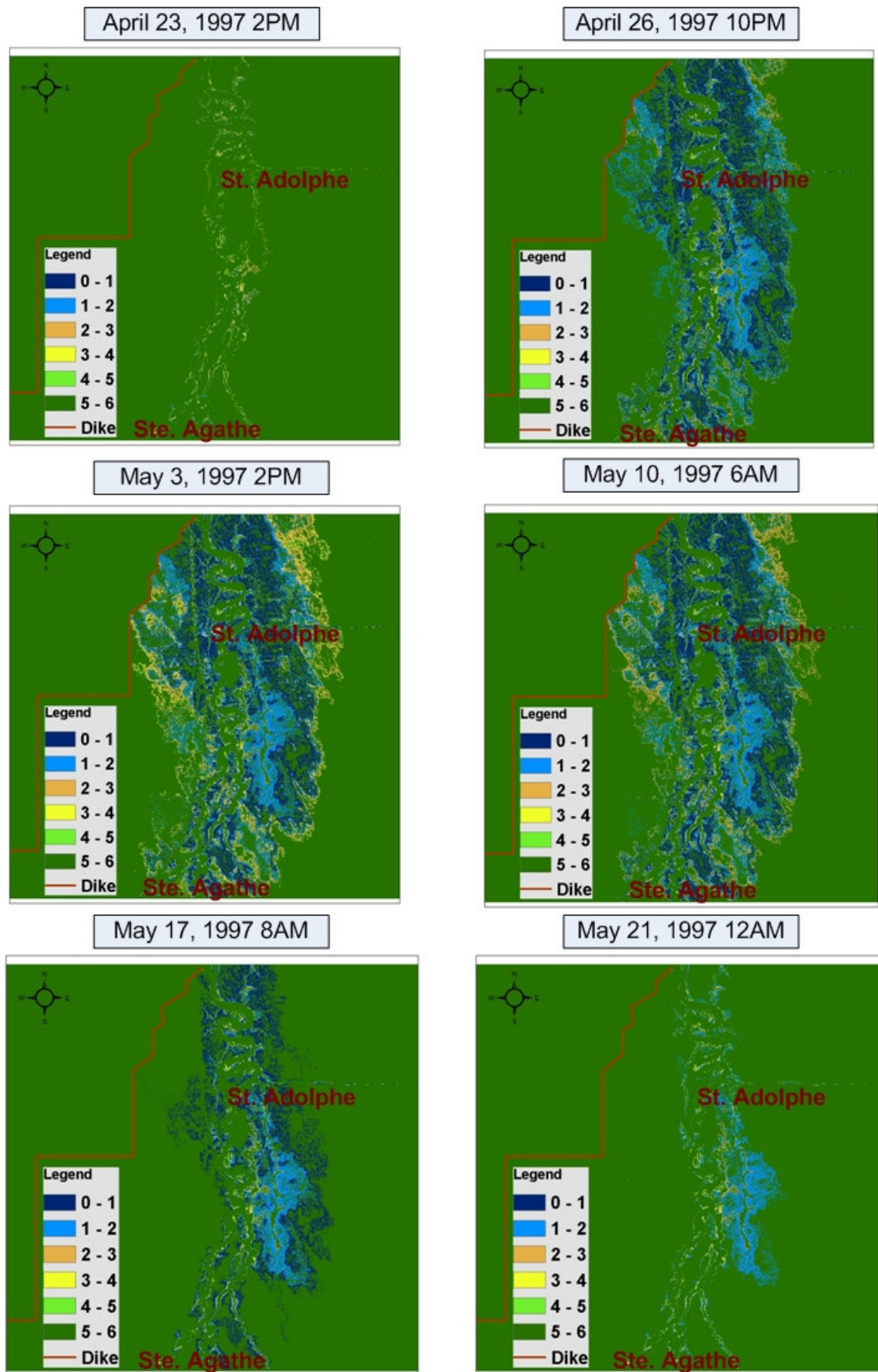


Figure 4.14: Fuzzy robustness index

dark green and range between 5 and 6. These regions have the highest ability to adapt based on the predefined change in partial levels of flood damage.

Figure 4.14 shows robustness index maps for different dates. On April 23, 1997, almost every location of the case study area has highest robustness in the range of 5 to 6. However, on April 26, 1997 areas that are closer to the river and the northern part of the case study area, which are bounded by dikes, show very low robustness ranging between 0 and 2. Regions such as these have a very low ability to adapt to change in the partial levels of flood damage. On May 3, 1997 and May 10, 1997, there are more areas closer to the Red River and the northern part of the case study area that show a low value of robustness index. Regions farther away from the Red River have a high robustness index, i.e. a high ability to adapt to change in partial levels of flood damage. Figure 4.14 also shows that on May 17, 1997, areas farther away from the Red River that were previously (May 10, 1997) less robust have transitioned into the green range, thereby representing high robustness. May 21, 1997 shows that most of the case study areas have high values of robustness, i.e. a high ability to adapt to change in the partial levels of flood damage.

Fuzzy Resiliency Index

Depending on degrees of severity, it normally takes time to recover from a flood event. A large period of time needed for a system to recover reflects low resiliency. Similarly, a system that recovers quickly indicates a high level of resiliency. A fuzzy resiliency index is calculated for the 1997 Red River basin flood in order to assess the ability of the area to recover from its flood event. In order to evaluate resiliency, the resiliency index ranges

from 0.2 (lowest) to 0.8 (highest). The values of resiliency index for the Red River basin are made clearer by interpolating the resulting maps with a new reclassification (Figure 4.15) of 6 zones, which better represents the range of resiliency index values. The range of 0.2 to 0.3, shown in dark blue, represents regions with very low resiliency. These regions have the highest recovery time, which means the lowest ability for a quick recovery. Light blue marks areas of low resiliency where the resiliency index ranges from 0.3 to 0.4. Orange marks the areas that have higher resiliency compared to areas shown in light blue. The value of resiliency index in this region is between 0.4 and 0.5. The next range of resiliency is between 0.5 and 0.6, which is shown in yellow. Light green marks the transition to regions with high resiliency and that have a resiliency index value in the range of 0.6 to 0.7. These regions require less recovery time. Regions with the least recovery time, and therefore the highest resiliency, are shown in dark green and have an index value ranging between 0.7 and 0.8.

The resiliency index map shows that on April 23, 1997, agricultural land and ring-diked communities are without a resiliency index, since they are not affected by flooding. However, on April 26, 1997 areas closer to the river begin to show a very low resiliency ranging between 0.2 and 0.3. Regions farther away from the River are not flooded. On April 26, 1997 the resiliency index for the community of Ste. Adophe ranges between 0.5 and 0.6, which is considered as a high value of resiliency in this study (Figure 4.15). On May 3, 1997 most of the study area was flooded and showed a higher recovery time and therefore lower resiliency. Although the community of St. Adolphe was completely protected from the flood, due to an increase in infrastructure damage cost the community

needed more time to recover and therefore showed a lower resiliency in the range of 0.4 and 0.5. Since the community of Ste. Agathe was completely flooded, the resiliency index was at its lowest. For agricultural areas the seeding date is considered for calculating the recovery date. If the flood recedes quickly, then the seeding date is closer. However, if the flood recession is slow or if water remains stagnant in some regions, then the seeding date will be delayed resulting in a higher recovery time and therefore low resiliency. On May 10, 1997, as the flood was receding, agricultural lands that were previously flooded suggested less recovery time as the seeding date was approaching. May 10, 1997 shows a decrease in agricultural areas with low resiliency. In this study the recovery time for ring-diked communities was based on the cost of infrastructure damage. Normally repair of infrastructure takes a considerably high amount of time. Therefore it can be assumed that even after the flooding is over, the damage to infrastructure will remain. Based on this assumption the results show that during the period of May 17, 1997 and May 21, 1997, for the ring-diked communities of St. Adolphe and Ste. Agathe, the recovery time did not change. During this time period for community of Ste. Adolphe the resiliency index remained unchanged and resulted in the range between 0.4 and 0.5. Similarly during this time period the resiliency index for community of Ste. Agathe did not change as well and remained in the range between 0.2 and 0.3. On May 21, 1997, most of the agricultural area recovered from flooding. Figure 4.15 shows that on May 21, 1997 rest of the agricultural areas that are yet to recover from flooding shows an increase in resiliency index when compared with the resiliency index of May 17, 1997. On May 21, 1997 areas closer to the River show a very high resiliency index, which indicates a high ability of the area to recovery quickly.

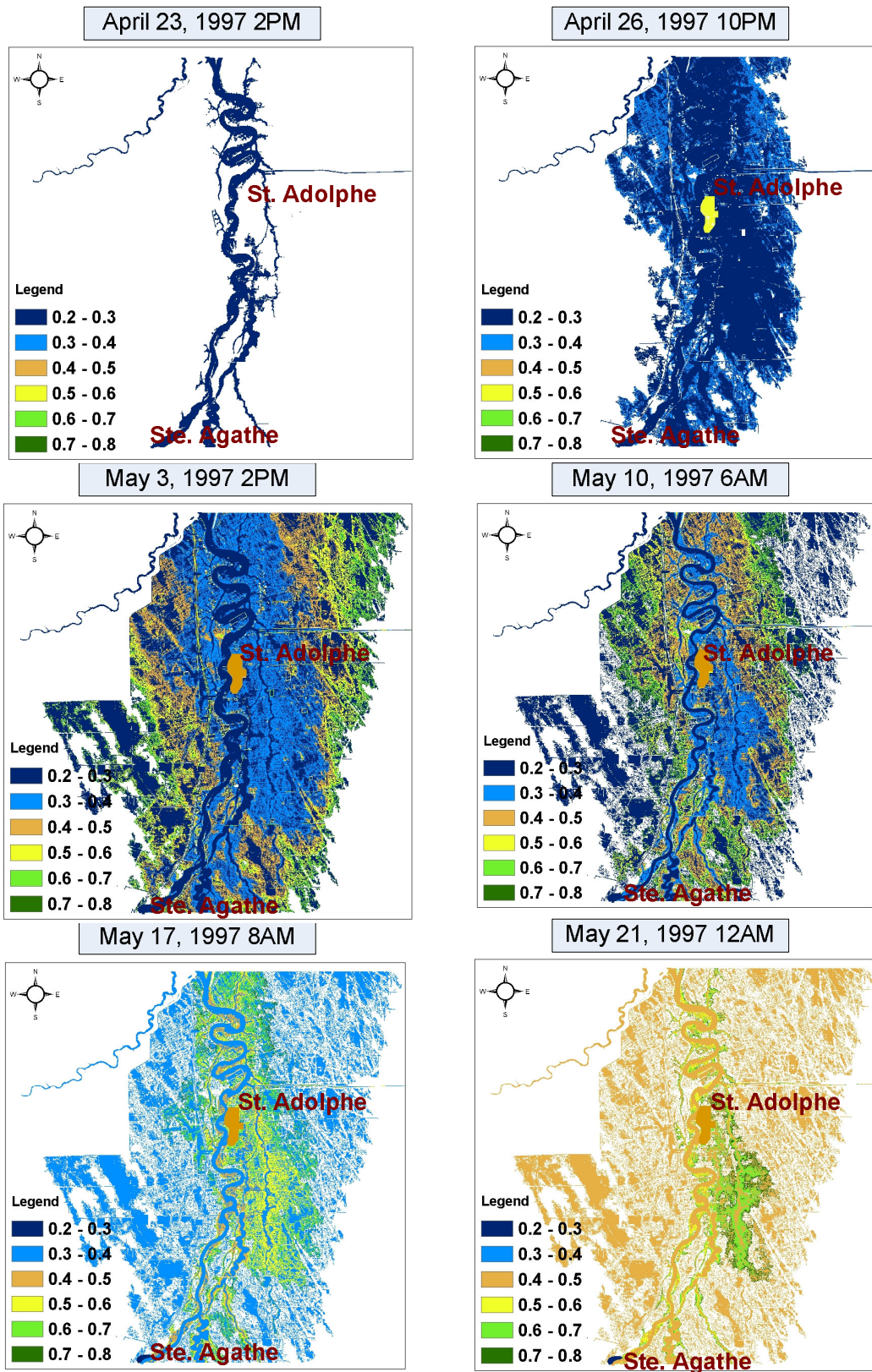


Figure 4.15: Fuzzy resiliency index

4.1.4 SYSTEM DYNAMICS MODELING OF THE RED RIVER CASE STUDY

The system dynamics modeling is used to simulate overland flooding. The model is developed for the Red River basin from south of the Winnipeg floodway to Ste. Agathe (Figure 4.16). Stella (HPS, 2001) is used for the system dynamics modeling. ArcView 9.3 (ESRI, 2009) is used for processing topographic information and visualization. The SD model simulates the flood propagation and provides the spatial and temporal variation of water surface elevations. In the SD model floodplain characteristics such as topography and information on infrastructure are used as inputs from the GIS.

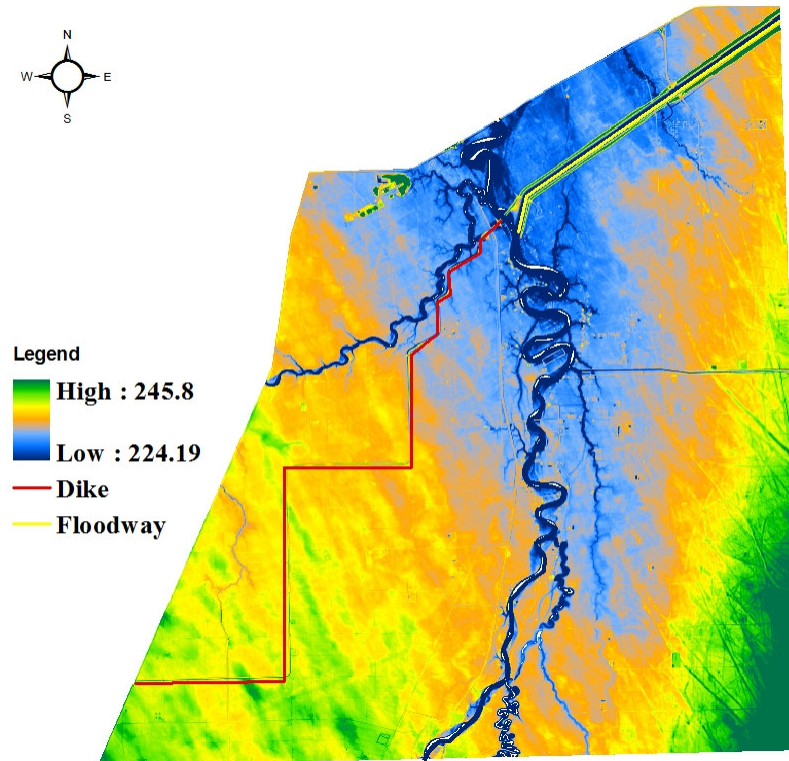


Figure 4.16: Topographic data of the Red River Case study

Overland flow in the floodplains is modeled in this work using a cell to cell routing approach. The cell-to-cell routing involves dividing the land surface into segments, and

routing flow from one segment to the next until it arrives at a final point. From several of the cell-to-cell routing models for overland flow, the routing method of Coe (1997) is used in the SD approach. This cell to cell routing method divides the land surface into routing cells. It is assumed that discharge occurs only when the volume of water in the cells exceeds their storage capacity. Therefore, the discharge rate is a function of the difference between the volume of water in the cell and the cell's storage capacity (Ahmad and Simonovic, 2004). The Von Neumann neighbourhood scheme is used for cell-to-cell routing. This scheme allows water from each cell to move to one or more of its four neighbouring cells. The excess water (exceeding storage capacity) is distributed to four neighbouring cells in descending order of slope difference.

The Muskingum method (Chow et al. 1988) has been used for routing flow in the river. Overland flow and river flow is modeled in the system dynamics simulation environment Stella, where basic building blocks, i.e., stocks, flows, connectors, and converters, are used to describe the model structure. Water volume in each cell is represented by a stock. Flows are used for inflows and outflows to model changes in water over time. Converters are used to provide information to the model and operate the system using logical/mathematical functions. The Flow routing sector describes the movement of water from cell to cell. Terrain information, such as surface elevation, ground slope and storage capacity in the cell, affects the flow from one cell to another. To solve the Muskingum equations of flow numerically, the region of interest is first discretized. The discretization enables the replacement of the continuous region by an array of points. In this research these points are taken as the center points of a grid. In the next step a finite difference

method is applied to these points to convert the differential equation into a set of difference equations. In Stella the set of equations is solved by Euler's method.

The SD model used for the simulation of overland flooding is based on the following assumptions:

- (i) The topography has each cell defined as a river section or as a floodplain;
- (ii) Flow of water is possible either from one cell in the river to the next cell in the river, or between cells if water level and ground slope permits;
- (iii) In the cell-to-cell routing model an assumption of linearity is made. This assumption is widely used in hydrology and in many routing methods such as the Muskingum method, the unit hydrograph, and the linear solutions of the St. Venant equations. Since the Muskingum method is used in this research as a cell-to-cell routing approach the assumption of linearity is valid.

Data Requirements

The SD model requires: (i) hydrologic data, and (ii) topographic data.

(i) Hydrologic Data

Daily water surface elevation near Ste. Agathe (St. No. 05OC012), precipitation, and evaporation losses are used in this case study.

(ii) Topographic Data

The same LIDAR data (provided by the IJC) that is used in the 2D hydrodynamic

modeling is also used for the SD model. This LIDAR data has a grid resolution of 5m by 5m. For simplification the topographic data is processed in GIS where grid cells are merged to obtain a coarse resolution of 2km by 2 km for the SD model. The river, dikes and floodway coverage are obtained from the Surveys and Mapping Branch at the Manitoba Department of Conservation. The study area is divided into cells with coverage representing river and flood control structures (dike, floodway, diversion, reservoir), and is shown in Figure 4.17.

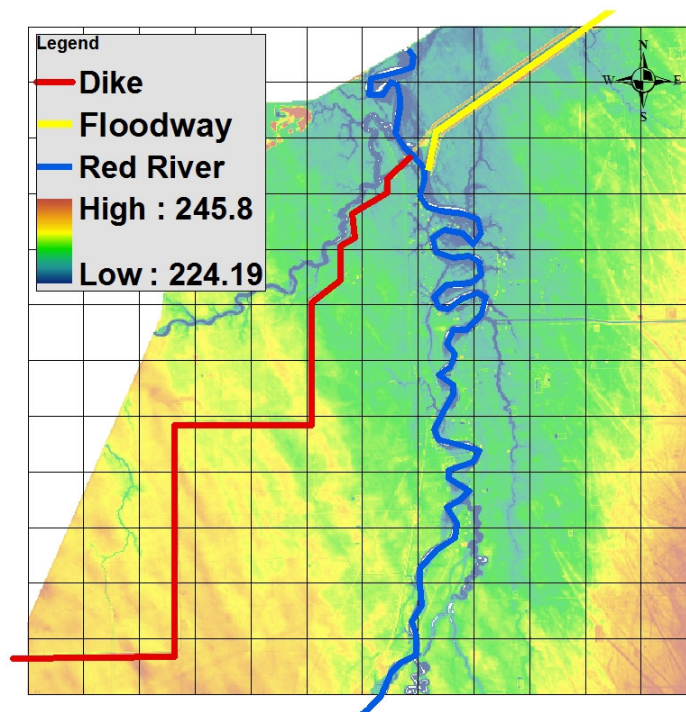


Figure 4.17: Study area divided into cells.

Description of System Dynamics Model for the Red River Section

The SD model deals with flow routing in the river and floodplains to describe the movement of water from cell to cell. The flow routing sector (Figure 4.18) in the model

uses the relative surface elevation of the neighbouring cells, ground slope elevation, presence of dikes, and storage capacity in the cells, to describe the cell-to-cell movement of water. The Red River basin has a flood control structure to regulate the flow. Operational strategies of flood control structure (floodway) are incorporated in the SD model to simulate the 1997 flood event. The model uses inflow, rain and evaporation as the main hydrologic and metrological inputs. The model also uses system constraints, operating curves, and flow capacity for additional information. In the overland flow model the operating rules are captured using logical statements such as IF-THEN-ELSE. The logical statements in Equation 4.1 (Ahmad and Simonovic, 2004) state the following: (i) if the floodway gates are closed then no flow is able to pass through the floodway, (ii) if the Red River flow is less than or equal to the safe carrying capacity of the river (1,400 m³/s) then flow is not diverted through the floodway, (iii) if flow in the Red River is more than the safe carrying capacity of the river (1,400 m³/s) and if the floodway gates are open, then excess flow is diverted to the floodway up to the maximum floodway capacity (1,850 m³/s).

$$\begin{aligned}
 & \text{IF (Floodway_Diversion_Control = 0) THEN (0)} \\
 & \text{ELSE IF (Red_Floodway_up} \leq 1400) \text{ THEN (0)} \\
 & \text{ELSE IF (Floodway_Diversion_Control = 1) AND (Red_Floodway_up} \geq 1400) \\
 & \text{THEN MIN ((Red_Floodway_up-1400), (1850)) ELSE (0)} \qquad (4.1)
 \end{aligned}$$

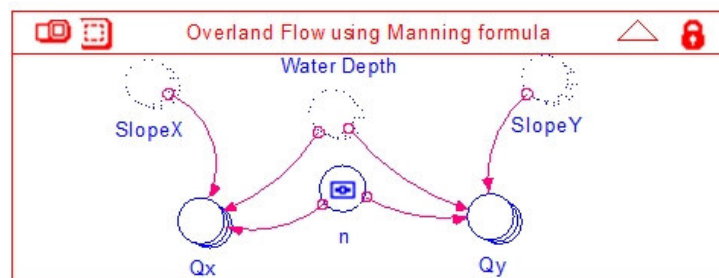
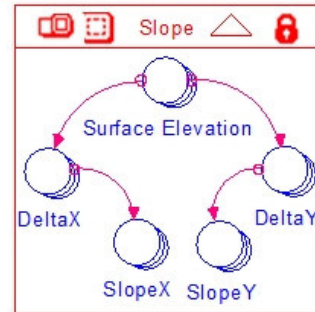
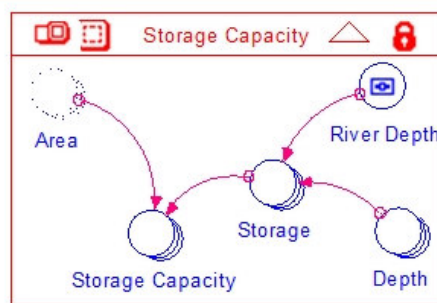
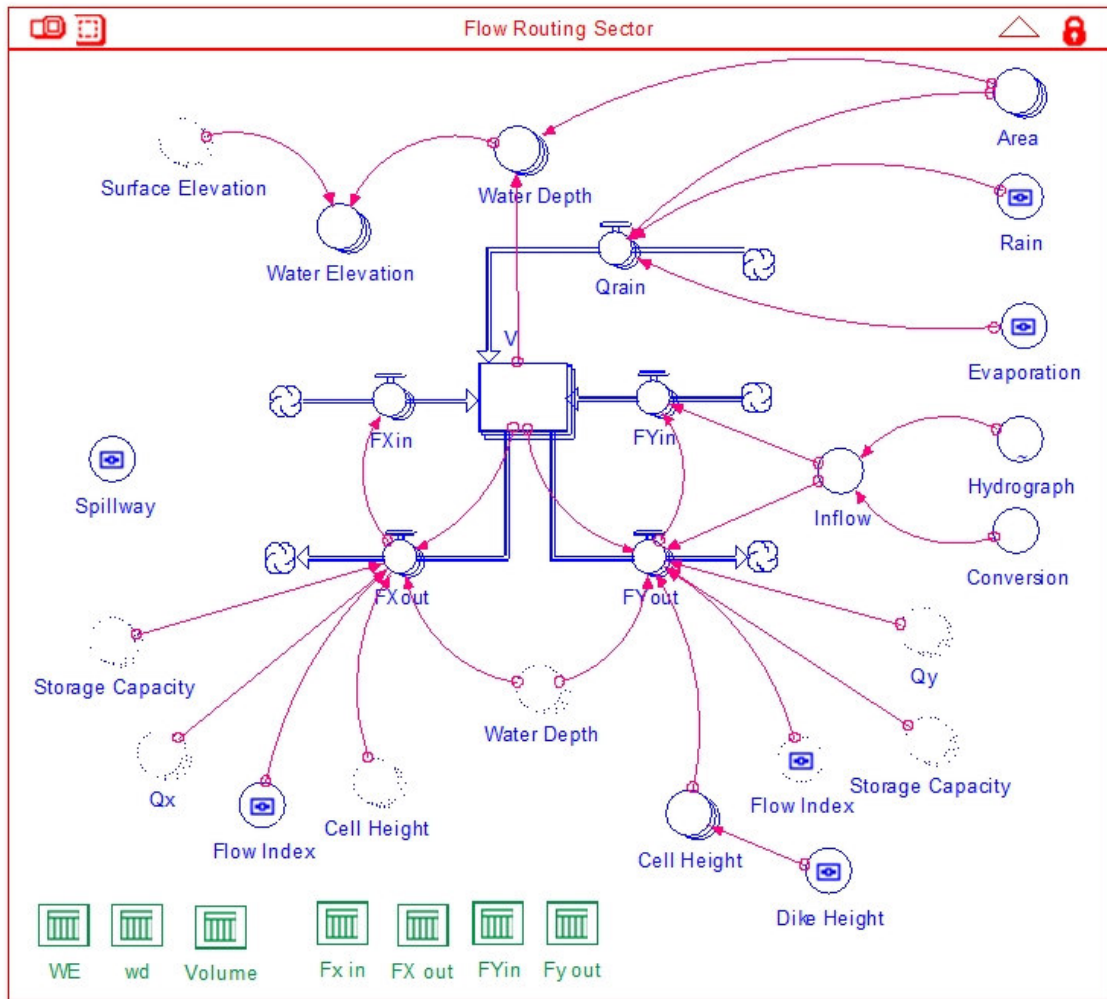


Figure 4.18: Flow routing sector.

The control screen of the SD model for the 1997 Red River flood simulation is shown in Figure 4.19. The User can change the control parameter, for instance rain, evaporation, dike height, river depth, mannings n, etc., using different sliders. For the operational strategy in the Red River basin, the module has a slider for carrying out the operation of the gates of the Red River floodway. Output of the SD model is given in tables. The results of the SD model consist in values for the variation of water surface elevations and discharges in the river and floodplain for every location and every time step. Several model runs are performed by modifying the model parameters and by changing the floodway operating rules. These modifications are necessary in order to more accurately reflect the extent of flooding and water surface elevation.

The application of the developed SD model is suitable to understand the following:

Impacts of Dike Height

The user is able to assess impacts of the dike by changing its height, removing, adding and even extending more dikes in the Red River basin. The consequence of such actions are meant to impact the spatial and temporal variability of flood extent and water surface elevation.

Impacts of Floodway Operation

The user can control the operation of the floodway in the SD model and can assess its impacts on flooding. The SD model can test different operating rules of floodway operation.

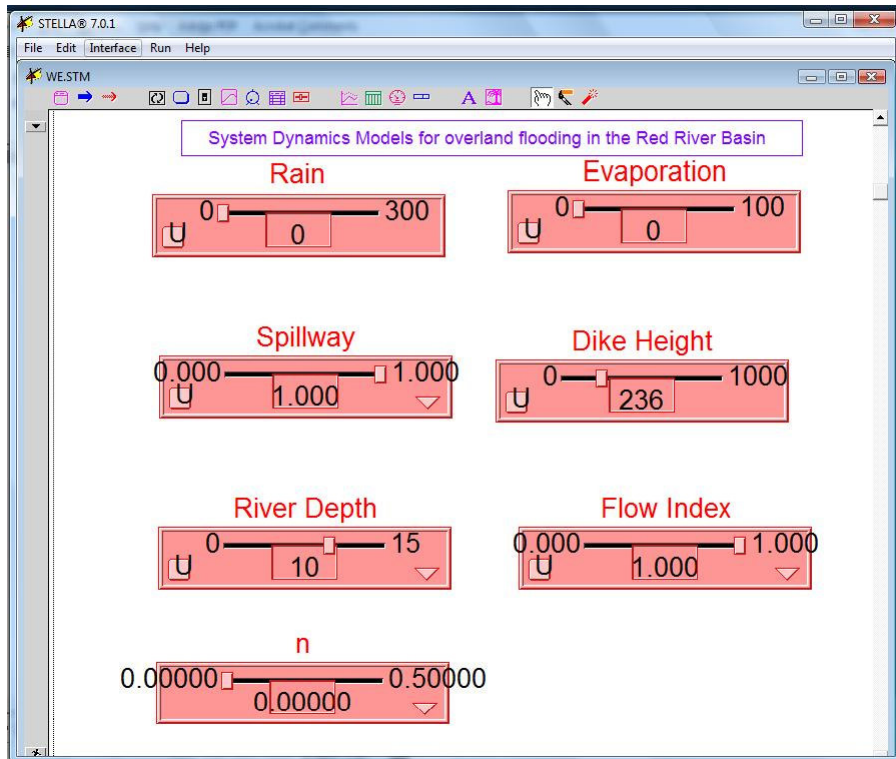


Figure 4.19: Control screen of the Red River section simulation model.

4.1.5 SPATIAL AND TEMPORAL FUZZY RISK ANALYSIS OF THE RED RIVER FLOOD OF 1997

The code in MATLAB is used to develop the fuzzy flood damage membership functions for agricultural land and ring-diked communities based on the flood damage data. The compliance of the flood damage membership function with different partial level (Figure 4.20) of flood damage membership functions is assessed for i -th time step at j -th location. The maximum value of compatibility is combined for i -th time step at j -th location to determine the fuzzy combined reliability-vulnerability index in time and space. The fuzzy performance indices, which include (i) combined reliability-vulnerability, (ii) robustness, and (iii) resiliency, are determined using Equations (3.36), (3.37) and (3.40), respectively.

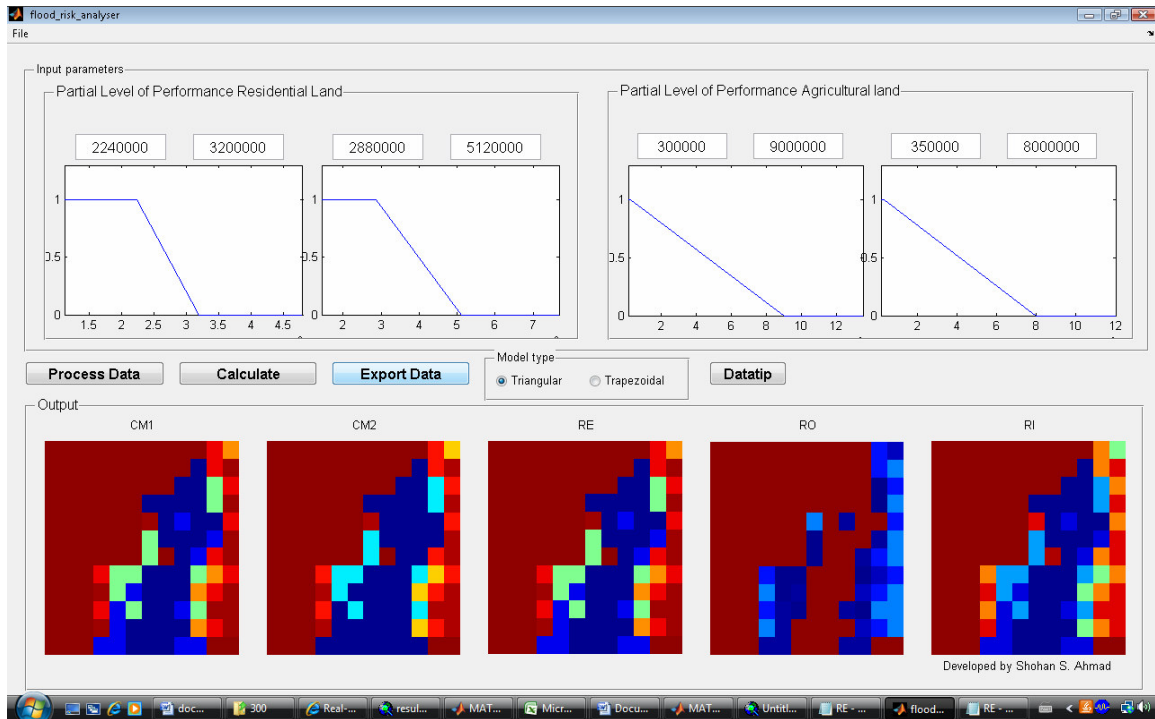


Figure 4.20: GUI with predefined partial level of flood damage for Red River Flood 1997

4.1.6 RESULTS AND DISCUSSIONS

Spatial and Temporal Variation of Flood Damage

Spatial and temporal variation of flood damage is shown using a red (light to dark) color ramp, with red representing a location with high damage and white representing a location with low damage (Figure 4.21). Some selected time steps are chosen to show the spatial and temporal variability of flood damage. Results show that on April 26, 1997 some agricultural areas south of the case study area show considerable flood damage. On April 28, 1997 more agricultural areas show a high level of flood damage. On May 3, 1997 and May 10, 1997 most of the agricultural land is submerged and flood damage is significantly high. Figure 4.21 shows that the ring-diked community of St. Adolphe was

protected from flooding. However, the community of Ste. Agathe suffered severe infrastructure damage.

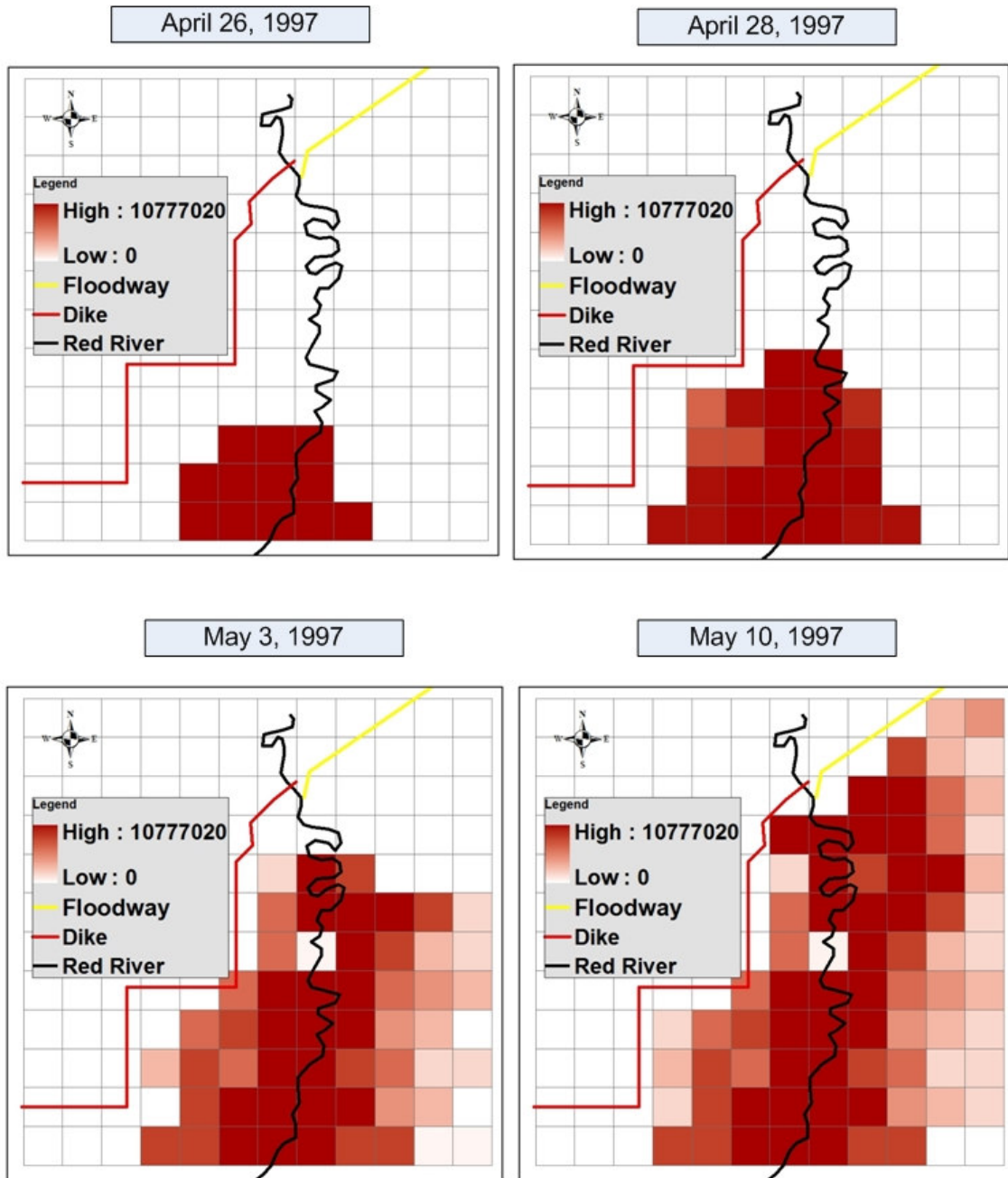


Figure 4.21: Spatial and temporal variation of flood damage (\$ per 4 sq. KM)

Combined Fuzzy Flood Reliability-Vulnerability Index

The combined reliability and vulnerability index for the Red River basin is expressed using a color ramp, with blue representing the location with lowest reliability and green the location with highest reliability (Figure 4.22). The combined fuzzy flood reliability-vulnerability index value ranges from 0 (dark blue) to 0.33 (light blue). Orange marks the areas of higher reliability and lower vulnerability in comparison with the regions closer to the river. The value of the combined fuzzy flood reliability-vulnerability index in this region is between 0.34 (dark orange) and 0.58 (light orange). The transition to regions with high reliability is indicated by the value of the combined index in the range of 0.59 (dark yellow) to 0.75 (light yellow). Green marks the regions that are safer and less vulnerable to floods, where the index value is between 0.76 and 1.

The spatial and temporal variability of the fuzzy combined reliability-vulnerability index is shown for selected time steps. The combined fuzzy reliability and vulnerability index map shows that on April 26, 1997, areas on the south of the case study area had less reliability and high vulnerability. With the propagation of flooding on April 26, 1997, more agricultural land shows less reliability. On May 3, 1997, a larger area was flooded and areas closer to the river started showing lower levels of reliability and higher levels of vulnerability. May 10, 1997 also shows a similar result of low reliability and high vulnerability. The community of St. Adolphe shows high reliability and less vulnerability for the 1997 flood event.

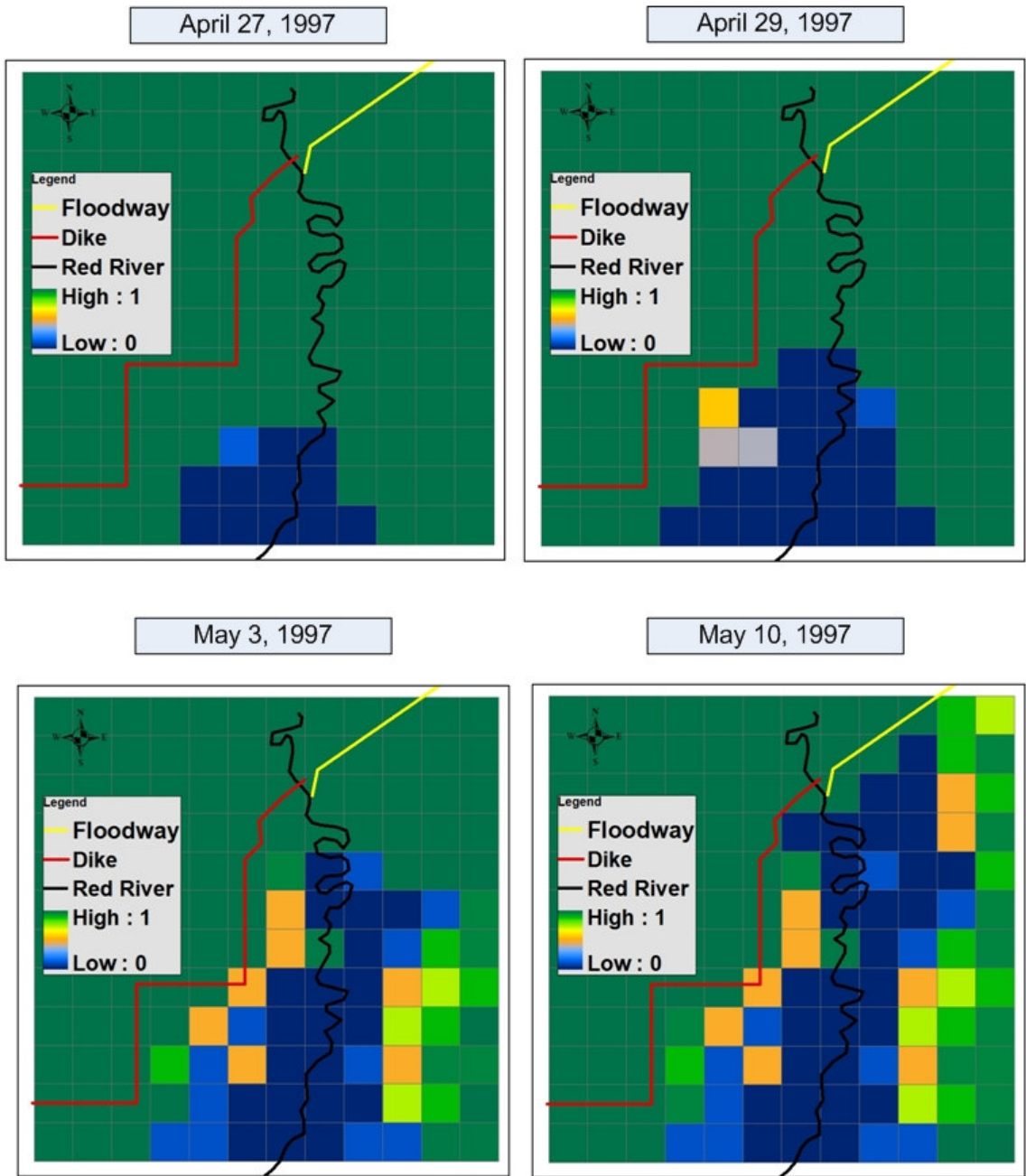


Figure 4.22: Fuzzy combined reliability-vulnerability index

Fuzzy Robustness Index

The ability of the Red River Basin to adapt to the change in partial levels of flood damage is assessed with a fuzzy robustness index. Two defined partial levels of flood damage are used to assess the robustness in the Red River case study. The fuzzy robustness index for the Red River basin is expressed using a color ramp, with blue representing the location with the lowest robustness of 0 and green the location with the highest robustness (Figure 4.23) of 6. The lower range of the fuzzy robustness index value ranges from 0 (dark blue) to 2 (light blue). These regions have the lowest ability to adapt to change in the partial levels of flood damage. Orange marks the areas of higher reliability and lower vulnerability in comparison with the regions closer to the river. The next range, between dark orange (2.1) and light orange (3.5), marks a higher robustness compared to the previous range in the color ramp.. The transition to regions with high robustness is indicated by the value in the range of 3.6 (dark yellow) to 4.5 (light yellow). Green marks the regions that are safer and less vulnerable to floods, where the index value is between 4.6 (light green) and 6 (dark green). These regions have the highest ability to adapt based on the predefined change in partial levels of flood damage.

Figure 4.23 shows robustness index maps for selected dates. On April 27, 1997 most of the case study area has its highest robustness. On April 29, 1997 areas south of the Red River Basin and areas closer to the river show a very low robustness ranging between 0 and 2. Regions such as these have a very low ability to adapt to change in the partial levels of flood damage. For May 3, 1997 and May 10, 1997, Figure 4.23 shows more areas closer to River with a low value of robustness index. It can be observed that

regions farther away from the River have a high robustness index, i.e. a high ability to adapt to change in the partial levels of flood damage.

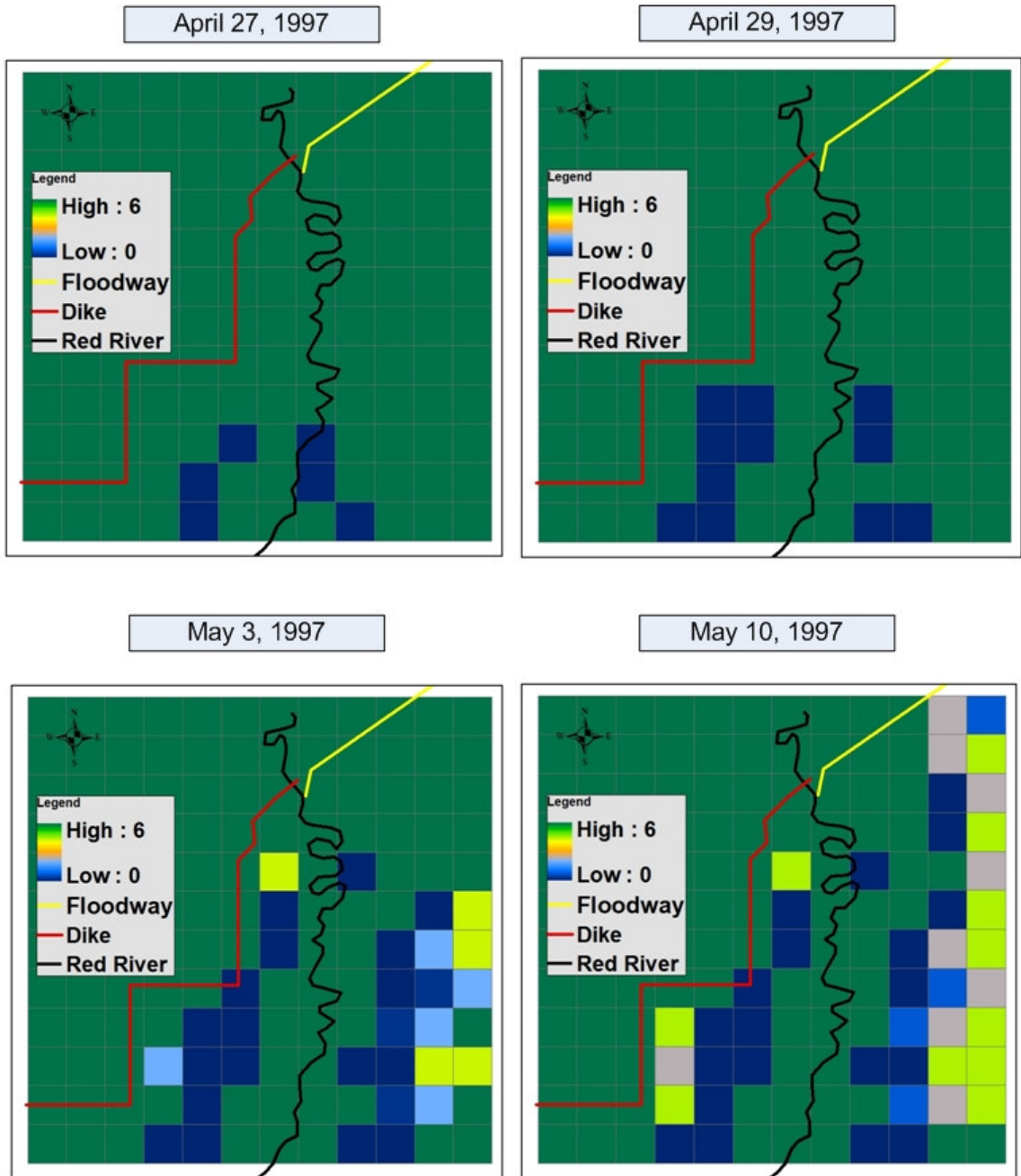


Figure 4.23: Fuzzy robustness index

Fuzzy Resiliency Index

The resiliency index for the Red River Basin is expressed using a color ramp ranging from 0.2 (dark blue) and 0.8 (dark green). Dark blue represents the location with lowest resiliency and dark green the location with highest resiliency (Figure 4.24). The range of 0.2 (dark blue) to 0.4 (light blue) represents regions with very low resiliency. These regions have the highest recovery time, which means that they have the lowest ability for a quick recovery. A resiliency index of 0.41 (Orange color) to 0.6 (yellow color) marks the areas that have a higher resiliency compared to areas shown in blue. The next range of 0.61 (light green color) to 0.8 (dark green color) represents regions with high resiliency. Therefore these regions need less time to recover from the flood event.

The resiliency index map shows that on April 27, 1997, areas south of the Red River Basin and areas closer to the river had the lowest resiliency index, and therefore required a long period of time to recover. On April 29, 1997, more regions closer to the river show less resiliency. The areas north of the case study show high resiliency. On May 3, 1997, and on May 10, 1997 most of the Red River Basin is submerged and shows low resiliency. Regions that are farther away from the River show a comparatively higher value of resiliency index. Figure 4.24 shows that for the 1997 flood the community of St. Adolphe was highly resilient.

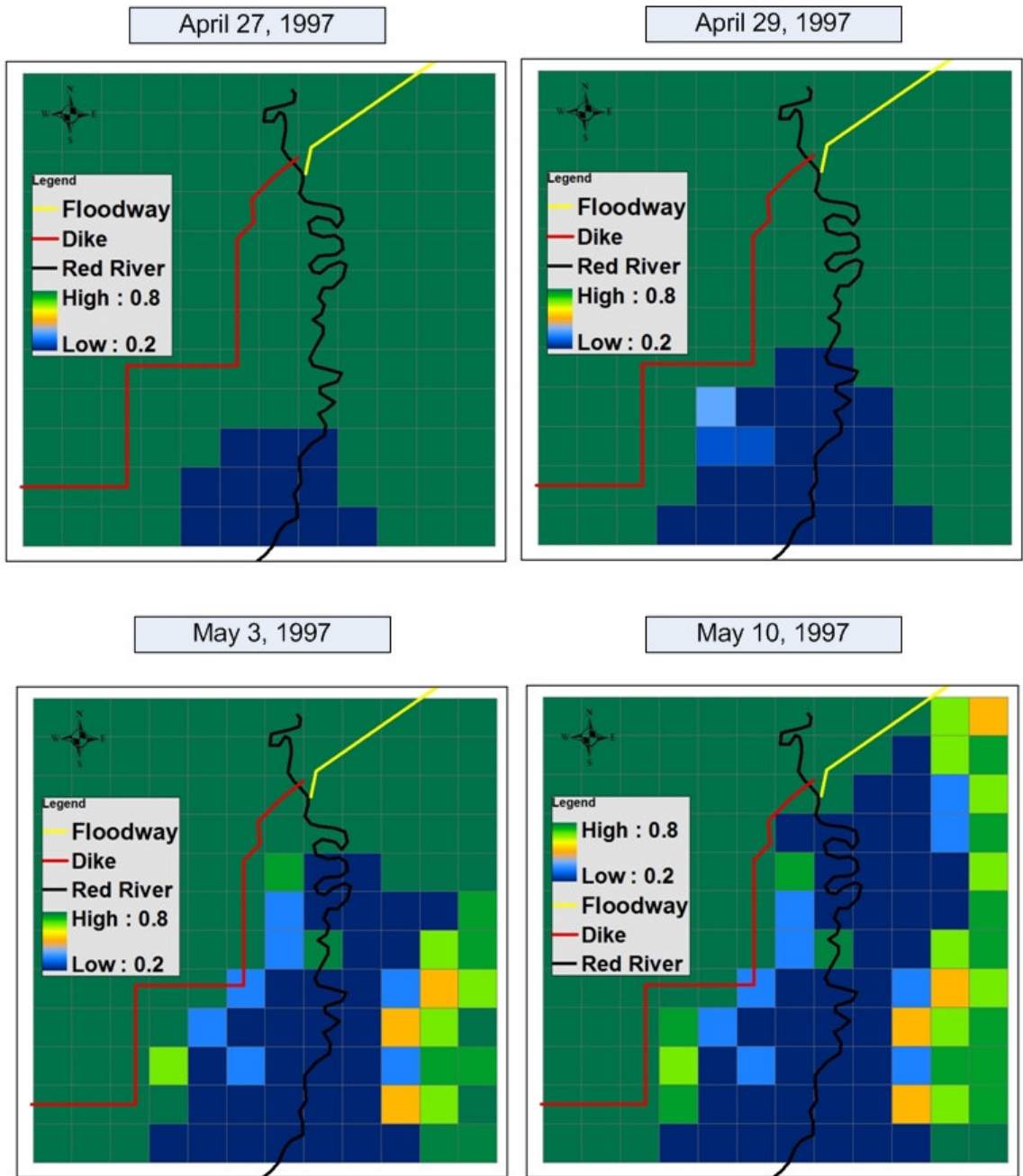


Figure 4.24: Fuzzy resiliency index

4.2 URBAN FLOOD RISK ANALYSIS: CEDAR HOLLOW CASE STUDY

Urban flood risk is a major problem for many cities around the world. Urban flood risk analysis is becoming an inevitable and necessary component of flood risk management. In this research the small residential area of Cedar Hollow, located in London, Ontario is chosen as the case study area to illustrate the methodology of urban flood risk analysis. The case study area is located (Figure 4.25) on the southeast side of Highbury Avenue and Fanshawe Park Road, and is currently under construction for residential development. The Thames River is on the south of the case study area. The topography in this area is gently undulating to hilly in the vicinity of the Arva Moraine is gradually sloping in the south urban area. In general, the topography has a downward slope in the south direction towards the Thames River.

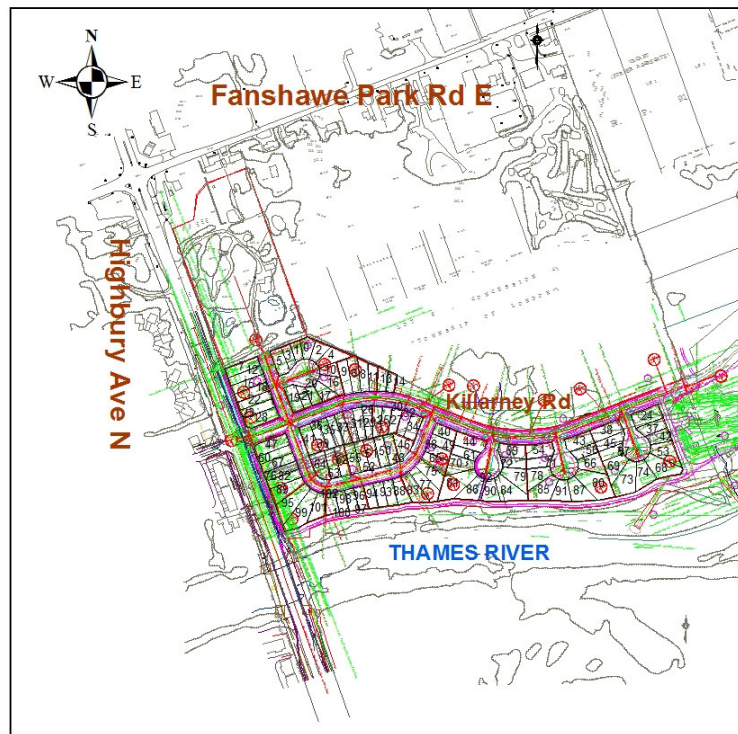


Figure 4.25: Location of Cedar Hollow, London, ON

The present modeling approach involves the linking of a two dimensional overland flow model with a one-dimensional storm sewer model to simulate urban flooding. The new methodology using fuzzy performance indices for urban flood damage and risk calculation, which is described in Section 3.2, is illustrated in the present case study.

4.2.1 COUPLED 1D HYDRAULIC AND 2D HYDRODYNAMIC MODELING

The modeling approach integrates a 1-D hydraulic model (MIKE URBAN) and a 2-D hydrodynamic model (MIKE 21) in a MIKE FLOOD environment. This process is used to link the dynamic interactions between the storm sewer system and overland flow in Cedar Hollow, London, ON. An independent overland flow model is created in MIKE 21 and a storm sewer network model in MIKE URBAN. Then the two models are coupled in MIKE FLOOD. As inputs for urban flood modeling, the MIKE 21 model requires high resolution topographic data containing surface elevation, roughness data and rainfall data.

Topographic Data

The topographic data set used for this study is provided by the Serge A Sauer Map Library of UWO. This data set is in DEM form and has a resolution of 10m by 10m. For the purpose of analysis in this study a higher resolution grid (0.25m by 0.25m) is prepared from this DEM. The DEM is pre-processed in GIS and exported as an ASCII file for import into MIKE 21. The MIKE Zero tool box has a MIKE2GRID conversion utility, which is used to convert the ASCII file to a DFS2 grid file. Since the DEM was prepared in 2004, the converted DFS2 grid file is only an approximate representation of the actual topography. Major residential development in the case study area involves a

change in elevations according to construction design and planning. Therefore the topographic data used in this study required that the elevation aberrations on the construction sites be manually corrected for an approximate description of the current topography. This approximation may have had an impact on the flood extent and flood inundation map.

Boundary Conditions

In MIKE 21 it is essential to provide boundary conditions for the model. Boundary conditions for MIKE 21 have two forms: (i) open, (ii) closed. For urban flooding a closed type of boundary is used by assigning the cells in the boundary with a true land value.

Roughness Data

A MIKE 21 model requires either roughness or bed resistance data to be assigned to the grid cells. There are two ways to assign roughness data in MIKE 21. A constant roughness value can be assigned for all the grid cells in the study area or a DFS2 grid file can be created such that each grid cell can be assigned a different roughness value. In this case the residential area of Cedar Hollow, London, ON was assigned with a roughness value (Manning's Coefficient, n) of 0.025.

Rainfall Data

Rainfall data is used as input to the MIKE 21 model. The rainfall data is applied directly to the grid cells in the case study area. The rainfall is converted to runoff and is routed hydraulically through the grid cells. In MIKE 21 rainfall can be applied in three ways: (i)

constant rainfall applied in every cell, (ii) DFS0 time series rainfall hyetograph applied to every cell, and (iii) DFS2 time series 2D grid to apply unique rainfall hyetograph to each cell of the study area. Since the case study area is relatively small, a DFS0 time series rainfall hyetograph is applied to every location of the case study area. In this study a 500-year, 6-h design rainfall was simulated based on extreme rainfall events to analyze surface inundation. The design storm hyetograph is shown in Figure 4.26.

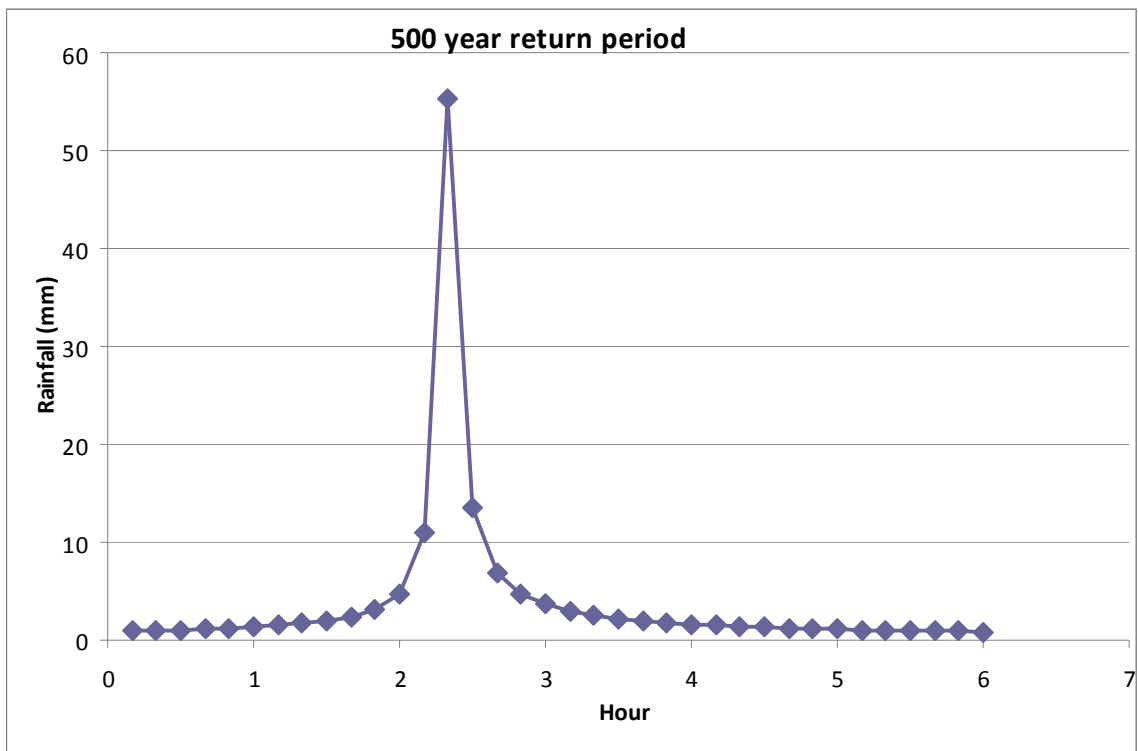


Figure 4.26: 500 year 6-hour design rainfall

4.2.2 URBAN FLOOD DAMAGE ANALYSIS

The innovative approach described in Section 3.2.2 for analysis of urban flood damage, which considers both (i) direct damage, and (ii) indirect damage, is used in the Cedar

Hollow case study. The damage analysis process consists of the following three steps:

Step One: Direct Damage Analysis

Direct damage computes the possible damage caused by flooding to building and infrastructure. MIKE FLOOD provides the necessary flood water depth for this analysis.

Direct damage is assessed using a depth-percent damage relationship. Almost every building of the Cedar Hollow infrastructure has two stories with basement. Figure 5.27 shows the depth-percent damage relationship used to determine direct damage.

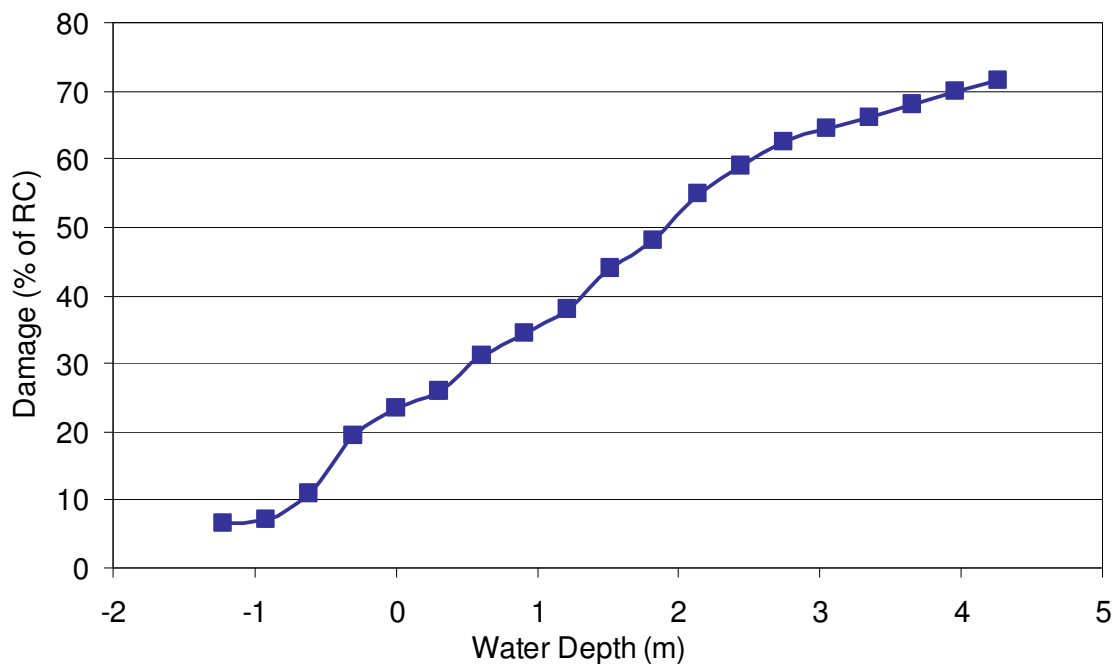


Figure 4.27: FIA based structure depth-damage curve, two or more stories with basement (Scawthorn, 2006)

Step Two: Indirect Damage Analysis

Other than direct damage, urban flooding causes disruptions and inconveniences to

people's lives. Urban flooding can either be trivial in its effects or can cause severe economic losses that are not related to infrastructure damage. In business sectors any interruption in operational activities may cause inconvenient disruptions in service to both suppliers and customers. The extent of such inconveniences depends upon the availability of alternate resources, types of business, duration of disruption, etc. In this case study disruption in business is determined based on the level of obstruction that residents might face due to flooding. A high level of road and other forms of transportation obstruction will translate into a high level of business disruption, particularly for those businesses whose productivity rates rely on access to transportation routes. For an illustration of the methodology, Figure 5.28 shows an obstruction vs. percentage damage relationship used in this study. In an actual case, a detailed investigation is needed by preparing a questionnaire for every resident in the case study area.



Figure 4.28: Road blockage vs. percent damage relationship

Step Three: Assessment of Total Urban Flood Damage

Total damage is assessed based on direct damage (%) and indirect damage (%). A weighted approach is used where direct damage and indirect damage are assigned with weights according to Equation 3.33.

4.2.3 SPATIAL AND TEMPORAL URBAN FLOOD RISK ANALYSIS

Using Equations (3.27), (3.28) and (3.31), the spatial and temporal flood risk analysis of Cedar Hollow is performed by determining a fuzzy combined reliability-vulnerability, robustness and resiliency, respectively. The fuzzy flood damage membership functions for residential land are developed based on the flood damage data. The GUI in Figure 4.29 shows different partial level of flood damage membership functions used in the Cedar Hollow case study.

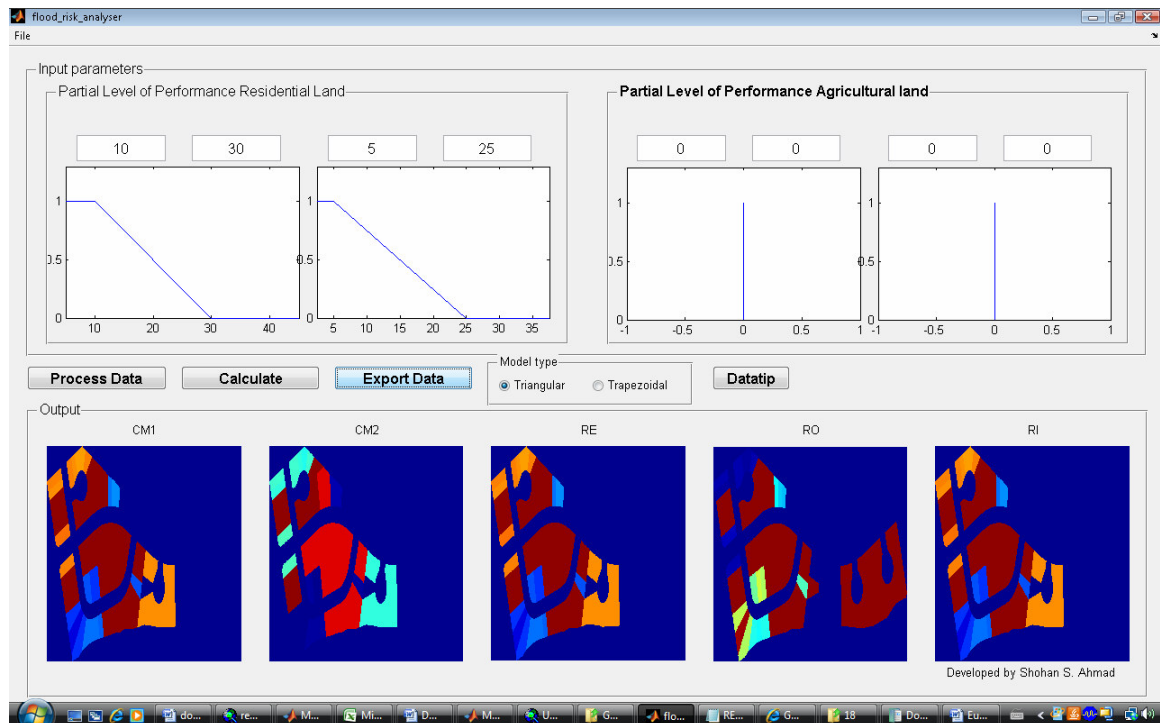


Figure 4.29: GUI with predefined partial level of flood damage for Cedar Hollow

4.2.4 RESULTS AND DISCUSSION:

Spatial and Temporal Variability of Water Surface Elevations

The result of the MIKE 21 model is a time variant 2D grid file that records flood water depth, velocity, flux, etc., at specified time intervals for every location (grid cells) in the case study area. From this, the urban flood extent and the flood water depth are assessed for the storm event. Figure 4.30 shows water surface elevations at the selected time steps of the rainfall hyetograph by using a blue color ramp. During the 6 hour design storm, at 2 hour 10 minutes some of the locations on the road are flooded. The next time step, at the 2 hour 20 minute stage, shows a propagation of overland flow obstructing the roads and also flooding the residential land parcels. At the 2 hour 40 minute and 3 hour time stages, more land parcels are flooded and an increase in water depth is visible.

Spatial and Temporal Variability of Flood Damage

Results of direct damage, indirect damage and total damage are shown in Figure 4.31, 4.32, and 4.33, respectively. Urban flood damage is shown for the Cedar Hollow case study and ranges from 0 percent, being the lowest, to 100 percent, being the highest level of damage.

In the case of direct damage, the range of values are shown with a new reclassification that has (Figure 4.32) 5 zones, thereby offering a better representation of direct damage. The light yellow, reflecting the range of 0 and 10 percent, shows the lowest direct damage. The next range of 10 to 20 percent of direct damage is shown in dark yellow.

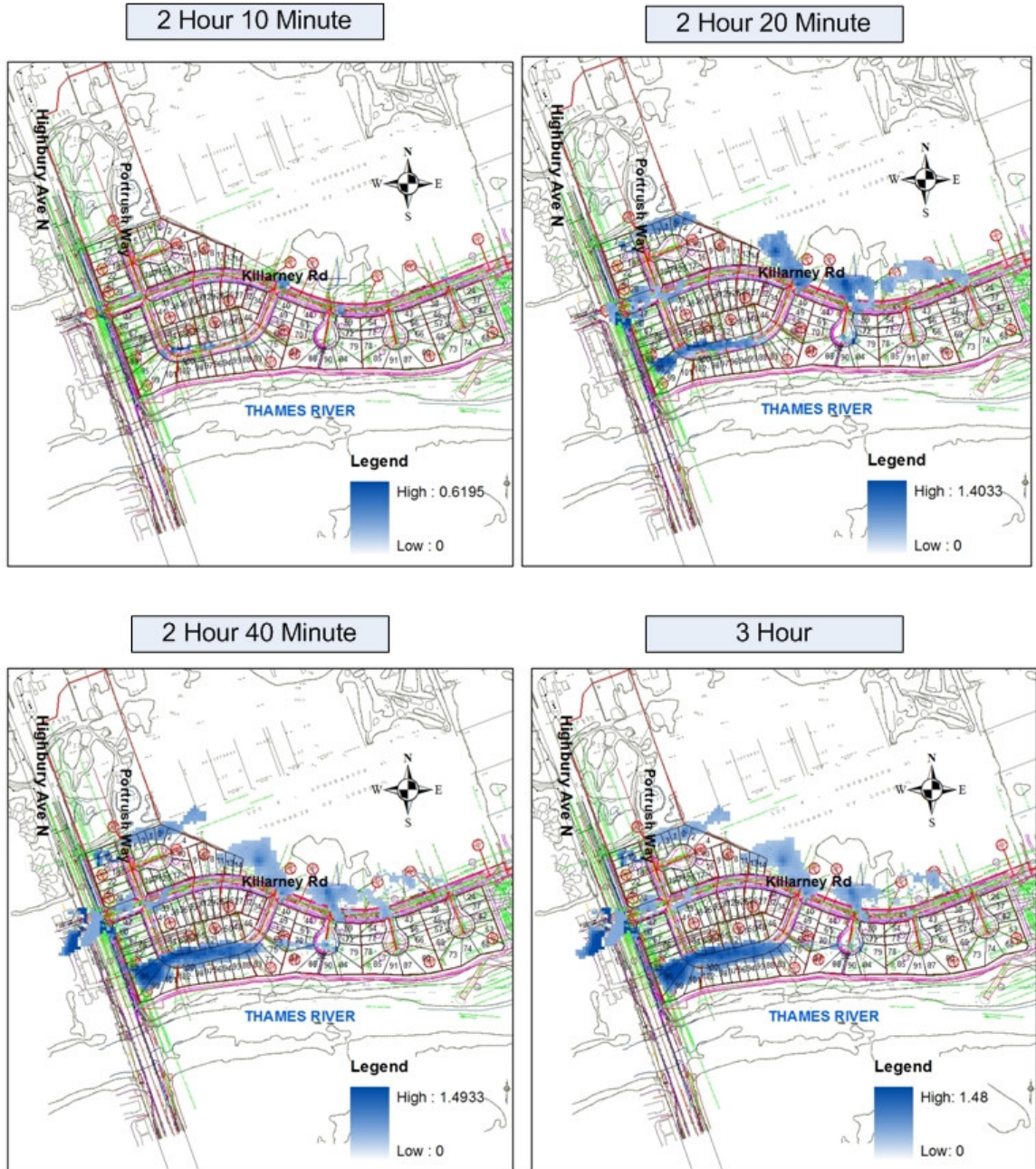


Figure 4.30: Spatial and temporal variation of water surface elevation (meter)

The parcels shown in orange have a higher percentage of direct damage (20 to 30) compared to previous ranges. The next range of 30 to 40 percent direct damage is shown in light brown. The next range of 40 percent and 100 percent representing the highest direct damage is shown in dark brown. From analyzing the maps in Figure 4.32, it can be observed that direct damage increases at the peak period of the rainfall hyetograph. During the 6 hour design storm, at the 2 hour 40 minute and 3 hour time stages, some of the land parcels on the west side of the case study area show considerable direct damage.

Figure 4.33 show the results of indirect damage at selected time steps. In the case of indirect damage, the range of values are shown (Figure 4.33) in 5 zones with Light yellow (in the range of 0 and 20 percent) indicating the lowest indirect damage and dark brown (in the range of 80 to 100 percent) representing the highest damage. The classification is useful in understanding the spatial and temporal variability involved in indirect damage. It can be observed that, generally speaking, residential land parcels that are located farther away from the community entrance suffer a higher level of obstruction. Also supplies and flood relief will reach these land parcels last. Therefore, in the case of these land parcels (in east of the study area) indirect damage will be considerably higher. With propagation of overland flooding more areas become obstructed and as a result the number of residential parcels with indirect damage increases. Total damage is assessed based on Equation 3.33. The color classification used in Figure 4.31 for direct damage is also used in Figure 4.33 to describe the spatial and temporal variability of total flood damage.

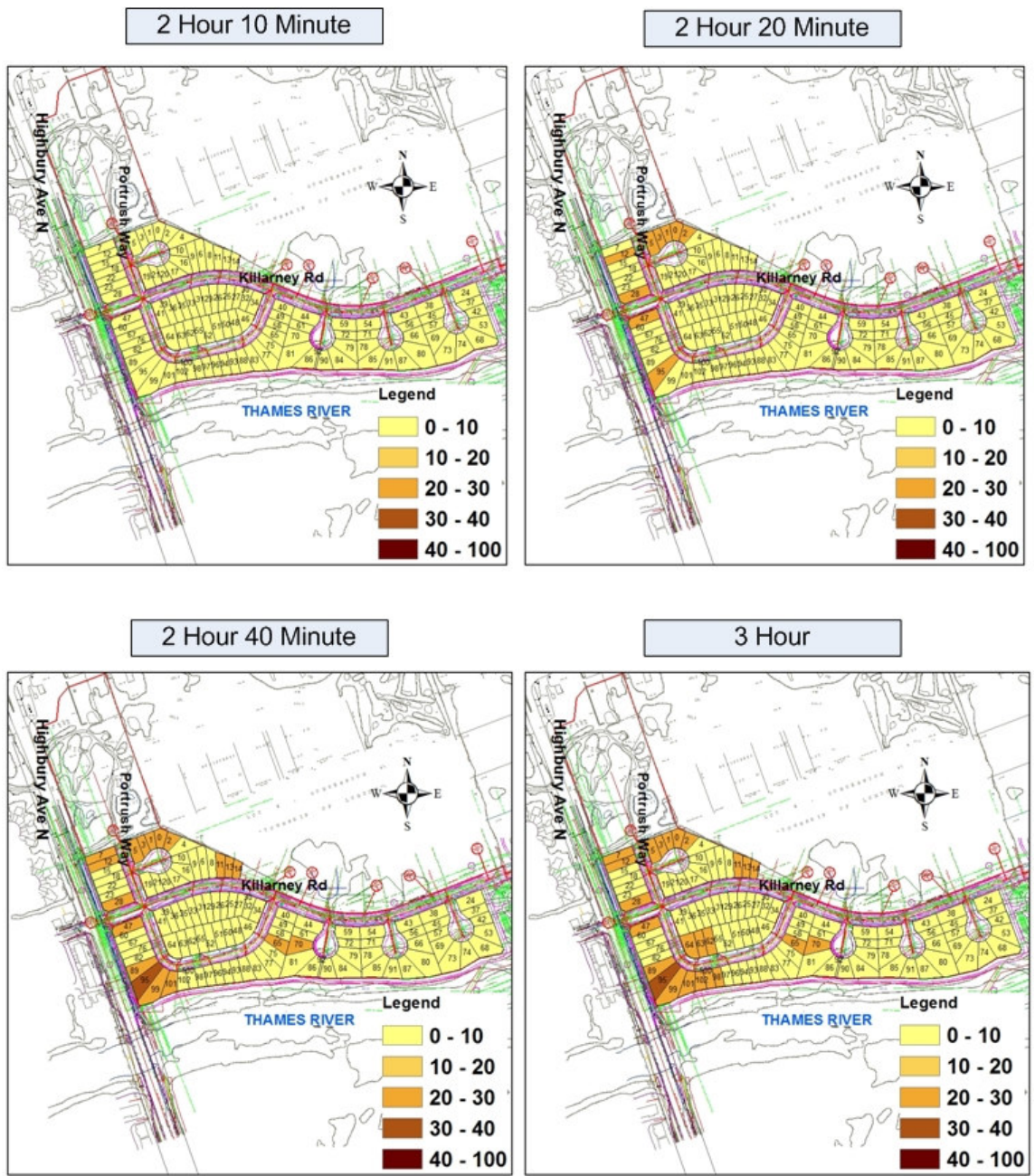


Figure 4.31: Spatial and temporal variation of direct damage
 (Results shown for selected times during the 6 hour design storm)

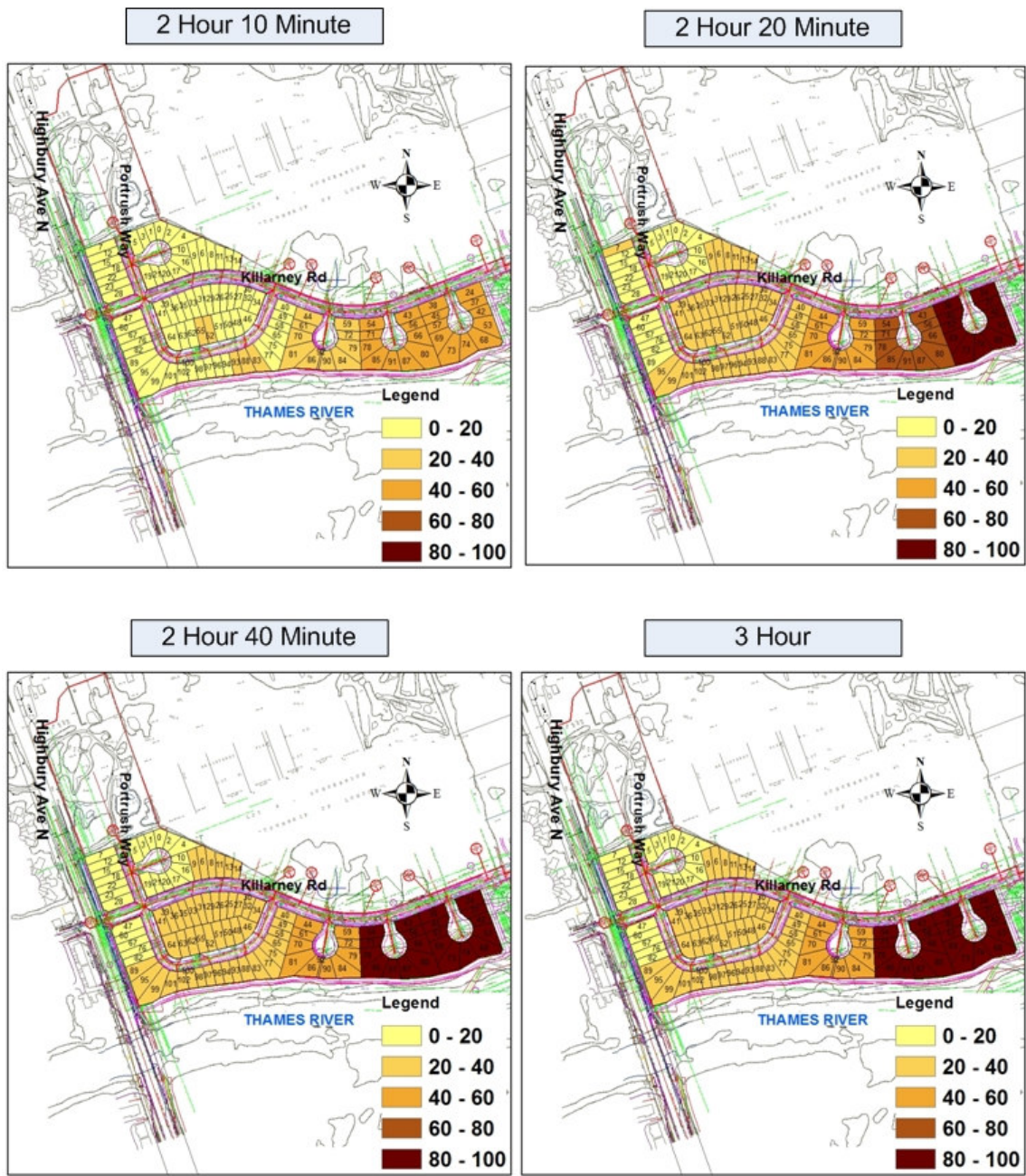


Figure 4.32: Spatial and temporal variation of indirect damage
 (Results shown for selected times during the 6 hour design storm)

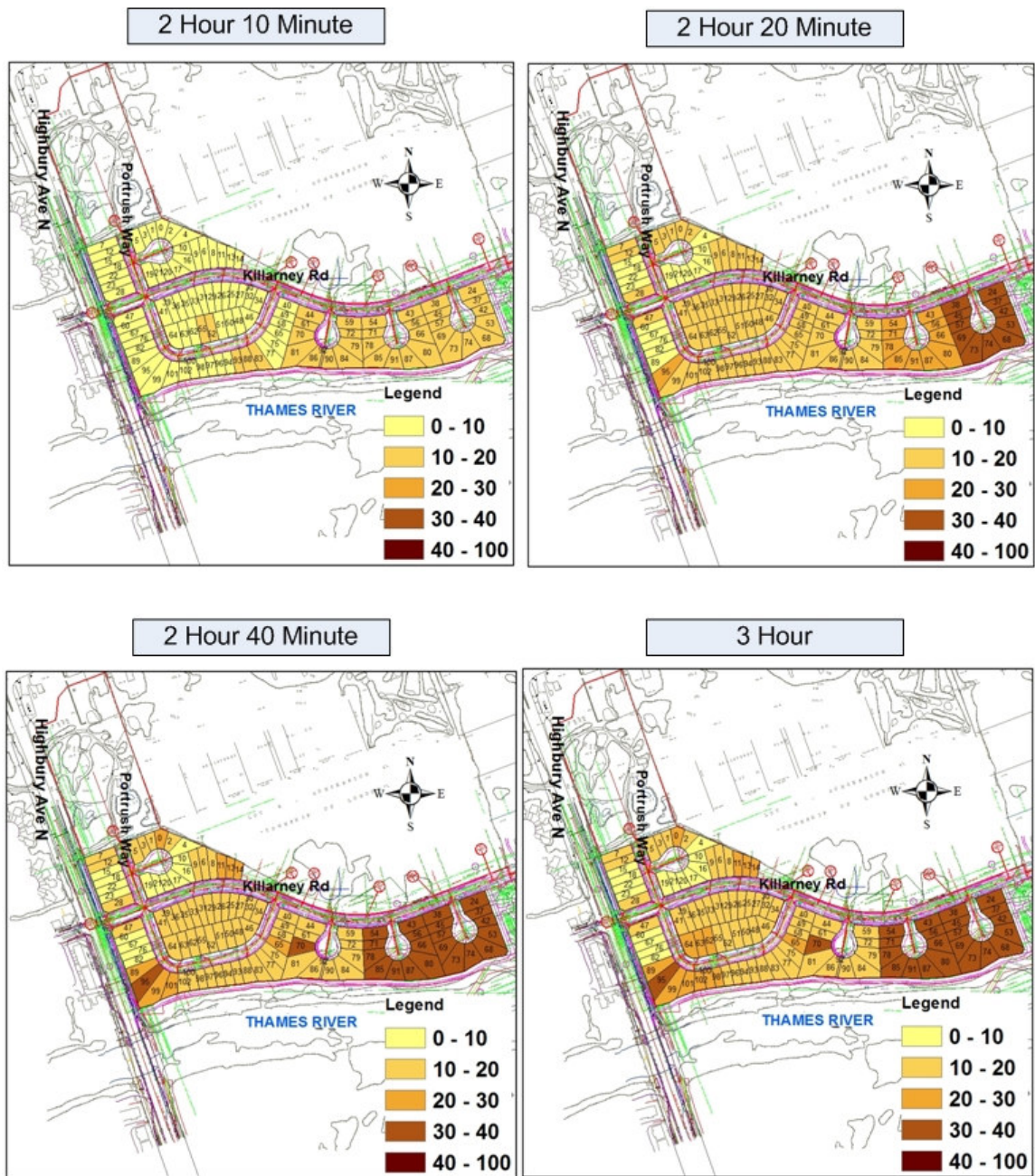


Figure 4.33: Spatial and temporal variation of total flood damage
 (Results shown for selected times during the 6 hour design storm)

Combined Fuzzy Flood Reliability-Vulnerability Index

The combined reliability and vulnerability index for Cedar Hollow, London, ON is expressed in the ranges from 0, (lowest) to 1 (highest). The range of values of the fuzzy reliability-vulnerability index are shown (Figure 4.34) in 5 zones. Dark blue indicates the range of 0 to 0.20, which represents the regions with the lowest reliability. Light blue marks the areas of low reliability where the combined reliability-vulnerability index ranges from 0.21 to 0.40. These areas have a slightly higher reliability compared to the regions shown in dark blue. Orange marks the areas that have a higher reliability compared to areas shown in light blue. The value of the reliability index in this region is between 0.41 and 0.60. Areas in light green have a reliability index in the range of 0.61 to 0.80. Regions with the highest reliability index, which consist of a range of 0.81 to 1.0, are shown in dark green.

Temporal analysis of Figure 4.34 shows that during the 6 hour design storm, at the 2 hour 10 minute time stage most of the case study area is highly reliable. Although residential land parcels on the west have a slightly lower reliability than most of the case study area at this time, as a consequence of obstruction on the road from flood water, at the 2 hour 20 minute time stage (during the 6 hour design storm) their level of obstruction has increased considerably for a land parcel resulting in a lower reliability and a high vulnerability. The situation on the west of the study area worsens even further during the 6 hour design storm, at the 2 hour 40 minute and 3 hour time stage. Most of the study area on the east side is comparatively reliable, while some exceptions found in these land parcels, namely those that have experienced higher levels of flooding, show

significant direct damage and less reliability (Figure 4.34).

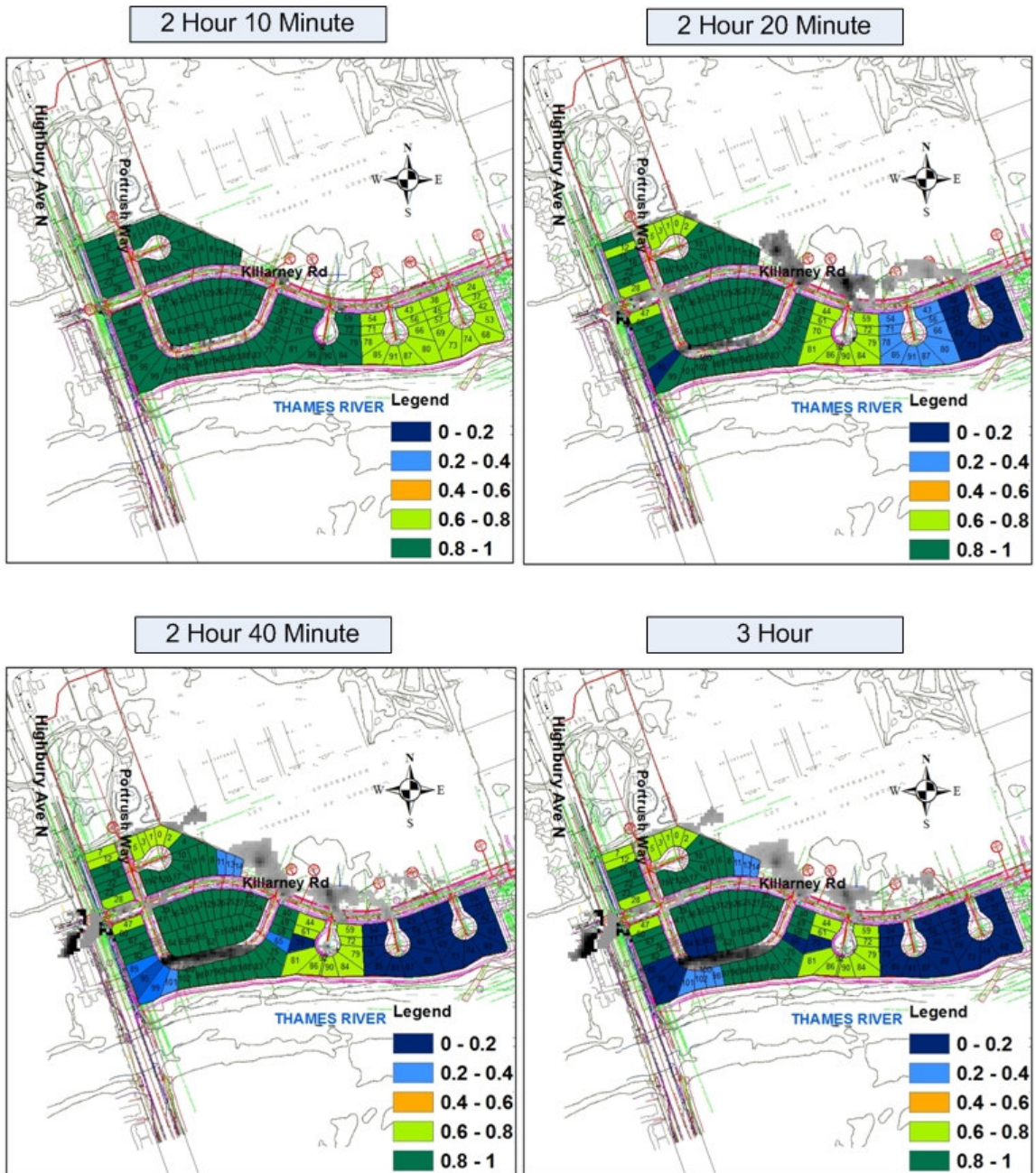


Figure 4.34: Fuzzy combined reliability-vulnerability index

(Results shown for selected times during the 6 hour design storm)

Fuzzy Robustness Index

A fuzzy robustness index is calculated for Cedar Hollow in order to assess the ability of the area to adapt to changes in the partial levels of flood damage. In this case, a fuzzy robustness index is developed based on the two defined partial levels of flood damage. The fuzzy robustness index of a system depends upon the change in fuzzy compatibility. The higher the change in compatibility measure, the lower is the value of robustness index, and vice-versa. The higher the value of the robustness index, the higher the system's ability to adapt to changing conditions. The fuzzy robustness index in this case ranges from 1 (lowest) to 2.5 (highest), with 6 zones (Figure 4.35) demarcating degrees of robustness. Dark blue is used to represent the range of 1 to 1.25, which indicates regions with the lowest robustness. These regions have a very low ability to adapt to changes in the partial levels of flood damage. The next zone, represented by light blue, marks the areas of low robustness where the robustness index ranges from 1.25 to 1.5. These areas have a slightly higher robustness compared to the regions shown in dark blue. Grey is used to represent areas with a higher robustness of 1.5 to 1.75 compared to areas shown in light blue. The transition to higher robustness is shown in yellow where the robustness index ranges between 1.75 and 2. The next range marks an even higher robustness in the range of 2 to 2.25 and is shown in light green. Finally, the highest range of robustness index, from 2.25 to 2.5, is shown in dark green. This region has the highest ability to adapt based on the predefined change in partial levels of flood damage. The spatial and temporal variability of the fuzzy robustness index is shown in Figure 4.35.

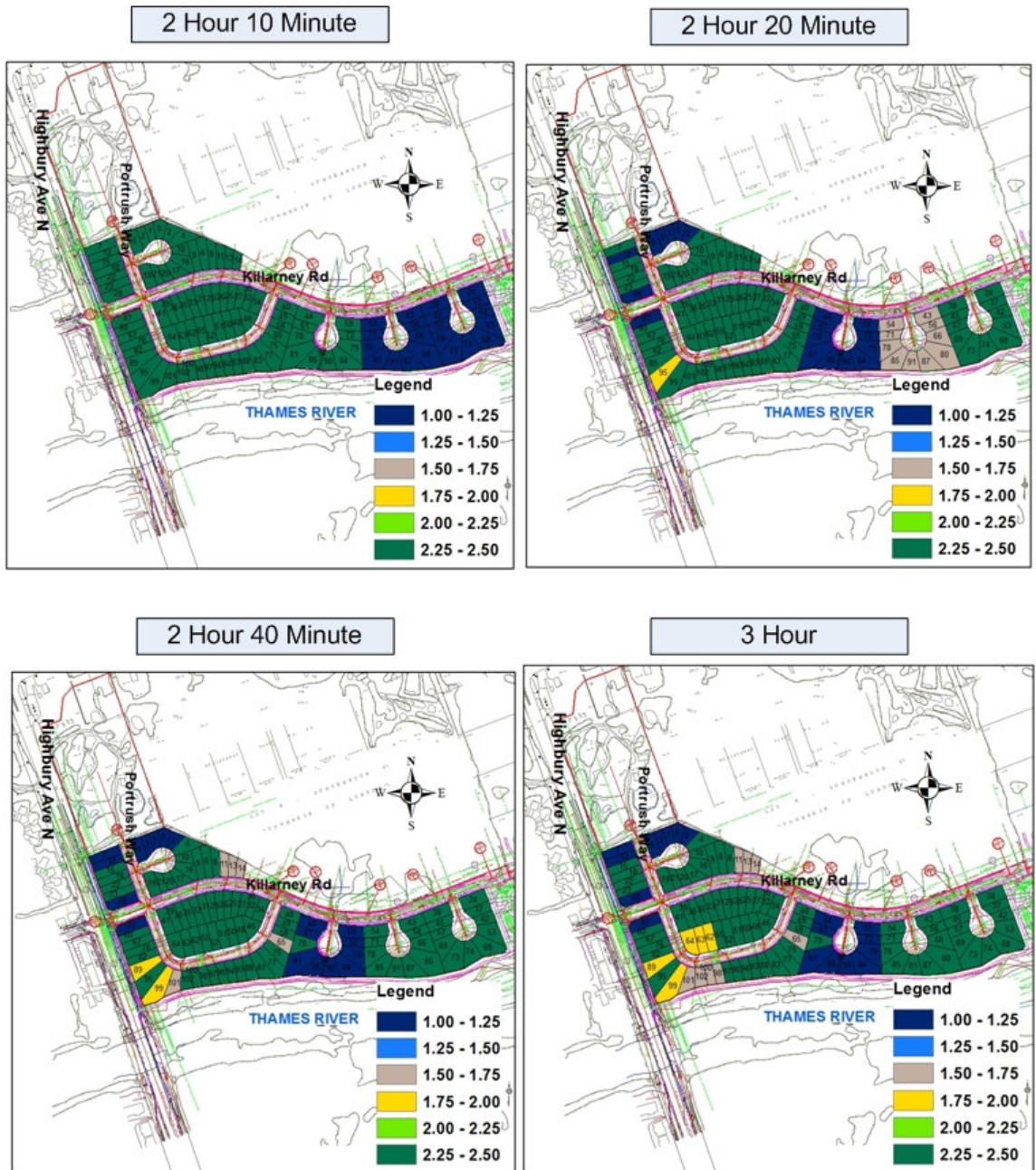


Figure 4.35: Fuzzy robustness index

(Results shown for selected times during the 6 hour design storm)

Fuzzy Resiliency Index

For the Cedar Hollow case study area used in this research, the calculation of fuzzy resiliency index requires information on the recovery time from direct and indirect damage. A detailed investigation is necessary to collect this information from the residents of Cedar Hollow and to determine the appropriate recovery time. Since the case study area is still undergoing construction a detailed investigation of the recovery time is not possible at this time.

5 SUMMARY AND CONCLUSIONS

Floods are the most frequent of natural disasters that affect lives, damage property and degrade the quality of the environment. Since the development of structural flood control measures takes time and is expensive, non-structural flood management measures are essential in minimizing the damage caused by floods. An effective approach to flood risk assessment, such as the one developed in this study, can help reduce flood damage. The physical processes of flood formation and flood risk are both spatially and temporally variable. Therefore, the performance of flood management can be greatly influenced by changing conditions in time and location. In addition, each element of the system must be identified within a spatial and temporal context to understand the interrelationships and interactions within the system. Flood management is multidisciplinary and requires the integration of engineering, social, and economic modeling tools.

The current approaches being used for dynamic modeling are not able to provide adequate solutions to flood management because the engineering, social, and economic modeling tools are not integrated and do not explicitly represent the spatial and temporal dimensions of risk assessment. The current risk assessment models used in practice have certain limitations in their ability to capture the characteristics of flooding that are uncertain, ambiguous, vague, spatial and temporal in nature. The limitations that are associated with current flood management practice provide a motivation to formulate a new approach. This study presents an innovative methodology for addressing the dynamic processes of flooding and flood risk and also addresses spatial and temporal variability.

5.1 FLOOD RELIABILITY ANALYSIS

The spatial and temporal variability of floods can play a significant role in the assessment of risk. However, both the spatial and temporal characteristics of flood, their interrelationship, and interaction within the system are very rarely taken into consideration. In river flood management, flood risk maps are used to show areas at risk of inundation, but they rarely take into account the spatial and temporal uncertainty of flooding. Therefore, people living in floodplain, and also in urban areas, may have an inaccurate perception of the flood risk to which they are exposed. In the case of urban flooding, residents need to know their level of exposure, potential for damage, and other associated risks, particularly in the case of severe flooding caused by heavy precipitation or overland flooding from a nearby river. River and urban flood risk maps that take into account the spatial and temporal uncertainty of flooding can reduce damage to properties and also reduce inconvenience to people's lives.

The problem of data insufficiency is a common problem in flood risk analysis. The principle of uncertainty in flood risk analysis arises from the inability to capture real world phenomena due to lack of knowledge, model prediction errors, or errors in human judgment. The probabilistic approach fails to represent the lack of knowledge, subjectivity and human error associated with flood risk analysis. Fuzzy set theory can address such uncertainties. Therefore, to represent the spatial and temporal variability and uncertainty associated with flood risk assessment and the management process, a new approach has been undertaken where three fuzzy performance indices are used to assess the spatial and temporal variability of flood risk.

The new methodology presented in this thesis addresses the spatial and temporal variability of various sources of uncertainty in flood management. Most of the risk assessment models used in current practice have some limitations in their ability to capture the impact of subjective uncertainty, ambiguity, vagueness of information, data unavailability, and decision makers' perceptions. All these factors, moreover, can further change in time and for different locations. The impacts of the spatial and temporal variability of the extent of damage caused by flooding can play a significant role in the assessment of risk, although they are very rarely taken into consideration. Development of a three dimensional (3-D) fuzzy set, with the first dimension used for the temporal variability of flood damage, the second dimension for the spatial variability of flood damage, and the third its membership degree, allows for addressing the variability of various sources of both spatial and temporal uncertainty. 3-D representation of the acceptance level of partial flood damage also allows for the expression of decision makers risk preferences and the examination of their impacts on flood management decisions. Three fuzzy performance indices: (i) combined fuzzy flood reliability-vulnerability index; (ii) fuzzy flood robustness index; and (iii) fuzzy flood resiliency index, are used in this research for spatial and temporal analysis of riverine and urban floods. A combined fuzzy flood reliability-vulnerability index is used to assess the frequency and severity of a flood threat. A fuzzy flood robustness index is used to assess the ability of an affected area to adapt to a wide range of possible flooding conditions. The time required for an area to recover from flooding has been assessed using a fuzzy flood resiliency index. The implementation of the fuzzy performance indices provides an effective and efficient approach to capture the spatial and temporal variability associated

with flood risk and to assist in the minimization of flood damage.

The number of urban and river floods and the damage associated with them are an ongoing concern all over the world. There is a need for more effective mitigation measures and risk management strategies to minimize flood damage. In the case of urban areas, the consequence of flood damage may be higher based on the size of the population, population density, economic activity, type of infrastructure, etc. The frequency and magnitude of river and urban floods are expected to increase as a result of climate change and the damage is also expected to be much higher with the increasing rates of population growth.

Absolute protection from floods is not possible. Flood risk mitigation mostly focuses on (i) structural, and (ii) non-structural measures. Common structural measures for river flood mitigation include levees or flood walls, diversion structures, channel modifications, flood control reservoirs etc. The structural measures undertaken for storm water management include the use of gutters, small drains, pipes, detention ponds, retention facility, channels, wetlands, reservoirs, treatment plants, culverts etc. Non-structural measures include flood zoning, flood warning, waterproofing, and flood insurance. Promoting flood awareness among local people by informing them about the risks and also preparing them for the event of a flood can significantly reduce flood damage. The development of structural measures alone cannot guarantee absolute protection from floods, so it is necessary that structural measures are combined with non-structural measures for more efficient river and urban flood risk management. The use of

fuzzy performance indices and the preparation of risk maps are intended to address the need for better flood risk management in both river and urban environments.

5.1.1 RIVER FLOOD RISK ANALYSIS

The Red River basin, from the community of St. Agathe to the south of the Winnipeg floodway in Manitoba, Canada, is used to illustrate the applicability of a spatio-temporal fuzzy risk analysis in river flood management. This research presents two modeling tools for simulating spatial and temporal variations of flows and water surface elevations in the Red River basin: (i) a two-dimensional hydrodynamic modeling, and (ii) system dynamics modeling. The spatial and temporal fuzzy risk analysis of the Red River flood of 1997 is performed and results are shown in maps as (i) fuzzy combined reliability-vulnerability index, (ii) fuzzy robustness index, and (iii) fuzzy resiliency index.

2D Hydrodynamic Modeling

2D hydrodynamic river modeling is presented in this research as a powerful application for spatial and temporal analysis of flood risk variation. In the case of very flat floodplains with complex topographic features and the presence of infrastructure, flood wave propagation cannot be properly captured using 1D modeling tools. To accurately capture the overland flows, a 2-D modeling approach is required. As the Red River valley is very flat, a 2-D hydrodynamic modeling approach is used in the basin for flood risk management.

Advantages of 2D Hydrodynamic Modeling:

The main advantage of using the 2-D approach is that it provides information on variations in velocity and depth at any point of interest in the model domain. In this research, MIKE 21 is used for the 2-D hydrodynamic modeling, and it is capable of generating a modeling system for 2-D free-surface flows. Full Navier-Stokes equations, i.e. the continuity and X and Y -momentum equations, are used for the conservation of mass and momentum to describe the flow and water level variations in two-dimensional models. The modeling system solves the fully time-dependent non-linear equations of continuity and momentum using an Alternating Direction Implicit (ADI) finite difference scheme of second-order accuracy with the variables defined on a space staggered rectangular grid. The benefit of such 2D hydrodynamic modeling is that it produces an accurate outcome for the simulation of water level and fluxes in time and space. In this research, the MIKE 21 model results were satisfactory for assessing the flooding of the Red River Basin in 1997 in the region from Ste. Agathe to the Red River Floodway control structure (southern border of the City of Winnipeg).

Disadvantages of 2D Hydrodynamic Modeling:

The 2D hydrodynamic modeling approach also has some disadvantages. The interoperability of different software components is still a major area of concern. There is no direct communication between GIS and the hydrodynamic model, MIKE 21. All topographic data processed in the GIS must be converted to ASCII format prior to importing it to MIKE 21. With every change in topography, e.g., size, height or location of dike, the process has to be repeated. Another disadvantage is in the use of the LIDAR

airborne survey used to collect the topographic information in the study area. LIDAR technology is not capable of penetrating the water surface so this method does not provide any information on river cross-sections. Cross-section data are adopted from a different source that requires datum correction and geo-referencing. This merging of data introduces some error in the high-resolution LIDAR data, particularly as cross-sectional data for the Red River basin are taken from old surveys carried out in 1979 and the 1950's.

MIKE 21 cannot explicitly model the operation of the floodway. There is an indirect way to incorporate floodway operations, i.e., by using a sink function in the model and providing diverted flows at the floodway as input to the sink. However, there is a limitation with this approach, since the sink function only affects the continuity equation. The momentum term is unaffected in the Saint-Venant equation. Thus, backwater effects due to the operation of the floodway cannot be captured accurately. Also, 2D models, compared with 1-D models, require a significant amount of additional data (especially topographic data) and time to set up and run. Any change in topography, such as an addition of a dike, will require a change in topographic data and the necessitation of incorporating such changes. In general, this process is more time consuming than the process used in 1-D models. Nevertheless, 2D models provide a better description of flow paths and velocities.

However, the major concern with 2-D modeling is the lengthy computation time. Due to the necessity of a detailed description of topography and the inclusion of additional terms

for mass and momentum equations, the 2-D models require more time and computational resources to simulate a hydrologic event. For the Red River Basin case study the computation time for the 2D hydrodynamic model, which used a time step of 2 seconds, a 30 days duration of event, and a spatial resolution of 25 m, is around 14 days for MIKE 21. This makes it very difficult to run the 2D model in a real-time flood event. However, with rapid advancements in computing power this will not be an issue in the near future.

Despite all the disadvantages of the 2D hydrodynamic modeling approach, with respect to the topography of the Red River Basin the 2D hydrodynamic model is the best approach for accurately predicting spatial and temporal variation of water surface elevation, velocity, flux etc., in the computational domain.

System Dynamics Modeling

The system dynamics modeling approach presented in this thesis has the potential to enhance the modeling capabilities in river flood risk management, where the main interest is the modeling of spatial and temporal processes. System dynamics modeling can benefit application areas such as modeling the spread of pollution, hydrologic and atmospheric processes modeling, and disaster management. Within disaster management, the areas where the proposed approach can significantly enhance the modeling capability are the following: the spread of infectious diseases, fire spread, overland flooding, and evacuation planning. In this research the system dynamics approach is applied to solve the problem of overland flooding for flood risk management. The study area is divided into cells. The overland flow is modeled for the river using the Muskingum routing

method, while for the floodplains a cell-to-cell routing approach is used. The routing model is developed using the system dynamics modeling tool. In this research, results of the system dynamics simulation appear in the form of the spatial and temporal variations of flood water elevations, which provide the input required in order for the spatial and temporal risk analysis process to calculate fuzzy performance indices. The focus of the presented research work in system dynamics is to develop an approach that can address the dynamics of flood propagation.

Advantages of System Dynamics Modeling:

A system dynamics approach captures feedback-based dynamic processes and negotiates time and space in an explicit way. The main advantage of using the system dynamics approach is in its ability to model dynamic processes in time and space. The strengths of the simulation model used in this study, which is based on the system dynamics approach, include the increased speed of model development, the ease of model structure modification, and the capability of performing sensitivity analyses. Based on the implementation of a system dynamics approach for overland flooding, the model shows great potential for capturing the dynamic process of floods and for addressing the spatial and temporal variability that is so crucial in flood risk management. The system dynamics approach also provides a way for decision makers to participate in the model building process, thus increasing their trust in the model. The decision maker's comments provide direction for follow-up simulations and modifications in the model structure.

Disadvantages of System Dynamics Modeling:

For flood management application, simplified routing methods are used for hydrodynamic modeling, such as the Muskingum method for river flow and the cell-to-cell routing method for floodplains. The Muskingum method is relatively easy to implement in system dynamics and in the case of rivers with a mild slope this method provides a reasonably good approximation. There are more accurate methods available for flow description; however, in system dynamics models there is no easy way to fully describe two-dimensional flow using continuity and momentum equations. This is partly because the modeling tool (Stella) does not allow the direct writing of differential equations. The system dynamics modeling tool (Stella) automatically generates differential equations from graphical icons, which are used to develop the model. Therefore, for modeling a flat basin such as the Red River, the Muskingum method is used in this research. However, due to the presence of downstream control structures in the Red River basin, this method was not able to model the back water effects that were so heavily responsible for the severe flood damage around the town of St. Agathe.

The second challenge for the system dynamics model was using an array structure to capture the flow process in the river and floodplain. In the system dynamics model with discretized space (using array), it was very difficult to produce a stock-flow structure that could describe a physical process in two dimensions.

The system dynamics modeling approach, in this study, is based on the cell-to-cell routing approach which involves dividing the land surface into segments, and routing

flow from one segment to the next until it arrives at a final point. Therefore, for the Red River basin the case study was divided into segments. The assumption in the cell to cell routing approach is that the land surface within each of these segments is homogeneous, which leads to further limitations.

Another disadvantage in system dynamics modeling is its inability to communicate between SD and GIS. Due to this limitation the data exchange between SD and GIS was achieved through the spreadsheets. Considering the large area in the Red River Basin case study and the limitation of direct data exchange between SD and GIS, the number of cells used to represent the case study area was not sufficient. This led to approximations in surface elevation for each discretized space.

Due to such limitations of the system dynamics approach, specifically in this research and its aim of simulating overland flooding, the model results were not as satisfactory as compared to the model results obtained from 2D hydrodynamic modeling. Furthermore, system dynamics modeling is not capable of simulating urban flooding as a result of heavy rainfall and the insufficient capacity of sewer systems. There is no way to dynamically link a storm sewer model with an overland flow model in SD to simulate urban flooding. Considering all these disadvantages, the system dynamics model was not used in simulating overland flooding for urban flood risk analysis.

5.1.2 URBAN FLOOD RISK ANALYSIS

This research used hydrodynamic modeling to predict flooding in a complex urban

environment. A novel approach was used to dynamically model the interaction between the storm sewer system and street network. A 1D storm sewer model (MIKE URBAN) was dynamically linked with 2D overland flow model (MIKE 21) to generate flood inundation extent, flood water depth and duration of flooding. In order to illustrate the methodology used in this research, the Cedar Hollow community in London, ON was chosen as a case study area. The coupled hydrodynamic modeling approach proved an essential tool for modeling the flow exchange between sewer system and overland flow, thereby predicting flood inundation in urban environments. The coupling of a 2D hydrodynamic overland flow model with a 1D hydrodynamic storm sewer model for urban flood modeling has many advantages compared to traditional methods. The modeling approach also has some challenges.

Advantage of Hydrodynamic Modeling for Urban Flooding:

One of the most important benefits of this approach is the ease of model development. A 1D storm sewer model, such as MIKE URBAN, requires node location, pipe sizes, pipe slopes and invert elevations as inputs. Model development of a 2D overland flow model such as MIKE 21 uses topography, rainfall and roughness data. The model development depends heavily on the available digital data, which reduces field work and surveying. Availability of high resolution LIDAR makes it further possible to prepare high quality topographic data as input into the hydrodynamic model. With the advancement in computer technology it has become possible for a 2D hydrodynamic model to solve full Navier-Stokes equations numerically using such high resolution LIDAR data.

Disadvantage of Hydrodynamic Modeling for Urban Flooding:

A disadvantage of using hydrodynamic modeling for urban flood simulation is the model's dependability on high resolution topographical data. The problem in many cases is that the available topographic data lacks an acceptable quality, which becomes difficult to use in models. The processing of LIDAR data in complex urban areas, where there are lots of buildings/infrastructures, may also result in a certain level of inaccuracy. In the case of rapid urban development, there can be several changes to the land that the existing topographical data does not account for, such as cutting and filling land areas for construction and other land development. In such circumstances LIDAR data should not be used without a proper investigation of its quality, and therefore usability. The case study area used in this research, for instance, is still undergoing construction. Therefore the LIDAR data required some modification with the help of design drawings that show the design elevation for Cedar Hollow. Accordingly, it is possible that, in the case of this research, the processing of the LIDAR data may contain certain levels inaccuracy.

5.2 THE USE OF SPATIAL AND TEMPORAL FUZZY RELIABILITY ANALYSIS IN PRACTICE

Most of the current flood risk mapping focuses on the presentation of depth-damage exceedence probability for a certain flood return period. The risk associated with a 100 year event shows a one percent chance of risk being either equal to or being exceeded in any given year. This risk is associated only with the outer edge of the 100-year floodplain. Therefore, for river flooding the areas closer to the river face a higher risk of a real flood event, and for urban flooding it is the areas with lower elevations that are at a

higher risk for a flood event. The problem, then, is that people tend to believe that during a 100-year flood in a 100-year floodplain, the entire floodplain has a risk of one percent exceedence probability. Traditional approaches to preparing for the possibility of flooding and the extent of potential damage and severity, shown in the maps using a probability-exceedence approach, can be misleading since they do not consider the spatial and temporal variation of flood risk. The maps presenting the spatial and temporal reliability indices provided in this research represent a highly valuable and practical tool for risk assessment as they provide a detailed quantitative analysis by taking into account the spatial and temporal variability of risk.

Traditionally, flood risk maps are used to provide qualitative (low, moderate or significant) risk ratings to inform the public of the potential flood danger. The fuzzy reliability maps represent reliability in terms of a 0 – 1 scale. This quantitative value provides additional information to help affected stakeholders understand if they are at risk of river and urban flooding and to what extent. This information can assist the emergency management process, and in addition offer vital data that might be helpful in the case of evacuation from the flooded areas. Property owners can develop more accurate and effective approaches to planning contingency strategies in the event of flooding. These maps can also help authorities and government agencies in pursuing sustainable development in land-use planning and infrastructure placement. In river-flood prone areas, residential and commercial development can more accurately account for regions where the reliability index is higher. In the case of urban-flood prone areas, the residential and commercial development can more accurately consider regions with

higher reliability indices and better ensure that they have an efficient storm sewer system. With the help of this information, buildings can be built on raised lands where the reliability index is normally very high. To prevent future damage, planners can also restrict the construction of buildings in locations that have low flood reliability. However, locations closer to the river, lakes etc. may have a higher value as recreational areas. If a building or infrastructure is already within a high vulnerability zone then the fuzzy reliability maps can be used for planning various temporary flood proofing measures. Long-term regional planning can benefit from the fuzzy reliability maps by determining any strategic directions for future developmental activities, particularly as these will not increase the vulnerability of people and infrastructure to flood events and will also contribute to a more resilient community structure.

The maps of fuzzy reliability indices are a potentially very effective tool for the insurance industry in setting flood insurance premiums. Higher insurance premiums may be issued for homes that are at a high risk of river and urban flooding, i.e. that have a low reliability index in the map, and lower premiums issued for homeowners in locations with a high reliability index. Premiums set by the insurance industry on the basis of the fuzzy reliability analysis of flooding can be used in the decision process of selecting the location for a future development project.

Spatial and temporal uncertainty associated with flooding makes the risk analysis process a very complex issue. The proposed methodology addresses spatial and temporal uncertainties related to flooding. In this study, the spatial and temporal representation of

fuzzy performance indices is proven to be an effective and efficient approach in capturing the spatial and temporal variation of flood risk and assisting in the minimization of (i) river, and (ii) urban flood damage.

5.3 RECOMMENDATIONS FOR FUTURE WORK

Some possible research directions for future work are outlined in this section.

5.3.1 INTELLIGENT DECISION SUPPORT SYSTEM

The system developed in this research, is an interactive model that users, i.e. flood manager or decision makers, can apply to assess flood risk in time and various locations in space. Future research work can focus on integrating this model into a computerized intelligent decision support system, which through an interactive consultation interface will support a dialogue with the user. Such future work might also provide consultation with the knowledge base and the numerical models, which could be highly instructive for analyzing an efficient flood management system and also for determining suitable flood damage reduction measures.

5.3.2 APPROPRIATE SHAPE OF FUZZY MEMBERSHIP FUNCTION

The fuzzy risk methodology developed in this research requires the generation of a fuzzy membership function. The shape of the membership function that best represents the flood damage should be selected on the basis of available damage information and the stakeholder's knowledge of the system. Future work can focus on integrating the intelligent decision support system mentioned in Section 6.3.1 with a way to develop an

appropriate shape of the membership function, which would vary depending on the specifics of each case study. Despic and Simonovic (2000) provide a review of methods for developing an appropriate membership function for flooding that combines available data, expert opinion, and stakeholder preferences. Such preferences are likely to aim at improvements to the flood management process.

5.3.3 MULTI-OBJECTIVE DECISION SUPPORT SYSTEM

The use of spatial and temporal fuzzy reliability measures for multi-objective decision making can be a vital tool in floodplain management. To determine the preferences from multiple decision makers involved in the floodplain management, both the methodology developed on the basis of Akter, Simonovic and Salonga (2004) to obtain the stakeholders' input in an appropriate form, and the Spatial fuzzy multi-criteria decision making tool developed by Simonovic and Nirupama (2005), can be used to rank all alternatives in space according to three reliability measures under the decision makers preferences.

REFERENCES

- Ahmad, S. and Simonovic, S. P. (2000a). System dynamics modeling of reservoir operations for flood management. *J. Comput. Civ. Eng.*, 14(3): 190–198.
- Ahmad, S. and Simonovic, S. P. (2000b). Dynamic modeling of flood management policies. *Proc., 18th Int. Conf. of the System Dynamics Society, Sustainability in the Third Millennium*, Bergen, Norway.
- Ahmad, S. and Simonovic, S. P. (2000c). System dynamics modeling of reservoir operations for flood management. *J. Comput. Civ. Eng.*, 14(3), 190–198.
- Ahmad, S. and Simonovic, S. P. (2004). Spatial System Dynamics: New Approach for Simulation of Water Resources Systems. *Journal of Computing in Civil Engineering*, ASCE, 18(4):331-340.
- Ahmad, S. S. and Simonovic, S. P. (2007). A methodology for spatial fuzzy reliability analysis. *Applied GIS*, 3(1): 1-42.
- Akter, T. and Simonovic, S. P. (2005). Aggregation of fuzzy views of a large number of stakeholders for multi-objective flood management decision-making. *Journal of Environmental Management*, 77, (2), 133-134.
- Ang, H-S. and Tang, H. (1984). *Probability Concepts in Engineering Planning and Design*. New York, USA: John Wiley & Sons, Inc.
- Apel, H., Thielen, A. H., Merz, B. and Blöschl, G. (2004). Flood Risk Assessment and Associated Uncertainty, *Nat. Hazards Earth Syst. Sci.*, 4, (2), 295-308.
- Asante, K. O. (2000). Approaches to continental scale river flow routing, *Doctoral Dissertation*, Submitted to the Graduate School, The University of Texas at Austin.

- Baker, W. L. (1992). Effects of settlement and fire suppression on landscape structure. *Ecology*, 73(5): 1879-1887.
- Barbara, P. and Donnell (2006). *User Guide To RMA2 WES Version 4.5*. US Army, Engineer Research and Development Center Waterways Experiment Station Coastal and Hydraulics Laboratory.
- Bedient, P. B. and Huber, W. C. (1988). *Hydrology and floodplain analysis*. Addison-Wesley, New York.
- Bender M. J. and Simonovic, S. P. (2000). A Fuzzy Compromise Approach to Water Resources Systems Planning Under Uncertainty. *Fuzzy Sets and Systems*, 115, 35-44.
- Bolle, A., et al. (2006). Hydraulic modelling of the two-directional interaction between sewer and river systems. *Proc., Urban Drainage Modelling and Water Sensitive Urban Design*, Monash Univ., Melbourne, Australia.
- Borsuk, M., Clemen, R., Maguire, L. and Reckhow, R. (2001). Stakeholder values and scientific modeling in the Neuse river watershed. *Group Decision and Negotiation*, 10, 355–373.
- Carr, R. S. and Smith, G. P. (2006). Linking of 2D and pipe hydraulic models at fine spatial scales. *Urban drainage modelling and water sensitive urban design*, Monash Univ., Melbourne, Australia.
- CBC news. (2010). Madeira flood kills at least 42, Retrieved July 1, 2010, from <http://www.cbc.ca/world/story/2010/02/21/madeira-flood-toll-rises.html>
- Chen, A. S., Djordjevic, S., Leandro, J. and Savic, D. (2007). The urban inundation model with bidirectional flow interaction between 2D overland surface and 1D sewer networks. *Proc., 6th NOVATECH Int. Conf., Workshop I*, Graie, Lyon, France, 465–

- 472.
- CHI. (2006). *The Flexible, Powerful, and Decision Support System, Detailed Description*. Computational Hydraulics International.
- Chow, V. T., Maidment, D. R. and Mays, L. W. (1988). *Applied hydrology*, McGraw-Hill, Inc., NY.
- Coe, M. (1994). Simulating continental surface waters: an application to holocene northern Africa, *Journal of Climate*, 10: 1680–1689
- Costanza, R., Sklar, F. H. and White, M. L. (1990). Modeling coastal landscape dynamics: Process-based dynamic spatial ecosystem simulation can examine long term natural changes and human impacts. *BioScience*, 40(2), 91–107.
- Coyle, R. G. (1996). *System dynamics modeling*, Chapman and Hall, London.
- Despic, O. and Simonovic, S. P. (2000). Aggregation operators for soft decision making. *Fuzzy Sets System*, 115, (1), 11–33.
- DHI. (2004). *MOUSE Pipe Flow Reference Manual*. DHI Water and Environment.
- DHI. (2008a). *Mike11 User manual*. DHI Water and Environment.
- DHI. (2008b). *Mike21 Flow Model, Hydrodynamic Flow Module, User Guide*. DHI Water and Environment.
- DHI. (2009). *MikeUrban User manual*. DHI Water and Environment.
- DHI. (2009). *MikeFlood User manual*. DHI Water and Environment.
- Downer, C. W. and Ogden, F. L. (2006). *Gridded Surface Subsurface Hydrologic Analysis (GSSHA) User`s Manual*. US Army Corps of Engineers, Engineer Research and Development Center.
- Duckstein, L., Plate, E. and Benedini, A. (1987). *Water Engineering Reliability and*

- Risk: A system Framework. *Engineering Reliability and Risk in Water Resources*, NATO ASI Series, No. 124, pp.1-18.
- El-Baroudy, I. and Simonovic, S. P. (2004). Fuzzy criteria for the evaluation of water resource systems performance. *Water Resource Research*, 40, (10).
- EPA. (1995). *SWMM Windows User Interface*. United States Environmental Protection Agency.
- ESRI. (2009). <http://www.esri.com>.
- Euro news. (2010). Polish flood death toll rises to nine, Retrieved July 1, 2010, from <http://www.euronews.net/2010/05/21/polish-flood-death-toll-rises-to-nine/>
- Ford, A. (1999). Modeling the environment. An introduction to system dynamics modeling of environmental systems, Island Press, Washington, D.C.
- Forrester, J. W. (1961). *Industrial dynamics*, Pegasus Communications Inc., Williston, Vt.
- Fletcher, E. J. (1998). "The use of system dynamics as a decision support tool for the management of surface water resources." *Proc., 1st Int. Conf. on New Information Technologies for Decision-Making in Civil Engineering*, Montreal, 909–920.
- Ganoulis, J. G. (1994). *Engineering Risk Analysis of Water Pollution: Probabilities*. Netherlands, Weinheim: VCH.
- Guesgen, H. W. (2005). Fuzzy Reasoning about Geographic Regions. In E. P. Petry, V. B. Robinson, & M. A. Cobb (Eds.), *Fuzzy Modelling with Spatial Information for Geographic Problems*. (pp. 1-14). Berlin, Germany: Springer press.
- Haimes, Y. Y. (1998). *Risk Modeling, Assessment, and Management*. Wiley Series in

- systems Engineering, USA.
- Hashimoto, T., Stedinger, J. R. and Loucks, D. P. (1982a). Reliability, Resiliency, and Vulnerability Criteria for Water Resources System Performance Evaluation. *Water Resources Research*, Vol. 18, No. 1, pp. 14-20.
- Hashimoto, T., Loucks, D. P. and Stedinger, J. R. (1982b). Robustness of Water Resources Systems. *Water Resources Research*, Vol. 18, No. 1, pp. 21-26.
- Horritt, M. and Bates, P. D. (2002). Evaluation of 1D and 2D numerical models for predicting river flood inundation. *J. Hydrol.*, 268, 87–99.
- HPS Inc. (2001). *Tutorial and technical documentation STELLA 5.1.1*, Hanover, N.H.
- Hydrologic Engineering Center. (1989). *EAD – Expected Annual Flood Damage Computation, User's Manual*. United States Army Corps of Engineers.
- Hydraulic Engineering Center. (2010). *HEC-RAS River Analysis System, Hydraulic Reference Manual, Version 4.1*. United States Army Corps of Engineers.
- IJC. (1997). International Joint Commission, Red River flooding: short-term measures. *Interim report of the international Red River basin task force*, Ottawa, Washington.
- Kacprzyk, J. and Nurmi, H. (1998). Group Decision Making Under Fuzziness, In R. Slowinsky (Eds.), *Fuzzy Sets in Decision Analysis*, Operation Research and Statistics, Kluwar Academic Publishers.
- Kaufmann, A. and Gupta, M. (1985). *Introduction to Fuzzy Arithmetic: Theory and Applications*. Van Nostrand Reinhold Company Inc, New York, USA.
- Kaushik, C. (2006). Urban flood modeling - A comparative study for 1D and 2D models, UNESCO-IHE, Delft, The Netherlands.
- Kawaike, K. and Nakagawa, H. (2007). Flood disaster in July 2006 in the Matsue city

- area and its numerical simulation. *32nd Congress of IAHR—Harmonizing the Demands of Art and Nature in Hydraulics*, IAHR, Venice, Italy.
- Keyes, A. M. and Palmer, R. (1993). The role of object-oriented simulation models in the drought preparedness studies. *Proc., Water Management in the '90s: A Time for Innovation*, ASCE, New York, 479–482.
- KGS. (2000). Red River basin stage-damage curves update and preparation of flood damage maps. Report submitted to Int. Joint Commission, Ottawa, Washington DC.
- Kite, G. W., Dalton, A. and Dion, K. (1994). Simulation of stream flow in a macro scale watershed using general circulation model data, *Water Res. Research*, 30(5): 1547-1559.
- Klohn-Crippen. (1999). Red River one-dimensional unsteady flow model, *final report submitted to International Joint Commission*, Richmond, BC.
- Kubal, C., Haase, D., Meyer, V. and Scheuer, S. (2009). Integrated Flood Risk Assessment – Adapting a Multicriteria Approach to a City. *Nat. Hazarad Earth Syst. Sci.*, 9, 1881-1895.
- Lowrance, W. W. (1976). *Of Acceptable Risk*. William Kaufman, Inc., Los Altos, CA.
- Li, L. and Simonovic, S. P. (2002). A system dynamics model for predicting floods from snowmelt in North American prairie watersheds. *Hydrolog. Process.*, 16, 2645–2666.
- Li, H. X., Zhang, X. X. and Li, S. Y. (2007). A Three Dimensional Fuzzy Control Methodology for a Class of Distributed Parameter Systems. *IEEE Trans. Fuzzy Syst.*, vol. 15, no. 3.
- Leandro, J., Djordjevic, S., Chen, A. S. and Savic, D. (2007). The use of multiple-linking-element for connecting surface and subsurface networks. *Proceeding of 32nd*

- Congress of IAHR—Harmonizing the Demands of Art and Nature in Hydraulics*,
IAHR, Venice, Italy.
- Leandro, J., Chen, A. S., Djordjevic, S. and Savic, D. A. (2009). Comparison of 1D/1D and 1D/2D Coupled(Sewer/Surface) Hydraulic Models for Urban Flood Simulation. *J. Hydraul. Eng.*, 135, (9), 495–504.
- Levy, J. K., Zhang and Hall, J. (2005). Advances in flood risk management under uncertainty. *Stoch Environ Res Risk Assess.* 19, 375 – 377.
- Lhomme, J., Bouvier, C., Mignot, E. and Paquier, A. (2006). One dimensional GIS-based model compared to two-dimensional model in urban floods simulations. *Water Sci. Technol.*, 54 (6–7), 83–91.
- Lin, B., Wicks, J. M., Falconer, R. A. and Adams, K. (2006). Integrating 1D and 2D hydrodynamic models for flood simulation. *Water Management*, 159, 19–25.
- Maidment, D. R. (ed.) (1993). *Handbook of hydrology*, McGraw-Hill, Inc., NY.
- Mark, O., Weesakul, S., Apirumanekul, C., Aroonnet, S. B. and Djordjević, S. (2004). Potential and limitations of 1D modelling of urban flooding. *J. Hydrol.*, 299 (3–4), 284–299.
- Mark, O., Weesakul, S., Apirumanekul, C., Aroonnet, S. B. and Djordjević, S. (2004). Potential and limitations of 1D modelling of urban flooding. *J. Hydrol.*, 299 (3–4), 284–299.
- Matthias, R. and Frederick, P. (1994). Modeling spatial dynamics of sea-level rise in a coastal area. *Syst. Dyn. Rev.*, 10(4), 375–389.
- Miller, J. R., Russell, G. L., and Caliri, G., (1994). Continental-scale river flow in climate models, *Journal of Climate*, 7: 914 – 928.

- Morris-Oswald, M. and Simonovic, S. P. (1997). *Assessment of the Social Impacts of Flooding for use in Flood Management in the Red River Basin*. Report prepared for the International Joint Commission, Slobodan P. Simonovic Consulting Engineer Inc., Winnipeg (available from Slobodan P. SIMONOVIC Consulting Ltd., 10 Pitcarnie Cr., London, Ontario, N6G 4N4, Canada).
- Munick Re, NatCatSERVICE. (2010). Great natural Catastrophes 1950-2009, Retrieved September 29, 2010, from http://www.munichre.com/en/reinsurance/business/non-life/georisks/natcatservice/significant_natural_catastrophes.aspx
- Naden, P. S. (1992). Spatial variability in flood estimation for large catchments: the exploitation of channel network structure, *Hydrological Science Journal*, 37: 53-71.
- National Research Council. (2000). *Risk Analysis and Uncertainty in Flood Damage Reduction Studies*. National Academy Press, Washington, D.C.
- Nasello, C. and Tucciarelli, T. (2005). Dual multilevel urban drainage model. *J. Hydraul. Eng.*, 131 (9), 748–754.
- Paquier, A., Tanguy, J. M., Haider, S. and Zhang, B. (2003). Estimation des niveaux d'inondation pour une crue éclair en milieu urbain: Comparaison de deux modèles hydrodynamiques sur la crue de Nîmes d'Octobre 1988. *Rev. Sci. Eau.*, 16 (1), 79–102.
- Pelling, M. (2003). *The Vulnerability of Cities: Natural Disasters and Social Resilience*, London.
- Phillips, B. C., Yu, S., Thompson, G. R. and de Silva, N. (2005). 1D and 2D modelling of urban drainage systems using XP-SWMM and TUFLOW. *Proc., 10th Int. Conf. on*

- Urban Storm Drainage*, DTU, Copenhagen, Denmark.
- Press, S. J. (2003). *Subjective and Objective Bayesian Statistics: Principles, Models, and Applications*. John Wiley & Sons, Inc, USA.
- Palmer, R. N. (1998). A history of shared vision modeling in the ACTACF comprehensive study: A modeler's perspective. W. Whipple Jr., ed., *Proceedings of Special Session of ASCE's 25th Annual Conf. on Water Resources Planning and Management*, ASCE, Reston, Va., 221–226.
- Press, S. J. (2003). *Subjective and Objective Bayesian Statistics: Principles, Models, and Applications*. John Wiley & Sons, Inc, USA.
- Prodanovic, P. and Simonovic, S. P. (2002). Comparison of fuzzy set ranking methods for implementation in water resources decision-making. *Canadian Journal of Civil Engineering*, 29, 692-701.
- Reuters. (2010). Rains kill at least 95 in Rio, paralyze city Retrieved July 1, 2010, from http://www.reuters.com/article/idUSTRE6352XH20100406?loomia_ow=t0:s0:a49:g43:r1:c1.000000:b29605500:z0
- River Sides. (2005). The Toronto Rain Storm 2005. Toronto Home Owners Guide to Rainfall, Retrieved July 1, 2010, from http://riversides.org/rainguide/riversides_hgr.php?cat=1&page=78&subpage=82
- Rossman, L. A. (2005). *Storm water management model—User's manual*, version 5.0, EPA—United States.
- Royal Commission. (1958). *Report on flood cost benefit*, Winnipeg, Manitoba.
- Royston, J., Dost, A., Townshend, J. and Turner, H. (1999). Using system dynamics to help develop and implement policies and programs in health care in England. *System*

- Dynamics Review*, 15(3), 293-313.
- Sausen, R., Schubert, S. and Dumenil, L. (1994). A model of river runoff for use in coupled atmosphere-ocean models, *Journal of Hydrology*, 155: 337 – 352.
- Scawthorn, C., Flores, P., Blais, N., Seligson, H., Tate, E., Chang, S., Mifflin, E., Thomas, W., Murphy, J., Jones, C. and Lawrence, M. (2006). HAZUS-MH Flood Loss Estimation Methodology II. Damage and Loss Assessment. *Natural Hazards Review*, 7 (2), 72-81.
- Shi, X., Zhu, A-X. and Wang, R. (2005). Fuzzy Representation of Special Terrain Features Using a Similarity-based approach. In E. P. Petry, V. B. Robinson, & M. A. Cobb (Eds.), *Fuzzy Modelling with Spatial Information for Geographic Problems*. (pp. 233-252). Berlin, Germany: Springer press.
- Simonovic, S. P. (1997). Risk in sustainable Water Resources Management. In *Sustainability of Water Resources Under Increasing Uncertainty, IAHS Publ.*, 240, 3-17.
- Simonovic, S. P., Fahmy, H. and Elshorbagy, A. (1997). The use of object-oriented modeling for water resources planning in Egypt. *Water Resour. Manage.*, 11(4), 243–261.
- Simonovic, S. P. (1999). Social Criteria for Evaluation of Flood Control Measures – Winnipeg Case Study. *Urban Water (special issue ‘Non-Structural Measures in Urban Flood Control’ ed. B. Braga)*, Vol.1, No.2, 167-175.
- Simonovic, S. P. (2002). World water dynamics: Global modeling of water resources. *J. Environ. Manage.*, 66(3), 249–267.

- Simonovic, S.P. (2002). Understanding risk management, *Proceedings of the 30th Annual conference of CSCE*, Montreal, Quebec, June, paper GE108, pp.12.
- Simonovic, S. P. and Nirupama (2005). A spatial multi-objective decision making under uncertainty for water resources management. *Journal of Hydroinformatics*, 7, (2), 117-133
- Simonovic, S. P. and Ahmad, S. S. (2007). A New Method for Spatial Analysis of Risk in Water Resources Engineering Management. *The Open Civil Engineering Journal*, 1, 1-12.
- Simonovic, S. (2009). A New Method for Spatial and Temporal Analysis of Risk in Water Resources Management. *Journal of Hydroinformatics*, 11(3-4):320-329.
- Simonovic, S.P. (2009). *Managing water resources: Methods and tools for a systems approach*, UNESCO, Paris and Earthscan James & James, London, pp.576.
- Simonovic, S. P. (2011). *Systems Approach to Management of Disasters: Methods and Applications*. John Wiley & Sons, Inc.
- Slovic, P. (2000). *The Perception of Risk*. Earthscan Publication Ltd., London, UK.
- Smith, J., Phillips, B. C. and Yu, S. (2006). Modeling Overland Flows and Drainage Augmentations in Dubbo, *Proceedings of the 46th Floodplain Management Authorities Conference*, Lismore, February 28 – March 2.
- Sterman, J. D. (2000). *Business dynamics: Systems thinking and modeling for a complex world*, McGraw-Hill, New York.
- Stuart, J. and Appelbaum, A. M. (1985). Determination of Urban Flood Damage. *Journal of Water Resources Planning and Management*, 111 (3), 269-283.

- Teegavarapu, R. S. V. and Simonovic, S. P. (2000). System dynamics simulation model for operation of multiple reservoirs. *Proceedings of the 10th World Water Congress*, Melbourne, Australia.
- Theobald, D. M. and Gross M. D. (1994). EML, a modeling environment for exploring landscape dynamics, *Computers, Environment and Urban Systems*, 8(3), 193-204.
- TUFLOW. (2006). *User Manual*. TUFLOW Flood and Tide Simulation Software.
- Tung, Y. and Yen, B. (2005). *Hydrosystems Engineering Uncertainty Analysis*. Civil Engineering Series, ASCE Press, McGraw Hill Construction, McGraw Hill, New York, NY., USA.
- Verma, D. and Knezevic, J. (1996). A Fuzzy Weighted Wedge Mechanism for Feasibility Assessment of System Reliability during Conceptual Design. *Fuzzy Sets and System*, Vol. 38, pp.179-187.
- Verstraete, J., Tre', G. D., Caluwe, R. D., and Hallez, A. (2005). Field Based Method for the Modelling of Fuzzy Spatial Data. In E. P. Petry, V. B. Robinson, & M. A. Cobb (Eds.), *Fuzzy Modelling with Spatial Information for Geographic Problems*. (pp. 41-69). Berlin, Germany: Springer press.
- Vick, S. G. (2002). *Degrees of Belief: Subjective Probability and Engineering Judgment*, ASCE Press, USA.
- Vörösmarty, C. J., Moore, B., Grace, A. L., Gildea, M. P., Melillo, M., Peterson, B. J., Rastetter, E. B. and Steudler, P. A. (1989). Continental scale models of water balance and fluvial transport: an application to South America, *Global Biogeochemical Cycles*, 3(3): 241–265.
- Wallingford Software. (2006). *Infoworks CS*, version 7.5, documentation, Wallingford.

- Weather, H. S. (2006). Flood hazard and management: a UK perspective. *Phil. Trans. R. Soc. A.*, 364, 2135-2145.
- Westervelt, J. D. and Hopkins, L. D. (1999). Modeling mobile individuals in dynamic landscapes. *Int. J. Geograph. Inf. Sci.*, 13(3), 191–208.
- WL | Delft Hydraulics. (2005). *SOBEK River/Estuary User Manual*, SOBEK Help Desk.
- XP Software Inc. (2010). *Stormwater and Wastewater Management Model, Getting Started Manual*.
- Zimmermann, H.-J. (1996). *Fuzzy Set Theory and its Applications, Third Edition*. Massachusetts, USA: Kluwer Academic Publishers.
- Zhong, Z. (1998). General hydrodynamic model for sewer/channel network systems. *J. Hydraul. Eng.*, 123(3), 307–315.

**APPENDIX: A (Computational Tools for the Implementation of River
Flood Risk Assessment Methodology)**

Appendix A presents the computational tools developed for the implementation of proposed methodology for river flood risk analysis using (i) 2-D hydrodynamic modeling, and (ii) system dynamics modeling. For river flood risk analysis, the methodology presented in Chapter 3 is illustrated using the Red River flood of 1997 (Manitoba, Canada) as a case study.

Modeling Dynamic Processes of River Flooding: 2-D Hydrodynamic Modeling Approach

The MIKE 21 hydrodynamic model, along with its input data and results, are given in Appendix A of the DVD attached. Equation 3.4 and 3.5 include Chezy resistance for Mike21 model formulation. However, in Mike21 there is option to choose either Chezy resistance or Mannings number. For the Red River case study Mannings number is used. The following table lists the names of the input files for MIKE 21 model together with MIKE 21 model results, which are included in Appendix A of the DVD attached.

Table A1: MIKE 21 model files and results

Data	File name	File location in DVD
Discharge near Ste. Agathe (St. No. 05OC012)	Dagathe.dfs0	Appendix A/HD/Mike21
Stage data taken above the Red River Floodway control structure (St. No. 05OC021)	Sfloodway.df0	Appendix A/HD/Mike21
Bathymetry data	Bathymetry.df2	Appendix A/HD/Mike21
Manning Number	0.067	
MIKE 21 model	Mike21.m21	Appendix A/ HD/Mike21
MIKE 21 result (Water surface elevation)	WS	Appendix A/ HD/Mike21_result

River Flood Damage Analysis

The computer program for the river flood damage analysis, for agricultural and residential land, is written in Microsoft Visual Studio (found in Appendix A of the DVD attached). The following is a description of the Microsoft Visual Studio file *FloodDamageMax.cpp*, which is used in this research for an analysis of the temporal and spatial variability of flood damage.

The *FloodDamageMax.cpp* reads GIS data i.e. ASCII files of water surface elevations as input into the program. These ASCII files are MIKE 21 model output containing water surface elevations for the required duration of the flood event and at a specific time interval. For analysis of flood damage for the Red river case study the program *FloodDamageMax.cpp* prompts the user with information necessary such as: availability of landuse, extra number of days required after recession of flood, average crop price, top level of dike, base level of incipient flooding, area of ring dike, total reported damage for community, percentage variation for minimum recovery time, and percentage variation for maximum recovery time.

Agricultural Damage:

The program (*FloodDamageMax.cpp*) uses water surface elevation for the entire duration of the flood event to generate a flood stage hydrograph at every location and determines the recession date at every location. Each location has a unique stage hydrograph and recession date. Then it asks the user on the additional time required for drying. The percentage of average yield is determined using the graphical relationship between the

relative yield and seeding date (Figure 3.3). Once this has been performed, Equation 3.7 is used to determine the agricultural damage for i -th time step at j -th location, D_{ij} .

Residential Damage:

Using Equation 3.9, the program (*FloodDamageMax.cpp*) calculates damage for residential and ring-dike communities. This equation represents a depth damage function (as shown in Figure 3.4) to estimate incremental damage. In order to utilize the Red River Basin case study for a damage analysis of ring-diked communities, such as St. Adolphe, the present research required the possession of relevant figures and information: (i) in 1997, the total reported damage was \$515,000, which is considered at a value of 100% when the flood water level reaches the top of the dike (Figure 3.4), and (ii) the total potential infrastructure damage was reported at \$4,142,702, which figures as 804% of the total reported damage (KGS, 2000). The total potential infrastructure damage is assumed (KGS, 2000) once the flood water level exceeds the top level of the dike. Other relevant information for the community of St. Adolphe required in the program is the following: top level of the dike is 236 meters, level of incipient flooding is 231 meters, and the area within the ring-dike is 1,121,747 Sq. meter.

Spatial and Temporal Variability of River Flood Damage

Temporal Variability of Flood Damage

The temporal variation of flood damage is considered for the Red River Basin by changing flow only. Temporal variability of flood damage is assessed by determining

minimum ($D_{i \text{ Min}}$), mean ($D_{i \text{ Mean}}$) and maximum ($D_{i \text{ Max}}$) flood damage. Mean flood damage, $D_{i \text{ Mean}}$ is determined using the observed discharge near Ste. Agathe (St. No. 05OC012). To assess the temporal variability of flood damage, the minimum flood damage, $D_{i \text{ Min}}$ is determined by decreasing the observed discharge data near Ste. Agathe by 5%, while maximum flood damage, $D_{i \text{ Max}}$ is determined by increasing the observed discharge data near Ste. Agathe by 5%. Uncertainty related to properties of spatial variability is not considered in determining the temporal variability of flood damage. Therefore the following information remained the same while determining the temporal variation of flood damage:

- average crop value: \$42.1
- additional time required for drying: 14 days
- the total reported 1997 damage: \$515,000
- the total potential infrastructure damage: \$4,142,702
- Top level of the dike (St. Adolphe): 236 meter,
- level of incipient flooding (For St. Adolphe): 231 meter, and
- the area within the ring-dike: 1,121,747 Sq. meter.

Spatial Variability of Flood Damage

The spatial variation of flood damage is considered for the Red River Basin by changing variables that are spatially dependent. Spatial variability of flood damage is assessed by determining minimum ($D_{j \text{ Min}}$), mean ($D_{j \text{ Mean}}$) and maximum ($D_{j \text{ Max}}$) flood damage. Mean flood damage, $D_{j \text{ Mean}}$ is determined using the average crop value of \$42.1 (for agricultural damage) and the total reported 1997 damage of \$515000 (for residential

damage). Spatial variability of flood damage is considered by changing the average crop value and the total reported 1997 damage. Therefore for agricultural land, the minimum flood damage, $D_{j \text{ Min}}$ and maximum flood damage, $D_{j \text{ Max}}$ is determined by considering an average crop value of \$37.9 and \$46.3, respectively. For a ring-diked community like St. Adolphe, the minimum flood damage, $D_{j \text{ Min}}$ and maximum flood damage, $D_{j \text{ Max}}$ is determined by considering the total reported flood damage for 1997 at \$463,500 and \$566,500, respectively. Uncertainty related to properties of temporal variability is not considered in determining the spatial variability of flood damage. The following information remained the same while determining spatial variation of flood damage:

- Observed discharge near Ste. Agathe (St. No. 05OC012),
- additional time required for drying: 14 days,
- the total potential infrastructure damage: \$4,142,702,
- Top level of the dike (St. Adolphe): 236 meter,
- level of incipient flooding (For St. Adolphe): 231 meter, and
- the area within the ring-dike: 1,121,747 Sq. meter.

Results of temporal variation of flood damage ($D_{i \text{ Min}}$, $D_{i \text{ Mean}}$, and $D_{i \text{ Max}}$) and spatial variation of flood damage ($D_{j \text{ Min}}$, $D_{j \text{ Mean}}$, and $D_{j \text{ Max}}$) for selected time steps are given in Appendix A of the DVD attached.

Spatial and Temporal River Flood Risk Analysis

The implementation of the fuzzy performance indices is written in MATLAB. MATLAB is used with inbuilt functions and the vectorization of matrix operations, which allow

whole data sets to be manipulated easily. A Graphic User Interface (GUI) is created to allow the easy operation of the program on different data sets, to give a graphical representation of the partial level of damage curves, and to choose either triangular or trapezoidal membership functions for a 2-D fuzzy set for (i) the temporal variability of flood damage, and (ii) the spatial variability of flood damage.

The following are descriptions of the MATLAB files used in this research for the development of fuzzy performance indices.

process_triangular.m computer program performs the following tasks:

- 1 read in GIS data i.e. ASCII files containing values of temporal variability of flood damage ($D_{i \text{ Min}}$, $D_{i \text{ Mean}}$, and $D_{i \text{ Max}}$) and spatial variability of flood damage ($D_{j \text{ Min}}$, $D_{j \text{ Mean}}$, and $D_{j \text{ Max}}$) for specific dates/times;
- 2 generates *2-D fuzzy set for temporal variability of river flood damage* (Figure 3.7) as defined in Equation 3.13 for a triangular fuzzy membership membership function;
- 3 generates *2-D fuzzy set for spatial variability of river flood damage* (Figure 3.8) as defined in Equation 3.15 for a triangular fuzzy membership membership function;
- 4 using *2-D fuzzy set for temporal variability of river flood damage* and *2-D fuzzy set for spatial variability of river flood damage* generates a *3-D fuzzy set for both temporal and spatial variability of river flood damage* (Figure 3.9);
- 5 Determines the center of gravity (Figure 3.10) of the *2-D fuzzy set for temporal*

variability of river flood damage using Equation 3.17 to determine D_{i_g} ;

- 6 the program then generates a new *2-D fuzzy set for spatial variability of river flood damage* at D_{i_g} (Figure 3.11) which is defined in Equation 3.18 as *2-D fuzzy set for temporal and spatial variability of river flood damage*; and
- 7 Calculates weighted area of the *2-D fuzzy set for temporal and spatial variability of river flood damage*, WA_{ij} using Equation 3.26.

process_trapezoidal.m computer program performs the following tasks: :

- 1 read in GIS data, i.e. ASCII files containing values of temporal variability of flood damage ($D_{i \text{ Min}}$, $D_{i \text{ Mean}}$, and $D_{i \text{ Max}}$) and spatial variability of flood damage ($D_{j \text{ Min}}$, $D_{j \text{ Mean}}$, and $D_{j \text{ Max}}$) for specific dates/times;
- 2 determines the Modal values for temporal variability of flood damage and spatial variability of flood damage to develop trapezoidal fuzzy membership functions;
- 3 generates *2-D fuzzy set for temporal variability of river flood damage* for a trapezoidal fuzzy membership function;
- 4 generates *2-D fuzzy set for spatial variability of river flood damage* for a trapezoidal fuzzy membership function;
- 5 using *2-D fuzzy set for temporal variability of river flood damage* and *2-D fuzzy set for spatial variability of river flood damage* generates a *3-D fuzzy set for both temporal and spatial variability of river flood damage*;
- 6 Determines the center of gravity of the *2-D fuzzy set for temporal variability of river flood damage* to determine D_{i_g} ;
- 7 the program then generates a new *2-D fuzzy set for spatial variability of river*

flood damage at D_{i_g} as 2-D fuzzy set for temporal and spatial variability of river flood damage; and

- 8 Calculates weighted area of the 2-D fuzzy set for temporal and spatial variability of river flood damage, WA_{ij} .

compatibility.m computer program performs the following tasks:

- 1 Loop through all trapezoids with valid data;
- 2 Linearly interpolate trapezoids and find minimum between fuzzy membership function of partial level of flood damage $\tilde{M}_{ij}(D_{ij})$ and fuzzy flood damage membership function $\tilde{S}_{ij}(D_{ij})$ to calculate the overlap area;
- 3 calculates the weighted overlap area between the fuzzy flood damage membership function and the partial level of flood damage membership function, WOA_{ij} ;
- 4 Calculates compatibility measure CM_{ij} using Equation 3.21.

flood_startup.m file does the following:

- 1 Initiates a Graphic User Interface (GUI) (Figure A1) by providing access to a Flood Risk Analyzer option, which has a call back function in MATLAB that links with the *flood_risk_analyser.m* file.

flood_risk_analyser.m computer program performs the following tasks::

- 1 Initiates a Graphic User Interface (GUI) for Flood Risk Analyzer (Figure A2).
- 2 The GUI uses a call back function to link (i) *process_triangular.m* file or *process_trapezoidal.m* file, and (ii) *compatibility.m* file and to compare two

compatibility measures based on user defined *fuzzy membership function of partial level of flood damage* $\tilde{M}_{ij}(D_{ij})$.

- 3 The GUI provides the option to select the File menu and load either ASCII data or mat data for files containing values of temporal variability of flood damage ($D_{i \text{ Min}}$, $D_{i \text{ Mean}}$, and $D_{i \text{ Max}}$) and spatial variability of flood damage ($D_{i \text{ Min}}$, $D_{i \text{ Mean}}$, and $D_{i \text{ Max}}$) for a specific date/time .
- 4 Select model type, i.e. either *triangular* or *trapezoidal*.
- 5 Then, by pressing the Process Data button, the program performs the operation mentioned in *process_triangular.m file* or *process_trapezoidal.m* based on model type (Figure A2).
- 6 Then, the lower ($D_{ij \ 1}$) and upper ($D_{ij \ 2}$) bounds of the partial level of flood damage (Figure 3.6) are entered for 1st and 2nd partial levels for residential and agricultural land (Figure A3).
- 7 Then, by pressing the Calculate button, the program finds the compatibility measure, cm; reliability index, RE; and robustness index, RO values. The program further enables the to presentation of the vause of resiliency index, RI, determined from the code written in Microsoft Visual Studio.
- 8 The program then plots the data and generates maps of the reliability index, RE; the robustness index, RO; and the resiliency index, RI (Figure A4).
- 9 The data can then be exported either as ASCII or mat format by pushing the Export Data button ,
- 10 The user can also select a point on any of the maps by pressing the Datatip button to get the 3-dimensional plot showing: (i) 3-D fuzzy set for temporal and spatial

variability of flood, (ii) the center of gravity (D_{i_g}) of the 2-D fuzzy set for temporal variability of flood damage, and also (iii) the 2-D fuzzy set for both temporal and spatial variability of flood damage. Next, deselect the Datatip to close the 3-dimensional plot (Figure A5 and Figure A6).

- 11 Results for selected time steps of the reliability index, RE; the robustness index, RO; and the resiliency index, RI, are given in Appendix A of the DVD attached.



Figure A1: GUI for *flood_startup*

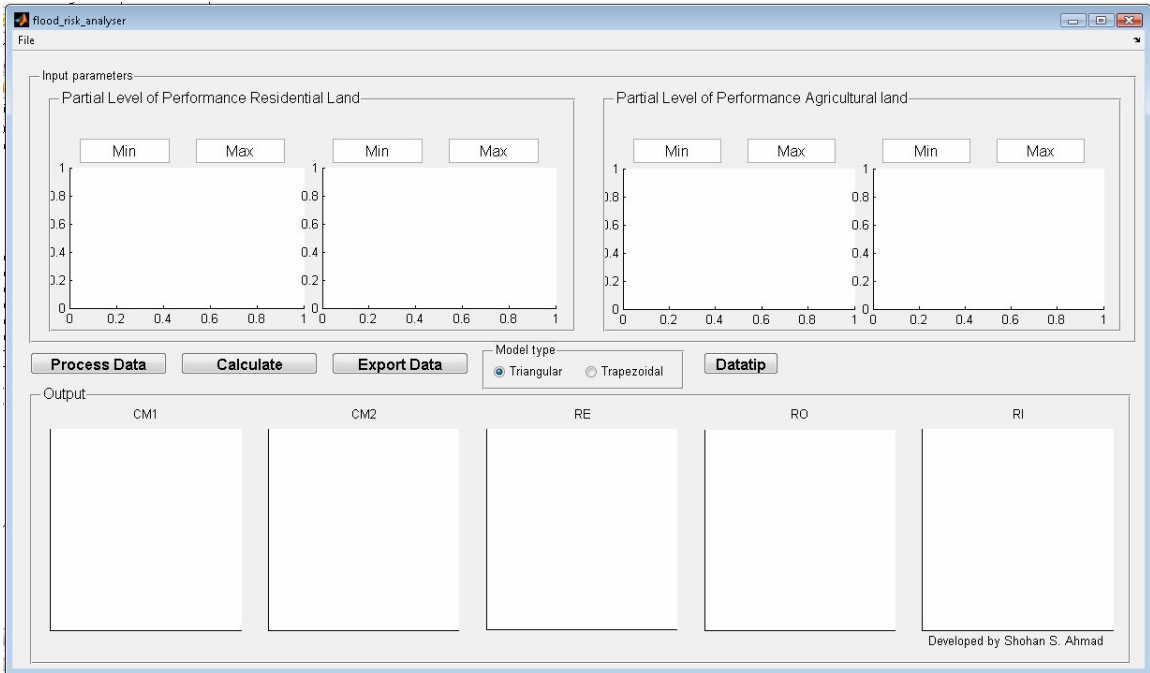


Figure A2: GUI for *flood_risk_analyzer*

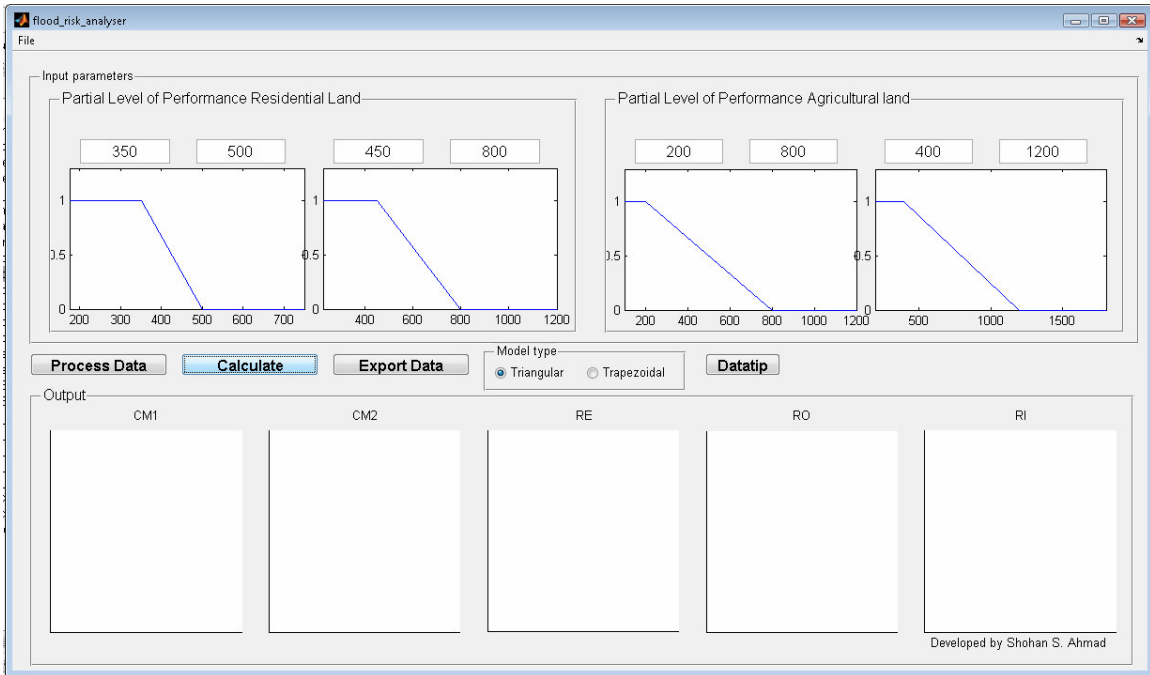


Figure A3: GUI showing partial level of flood damage for Red River Basin case study

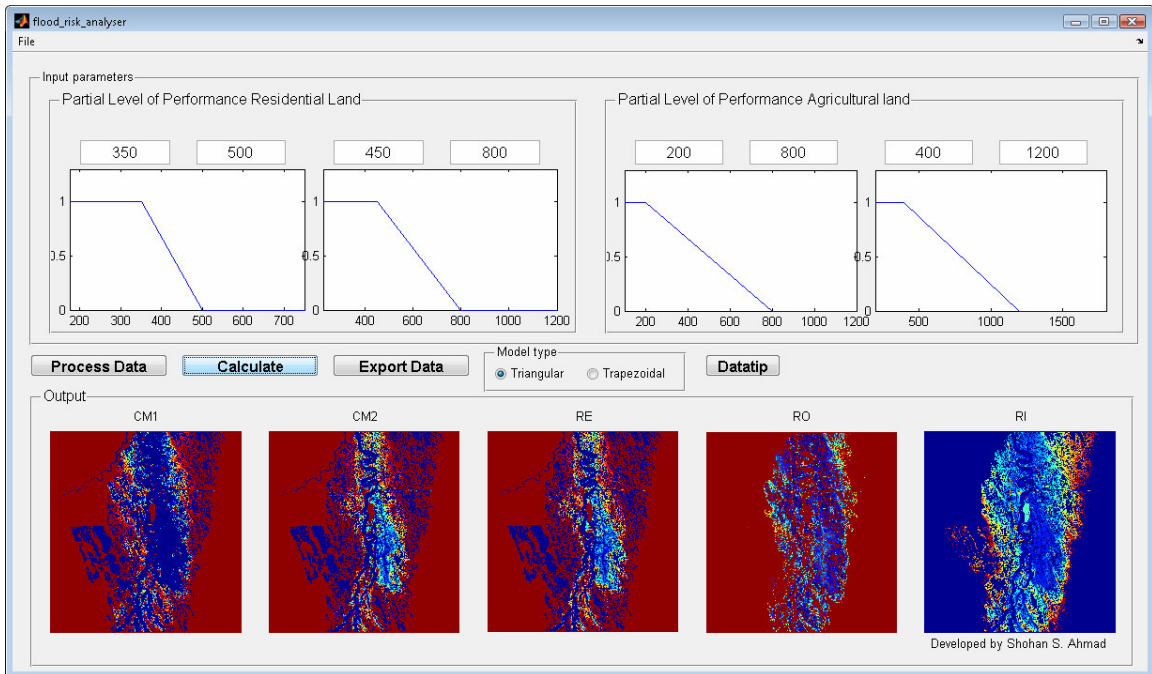


Figure A4: GUI showing maps of reliability indices

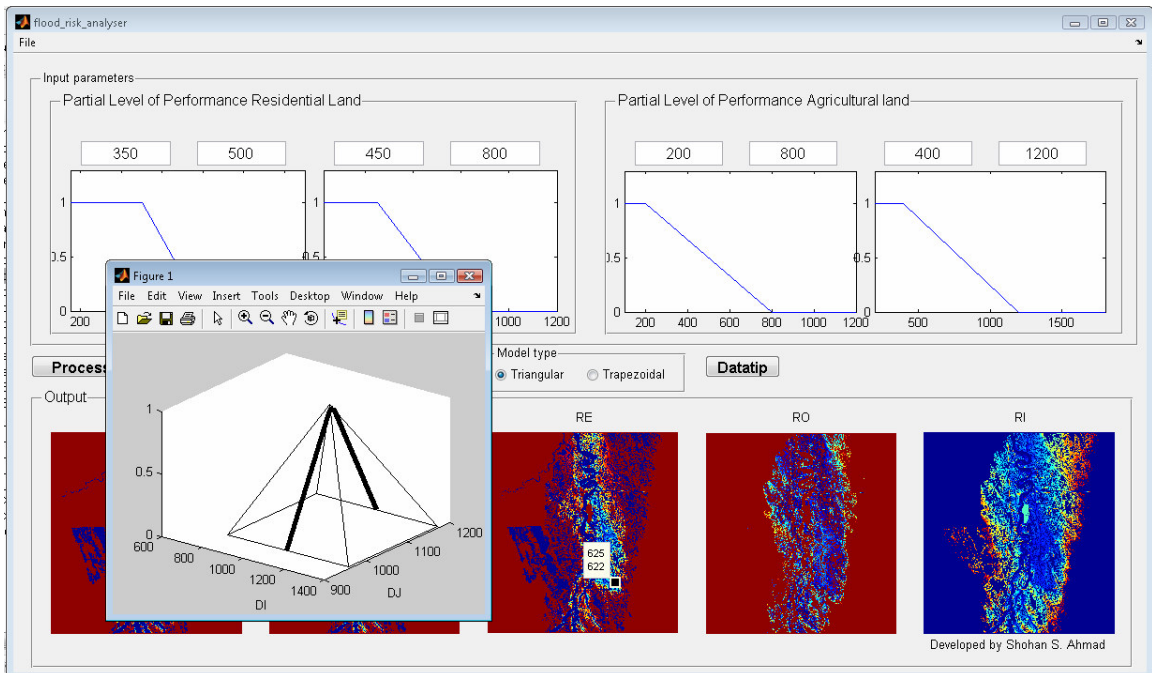


Figure A5: GUI showing 3-D fuzzy set for temporal and spatial variability of flood damage for triangular membership function

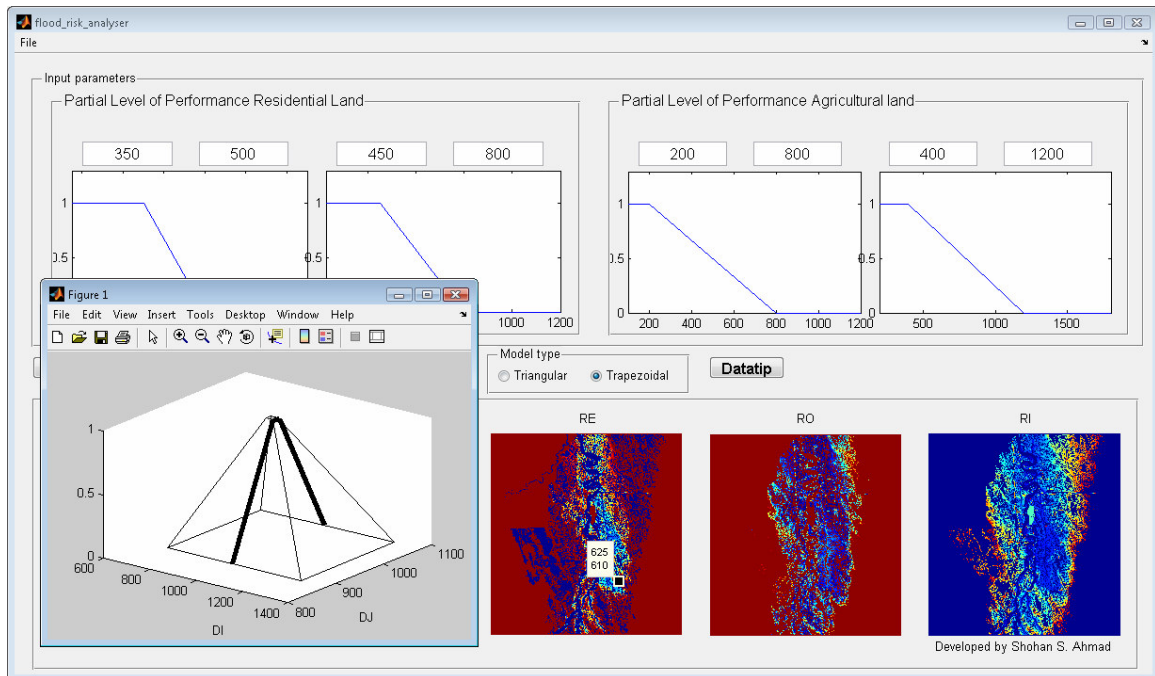


Figure A6: GUI showing 3-D fuzzy set for temporal and spatial variability of flood damage for trapezoidal membership function

The following table lists the names of the program files that are used for damage and risk analyses and their results, which are included in Appendix A found in the DVD attached.

Table A2: Model files and results

Data/File type	File name	File location in DVD
Damage analysis program	<i>FloodDamageMax.cpp</i>	Appendix A/HD/V_Studio
Result of damage analysis	Di Min, Di Mean, Di Max, Dj Min, Dj Mean, and Dj max	Appendix A/HD/ damage_result
Risk analysis	<i>process_triangular.m file</i>	Appendix A/HD/MATLAB
Risk analysis	<i>process_trapezoidal.m file</i>	Appendix A/HD/MATLAB
Risk analysis	<i>compatibility.m file</i>	Appendix A/HD/MATLAB
Risk analysis	<i>flood_startup.m file</i>	Appendix A/HD/MATLAB
Risk analysis	<i>flood_risk_analyser.m file</i>	Appendix A/HD/MATLAB
Results of re, ro, ri	re.txt, ro.txt, ri.txt	Appendix A /HD/MATLAB_result

Modeling Dynamic Processes of River Flooding: System Dynamics Modeling

Approach

Stella (HPS, 2001) is used as the system dynamics modeling tool to simulate the Red River flood of 1997. The system dynamics model, along with its input data and results, are given in Appendix A of the DVD attached. The computer program for the river flood damage analysis, for agricultural and residential land, is written in Microsoft Visual Studio (found in Appendix A of the DVD attached).

Architecture of the System Dynamics Model for Overland Flooding

The model architecture adopted for the development of the overland flooding model uses a system dynamics approach, which is shown in Figure A7. The system dynamics and geographic information system are loosely coupled to model overland flooding. GIS provides watershed characteristics and information on infrastructure in the floodplain, whereas the SD model describes the river and overland flow process. Initially, terrain information from the digital elevation model (DEM) is extracted from the GIS and provided for the SD model (as shown in Figure A7). Then, the dynamic modeling is performed in SD for overland flooding using the cell to cell routing approach. The Muskingum method is used to represent flow in the river section, which enables the generation of flood water levels. The Von Neumann neighborhood scheme is used for cell-to-cell routing. Implementation of the cell-to-cell routing approach requires the discretization of the watershed. The results of the system dynamics model provide the spatial and temporal variation of flood water depth. The spatial and temporal distributions of flood water depths are communicated back to GIS to generate maps.

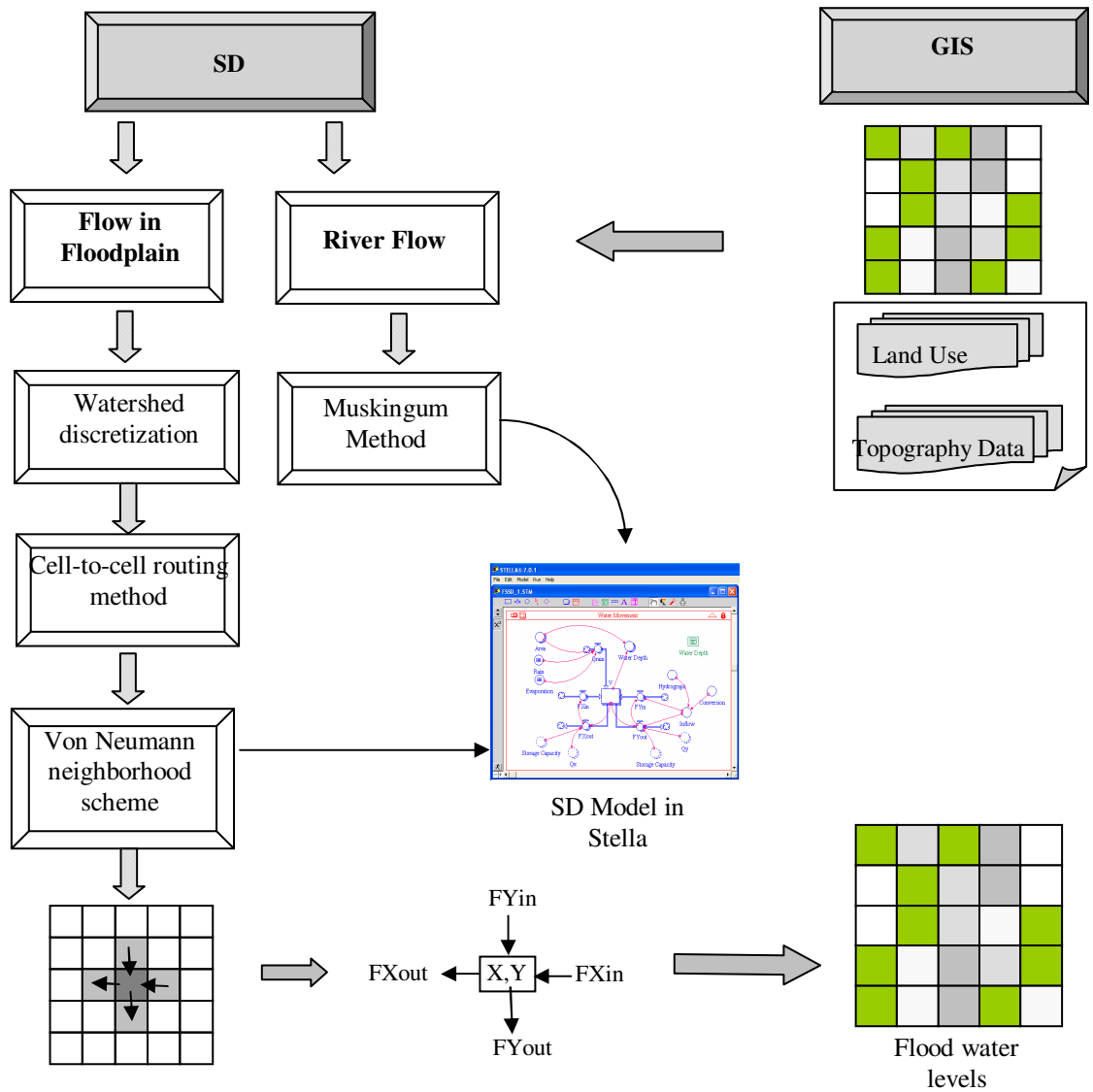


Figure A7: Framework for developing System Dynamics Model

The system dynamics model is developed graphically on the screen by using basic building blocks, i.e., stocks, flows, connectors, and converters, all of which are available in the model development tool. For example, in the case of a reservoir the system dynamics model would represent storage as a stock. Varying inflows and outflows cause changes in storage volume over time. Inflows and outflows are represented by the

building block “flow.” Converters are provided to extend the range of calculations that can be performed on flows and to house data and logical/mathematical functions that are necessary to operate the system. Operating rules for flood control structures (reservoir, floodway) are also implemented through converters. Connectors (directed arrows) link various elements of the model, i.e., converters, flows, and stocks, to indicate relationships and influence.

The following table lists the names of the input files for system dynamics model together with the system dynamics model results, which are in Appendix A found in the DVD attached.

Table A3: System dynamics model files and results

Data/File type	File name	File location in DVD
Discharge near Ste. Agathe (St. No. 05OC012)	St.agathe.xls	Appendix A/ SD/SD
System dynamics model	Redriver.STM	Appendix A/SD/SD
System dynamics model result (water surface elevation)	WS.txt	Appendix A/SD/SD_result

River Flood Risk Analysis

After generation of the water surface elevations using system dynamics modeling approach, river flood damage analysis is performed using *FloodDamageMax.cpp* given in Appendix A of the DVD attached. The analysis of river flood damage is described previously using *FloodDamageMax.cpp*. Similar procedure is followed to determine the *temporal variability of flood damage* and *spatial variability of flood damage*. Then the reliability index, r_e ; the robustness index, r_o ; and the resiliency index, r_i , is determined

using *process_triangular.m file*, *process_trapezoidal.m file*, *compatibility.m file*, *flood_startup.m file*, *flood_risk_analyser.m file*. Results for selected time steps of the reliability index, re; the robustness index, ro; and the resiliency index, ri, are given in Appendix A. Figure A8 shows a GUI for the Red River basin case study using the water surface elevation generated from the system dynamics modeling approach.

The following table lists the names of the program files that are used for damage and risk analyses and their results, which are included in Appendix A found in the DVD attached.

Table A4: Model data inputs and results

Data/File type	File name	File location in DVD
Damage analysis program	<i>FloodDamageMax.cpp</i>	Appendix A/SD/V_Studio
Result of damage analysis	Di Min, Di Mean, Di Max, Dj Min, Dj Mean, and Dj max	Appendix A/SD/damage_result
Risk analysis	<i>process_triangular.m file</i>	Appendix A/SD/MATLAB
Risk analysis	<i>process_trapezoidal.m file</i>	Appendix A/SD/MATLAB
Risk analysis	<i>compatibility.m file</i>	Appendix A/SD/MATLAB
Risk analysis	<i>flood_startup.m file</i>	Appendix A/SD/MATLAB
Risk analysis	<i>flood_risk_analyser.m file</i>	Appendix A/SD/MATLAB
Results of re, ro, ri	Re.txt, ro.txt, ri.txt	Appendix A/SD/MATLAB_result

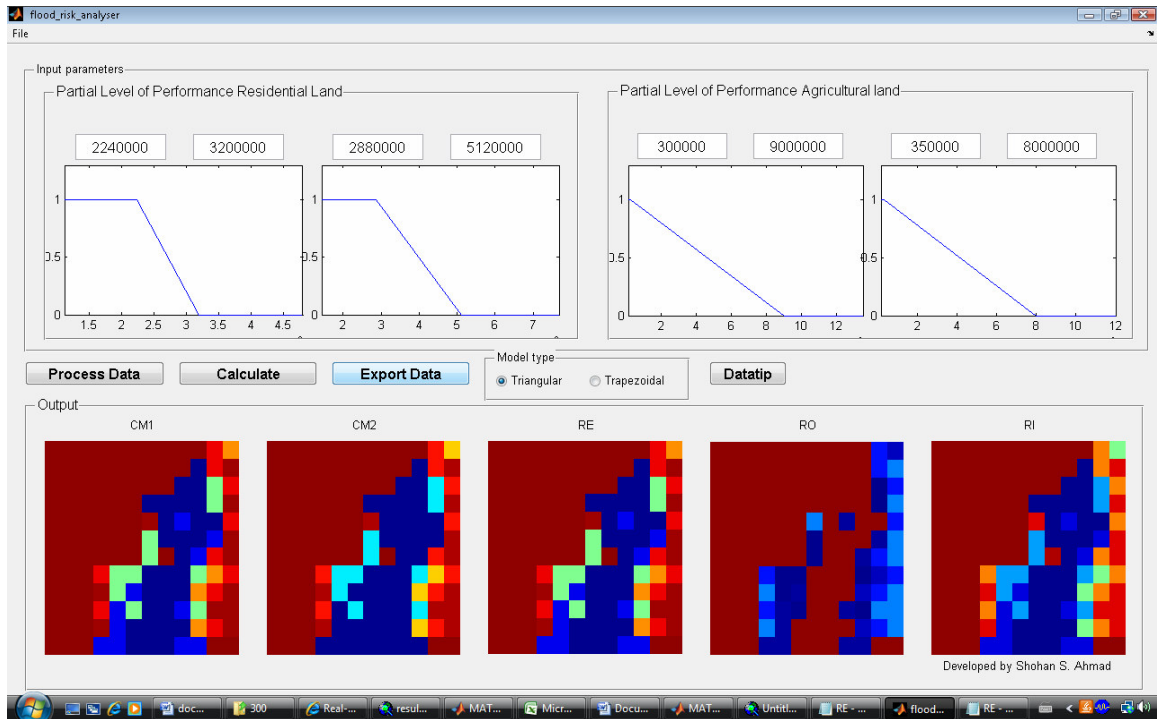


Figure A8: GUI showing partial level of flood damage and maps of reliability indices

**APPENDIX: B (Computational Tools for the Implementation of Urban
Flood Risk Assessment Methodology)**

Appendix B presents the computational tools developed for the implementation of proposed methodology for urban flood risk analysis. The methodology for urban flood risk analysis presented in Chapter 3 is illustrated using a small residential area called Cedar Hollow, London, ON as a case study. The following sections describe the development of the 1D/2D hydrodynamic model, damage analysis, and the flood risk analysis process for urban flood risk analysis.

Modeling Dynamic Processes of Urban Flooding

The 1D/2D Hydrodynamic Modeling Approach integrates a 1-D hydraulic model (MIKE URBAN) and a 2-D hydrodynamic model (MIKE 21) in a MIKE FLOOD (DHI, 2009) environment. A 1D storm sewer model built in MIKE URBAN and a 2D overland flow model built in MIKE 21, along with the necessary input data used in the models, and model results are included in Appendix B of the DVD attached.

MIKE URBAN Storm Sewer Model

MIKE URBAN is a 1-D hydrodynamic pipe flow model. MIKE URBAN solves complete 1-D Saint Venant equations for modeling hydraulics in open channel and closed conduits. When MIKE URBAN is coupled with MIKE 21 to solve overland flooding, the required inputs to the MIKE URBAN storm sewer model consist of storm sewer node locations, pipe sizes and locations, pipe slopes, pump specification, invert elevations, and boundary conditions.

Storm Sewer Nodes and Links

With a GIS interface in MIKE URBAN it was very easy to accurately locate manholes and input them into the storm sewer model as nodes. Nodes were linked to each other with MOUSE Links between two manholes. Then pipe specifications such as pipe length, pipe size, upstream invert elevation, downstream invert elevation and pipe roughness were used as inputs in the storm sewer model. Although the ground elevation of the manhole was entered in the storm sewer model when coupled with MIKE 21, the model automatically determined the ground elevation of the manhole from topographic data.

Runoff Calculation

MIKE 21 calculates runoff. Therefore additional information is not required in MIKE URBAN for runoff calculation, particularly when MIKE URBAN is coupled with MIKE 21 in a MIKE FLOOD environment.

Model Setup in MIKE FLOOD

MIKE FLOOD is used as a coupling tool to ensure the dynamic interaction between MIKE URBAN and MIKE 21. In setting up the MIKE FLOOD, the coupling process requires an urban link setup.

Urban Link Setup: The 'Urban Link' utilizes 'Link Urban node to MIKE 21' to couple MIKE URBAN manholes with the corresponding grid cells in MIKE 21. This enables a dynamic link between the manhole and the grid cell, where water can drain from the MIKE 21 model into the MIKE URBAN model or surcharge from the MIKE URBAN

model can drain into the MIKE 21 model. Setting up the Urban Link requires additional parameters for the orifice equation, weir equation, or an exponential function.

The following table lists the names of the input files for the MIKE 21 and MIKE URBAN model together with the model results, which are included in Appendix B of the DVD attached.

Table B1: MIKE URBAN and MIKE 21 model data inputs and results

Data	File name	File location in DVD
Topographic data	topocedar.dfs2	Appendix B/MikeU_21
Rainfall hyetograph	rainfall.dfs0	Appendix B/MikeU_21
Manning's Coefficient	of 0.025	
MIKE URBAN Model	CedarMikeU.mu	Appendix B/MikeU_21
MIKE 21 model	CedarMike21.m21	Appendix B/MikeU_21
MIKE FLOOD model	CedarMFlood.mf	Appendix B/MikeU_21
pipe length, pipe size, upstream invert elevation, downstream invert elevation and pipe roughness	Within MIKE URBAN Model	Appendix B/MikeU_21
MIKE 21 result (Water surface elevation)	Ws.txt	Appendix B/MikeU_21_result

Urban Flood Damage Analysis

The calculation of an urban flood damage analysis for the residential area of Cedar Hollow in London, ON is carried out in ArcGIS using GIS Macro extension. The GIS Macro extension is included in Appendix B as a document file in the DVD attached with this thesis.

The GIS Macro extension in ArcGIS reads in the MIKE 21 model output of water surface elevations as GIS data, i.e. as ASCII files (given in Appendix B of the DVD attached) for

the required duration of the flood event and at a specific time interval. In this research GIS Macros is used for assessing (i) direct damage, which is based on a depth-percent damage relationship, and (ii) indirect damage which is based on obstruction vs. percentage damage relationship. The total damage is assessed based on the weighted approach. Equation 3.33 is used to determine residential flood damage for i -th time step at j -th location, D_{ij} . For the Cedar Hollow case study the weight of direct damage, w_1 is taken as 60% and the weight of indirect damage, w_2 is taken as 40%. The weights assigned for this case study are used exclusively for the purposes of illustrating the methodology. Since the residential community of Cedar Hollow is still undergoing development, and even in very few finished houses residents are yet to move in, it was therefore not possible to initiate a survey and questionnaire to carry out a proper investigation in determining the appropriate values for the weights.

Spatial and Temporal Variability of Urban Flood damage

Temporal variation of urban flood damage is considered for Cedar Hollow by changing the time variant property of rainfall intensity only. The mean flood damage D_i Mean is determined using the 6-h design rainfall with a return period of 500 years (Figure 4.26). In order to determine temporal uncertainty related to flood damage, the 6-h design rainfall with a return period of 500 years is varied by a certain percentage. For illustration of the methodology, the design rainfall is decreased by 10% to determine minimum water surface elevation and increased by 10% to determine maximum water surface elevation. Then (i) direct damage (using depth-percent damage relationship) and (ii) indirect damage (using obstruction vs. percentage damage relationship) are assessed to determine

the temporal variation of flood damage, i.e. minimum flood damage ($D_{i \text{ Min}}$) and maximum flood damage ($D_{i \text{ Max}}$). Uncertainty related to properties of spatial variability is not considered in determining the temporal variability of flood damage. Therefore the following information remained the same while determining the temporal variation of flood damage:

- depth-percent damage relationship
- obstruction vs. percentage damage relationship

Spatial variation of flood damage is considered for Cedar Hollow by changing variables that are spatially dependent. In this case study the depth-percent damage relationship and obstruction vs. percentage damage relationship are considered to be spatially variable. The variation of the depth-percent damage relationship and obstruction vs. percentage damage relationship is used to determine the spatial variability of flood damage, i.e. minimum flood damage, $D_{j \text{ Min}}$; and maximum flood damage, $D_{j \text{ Max}}$. Uncertainty related to properties of temporal variability is not considered in determining the spatial variability of flood damage. The following information remained the same while determining the spatial variation of flood damage:

- the 6-h design rainfall with a return period of 500 years

Results of the temporal variability of urban flood damage ($D_{i \text{ Min}}$, $D_{i \text{ Mean}}$, and $D_{i \text{ Max}}$) and the spatial variability of urban flood damage ($D_{j \text{ Min}}$, $D_{j \text{ Mean}}$, and $D_{j \text{ Max}}$) are given for selected time steps in Appendix B of the DVD attached.

Spatial and Temporal Urban Flood Risk Analysis

The implementation of the fuzzy performance indices is written in MATLAB. A Graphic User Interface is used to allow the easy operation of the program on different data sets, to give a graphical representation of the partial level of performance curves, and to choose either triangular or trapezoidal membership functions. The following are descriptions of the MATLAB files used in this research for the development of fuzzy performance indices.

process_triangular.m computer program performs the following tasks::

- 1 read in GIS data, i.e. ASCII files containing values of temporal variability of flood damage ($D_{i \text{ Min}}$, $D_{i \text{ Mean}}$, and $D_{i \text{ Max}}$) and spatial variability of flood damage ($D_{j \text{ Min}}$, $D_{j \text{ Mean}}$, and $D_{j \text{ Max}}$) for specific dates/times;
- 2 generates *2-D fuzzy set for temporal variability of urban flood damage* (Figure 3.7) as defined in Equation 3.13 for a triangular fuzzy membership membership function;
- 3 generates *2-D fuzzy set for spatial variability of urban flood damage* (Figure 3.8) as defined in Equation 3.15 for a triangular fuzzy membership membership function;
- 4 using *2-D fuzzy set for temporal variability of urban flood damage* and *2-D fuzzy set for spatial variability of urban flood damage* generates a *3-D fuzzy set for both temporal and spatial variability of urban flood damage* (Figure 3.9);
- 5 Determines the center of gravity (Figure 3.10) of the *2-D fuzzy set for temporal variability of urban flood damage* using Equation 3.17 to determine D_{i_G} ;

- 6 the program then generates a new *2-D fuzzy set for spatial variability of urban flood damage* at D_{i_g} (Figure 3.11) which is defined in Equation 3.18 as *2-D fuzzy set for temporal and spatial variability of urban flood damage*; and
- 7 Calculates weighted area of the *2-D fuzzy set for temporal and spatial variability of urban flood damage*, WA_{ij} using Equation 3.26.

process_trapezoidal.m computer program performs the following tasks:

- 1 read in GIS data, i.e. ASCII files containing values of temporal variability of urban flood damage ($D_{i_{Min}}$, $D_{i_{Mean}}$, and $D_{i_{Max}}$) and spatial variability of urban flood damage ($D_{j_{Min}}$, $D_{j_{Mean}}$, and $D_{j_{Max}}$) for specific dates/times;
- 2 determines the Modal values for temporal variability of urban flood damage and spatial variability of urban flood damage to develop trapezoidal fuzzy membership functions;
- 3 generates *2-D fuzzy set for temporal variability of urban flood damage* for a trapezoidal fuzzy membership membership function;
- 4 generates *2-D fuzzy set for spatial variability of urban flood damage* for a trapezoidal fuzzy membership membership function;
- 5 using *2-D fuzzy set for temporal variability of urban flood damage* and *2-D fuzzy set for spatial variability of urban flood damage* generates a *3-D fuzzy set for both temporal and spatial variability of urban flood damage*;
- 6 Determines the center of gravity of the *2-D fuzzy set for temporal variability of urban flood damage* to determine D_{i_g} ;
- 7 the program then generates a new *2-D fuzzy set for spatial variability of urban*

flood damage at D_{i_g} as 2-D fuzzy set for temporal and spatial variability of urban flood damage; and

- 8 Calculates weighted area of the 2-D fuzzy set for temporal and spatial variability of urban flood damage, WA_{ij} .

compatibility.m computer program performs the following tasks:

- 1 Loop through all trapezoids with valid data;
- 2 Linearly interpolate trapezoids and find minimum between fuzzy membership function of partial level of flood damage $\tilde{M}_{ij}(D_{ij})$ and fuzzy flood damage membership function $\tilde{S}_{ij}(D_{ij})$ to calculate the overlap area;
- 3 calculates the weighted overlap area between the fuzzy flood damage membership function and the partial level of flood damage membership function, WOA_{ij} ;
- 4 Calculates compatibility measure CM_{ij} using Equation 3.21.

flood_startup.m computer program performs the following tasks:

- 1 Initiates a Graphic User Interface (GUI) (Figure B1) by providing the option of pressing a button for the Flood Risk Analyzer, which has a call back function that links with the *flood_risk_analyser.m* file.

flood_risk_analyser.m computer program performs the following tasks:

- 1 Initiates a Graphic User Interface (GUI) for Flood Risk Analyzer (Figure B2).
- 2 The GUI uses a call back function to link (i) *process_triangular.m* file or

process_trapezoidal.m file, and (ii) *compatibility.m* file and then compares two compatibility measures based on a user defined as the *fuzzy membership function of partial level of flood damage* $\tilde{M}_{ij}(D_{ij})$.

- 3 The GUI provides the option to select the File menu and load either ASCII data or mat data for files containing values of temporal variability of flood damage ($D_{i \text{ Min}}$, $D_{i \text{ Mean}}$, and $D_{i \text{ Max}}$) and spatial variability of flood damage ($D_{i \text{ Min}}$, $D_{i \text{ Mean}}$, and $D_{i \text{ Max}}$) for a specific date/time .
- 4 Select model type, i.e. either *triangular* or *trapezoidal*.
- 5 Then, by pressing the Process Data button, the program performs the operation mentioned in *process_triangular.m* file or *process_trapezoidal.m* based on model type (Figure B2).
- 6 Then lower ($D_{ij \ 1}$) and upper ($D_{ij \ 2}$) bounds of the partial level of flood damage are entered for 1st and 2nd partial levels for residential land (Figure B2).
- 7 Then, by pressing the Calculate button the program finds values for the compatibility measure, cm; the reliability index, RE; and the robustness index, RO . The program further initiates an operation that allows for the presentation of the vause of resiliency index, RI, determined from the code written in Microsoft Visual Studio.
- 8 The program then plots the data and generates maps of reliability index, RE; robustness index, RO; and resiliency index, RI (Figure B3).
- 9 The data can then be exported either as ASCII or mat format by pushing the Export Data button ,
- 10 The user can also select a point on any of the maps by pressing the Datatip button

to get the 3-dimensional plot showing: (i) 3-D fuzzy set for temporal and spatial variability of flood, (ii) the center of gravity (D_{i_g}) of the 2-D fuzzy set for temporal variability of flood damage, and also (iii) the 2-D fuzzy set for both temporal and spatial variability of flood damage. The user can then deselect the Datatip to close the 3-dimensional plot (Figure B3). Results for selected time steps of the reliability index, re ; robustness index, ro ; and resiliency index, ri ; are given in Appendix B of the DVD attached.

The following table lists the names of the program files that are used for damage and risk analyses and their results, which are included in Appendix B found in the DVD attached.

Table B2: Model files and results

Data/File type	File name	File location in DVD
Damage analysis using GIS mAcros	GISMmacro.doc	Appendix B/damage
Result of damage analysis	D_i Min, D_i Mean, D_i Max, D_j Min, D_j Mean, and D_j max	Appendix B/damage_result
Risk analysis	<i>process_triangular.m file</i>	Appendix B/MATLAB
Risk analysis	<i>process_trapezoidal.m file</i>	Appendix B/MATLAB
Risk analysis	<i>compatibility.m file</i>	Appendix B/MATLAB
Risk analysis	<i>flood_startup.m file</i>	Appendix B/MATLAB
Risk analysis	<i>flood_risk_analyser.m file</i>	Appendix B/MATLAB
Results of re , ro , ri	re.txt, ro.txt, ri.txt	Appendix B/MATLAB_result

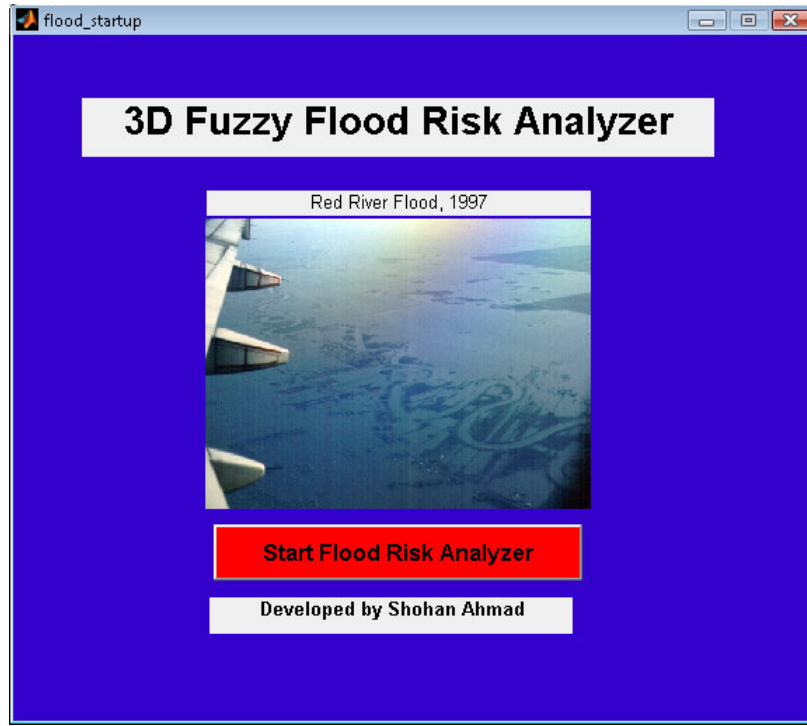


Figure B1: GUI for *flood_startup*

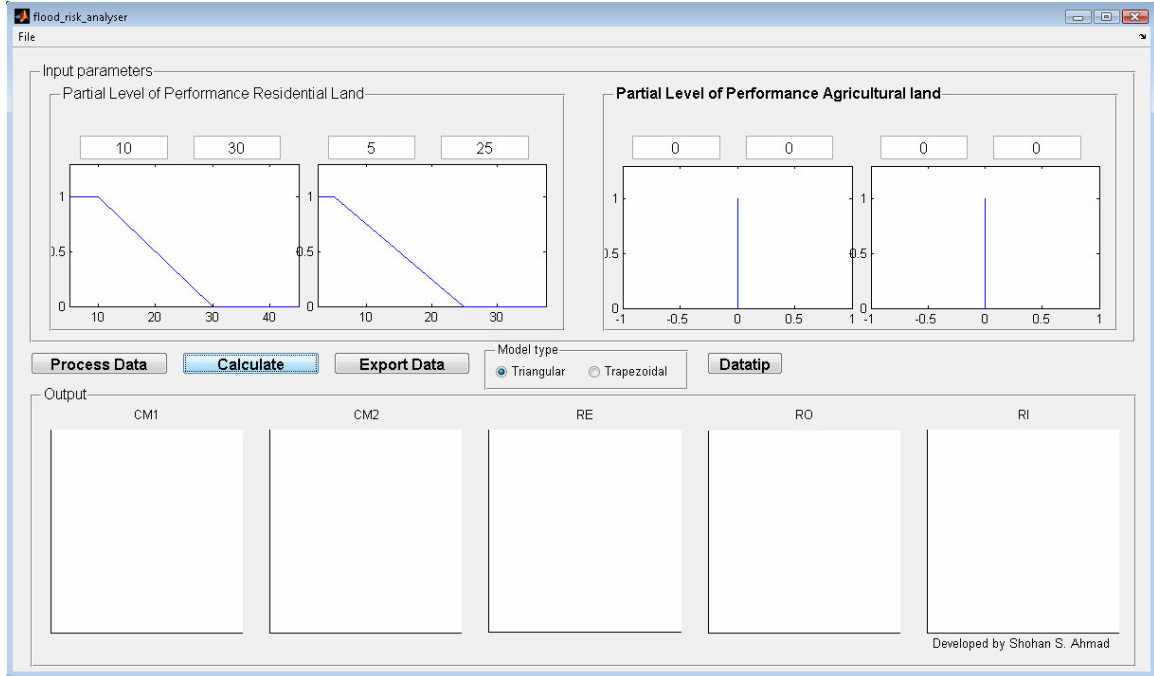


Figure B2: GUI showing partial level of flood damage for Cedar Hollow case study

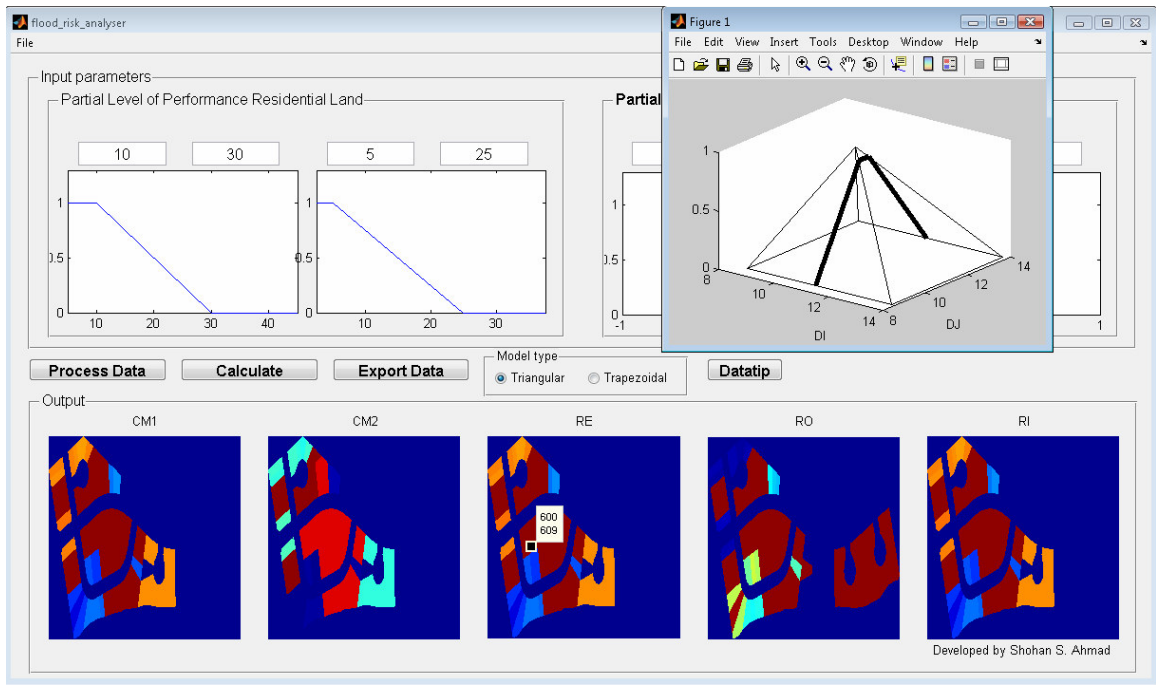


Figure B3: GUI showing maps of reliability indices and 3-D fuzzy set for temporal and spatial variability of flood damage for triangular membership function

CURRUCULUM VITAE

Name: Shohan S. Ahmad
Place of Birth: Calgary, Alberta, Canada
Date of Birth: May 20, 1978

EDUCATION

2006 **M.E.Sc.** in Civil & Environmental Engineering
The University of Western Ontario (UWO), London, ON

2004 **B.Sc.** in Water Resources Engineering
Bangladesh University of Engineering & Technology, Dhaka, Bangladesh

AWARDS AND HONOURS

2007 **CSCE Hydrotechnical Engineering Award**
(2007 Student Award for *best master's thesis in Canada* related to water resources engineering and water management. Presented by the CSCE Hydrotechnical Division at the CSCE Hydrotechnical Conference in Winnipeg in August, 2007)

2007- 2010 Natural Sciences and Engineering Research Council of Canada, Post Graduate Scholarship (**NSERC PGS D3**)

2007- 2008 Ontario Graduate Scholarship (**OGS**) (Declined)

2005- 2006 Natural Sciences and Engineering Research Council of Canada, Canada Graduate Scholarship (**NSERC CGS M**)

1998- 2004 Deans Award, Bangladesh University of Engineering and Technology

1998- 2004 Bangladesh University of Engineering and Technology Merit Scholarship

JOURNAL PUBLICATIONS

- 1) **Ahmad, S. S.** and S.P. Simonovic (2010). A Three Dimensional Fuzzy Methodology For Flood Risk Analysis, *Journal of Flood Risk Management*, (Accepted).
- 2) **Ahmad, S. S.** and S.P. Simonovic (2007). A Methodology for Spatial Fuzzy Reliability Analysis, *Applied GIS Journal*, 3(1):1-42.
- 3) Simonovic, S.P. and **S. S. Ahmad** (2007). A New Method for Spatial Fuzzy Reliability Analysis of Risk in Water Resources Engineering Management, *Open Civil Engineering Journal*, 1:1-12.

CONFERENCE PUBLICATIONS

- 1) **Ahmad, S.S.** and Simonovic, S.P. (2008). 2-D Hydrodynamic Modeling For Evaluation of Flood Risk in Space and Time, *4th International Symposium of Flood Defence, CSCE, Toronto, Ontario.*
- 2) Hossain, M.M, **Ahmad, S.S.** and Baki, A.B.M. (2008). The Flood Problem and Mitigation Methods in Bangladesh, *4th International Symposium of Flood Defence, CSCE, Toronto, Ontario.*
- 3) Ahmad, S.S. and Simonovic, S.P. (2007). A New Method for Spatial and temporal Analysis of Flood Risk, *18th Canadian Hydrotechnical Conference, CSCE, Winnipeg, Manitoba.*
- 4) El-Baroudy, I., **S.S. Ahmad,** and S.P. Simonovic (2006). Fuzzy reliability analysis for the evaluation of water resource systems performance, *CD Proceedings, 59th Annual Conference – CWRA, paper C4, pp.10.*